Oxidative Coal Dissolution a Systematic Study

by

Cristhian Camilo Cantillo Olave

A thesis submitted in partial fulfillment of the requirements for the degree of

Master of Science

in

Chemical Engineering

Department of Chemical and Materials Engineering
University of Alberta

Abstract

The coal industry in Canada boasts abundant reserves, with significant potential for value addition through innovative processes. Oxidative coal dissolution (OCD) emerges as a promising method to generate high-value products from coal, using air as the oxidant, making it a cost-effective and environmentally favorable approach. This thesis focuses on evaluating the impact of critical operating parameters on OCD, seeking to enhance its efficiency and product selectivity for large-scale applications.

The research started with a comprehensive overview of coal composition, ranks, and properties, followed by an exploration of the oxidation process itself. The study narrows down the scope to oxygen in air as the oxidant and explores the engineering challenges associated with OCD, including different operating parameters such as oxidant type, oxidant availability, temperature, time, water-to-coal ratio, and pH control.

An initial set of experiments at atmospheric pressure with temperatures up to 95 °C revealed that OCD at low temperatures has limited carbon yield to liquid products. To overcome this, OCD reactions at elevated pressures of 5 MPa and temperatures ranging from 90 to 180 °C were conducted. These conditions significantly improve carbon yield to liquid products, providing a better understanding of carbon conversion and product distribution. However, overoxidation remains a challenge at higher temperatures and pressures, leading to increased carbon conversion to gaseous products. To address this issue, further experiments at 1 MPa pressure at same temperature range were performed, improving carbon selectivity to liquid products, though at the

cost of decreased yield. It was found that the optimal selectivity and yield towards liquid products occur at 150 °C,

Additionally, an unexpected increase in heating value was observed in the residue product after OCD reactions at 90 °C, contradicting conventional expectations. To explore this phenomenon further, additional reactions were conducted using nitrogen instead of air, revealing that the decrease in the oxygen-to-carbon molar ratio responsible for the heating value increase is not solely attributed to the oxidative coal dissolution process. Instead, a hypothesis suggests that under specific reaction conditions, a portion of initially bonded oxygen within the coal molecule is liberated, possibly promoting the exudation of oxygen-rich organic compounds from the coal porous structure.

Keywords: OCD, Oxygen in air, Temperature changes, Oxidant availability, Carbon yield, heating value.

Acknowledgements

I want to extend my heartfelt gratitude to my supervisor, Dr. Arno de Klerk, for his guidance and support throughout this journey. Thank you for granting me the privilege of being part of an amazing research group. Your mentorship extended beyond research, encompassing a profound understanding of the holistic nature of learning and life.

I want to extend my sincere thanks to both current and former members of our research group, with whom I have shared innumerable moments of camaraderie and exchanged anecdotes and traditions. Many of these interactions have transformed into beautiful friendships, a gift I did not anticipate but now hold profound meaning in my life.

Gratitude is also owed to Omex, with whom I engaged in countless meaningful conversations over a cup of coffee, almost every morning when we both coincided at the university.

The unwavering support of my mother has been fundamental throughout this journey, despite the significant impact my decision to embark upon this path had on her life. To my beloved aunt Myrian and my precious siblings, I am indebted for their affection and shared laughter every time we talked, despite the distance.

To my princess, Luisa, thank you for all the respect, care and strength throughout this journey; your love is the most treasured gift of all.

Finally, I also want to express my gratitude to Mancal Coal Inc. for providing the financial support for this project to happen.

Table of content

List of tables

List of figures

1. Introduction to oxidative coal dissolution and key operating parameters

1.1 Background

In Canada, coal is the most abundant fossil, with 6.6 billion tonnes of recoverable coal reserves [1]. Additionally, more than 90% of Canada's coal deposits are located in western provinces. There are 2 trillion tonnes of coal at depth in the Alberta Plains that may be suited for exploration. In terms of production, by 2017, the output of Coal in Canada was 60.9 million tonnes, and most of the internal coal consumption is either used for power and heat plants with about 33.2 million tonnes, or for steel industries as coking coal with about 3.2 million tonnes, the remainder is exported [2]. Coal uses worldwide, and its distribution by rank is shown in Figure 1-1.
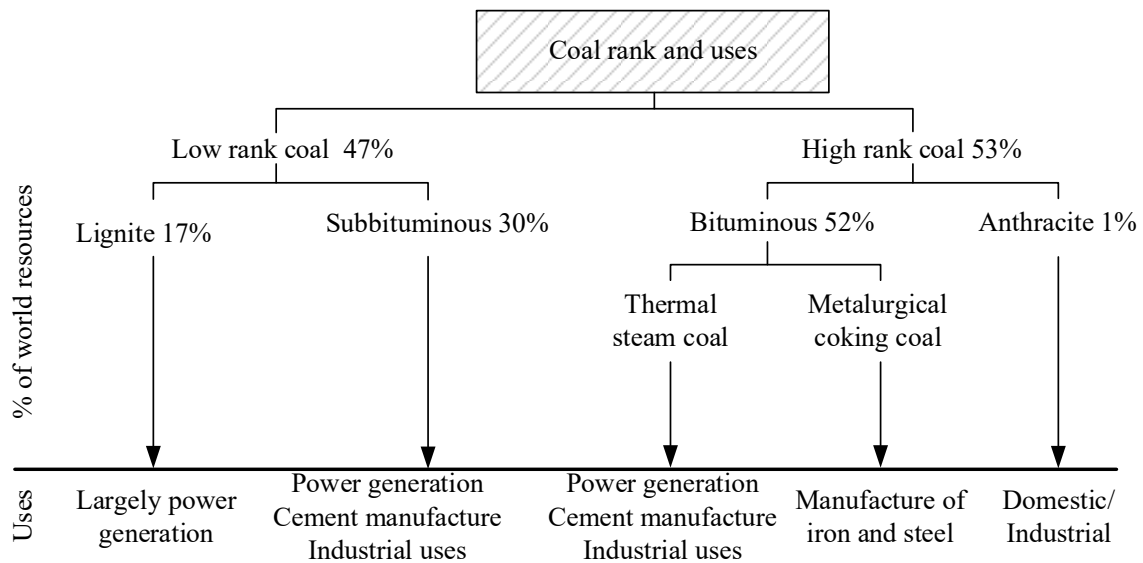
Figure 1-1 resources of coal by rank and uses [3].

But coal has not always been used as a source of fuel. More than 6000 years ago, it had an aesthetical value. In China, people used it to carve ornaments such as ear-piercing from black lignite. The first hard evidence of coal being used as fuel dates from the Han dynasty (206 bce to 220 ce). Among the different uses throughout history, people used coal for safety reasons, burning it to generate smoke and keep away snakes. It was also critical for the industrial revolution, and nowadays, it is the major thermal energy source in the world, as shown in Figure 1-2. Similarly,

new applications of coal with different objectives and new products will appear in the future through processes such as Oxidative coal dissolution (OCD), which is the topic of this study.
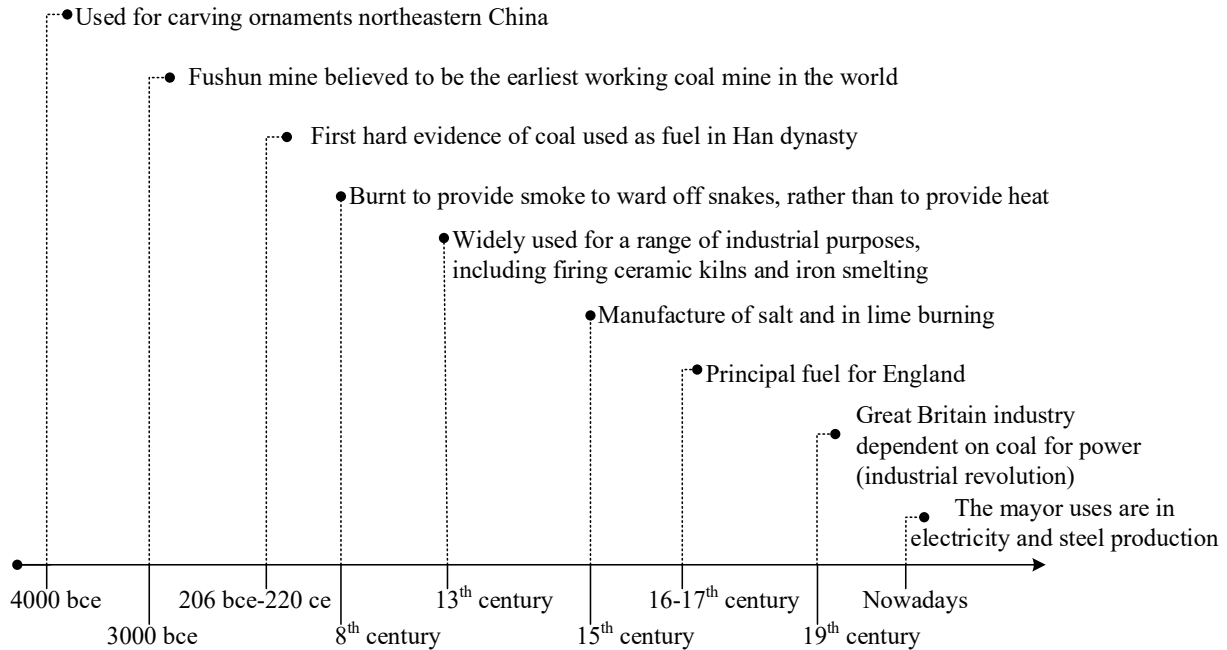
Figure 1-2 Uses of Coal through history [4].

Historically, mild coal oxidation was investigated to elucidate spontaneous combustion of coal during storage, and through oxidative dissolution to gain insight into the chemical constitution of coal [5][6]. Later work expanded oxidative coal dissolution to evaluate liquid fertilizer production [7]. More recent studies confirmed that a high yield of dissolved coal can be obtained, and there is an interest in using oxidative coal dissolution as a method to produce higher-value coal products. However, there are two prominent knowledge gaps. First, except for *Hayashi et al.* [8], other oxidative coal dissolution studies did not keep this conversion's economic aspects in mind. Second, little is known about conversion pathways that could be used to convert the oxidized coal into marketable products.

1.1.1 Why should coal be oxidatively dissolved?

Coal reserves are much higher than the world's consumption, and due to the increase and strengthening of environmental protection to the applications of coal use described in Figure 1-1,

it is important to explore other uses for coal. Therefore, oxidative coal dissolution comes as a conversion process that potentially generates some benefits through new opportunities for developing value-added products.

The approach to value addition in this project is via liquid phase conversion, and this work is specifically realated to the first step through oxidative coal dissolution under mild conditions. Liquid-phase oxidation of low rank coal is one of the promising methods of obtaining organic compounds in the liquid phase from the solid feed material [9]. It is not only a way to obtain organic acids, but also it can potentially improve residue properties, removing heteroatoms [10].

Oxidative coal dissolution has the further advantage of using air a reagent, as opposed to the use of hydrogen for reductive coal liquefaction. Although oxidation increases the oxygen content of the liquid products, part of the investigation that falls outside this project's scope is investigating pathways for selective CO_2 removal from the oxidized products. Various technologies have been developed in coal liquefaction with hydrogen at a pilot plant scale. Some of the most commonly known are H-coal, Exxon Donor Solvent (EDS), Solvent Refined Coal, and two stages liquefaction processes [11]-[13]. However, they require high pressure and temperature and in some cases the presence of a catalyst to transform coal into valuable liquid products. Nonetheless, no equivalent process development for oxidative coal dissolution exists.

1.1.2 What are the engineering challenges?

There are many challenges in the liquid phase oxidation of coal. First and foremost, the effect of reaction parameters on product distributions, which is crucial for process development, is not clear. From literature [8][14], and previous work developed in our research group [10], technically, oxidative coal dissolution is feasible. However, it is necessary to develop a reliable operating range for oxidative coal dissolution with the economics of the process in mind.

There are six operating parameters that will affect conversion, cost, and viability on a large scale: oxidant type, oxidant availability, temperature, use of additives for pH control, water-to-coal ratio, and time.

Despite the academic interest in different alternatives, there are some points to consider when selecting an oxidant: price, ease of handling, nature of the by-products, and percentage of oxygen available. Depending on the scale, production options change and bulk industrial oxidation processes are largely limited to air. Therefore, based mainly on cost, the oxidant is restricted to O_2 in air as an oxidant. With this clear, the reaction rate is affected by the oxygen availability that is correlated to the oxygen partial pressure. The reaction occurs in the presence of water, with the coal pores being water-filled. Thus, oxygen availability is related to the availability of dissolved oxygen in water, which in turn is dependent on the operating temperature and pressure. Changes in selectivity impact product upgrading and potentially the type of final products that can be produced and commercialized.

Temperature also impacts oxidation rate and affects selectivity, which needs to be understood at mild conditions, typically temperatures below 250°C. At the same time, the increase in temperature also affects the capital cost and the operating cost at a large scale. Considering that the liquid phase reaction medium is primarily water, a higher temperature than the boiling point of water would require additional pressurized systems to keep the reaction in the liquid phase.

Most of the work reported in the literature requires a large amount of alkali consumption. It is suspected that alkali is employed to increase water solubility of products like phenolics and carboxylic acids as phenolates and carboxylates. If so, adding alkali is not an oxidative dissolution requirement and can be totally or partially avoided if the oxidized coal can be recovered as a multi-phase product. Alkali addition would increase operating costs and downstream water treatment. Beyond the obvious impact on material selection, a fundamental understanding of the need and benefit of pH control is required.

The increase of water-to-coal ratio directly impacts the process operation, since more material volume makes the product recoveries more challenging in many ways. It increases the utility services, such as water and electricity, impacts the water treatment process downstream and the solvents needed for the product recovery, and also requires more unit capacity and capital cost for the same coal feed rate. Conversely, the decrease of water-to-coal ratio is limited by different

4

aspects, such as solubility and rheological constraints on water-coal slurry fluidity. Therefore, the aim is to see with how little water the process can be performed. On the other hand, it is necessary to analyze the impact of water-to-coal ratio on reaction engineering too. For example, if over-oxidation can be reduced by increasing oxidized coal removal by a higher water-to-coal ratio, then it is important to understand this relationship.

Reaction time has been studied at different conditions to evaluate the impact on oxidation conversion and product yield. *Francis* [15] describes a relationship between time and the various stages of coal oxidation which lead to differences in product selectivity. Time is probably the variable with the highest impact on operational cost and equipment capacity design. Therefore, an evaluation of the product selectivity with time needs to be performed. Figure 1-3 summarize the key engineering challenges faced by the different operating conditions evaluated in this project.

Figure 1-3 Key engineering challenges at different operating conditions

1.2   Objective

This project's objective was to understand and evaluate the effects of critical operating parameters in oxidative coal dissolution using oxygen in air as oxidant.

1.3   Scope of work

To limit the scope of the investigation and consider the conversion cost and viability on a large scale, no other oxidants than air were considered purely based on economics. Additionally, the project is not specifically aimed at subsurface coal conversion, because attention would have to be

given to coal porosity and permeability, but these aspects are not considered. For reasons of cost and the challenge of recovering dissolved catalyst, this work did not consider catalysts.

The literature on oxidative coal dissolution was consulted, particularly focusing on the processes at mild conditions, reaction chemistry and engineering (Chapter 2). The experimental investigation was limited to the coal feed characterization (Chapter 3), the development of scoping experiments at atmospheric pressure, including changes in temperature and time (Chapter 4), the effect of temperature on reaction selectivity at 5 MPa (Chapter 5), and the effect of temperature on reaction selectivity at 1 MPa (Chapter 6). Finally, there are the findings and conclusions with recommendations for future research on this topic (Chapter 7).

References

[1]   Thomas, L. *Coal Geology* 3rd ed.; John Wiley & Sons Ltda: Abergavenny, 2020.

[2]   International Energy Agency. Coal Information.; IEA Publications: France, 2019.

[3]   Speight, J. G. *Handbook of coal analysis. Chemical analysis: A series of monograph on analytical chemistry and its applications. Vol. 182*, 2ed.; Wiley: Hoboken, New Jersey, 2015.

[4]   Crane, R. *Coal*; Reaktion Books Ltda: London, 2021.

[5]   Howard, H. C. Chemical constitution of coal: as determined by oxidation reactions. In *Chemistry of coal utilization. Vol.1*; Lowry, H. H. ed; Wiley: New York, 1945, p.346-376.

[6]   Dryden, I. G. C. Chemical constitution and reactions of coal. In *Chemistry of coal utilization, Supplementary Volume*; Lowry, H. H. ed; Wiley: New York, 1963, p. 232-295.

[7]   Wender, I.; Heredy, L. A.; Neuworth, M. B.; Dryden, I. G. C. Chemical reactions and the constitution of coal. In *Chemistry of coal utilization, Second Supplementary Volume*; Elliott, M. A. ed; Wiley: New York, 1981, p. 425-521.

[8]   Hayashi, J.; Matsuo, Y.; Kusakabe, K.; Morooka, S. Depolymerization of lower rank coals by low-temperature O_2 oxidation. *Energy Fuels* **1997**, *11*, 227-235.

[9]   Mae, K.; Shindo, H.; Miura, K. A new two-step oxidative degradation method for producing valuable chemicals from low rank coals under mild conditions. *Energy Fuels* **2001**, *15*, 611-617.

[10]   Siddiquee, M. N.; De Klerk, A. Heteroatom removal as pretreatment of boiler fuels. *Energy Fuels* **2019**, *33*, 5790-5801.

[11]   Vasireddy, S.; Morreale, B.; Cugini, A.; Song, C; Spivey, J.S. Clean liquid from direct coal liquefaction: chemistry, catalysis, technological status and challenges. *Energy & Environmental Science* **2011**, *4*, 311-345.

[12]   Robinson, K.K. Reaction Engineering of direct coal liquefaction. *Energies* **2009**, *2*, 976-1006.

[13]   Yurchick, C. L. *Coal liquefaction process development*; Ph.D. Thesis, West Virginia University, 2012.

[14]   Liu, K.; Yang, J.; Jia, J.; Wang, Y. Desulphurization of coal via low temperature atmospheric alkaline oxidation. *Chemosphere* **2008**, *71*, 183-188.

[15]   Francis, W. *Coal. Its formation and composition*, 2ed.; Edward Arnold: London, 1961.

2. Literature review on oxidative coal dissolution

2.1 Introduction

Current research focuses on oxidative coal dissolution (OCD) as a conversion pathway that has the potential to add value to coal through further upgrading processes. Previous work performed in our research group [1] demonstrated that oxidative coal dissolution under mild conditions is feasible. The products after oxidation consist of a solid residue, partially desulfurized with a high carboxylic acid content and a water soluble liquid extract.

This chapter highlights the scientific background and the influence of the key operating parameters for OCD. To do so, first, it is essential to understand the chemical composition and ranks of coal that influence the present work. Next, this chapter explains the oxidation process itself, focusing on the stages of oxidation, mechanisms, and process variables that affect OCD reactions. Even though some liquid oxidation processes include different oxidants, mediums, and in specific cases, the use of catalyst, only oxygen in air as the oxidant in neutral or alkali medium (with NaOH) for pH control is considered based on cost and viability on a large scale. Finally, there is a description of liquid products identified and/or isolated after different OCD processes with a particular focus on yields of carboxylic acids.

2.2 Coal

Oxidative coal dissolution results depend to a great extent on coal composition and its properties. Coal is defined as a sedimentary rock composed mainly of organic carbonaceous macerals, which are the combustible part of coal, and inorganic minerals [2]. Coal also has an internal capillary structure that contains water as moisture and gases; this is an important feature for the chemical reaction process [3].

There are various methods for classifying coal. Morphology can be used to classify different types of coal. Internal layering, also known as banding, is present in most coals. Coal types and their subsets, or lithotypes, are classified according to whether or not there is banding and whether or

not the individual bands are bright or dull. Microscopic microlithotypes of coal are subdivided further into coal lithotypes and are made up of several kinds of microscopic coal constituents known as macerals [4].

2.2.1 Macerals

Macerals are a complex mixture of macromolecules composed of structural units or constituent molecules, which are those units of the macromolecules that survive mild chemical transformations over geological time [2]. The organic fragments of coal are divided into three maceral groups based on their appearance, chemical composition, and optical properties. Additionally, they can be traced to specific origins or components of the plant debris from which the coal formed in most cases. These maceral groups are vitrinite, exinite (or liptinite), and inertinite. Each maceral group is subdivided into further macerals and sub-macerals. Table 2-1 shows some coal macerals indicating the plant component from which they are composed.

In terms of maceral reactivity, vitrinite exhibits the highest susceptibility to oxidation compared to other groups of the same rank. Additionally, both vitrinite and liptinite are considered reactive with respect to hydrogen liquefaction, whereas inertinite demonstrates near-complete resistance to both oxidation and liquefaction, regardless of the rank [4][7]. Furthermore, vitrinite has been identified as the maceral group most prone to spontaneous combustion, although this characteristic is highly dependent on external factors such as bulk density and particle size. As the latter decreases, both the susceptibility to spontaneous combustion and the magnitude of its effect tend to increase [4].

Table 2-1 Components of coal macerals [5][6]

Maceral Group	Maceral	Composition/Characteristics
Vitrinite	Collinite	humic gels
	Tellinite	wood, bark, and cortical tissue
	Corpocollinite	cell filling
	Vitrodetrinite[a]	Detritus
Liptinite	Sporinite	fungal and other spores
	Cutinite	leaf cuticles
	Suberinite	subordinated cell walls (cork)
	Fluorinite	plant oils
	Resinite	resin bodies and waxes
	Alginite	alga remains
	Bituminite	amorphous (bacterial, algal, faunal)
	Chlorophyllinite	chlorophyll
	Liptodetrinite[b]	detritus
Inertinite	Micrinite	unspecified detrital matter, $<10\mu m$
	Macrinite	unspecified detrital matter, $10\text{-}100\mu m$
	Semifusinite	carbonized woody tissues
	Fusinite	carbonized woody tissues
	Sclerotinite	fungal sclerotia and mycelia
	Inertodetrinite[c]	detritus

[a]used to designate a maceral when it is not possible to distinguish between collinite and tellinite

[b]used to differentiate between sporinite and cutinite on morphological grounds

[c]because of its reflectivity, must be assigned to this maceral group, but that cannot be unequivocally identified with any particular maceral within the group.

2.2.2 Chemical composition

Coal does not have a defined chemical structure. Coal macromolecule is not composed of repeating monomeric units; however, coal can be described in terms of structural parameters [2]. The main parts of coal can be described as aromatic clusters connected through methylene bridge bonds and different lengths of aliphatic structures on them. Coal is a high molecular weight substance with a nonuniform structure, an abundance of aromatic rings and with a polymeric structure [6].

The chemical composition of coal is usually defined in terms of proximate analysis and elemental composition. Even though these techniques do not provide direct information about the coal structure, their data can be correlated to understand coal behavior [5]. And with additional parameters such as those given in Van Krevelen diagrams [6], it is possible to have a general idea

of the coal skeleton (see Figure 2-1). Transition through a coalification process defines the typical composition ranges for specific elements in coal and other important properties classified by ranks.
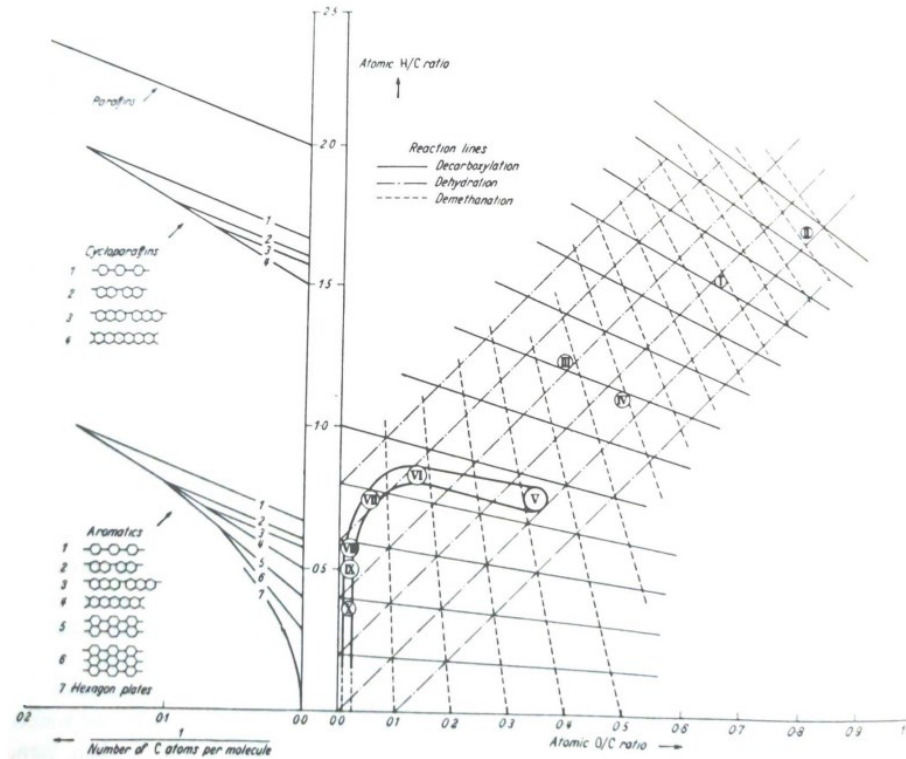
Figure 2-1 Van Krevelen H/C versus O/C diagram for different coal ranks: (I) Wood, (II) Cellulose, (III) Lignin, (IV) Peat, (V) lignite/Subbituminous coal, (VI) Low rank Bituminous coal, (VII) medium rank bituminous coal, (VIII) high rank bituminous coal, IX semi-antracite, X Antracite [6] Figure is reprinted with permission of the copyright holders

Rank classification

The rank of the organic fraction of coal is determined based on the degree of alteration that occurs as coal matures under the influence of time, temperature, and pressure. *Davidson* [2] interpreted the coalification process in two stages based on coal oxidation studies with sodium hypochlorite: First, a stable aliphatic carbon skeleton is generated from the original plant matter, and then benzene rings are produced. *Hatcher and Clifford* [8] proposed the reactions associated with the leading chemical changes from lignin to the different rank levels (Figure 2-2). The degree of coalification progressively increases from lignin and lignite through sub-bituminous coal,

bituminous coal to anthracite. Lignite and sub-bituminous coals are denominated low-rank coals, and bituminous and anthracite coals are named high-rank coals [9].
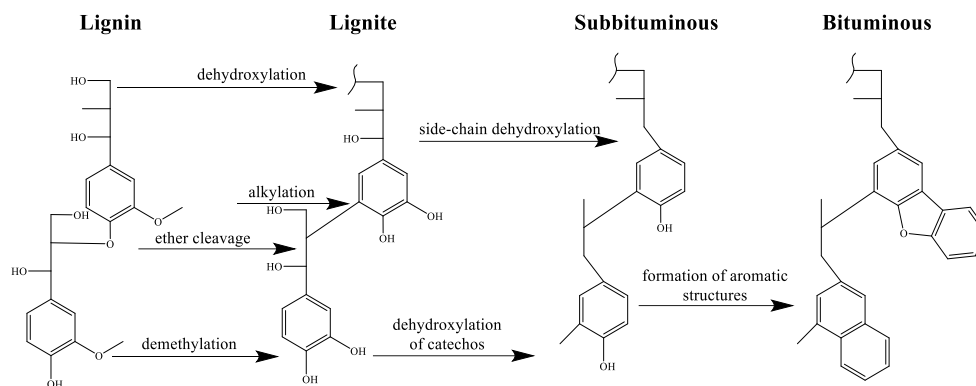
Figure 2-2 Chemical transition of coal in coalification process (adapted from [8])

Van Krevelen H/C and O/C diagram shown in Figure 2-1 presents a graphical method that permits a rough idea about the structure of carbon skeleton based on rank. With regard to elemental chemistry, an increase in carbon content and aromaticity with decreasing in oxygen and hydrogen content are the most prominent characteristics of the coalification process [2]. One basic model with the general structure evolution for coals of different ranks is shown in Figure 2-3 Although these structures are helpful to visualize the coalification process, including changes in carbon content and aromaticity previously mentioned, it is an over-simplification of the composition, which is more varied and complex.
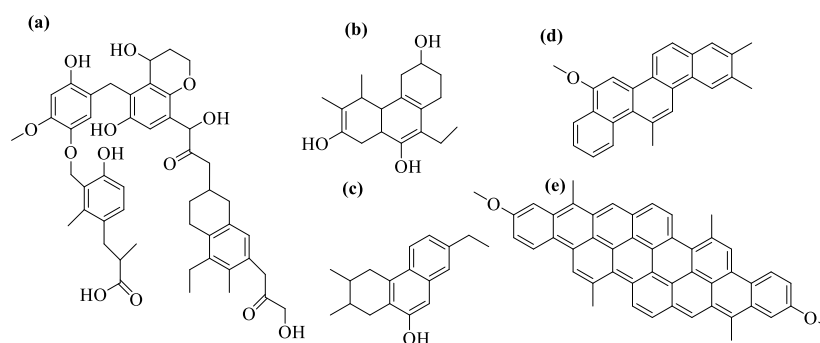
Figure 2-3 Basic structural model for coals of different ranks (a) brown coal(lignite), (b) subbituminous coal, (c) high volatile bituminous coal, (d) low volatile bituminous coal, (e) hard coal: anthracite [10]

12

As coals increase in rank, there is also a general decrease in moisture and an increase in heating value [11]. Density ranges decrease from lignite to bituminous coal. However, for anthracite, density range is more comprehensive, with a maximum relatively higher than lignite coal density. Table 2-2 [12] shows the relationship and typical ranges of important analytical parameters for the principal ranks of coal.

Table 2-2 Typical composition and physical property ranges for various rank coals [12]

	Lignite	Subbituminous	Bituminous	Anthracite
Moisture (%)	25-45	10-12	2-5	3-6
Volatile matter (%)	24-32	28-45	15-45	2-12
Fixed Carbon (%)	25-30	30-57	50-70	75-85
Ash (%)	3-15	3-10	4-15	4-15
Sulfur (%)	0.3-2.5	0.3-1.5	0.5-6	0.5-2.5
Hydrogen (%)	6-7.5	5.5-6.5	4.5-6	1.5-3.5
Carbon (%)	35-45	55-70	65-80	75-85
Nitrogen (%)	0.6-1.0	0.8-1.5	0.5-2.5	0.5-1
Heat of combustion[a] (MJ/kg)	14.0-17.4	17.4-23.3	27.9-33.3	27.9-31.4
Heat of combustion (Btu/lb)	6000-7500	7500-10000	12000-14500	12000-13500
Density (g/mL)[a]	1.40-1.45	1.35-1.40	1.28-1.35	1.35-1.70

[a] Calculated based on Dulong's correlation.

2.2.3 Mineral matter

Mineral mater represents all forms of inorganic material incorporated with coal, including all optical identifiable mineral species or phases and complexed metals and anions [5]. Even though there has been considerable discussion about the terms used to describe the origin of mineral matter, it is generally classified into two classes. One class present in the plant structure that formed coal "inherent", and the second class that was added to coal during the peat bog or later stages of coal formation "adventitious" [13][14].

A large number of minerals have been reported in the literature to be present in coal. Still, according to their relative abundance, the majority that can be classified as major constitutes are shown in Table 2-3 and described as follow:

- Clay minerals are the most common type of mineral in coal. The most known species are kaolinite and illite, and some experiments found that clay minerals dominate up to 73 % of the mineral matter [14]. Generally, this type of mineral is about 50 % of the total mineral matter content [5]

- Carbonate minerals are the salts of carbonic acid and the extensive possibilities for interchanging the more common metals, such as calcium, magnesium, iron, and manganese [14][15]

- Sulfide minerals existing principally as pyrite and marcasite [5][14]

Table 2-3 Mayor minerals associated with coal [5][14]-[16]

Mineral type	Species	Molecular composition
Clay	Illite	$KAl \cdot (AlSi_3O_{10})(OH)_2$
	Kaolinite	$A1_4Si_40_{10}(OH)_8$
	Montmorillonite	$Na_2(Al \cdot Mg)(Si_4O_{10})(OH)_2$
	Smectite	$A1_2Si_40_{10}(OH)_2$
Carbonates	Ankerite	$CaCO_3 \cdot MgCO_3 \cdot FeCO_3 \cdot CaCO_3(Mg,Fe,Mn)CO_3$
	Calcite	$CaCO_3$
	Dolomite	$CaCO_3 \cdot MgCO_3$
	Siderite	$FeCO_3$
Sulfides	Marcasite	FeS_2 (orthorhombic)
	Pyrite	FeS_2 (isometric)
	Sphalerite	ZnS
	Galena	PbS
Sulfates	Iron Sulfate	$FeSO_4 \cdot nH_2O$
Silicates	Quartz	SiO_2
Others	Barite	$BaSO_4$
	Feldspar	$(K \cdot Na_2)_2O \cdot Al_2O_3 \cdot 6SiO_2$
	Gypsum	$CaSO_4 \cdot 2H_2O$
	Halite	$NaCl$
	Phosphates	$Ca_{10}(PO_4)_6(OH)_2$ $Ca_{10}(PO_4)_6(F)_2$ $Ca_{10}(PO_4)_6(Cl)_2$
	Zircon	$ZrSiO_4$
	Epidote	$4CaO\ 3Al_2O_3\ 6SiO_2\ H_2O$
	Biotite	$K_2O\ MgO\ Al_2O_3\ 3SiO_2\ H_2O$
	Diaspore	$Al_2O_3\ H_2O$
	Magnetite	Fe_3O_4
	Lepidocrocite	$Fe_2O_3\ H_2O$
	Hematite	Fe_2O_3

- Sulfate minerals are not usually present in unweathered coals and exist primarily as variously hydrated iron sulfates [14][15]
- Silicate minerals with quartz as the dominant form and accounts make up to 20 % of all mineral mater [5][14]

In addition to those already mentioned, minor constitutes of minerals have been reported to be present in coal, and it is frequently challenging to determine whether the mineral was intimately associated with the coal or was in the rock units making up the roof, floor, or a parting within the seam [15].

Mineral matter in coal is commonly analyzed and characterized using data on ash and ash-forming constituents. Ash is the residue produced after the complete combustion of the organic portion of the coal. When the mineral matter is exposed to high temperatures, there is a generalized behavior to specific reactions identified in some of the species according to Table 2-4. Mayor inorganic compounds of coal ash are shown in Table 2-5.

Table 2-4 Generalized behavior of mineral matter at high temperatures [16][17]

Inorganic Species	Reactions on heating
Clays	Dehydration and sintering; reaction of products with FeS_2 from pyrite, CaO from carbonates, SiO_2, etc.
Pyrite	In air Oxidation to Fe_2O_3 or Fe_3O_4 ; reaction with silicates; in volatile matter test decomposes to FeS
Quartz	Reaction with aluminosilicates from clays, with CaO and Fe_2O_3 to form crystalline and molten silicate phases
Metal carboxylates	Decomposition to sulfates or can also react to SiO_2 to form silicates
Carbonates	Dissociation to oxides with loss of CO_2; residual oxides fix some organic and pyritic S as sulfate

Regarding the impact of mineral matter in coal applications as a fuel; problems, and limitations of the commercial use of coal include deposits in boiler, fouling, slagging, corrosion, and others. It has also been reported that calorific values of coals tend to decline with an increase in mineral matter content due to its endothermic reactions of decomposition and heat capacity [18].

Table 2-5 Major inorganic constituents of coal ash [16]

Compounds	Percentage in coal ash (%)
SiO_2	40-90
Al_2O_3	20-60
Fe_2O_3	5-25
CaO	1-15
MgO	0.5-4
Na2O	0.5-3
K2O	0.5-3
SO3	0.5-10
P_2O_5	0-1
TiO_2	0-2

Some minerals may also affect the reaction chemistry and composition of the coal. For example, clay minerals may participate in acid catalysis and pyrites may transfer sulfur to the organic matter.

2.3   Coal oxidation

Coal oxidation is a degradative process where coal macromolecules are attacked by the oxidant, generating products of lower molecular mass despite the addition of oxygen to some products [19]. Several studies about coal oxidation at mild conditions have been developed from various points of view. The two most common are related to the oxidation of solid coal by air, also called weathering process of coal and the aqueous oxidation of coal.

The weathering process results from coal's exposure to air while handling and transporting under different environmental conditions. It has been widely studied, mainly because one of the consequences of this type of oxidation is the spontaneous combustion of coal. Spontaneous combustion of coal occurs when the heat generated by in situ oxidation causes the coal to smoulder and ultimately burn without any external heat source [15].

On the other hand, liquid phase oxidation of coal at mild conditions has been studied with multiple purposes at different operating conditions and with a wide range of oxidant agents. Initially, liquid oxidation research was conducted as an effort to better understand the chemical constitution of coal [3][7], which is still used as a way to explore coal's molecular structure [20][21][22][23].

Efforts also broadened to evaluate liquid fertilizer production [24], the oxidative desulfurization of coal [1][25] and the production of higher value products from low rank coals [19][26][27][28].

2.3.1 Liquid phase oxidation of coal at mild conditions

Oxidative coal dissolution at mild conditions (reaction temperature <250°C), aside from well-known advantages in areas such as the study on spontaneous combustion and the understanding of coal constitution [13], is considered a potentially effective method for converting low-ranking coal into small molecules to produce commercial value-added chemicals in high yields [26].

Besides the importance of Van Krevelen diagrams on the identification of coal structures, they also give a graphical representation of reaction processes such as oxidation [6]. Figure 2-4(a), for example, identifies the variation H/C vs O/C for six different reactions, where it is clear that oxidation increases O/C ratio with the incorporation of oxygen to the structure. But it is not entirely true that H/C ratio keeps the same during the liquid oxidation process; instead, it changes according to the stage and intensity of oxidation. According to Figure 2-4(b) H/C ratio initially decreases, but in the second stage, it increases as it is described as part of the mechanism of oxidation.
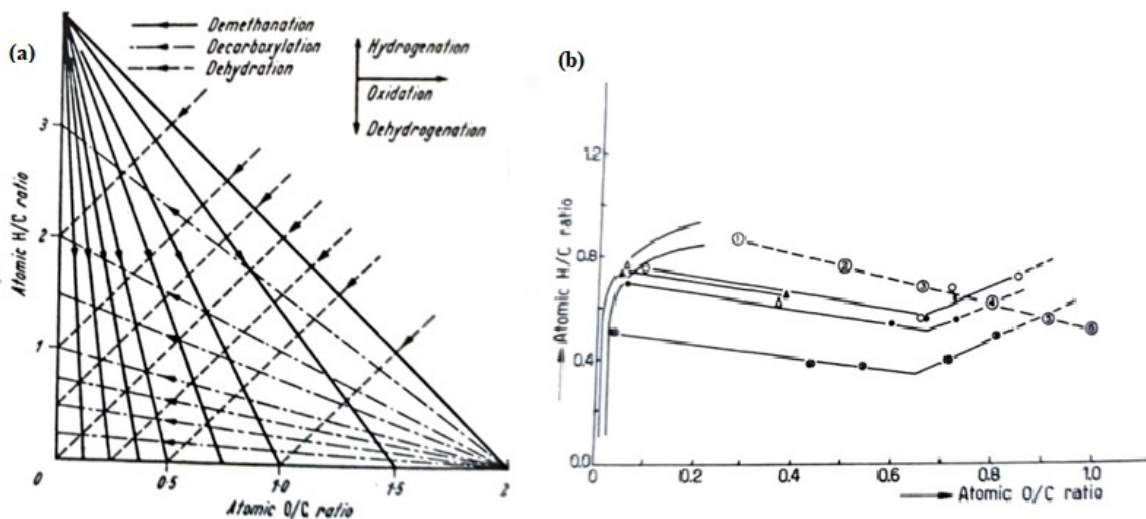
Figure 2-4 Van Krevelen H/C versus O/C diagram for: (a) representation of reaction processes and (b) Oxidation by aqueous agents [6]. Figures is reprinted with permission of the copyright holders

2.3.2 Stages of Coal Oxidation in aqueous media

Based on an experiment with alkaline potassium permanganate, which was found as the best agent to oxidize in a strictly quantitative way. The potassium permanganate rate of decomposition was used as a measure of the oxidation of coal, and it was established that the oxidation reaction apparently consists of three phases [13]:

1. A speedy initial reaction in low rank coals that was completed before the first period of oxidation (10 min). It can be described as the first stage or surface of oxidation.
2. A steady reaction for intermediate reaction times, that represents the formation of colloidal humic acids alkali-soluble, as part of the second stage of oxidation.
3. A slow long-continued reaction for extended periods of several hours, which represents the third stage of oxidation to water soluble acids.

Without diminishing the importance of the description, there is an inherent bias related to the use of partitioning between the organic phase (coal) and alkaline aqueous phase to determine the phases of the reaction.

Stage 1: Surface Oxidation

The first stage of coal oxidation, also called surface oxidation, is characterized by the addition of oxygen and forming oxygen-containing groups with acidic properties [26], particularly phenolic, anhydride acid, and carboxylic acid [5]. Even though coal visually appears to be little affected during the early part of this stage, it exhibits changes in caking and coking properties, the heat of combustion and susceptibility to further oxidation [7].

It involves the adsorption of molecular oxygen onto the coal surface, leading to the formation of oxygen-containing functional groups, such as hydroxyl (-OH) and carbonyl (-C=O) groups. These functional groups are generated via chemical reactions between oxygen molecules and the organic functional groups within the coal, which primarily consist of aliphatic and aromatic hydrocarbons.

In the case of aliphatic oxidation, the hydrogen-containing groups within the coal significantly contribute to the formation of carboxyl groups. Specifically, oxygen molecules first remove hydrogen atoms from these groups, followed by attachment to the radical carbon [7]. On the other hand, in the case of aromatic oxidation, the formation of oxygenates can occur via three pathways: without cleavage of the aromatic rings, accompanied by cleavage of the aromatic rings, or through oxidation of the side chains attached to the aromatic rings [29].

Overall, the initial stage of coal oxidation involves the transformation of the coal surface through the introduction of oxygen-containing functional groups, which can subsequently participate in further oxidation and degradation processes. The specific types of functional groups formed depend on the nature of the organic functional groups present in the coal and the type of oxidative conditions present.

Stage 2: Humic Acids

As oxidation continues, a significant fraction of the organic material of the coal is converted into what is collectively called "regenerated humic acids" or "humic acids." It is a product that contains sufficient hydrophilic, carboxyl, and hydroxyl groups to confer alkali solubility [6][7]. That solution can be flocculated with acids, and the precipitate is composed of substances with about 30-40 % oxygen [6]. Humic acids represent molecules of an intermediate complexity stage between the original coal substance and the simple water-soluble acid [7]. The collective term "humic acids" is therefore not a compound class, but a solubility class.

Stage 3: Water soluble acids

Once the process that produced the humic acids is continued for a sufficient time and depending on the severity of the oxidation methods applied, the humic acids are degraded to lower-molecular-weight acids, soluble in acid, neutral, and alkaline aqueous media. This oxidation to the soluble acids may take place in one step, without humic acids isolation. In any case, it appears that humic acid is an intermediate product, but for strong oxidation procedures, it is ephemeral [7].

2.3.3   Mechanisms of coal oxidation

At low temperatures and weak oxidation conditions, *Francis* [13] states that aqueous oxidation proceeds in the same way as in a nonaqueous medium. It starts by the normal mechanism for the oxidation of aliphatic groupings, which may be attached to cyclic structures or act as linkages between such structures. During this reaction, one oxygen is introduced into the residue for each hydrogen removed from the system. The contribution of this reaction decreases when unoxidized aliphatic linkages or grouping are no longer abundant. The process of oxidation in air leads to the formation of carboxyl groups through a mechanism that involves hydrogen transfer from nearby hydroxyl (-OH) groups. However, in aqueous media, where there is an abundance of accessible hydroxyl groups, this hydrogen transfer is not an essential step in forming carboxyl groups. The presence of a high concentration of hydroxyl groups in an aqueous environment provides an alternative source of hydrogen that can participate in the oxidation process, obviating the need for hydrogen transfer.

Van Krevelen [6] describes a two stages mechanism in aqueous oxidation with nitric acid. First, following the reaction progress explained by Francis and going further, by indicating that H/C ratio in coal decreases whereas O/C ratio increases. At this first subsequent stage, there is an oxidation of nonaromatic groups to carboxylic groups and oxidation of some aromatic rings to quinone structures. It is, on average, a rate of 1:4 of hydrogen removed and oxygen introduced from the coal molecule, respectively. In the second stage, H/C and O/C rates increase up to a 1:1 ratio of oxygen and hydrogen atoms introduction in coal molecule as shown in Figure 2-4(b). An example of the reactions for each stage is shown in Figure 2-5.
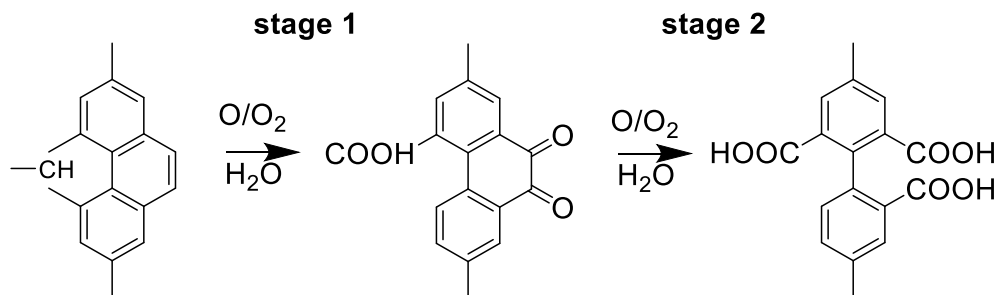
Figure 2-5 Model of Aqueous oxidation reaction following the description of Van Krevelen [6]

There are additional studies of coal oxidation mechanism in the liquid phase. The proposed models are similar to those mentioned before with one or two steps, focusing on the production of aliphatic and aromatic carboxylic acids as the main product. Some examples include oxidation with oxygen coming from hydrogen peroxide [21][27], sodium hypochlorite and ruthenium oxide [30].

There are also interesting mechanisms in a nonaqueous medium that postulate the reaction path for coal conversion into humic acids with oxygen in air at different temperatures. One of them, with the objective to explain the observed changes in coal oxidation process, is suggested by *Berkowitz* [5] It implies that air oxidation of coal can degrade aromatic as well as nonaromatic structures. It attaches an additional step of phenols formation before quinones appear, according to Figure 2-6(a). Then proceeds via quinones and acid anhydrides to carboxylic acids, as shown in Figure 2-6(b).
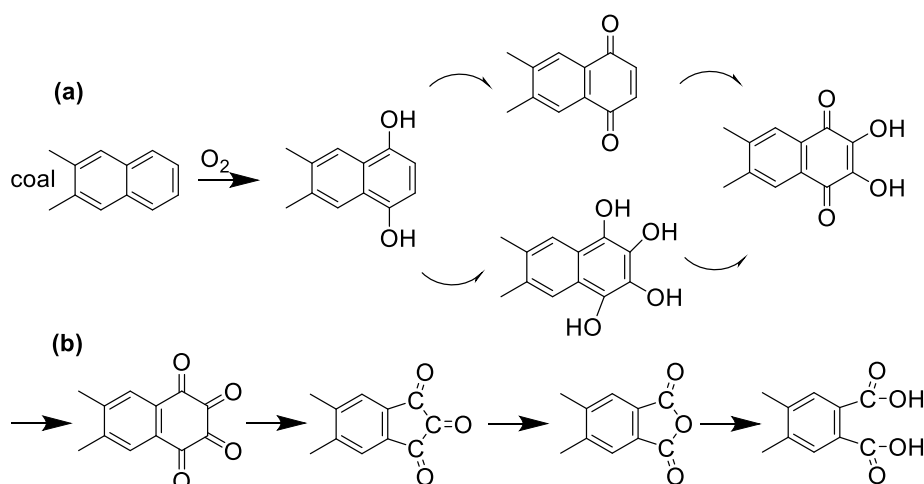
Figure 2-6 Postulated reaction mechanism for coal oxidation in air adapted from [5]

A more extensive mechanism for coal oxidation by air proposed by *Clemens et al.* [31] is shown in Figure 2-7. This mechanism also includes the carbonyl group as intermediate, and additionally, there are other possible products after the formation of carboxylic acids. First, (a-c) radicals are produced from a bridge bond in coal (in aqueous media due to -OH groups plentifully available that bridge bond can also be easily produced with it), and the oxygen attacks the radical to form the hydroperoxide. Then, (d) there is a decomposition of hydroperoxide and the release of more radical groups. Afterward, reactions involve the generation of aldehydes from oxygen radicals (e)

and carboxylic acids from aldehydes, carbon radicals and peroxyacetic acids (f-g). Last, if the reaction goes further, carbon monoxide (h) is formed from carbonyl radicals and (i-j) carbon dioxide, esters and anhydrides are developed by the reaction of alkane radicals and carboxylic acid radicals.

The aforementioned descriptions of oxidation were all based on studies of coal oxidation. Most of these descriptions are empirical, with only limited free radical reaction fundamentals being incorporated in the descriptions. The fundamental steps in oxidation can also be described using the literature developed through model compound oxidation.
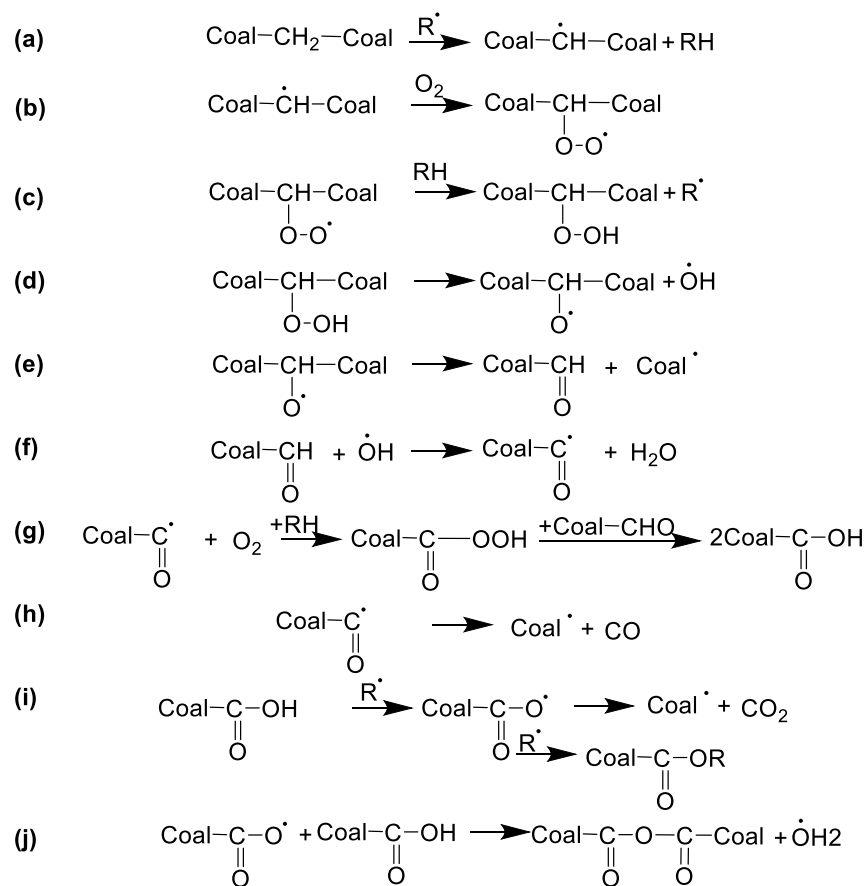
Figure 2-7 Proposed reaction mechanism for coal oxidation in air, by *Clements et al* [31]

The decision to limit the description to coal oxidation is one of scope. It is nevertheless recognized that both aliphatic and aromatic oxidation can take place in parallel, as was suggested by *Berkowitz* [5]. The description did not explore heteroatom oxidation and did not specifically explore the

formation of olefins and their oxidation, or any of the free radical side-reactions that may take place.

2.3.4 Operating parameters that affect oxidative coal dissolution

The study of coal oxidation variables is key to understand the reaction process and yield of products and to measure the viability of engineering challenges associated with scaling the process at a commercial level.

Oxidant

In terms of oxidants, various options have been studied for oxidative coal dissolution: oxygen, sodium hypochlorite, hydrogen peroxide and nitric acid as the most common (Table 2-6). Nevertheless, as mentioned previously, based on cost and the possibility of scaling up this process to an industrial level in the future, only oxygen in air as oxidant is considered in this project. Previous investigations in the other variables alongside their main findings are described in the following subsections.

Table 2-6 Typical oxidants for coal oxidation in aqueous media (adapted from [6])

Medium	Oxidant	Reaction conditions	Studies reported in the literature
Alkaline	O_2 NaOCl $KMNO_4$ CuO Eletro-chemical	20-320 °C / 1-61 atm 20-70 °C Ambient-105 °C 100-200 °C 25-90 °C	[1][19][22][25][28][32]-[34] [23][35]-[39] [40][41] [9] [42]
Acid	H_2O_2 HNO_3 $K_2Cr_2O_7$ O_2 $Na_2S_2O_8$ Photochemical Eletro-chemical	20-80 25-300 °C 100-109.5 °C 140-190°C/10-49 atm 60 °C/atm ambient 40-60 °C	[21][27][35][23][43]-[51] [9][46][50][52]-[54] [9][55] [56] [35] [9] [57]
"Neutral"	$Na_2Cr_2O_7$ O_3	250 °C 20-60 °C	[9][58] [51][59][60]

Temperature

Temperature plays a significant role in the oxidation of coal. During storage of coal piles, it can lead to spontaneous combustion. This hazard is a result of an imbalance between the heat generated by oxidation and the heat dissipated over the same period. If the rate of heat production through oxidation is greater than the rate of heat dissipation, a buildup of temperature will occur within the stockpile, leading to spontaneous combustion [6]. This phenomenon is complex and is influenced by multiple factors, including the intrinsic properties of the coal, the physical structure of the stockpile, and external environmental conditions.

The particle size and porosity of the coal pile are crucial factors that determine the likelihood of spontaneous combustion. Previous studies have demonstrated that the initial temperature required for spontaneous combustion decreases as the coal particle size decreases. Additionally, a decrease in coal rank also results in a decrease in the initial temperature required for spontaneous combustion, for coal with the same particle size [61].

While it is true that oxidation with air and oxygen at higher temperatures can accelerate the process, the extent of acceleration can vary depending on various factors such as reaction time, coal particle size and others. For instance, it has been reported that the oxidation rate of coal particles passing through a 6.4 mm sieve in an oxidative environment increased by approximately 1.7 times for every 10 °C rise in temperature within a range of 30 °C to 99.3 °C over the course of one week. [62]. There are important quantitative differences depending on the oxidation temperature for otherwise comparable experimental conditions. *Berkowitz* [5] noted that below 70°C, the oxidation rate is generally low, independent of coal rank, and mainly results in the formation of acids and peroxides. In the temperature range of 70-150°C, the oxidation rate is more dependent on coal porosity, and it tends to decrease with increasing rank or particle size. This indicates that the oxidation becomes transport limited instead of kinetically limited. Above 150°C, the generation of humic acids is accelerated, and acid degradation is less commonly observed up to 250°C.

Many of the experiments to obtain and identify water soluble acids and water insoluble acids with air and oxygen have been performed at the highest possible temperatures (220-260°C) to avoid acids degradation; some examples are [19][22][28][34]. *Hayatsu* [9] oxidized coal with oxygen in an aqueous alkaline medium and concluded that the most suitable temperature for the generation of water soluble acids appeared to be 260-270°C, where the yield was about 50-60 wt% of the original coal over a period of 1-2 hours and air pressure of 4.6-8 MPa. Nevertheless, Experiments conducted at mild conditions with temperatures in a range from 25-110 °C [1][32][33] confirmed the generation of water-soluble acids. Improvement in production and extraction when temperature increased at constant reaction time at those specific conditions were also confirmed [32][33].

Effect of temperature has also been studied for different oxidants more than oxygen at mild conditions. Most experiments were performed with hydrogen peroxide (H_2O_2) [47]-[49][51] at a range of temperatures from 20 to 80°C, also changing other parameters such as concentration and time. With nitric acid [52], the maximum yield of soluble acids was at the range of 170-185 °C in a 4-8 hour reaction time. Even though there is an interdependency with other variables such as the oxidant concentration, the temperature is one of the most important variables affecting products yields and properties.

Time

Reaction time have been studied at different conditions including temperature and oxidant availability to mainly evaluate the impact in oxidation conversion and products yield. At mild conditions, atmospheric oxygen oxidation in alkaline medium with 0.5N Na_2CO_3 and 85 °C yielded 70 % or more after 6 hours was reported [32]. With 6.4 atm of oxygen partial pressure, 1.16N NaOH, and 110 °C for the first 10 hours, the production rate of humic acids increased by a factor of 5; and after 10 hours, it remained constant [33]. At high temperatures (220-260°C) and 40-60 atm of oxygen partial pressure in an alkaline medium with approximately 0.69N of NaOH [19] most benzene polycarboxylic acids from lignite reached their maximum yield at 30 minutes.

In oxidative experiments with 3mol/L H_2O_2 at 60 °C [49], oxidation time was performed every hour within the range of 1 to 5, inclusive. The highest conversion rate of subbituminous coal which

was about 52 % did not exceed 4 hours. In catalytic oxidation of lignite with aqueous 1.5 wt% $H_5PV_2Mo_{10}O_{40}/H_2SO_4$ at 170 °C [56], the yield of carboxylic acids reaches the maximum in 1 hour. In an additional study where different ranks of coal were studied at 1N HNO_3, low-rank coal oxidized faster to obtain maximum yields of acids at a shorter time at constant temperature [24].

pH of the aqueous phase

Liquid oxidation of coal by oxygen has been studied in different mediums, and alkaline solution oxidation is the widely used method [56]. Thus, since years ago, the most relevant results have been obtained in this media [7]. It seems that the importance of alkali involves, on the one hand, the increased ionization of hydroxyl groups and, on the other hand, the protection of intermediates and products by neutralizing the formed carboxylic. In this way, intermediate products are kept in the water and away from the coal surface. Nevertheless, an excess amount of alkali in the oxidation system decreases oxygen solubility in water due to stronger ionic strength slowing down oxidation due to a lower oxygen concentration in water. Additionally, the system becomes adverse to the oxidation because it results in the salting out effect [19].

The phenomenon of the salting out effect can lead to the formation of a protective coating around the coal particles, thereby limiting their accessibility to the oxidizing agents and products removal. When alkali salts are formed into the water-coal slurry, they can interact with the coal particles and form a layer of precipitated around them. This layer can act as a barrier that slows down the penetration of the oxidizing agents into the coal, reducing the rate of oxidation.

The effect of alkali in coal oxidation and products yield has been studied under different conditions, at low pressure (1 atm) and temperature (92°C). With NaOH 0-0.5N concentrations range, the rate reaction and production of water soluble acids were favored. But at higher concentrations of alkali, there was a dramatic decrease in rate reaction attributed to a reduction of product removal from the coal surface owing to a salting-out effect [33].

In more extreme conditions, with temperatures rage (240-320°C) and pressure (49 atm), where the target products were benzene polycarboxylic acids (BPCAs), the results showed that, yield of coal

on a moisture, ash-free basis to benzene polycarboxylic acids was very low without alkali. The maximum yield at constant time was obtained at an alkali/coal mass ratio of 3. As the alkali/coal mass ratio was increased, the reaction time was longer to obtain the same yields due to passivation and the salting out effect [19][34].

An inherent challenge with the evaluation of the impact of pH is that oxidation products that are trapped in the organic phase (coal) and that are not dissolved in the aqueous phase, are not detected as converted products. It is an analytical limitation due to the complexity of the system. It is therefore difficult to decouple observations about pH from the impact of mass transport and product solubility in the aqueous medium.

Water-to-coal ratio

Unlike other parameters that have been widely investigated at different conditions, direct influence of water/coal ratio in oxidative reaction chemistry, reaction engineering and inorganic mater dissolution in the liquid phase have been explored to a limited extend. Nevertheless, it is important to mention an experiment with H_2O_2 30 % wt. as the oxidant at 60 °C under atmospheric pressure performed for 24h. In that study, water-to-coal ratio was changed from 5/1 to 20/1, and the findings indicated that at a higher water-to-coal ratio, oxidation rate and thus yield of organic acids increased. However, conversion to release CO_2 also increased [44].

Oxygen availability

Oxygen, compared with other oxidants for oxidative coal dissolution, is inexpensive and easy to obtain [56]. Coal's ability to absorb oxygen varies with rank: low absorption for anthracite and high absorption for subbituminous and lignite. Oxygen absorption is also higher for those coals with high moisture capacity [49].

The influence of oxygen concentration on coal oxidation differs from the temperature effect as it appears to not alter the selectivity of products; Moreover, the oxygen concentration is primarily responsible for changes in reaction rate [19]. As indicated by Henry's law, which states that high oxygen pressure results in a high oxygen concentration in water. Consequently, insufficient

oxygen concentration may result in underoxidation, while excessive concentration may cause overoxidation. The oxidation mechanism of coal, which is based on the formation of free radicals, is also influenced by the concentration of oxygen, as the ability of these radicals to bond with each other or with oxygen molecules is determined by the concentration. Therefore, the oxidation process of coal is influenced, to some extent, by the concentration of oxygen [19].

Siddiquee et al. [63] applied liquid phase oxidation of hydrocarbons with oxygen in microfluidic reactors, demonstrating that the availability of oxygen after hydrogen abstraction from an aliphatic carbon can be shown to change the probability of ketone, alcohol, or addition product formation. In their experiments, ketone selectivity increased when increasing oxygen availability, and selectivity to alcohol and addition product increased at lower oxygen availability.

At mild conditions, it has been reported that the oxidation of coal was a first order reaction with respect to oxygen initial concentration in an aqueous solution [64] and an aqueous alkaline media with NaOH [33]. For high initial pressure conditions, the conversion of low rank coals and yield of products increased with pressure and reaches a maximum before they start decreasing [19][56].

Coal particle size

Wang et al. [65] characterized the low-temperature weathering of coal with air as a complex process involving multiple phenomena. Initially, convective mass transfer facilitates oxygen diffusion to the external surface of coal particles, where it diffuses through a surrounding film. Concurrently, diffusive mass transfer takes place within coal pores. Second, chemical reactions occur between the oxygen and coal, resulting in the generation of reaction products, the release of heat, and the emission of byproducts. An illustration of the process is shown in Figure 2-8.

According to the process described above, coal oxidation takes place at the external surface of coal particles and the internal surface of coal pores. The external surface is correlated with the diameter of coal particles. In contrast, the internal surface depends on coal porosity [65]. Hence, the reaction rate is expected to rely on the particle diameter for high-rank coal with minimal or no internal pore

structure. While for highly porous coal with no mass-flow limitations, the reaction rate is likely to be independent of particle size [66].
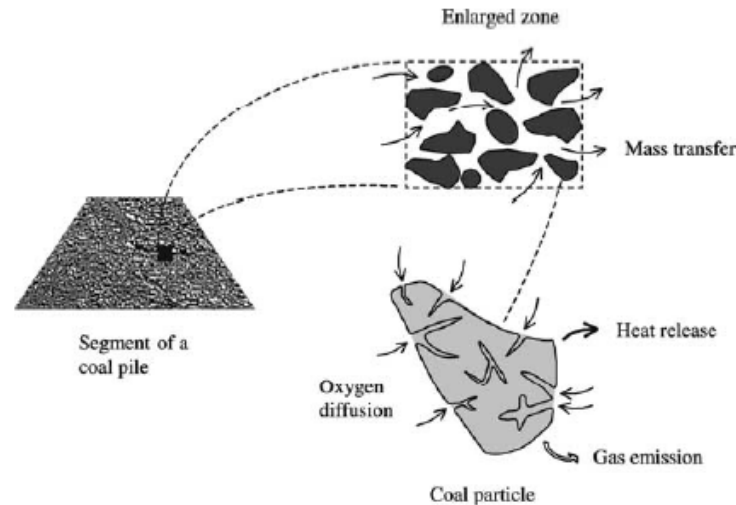
Figure 2-8 Fundamental phenomena in coal oxidation process [65]

There have been several studies of the effect of particle size on the oxidation rate; some experiments found that oxidation rates depended on particle size, increasing with a decrease in particle diameter. *Kapo and Calvert* [33] investigated the impact of coal oxidation with oxygen as the oxidant in aqueous NaOH. The study, varied particle sizes of coal, including particles that passed through mesh sizes 2 to 3 (>6.7 mm), 20 on 28 (>0.6 mm), and 80 on 100 (>0.15 mm). Their results showed that the reaction rate varied by a factor of 13, while the external area changed by a factor of 71, and the macropore area was only slightly affected with a factor of 1.07. *Itay et al.* [67] oxidized coal particle sizes ranging from 0.7-0.04 mm and air as the oxidant, with temperatures ranging from 25-140 °C. Their results demonstrated that the reactivity of the finer coal particles was significantly higher than that of the coarser materials. *Akgün and Arisoy* [68] also observed similar findings when studying coal oxidation with air at temperatures between 25-75 °C using coal particles ranging from 2-50 mm, indicating that the effect of coal oxidation is dependent on the particle size.

In contrast, *Kaji et al.* [69] conducted a study on coal oxidation with oxygen using coal particles ranging from 0.074-1.0 mm and temperatures ranging from 30-250°C. Their findings revealed that

there was no discernible effect of particle size on the rates of CO_2 and CO formation, indicating that particle sizes below 1.0 mm did not significantly impact the oxidation rate.

An analogous description can be derived for coal-water slurries, where the oxygen is dissolved in the aqueous phase and it is oxygen diffusion in the aqueous phase to the coal surface that is the transport process affecting the rate and extend of coal oxidation. The rate of oxygen transport is influenced by several factors, including the oxygen concentration in the aqueous phase, the temperature of the system, and the size and shape of the coal particles.

The particle size of coal has a significant impact on the transfer to dissolve oxygen in coal-water slurry to the coal. Smaller coal particle sizes lead to increased oxygen transport to the coal due to the larger surface area available. Conversely, larger coal particle sizes result in reduced oxygen transport due to the smaller surface area exposed. However, small particle sizes can also lead to increased viscosity and more challenging handling and transportation of coal-water slurries, since rheological behavior of coal-water mixtures is largely dependent on solids concentration, particulate size and particle size distribution [70].

In the production of coal-water slurry for hydrotransportation, the maximum permissible particle size is approximately 0.3 mm. Larger particles may cause pipeline blockage due to excessive settling [71]. Conversely, very fine particles (<53 μm) can significantly increase the dynamic viscosity of the slurry. Particle size distribution optimization is necessary based on coal type to minimize the dynamic viscosity of the slurry [72]. *Sing et al.* [71] studied coal-water slurries with coal concentrations ranging from 10-60 wt% and evaluated apparent viscosity, head loss, and specific enthalpy consumption through a 100 mm diameter pipeline. They found that the optimal coal particle size distribution for high stability had a greater proportion of particles between 0.1 mm to 0.05 mm. Therefore, it is essential to optimize coal particle size distribution to balance the competing demands of oxygen solubility, viscosity, and handling characteristics of coal-water slurries.

2.4 Products of Coal Oxidation

Even though the structure of all humic substances is still largely unknown, including those that are a product of the oxidative coal solutions, their major functional groups include carboxylic, phenolic, carbonyl, hydroxyl, amine, and aliphatic fractions, among others [73]. However, it is well known that final products of low-rank coals oxidation are characterized mainly by carbon dioxide, aliphatic acids, and aromatic carboxylic acid of lower molecular weight [7]. Even though this project works with oxygen as the oxidant, products obtained by different oxidants are generally similar qualitatively but differ quantitatively [24]. Thus, a review focused mainly on oxygen as the oxidant and identifying products with other oxidants, according to the different functional groups, is given in the following subsections.

2.4.1 Carboxylic Acids

Carboxylic acids are considered the main product in the oxidative coal dissolution (OCD) process. Figure 2-9 and Figure 2-10 show carboxylic acids identified and/or obtained in different OCD processes. Oxalic and mellitic acid were the first acids identified in OCD with alkaline permanganate in 1871. At 70 °C with the same oxidant, were identified oxalic, acetic and benzenoid acids. The latter with the best yield for low-rank coal(lignin) is 22-34 % [6]. In succeeding investigations with brown coals, up to 28 acids were identified [40].
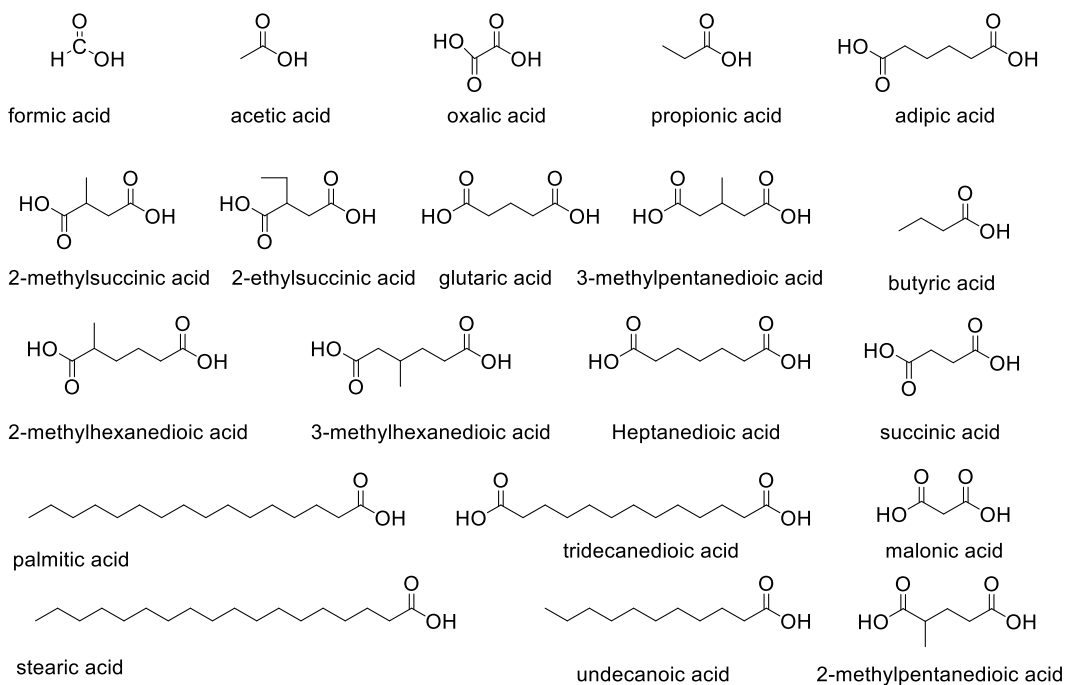
Figure 2-9 Aliphatic Carboxylic acids identified in OCD processes [32][39][40][49]
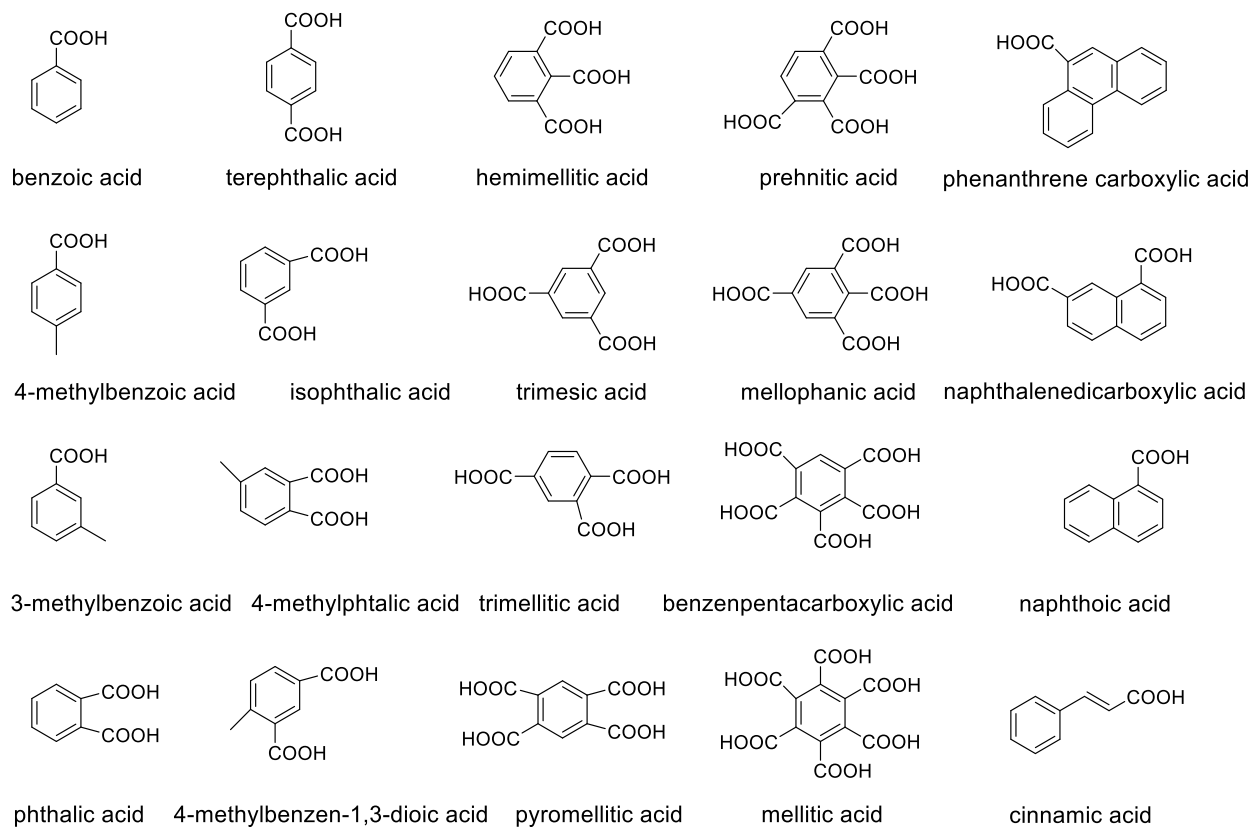
Figure 2-10 Aromatic Carboxylic acids identified in OCD processes [9][19][39][40][49][74]

From oxygen (O_2) oxidation, the products of OCD were reported in 1919-1920 and were obtained in alkali media. Some of the products identified included benzene carboxylic acids and aliphatic acids such as formic, acetic, oxalic and butyric [6][13]. Since then, and depending on the type of coal and operative conditions, various carboxylic acids at different yields have been identified and isolated. *Howard and Roy* [75], isolated trimetallic, pyrometillic, o-phthalic, isophthalic, prehnitic and benzenepentacarboxylic acid from OCD of a bituminous coal in alkali media, after oxidation using gaseous O_2 at 270 °C and about 61 atm. *Kapo and Calvert* [33] included benzenoid, oxalic and acetic acids as part of the organic acids obtained from different coals at mild conditions (60-100°C). Furthermore, *Matsuo et al.* [32] oxidized low-rank coals at 20-85 °C using 0.5N Na_2CO_3 as the aqueous solution. After extraction, 80-90 wt% yields daf were reached, with oxalic, formic, acetic, and malonic acids and carbon dioxide as the main products.

More recently, studies focused on the oxidation of lignite in alkaline medium at 220-320 °C and 40-60 atm [19][28][34], and acid medium at 140-190 °C and 10-49 atm [56] with O_2, to produce benzene polycarboxylic acids (benzoic, isophthalic, phthalic, metallic, trimetillic, pyromellitic, trimesic, hemimellitic, mellophanic, prehnitic, benxene pentacarboxilic and terephthalic acid), and aliphatic Acids (formic, acetic, succinic, malonic and oxalic acids). In those studies, operating variables were changed, and results indicated the best yield of benzene polycarboxylic acids is about 20 % and carboxylic acids 57 %.

OCD of bituminous and subbituminous coals with NaOCl at mild conditions has produced a considerable number of aliphatic acids (AAs) and benzene polycarboxylic acids (BPCAs) [23][36]-[39]. In the seventies, *Chakrabartty and Krestchemer* [36][37] isolated acetic, propionic, succinic, glutaric, adipic acids, contributing about 10-15 % to the total yield of acids. They also identified some benzene polycarboxylic acids (hexacarboxyl benzene, pentacarboxyl benzene, tetracarboxy1 benzene, tricarboxyl benzene and phthalic acids) with 75-80 % of the yield of the acid. Reaction conditions were 60-70 °C with 1.6N of NaOCl and initial pH of 12. In 2012, *Gong et al.* [39] oxidized two coals, also identified as bituminous and subbituminous, at an even lower temperature of 30 °C for 24 hours. They detected 26 aliphatic acids and 16 benzene polycarboxylic acids, including all previously mentioned with O_2 and NaOCl as the oxidants, except for acetic

acid. In addition, benzene polycarboxylic acid's relative content was also the highest for both coals, with an average extraction fractions of 61.2 % and 60.6 %, respectively.

The oxidant with more experiments reported in the literature about OCD apart from O_2, is H_2O_2. In terms of products after oxidations, in 1978, *Hayatsu et al.* [9] oxidized lignite and bituminous coal with H_2O_2 in acetic acid at 40-60 °C. The conversion of coal on a moisture, ash-free basis to water soluble products was up to 80 % for lignite coal. The major products divided as benzenecarboxylic acids 44 %, furan carboxylic acids 16 % and dibasic aliphatic acids 18 %. In oxidation with H_2O_2 in trifluoroacetic acid, benzenecarboxylic acids yield increased to 59 %, aliphatic acids kept almost constant 18 %, and there were identified phenol acids 4 %. *Miura et al.* [27][44] oxidized low-rank coals with 30 % H_2O_2 for 24 hours at 60 °C, resulting in a 60-70 % conversion determined by carbon balance analysis of the coal feed and products. The number of aliphatic acids such as oxalic, acetic, formic, acetic, glycolic and malonic acid increased to almost about half of the extract products identified. Subsequent studies with a lower concentration of H_2O_2 (5 %) at 40°C, did not detect benzene polycarboxylic acids and the predominant products were malonic and succinic acid [21]. Studies with subbituminous coals also identified about 30 carboxylic acid compounds [47][49], where benzene carboxylic acids are the majority, specially terephthalic and isophthalic acid [49].

Oxidation with HNO_3 has also generated a great variety of acids with different kinds of coals and at different operating conditions [6][9]. Most of the products are qualitatively similar to the products already mentioned with previous oxidants. Other methods that obtained acids as products were:

- Ozonization of humic acids derivated from oxidized bituminous coal. It was conducted for a 48 hours and led to the most substantial production of oxalic and carbonic acids, with peak yields observed after 24 hours of treatment. These two acids accounted for approximately 65 % of the initial carbon content of the coal sample, determined by carbon balance analysis of the coal feed and products [59]

- Photochemical oxidation, which was conducted on lignite and bituminous coal in a 10 % HCl aqueous solution under ultraviolet light irradiation for 8 days, with either pure oxygen

or oxygen in air as the oxidizing agent. This process resulted in product yields of 25-30 % [9], albeit without a detailed description of the yield calculation methodology

- Aqueous $Na_2Cr_2O_7$ oxidation at 250 °C for 40-72 hours with 50 to 59 % of coal yield on a moisture, ash-free basis to water soluble organic acids, humic acid-like materials and carbon dioxide. Aromatic carboxylic acids with higher molecular weight were extracted [9]

- Oxidation with performic acid as the oxidant, between ambient temperature and 50 °C for 24 hours. Yield of coal determined by carbon balance analysis of the coal feed and products was between 78 and 87 % and in 14 different types of coals cinnamic acid was always identified in the reaction products [74]

2.4.2   Alcohols and Phenols

Hydroxyl groups which are already present in coal, are predominantly phenolic, and decreases in abundance when coal rank increases. Low rank coals with 67 % carbon, have about 12 % hydroxyl and falls to almost zero after coalification to 90 % carbon [6]. Apart from that, coal degradation of aromatics, as well as nonaromatic structures through OCD, includes a step of phenols formation in its reaction mechanism (see Figure 2-6) [5]; therefore, it is common to find alcohols and phenols as a product of coal oxidation.

Phenolic acids have been found from oxidation of lignin with alkaline cupric oxide; lignite and bituminous coals with hydrogen peroxide in acetic acid (counting up to 22 % of the fraction of the product in lignite coals); high volatile bituminous coals with HNO_3, lignite and bituminous coals in aqueous $Na_2Cr_2O_7$; degradation of humic acid extracted from lignite with $KMnO_4$; and photochemical oxidation. It was also concluded that Lower rank coals gave higher yields of phenolic acids [9]. Furthermore, *Miura et al.* [27] reached about 8 % of methanol yield from low-rank coals conversion with 30 % H_2O_2 in 24 hours. Last, *Raj* [74] oxidized different types of coals with performic acid to study chemical parameters of coal. As a result, various phenols and phenolic acids where identified. Alcohol and phenol compounds identified in OCD processes are shown in Figure 2-11.
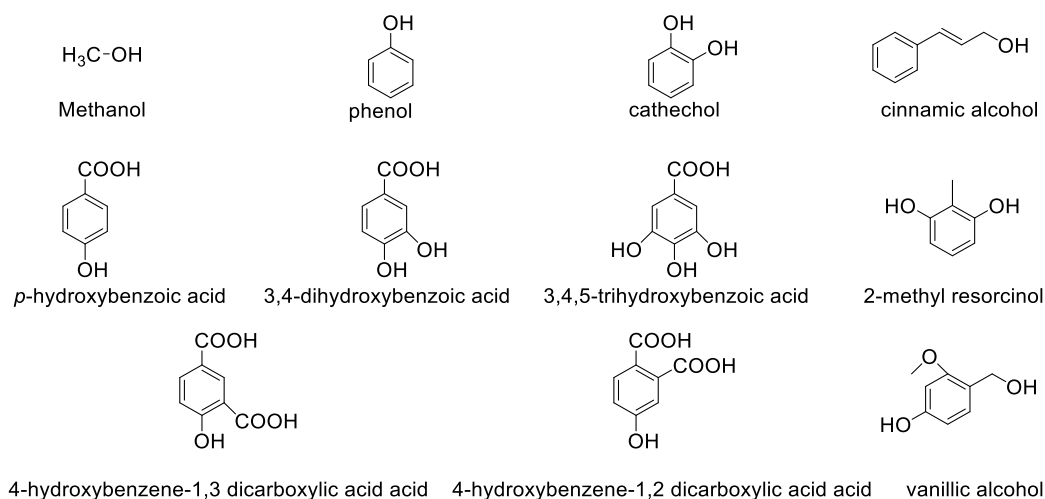
Figure 2-11 Alcohol and phenols identified in OCD processes [9][74]

2.4.3   Aldehydes and Ketones

Carbonyl groups are also part of the coal structure. In coals, with 83 % carbon oxygenates, identified as quinone carbonyl, correspond to 2.5-4.0 % of carbonyl oxygen [6]. Additionally, oxidation of coal includes some of the degradation steps of aromatic rings to quinone structures [5][6] and the formation of carbonyl groups as aldehydes or ketones [31].

Although most of the products with higher yield and commercial value in OCD are carboxylic acids, aldehydes and ketones have been identified in most of the cases as minor products. Oxidation in aqueous NaOCl solution [39], performic acid [74]; KMNO$_4$; alkaline nitrobenzene, and O$_2$ in alkaline medium [9]; are some of the experiments where products with aldehyde or ketone groups were identified. Figure 2-12 presents some of the aldehyde and ketone compounds identified in OCD processes.
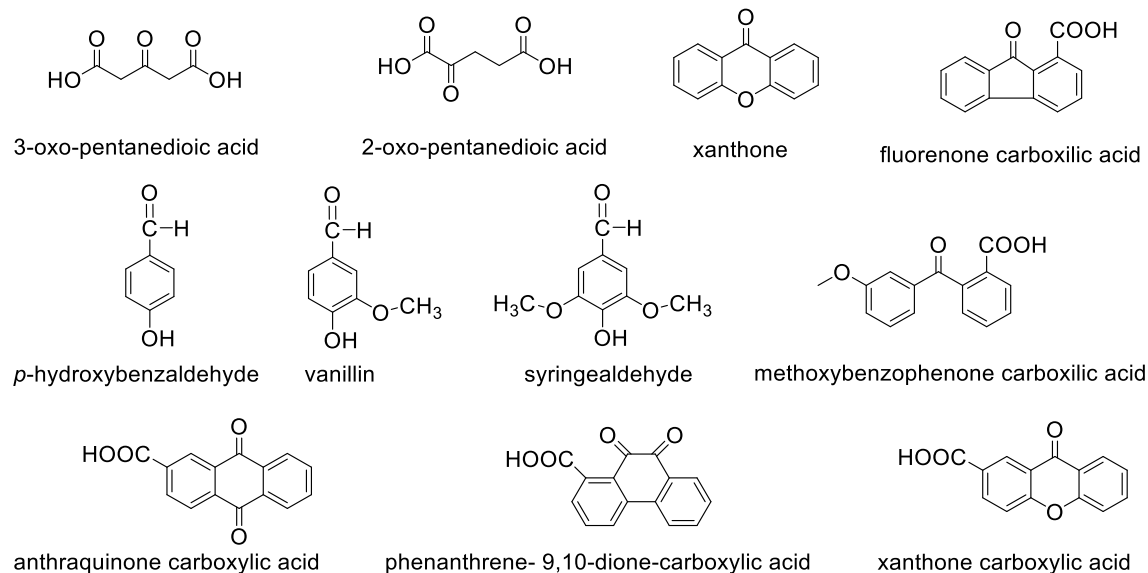
Figure 2-12 Aldehydes and ketones identified in OCD processes [9][39][74]

2.4.4 Ethers and Esters

Unlike alcohol, phenol, and carboxyl groups, of which the distribution changes depending on the coal rank, ether and ester groups keep constant based on oxygen percentage in the coal with about 20 % each [76]. Apart from that, in OCD processes, esters and anhydride groups are formed as intermediates or when carboxyl radicals are combined with alkane and carboxylic acid radicals [5][31]. Specifically, 6-dibenzopyrone was suggested as a possible intermediate in O_2 alkaline oxidation of bituminous coal [6].

Still the yield of ether and ester groups as products are very low, some ethers identified after OCD of bituminous coal at mild condition are dibenzofuran, benzonaphthofuran, and dibenzo-*p*-dioxin [24] . Less than 0.9 % of Ethyl-2,2-dimethyl-5oxo-heptanoate was detected in H_2O_2 oxidation products [49]. Aqueous $Na_2Cr_2O_7$ oxidation of lignite and bituminous coal resulted in a product within which dibenzofuran carboxylic acids where identified. Finally, some additional products were identified in the oxidation products of bituminous coals at higher temperatures 250-300 °C with HNO_3 and O_2 in alkali (xanthene, naphthofuran carboxylic acid) [9]. Some of the ether and esters compounds identified in OCD processes are shown in Figure 2-13.

37
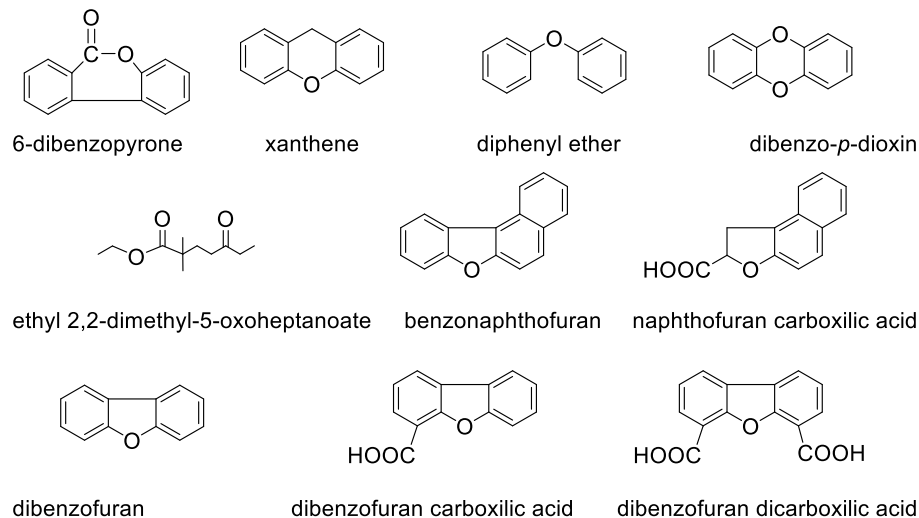
Figure 2-13 Ethers and esters identified in OCD processes [6][9][49][24]

2.4.5 Sulfur and Nitrogen Compounds

Sulfur content in coal normally varies from 0.3 to 6.0 wt% depending on the type of coal as it is described in Table 2-2. However, there are specific coals with much higher sulfur content than the typical with a correspondingly low oxygen content, particularly those located in Yugoslavia, Pakistan, some parts of Australia and India [4]. As a consequence, amounts of sulfur of up to 11 wt% have been registered [16]. Organic sulfur compounds in coal is about 50-70 % of total sulfur, and are distributed uniformly throughout the coal, the reminder being due to sulfur-containing minerals, such as iron pyrite. They occur in mercaptans, sulfides, and thiophenes, the latter always predominating over the others [6][77].

During oxidative coal dissolution, thiols, thioethers, and thiophenes present in the coal can be oxidized to their corresponding sulfoxides or sulfones, depending on the extent of oxidation. Thiols (R-SH) can be oxidized to disulfides (R-S-S-R), which can then be further oxidized to sulfoxides (R-S(O)-S-R) and sulfones (R-S(O)$_2$-S-R) in the presence of strong oxidizing agents. Thioethers (R-S-R') can also be oxidized to sulfoxides (R-S(O)-S-R') and sulfones (R-S(O)$_2$-S-R') in a similar manner.

Thiophenes (R-C$_4$H$_3$S) can undergo various types of oxidation reactions depending on the conditions used. In the presence of mild oxidizing agents such as air or oxygen, thiophenes can be

38

oxidized to the corresponding sulfoxides and sulfones. However, in the presence of strong oxidizing agents such as hydrogen peroxide or potassium permanganate, thiophenes can undergo ring-opening reactions and form carboxylic acids, ketones, and other oxygen-containing compounds.

Oxidative coal dissolution with oxygen at mild conditions has been studied for heteroatom removal of coal, with positive evidence mainly for desulfurization where thiophenes can be oxidized to sulfones improving the quality of residue product [1][25]. Some of the sulfur products associated with OCD are N,4-dimethylbenzenesulfonamide from H_2O_2 oxidations and which had a relative content of 22 % of the total converted products [49] and, dibenzothiophene carboxylic acid from aqueous $Na_2Cr_2O_7$ oxidation of lignite coal [9].

Nitrogen content in coal can be up to 2.5 wt% depending on the type of coal as it is described in Table 2-2. Nitrogen compounds in coals are primarily in cyclic structures such as pyridines and pyrroles, and small amounts of nitrogen-containing side chains could be in the form of amines and amides [1][6][77].

In oxidative coal dissolution, when amines, pyrroles, and pyridines are oxidized, the reactions can lead to the formation of a variety of carbon-centered oxygenated functional groups on the coal structure, such as carbonyl, carboxyl, and quinone groups. Amines can be oxidized to their corresponding oxides. For example, the oxidation of ethylamine can lead to the formation of ethylamine N-oxide. Pyrrole can be oxidized to pyrrole-2-carboxylic acid. Pyridine can be oxidized to pyridine N-oxide or pyridine N,N-dioxide.

It was possible to identify small amounts of pyridine derivatives oxidizing different coals with an aqueous solution of $Na_2Cr_2O_7$ at 250 °C (4-aminopyridine-3- carboxylic acid) [58]. At mild conditions, carboxylic acids benzene polycarboxylic acids as well as toluene carboxylic acids with some nitro groups were isolated and identified from: NaOCl (4-nitro-*o*-phthalic-carboxylic, 4-nitro-1,2,3-benzene-tricarboxylic, nitrobenzene-tetracarboxylic, and nitrobenzene-pentacarboxylic acids) [36]-[38]; HNO_3 (aniline, nitrobenzene-dicarboxylic, nitrobenzene-tricarboxylic, and nitrobenzene-tetracarboxylic acids, alkyl-pyridines, alkyl-quinolines and

39

benzoquinolines) and Na$_2$Cr$_2$O$_7$ (pyridine-tricarboxylic acid and pyridine-tricarboxylic acid) [9]. Additionally, by photochemical oxidation with either pure oxygen or oxygen in air as the oxidizing agent, substituted pyridines such as pyridine carboxylic acids, quinoline, and carbazoles were identified [9][24]. Figure 2-14 shows some of the sulfur and nitrogen compounds identified in OCD processes.

dibenzothiophene carboxilic acid   aniline   4-aminopyridine-3- carboxylic acid

4-nitro-o-phthalic-carboxylic acid   nitrobenzene-tetracarboxylic acid   N,4-dimethylbenzenesulfonamide

4-nitro-1,2,3-benzene-tricarboxylic acid   nitrobenzene-pentacarboxylic acid
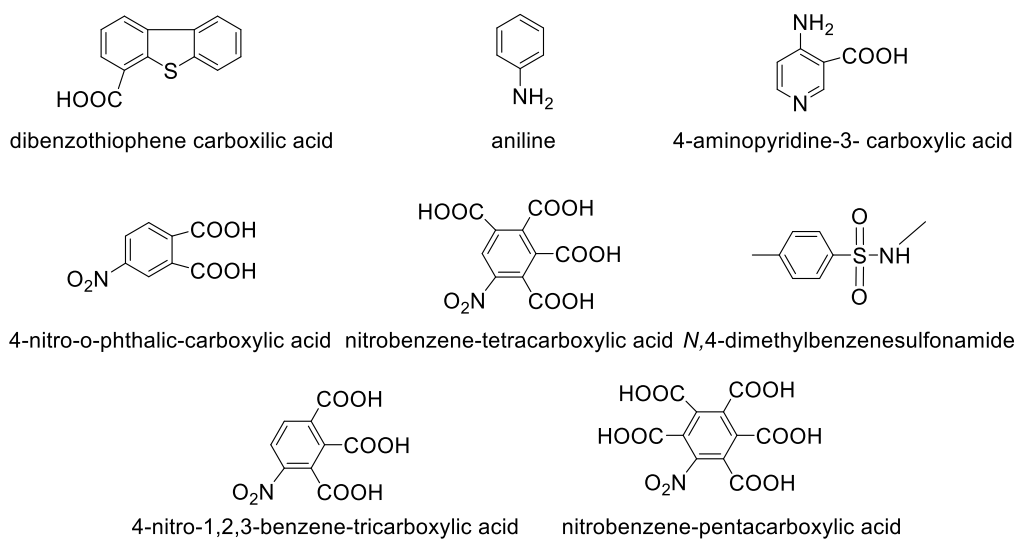
Figure 2-14 Sulfur and nitrogen compounds identified in OCD processes [9][49][58]

2.5   Conclusions

- The selection of an oxidant in oxidative coal dissolution appears to have little effect on the chemical products that result from the reaction. As a result, multiple oxidants that are frequently utilized in oxidative coal dissolution create the same types of chemical reactions. This suggests that the overall mechanism of oxidative coal dissolution may be comparable irrespective of the particular oxidant selected. However, the choice of oxidant can have an impact on the engineering and reaction rate of the process. It can also impact the materials and equipment used in the reaction. As a result, the decision to utilize air as an oxidant in this thesis can draw on the broader oxidation literature for interpretation. This indicates that air may be an acceptable oxidant for oxidative coal dissolution processes since it produces similar effects on the resulting products when compared to other oxidants. However, the particular conditions

and uses of the process should be taken into consideration since alternative oxidants may be more suitable for different scenarios.

- Oxidative coal dissolution is a complex chemical process that involves the reaction of coal with an oxidant in the presence of water. The products of the reaction can vary depending on the specific conditions and oxidant used, but typically include CO_2, CO, H_2O, and various oxygen-containing compounds such as carboxylic acids and alcohols. The specific mechanism of the process may vary depending on the specific conditions and oxidant used, but typically involves the attack of oxygen-containing species on the coal surface, followed by the release of various small molecules and the formation of oxygen-containing functional groups. Despite the complexity of the chemistry, several studies described in this literature review have shown that oxidative coal dissolution can lead to the depolymerization and dissolution of coal, making it a potentially useful for coal upgrading and utilization.

- The yields and selectivities of oxidative coal dissolution can vary depending on the specific conditions and oxidant used. However, several studies have reported promising results in terms of the production of carboxylic acids with a coal conversion on a moisture, ash-free basis to water soluble organic acids of up to 80 %. These results suggest that oxidative coal dissolution can be an effective method for the selective production of these classes of compounds. In addition, various studies discussed in this review have reported the production of other classes of compounds such as ketones, phenols, and esters, with selectivities that can also vary depending on the specific conditions and oxidant used. Overall, the selectivity of oxidative coal dissolution towards different compound classes changes by adjusting the reaction conditions such as the temperature, time, coal/water ratio, coal particular size and oxidant concentration.

- Despite the considerable number of investigations on aqueous oxidation of coal using oxygen in air or pure oxygen as the oxidant, and the potential advantages of oxidative coal dissolution in an alkaline medium, which include the enhanced solubilization of coal and coal oxidation products in water, research on oxidative coal dissolution in a neutral medium is limited to a few oxidants other than oxygen such are sodium dichromate and ozone. Moreover, to date,

there are no yield or selectivity references available for neutral medium oxidation conditions using air as the oxidant. Therefore, further investigations are needed to elucidate the effects of neutral medium oxidation conditions using air as the oxidant, in order to broaden our understanding of oxidative coal dissolution and potentially develop more efficient coal conversion technologies.

- The use of air as an oxidant in oxidative coal dissolution is often preferred due to economic considerations. However, the literature on the evaluation of operating parameters in aqueous oxidation of coal in relation to both economic and environmental considerations is limited. While there have been significant efforts to understand the chemistry of oxidative coal dissolution, there has been comparatively little research into the broader economic and environmental implications of this technology.

2.6   References

[1]   Siddiquee, M. N.; De Klerk, A. Heteroatom removal as pretreatment of boiler fuels. *Energy Fuels* **2019**, *33*, 5790-5801.

[2]   Davidson, R. M. Molecular structure of coal. In *Coal science Vol. 1*; Gorbaty, M. L., Larsen, J. W., Wender, I. eds.; Academic Press: Orlando, 1982, pp.83-160.

[3]   Dryden, I. G. C. Chemical constitution and reactions of coal. In *Chemistry of coal utilization, Supplementary Volume*; Lowry, H. H. ed.; Wiley: New York, 1963, pp. 232-295.

[4]   Stach, E. The microlithotypes of coal and their strength. In *Coal Petrology third revised and enlarged edition*; Stach, E., Mackowsky, M.-TH., Teichmüller, M., Taylor, G. H., Chandra, D., Teichmüller, R. eds.; Gebrüder Borntraeger: Berlin, 1982, p140-150.

[5]   Berkowitz, N. *An introduction to coal technology*; Academic Press: New York,1979.

[6]   Van Krevelen, D. W. *Coal. Typology-Physics-Chemistry-Constitution*, 3rd ed.; Elsevier: Amsterdam, 1993.

[7]   Howard, H. C. Chemical constitution of coal: as determined by oxidation reactions. In *Chemistry of coal utilization. Vol.1*; Lowry, H. H. ed; Wiley: New York, 1945, pp.346-376.

[8]   Hatcher, P. G.; Clifford, D. J. The organic geochemistry of coal: from plant materials to coal. *Organic Geochemistry* **1996**, *27*, 251-274.

[9]   Hayatsu, R.; Scott, R. G.; Winans, R. E. Oxidation of coal. In *oxidation in organic chemistry. Part D*; Trahanovsky, W. S. ed.; Academic Press: New York, 1982, pp. 279-354.

[10]   Ghani, M. J.; Rajoka, M. I.; Akhtar, K. Investigations in fungal solubilization of coal: mechanisms and significance. *Biotechnology and Bioprocess Engineering* **2015**; *20*, 634-642.

[11]   O'Keefe, J. M. K.; Bechtel, A; Christanis, K.; Dai, S.; DiMichele, W. A.; Eble, C.F.;Esterle, J.S.; Mastalerz, M.; Raymond, A. L.; Valentim, B. V.; Wanger, N. J.; Ward, C. R.; Hower, J. C. On the fundamental difference between coal rank and coal type. *International Journal of Coal Geology* **2013,** *118*, 58-87.

[12]   Riley, J. T. *Routine coal and coke analysis: collection, interpretation, and uses of analytical data*, 2nd ed.; ASTM International: West Conshohocken, 2014.

[13]   Francis, W. *Coal. Its formation and composition*, 2ed.; Edward Arnold: London, 1961.

[14]   Gluskoter, H. J.; Shimp, N. F.; Ruch, R. R. Coal analyses, trace elements, and mineral matter. In *Chemistry of coal utilization, Second Supplementary Volume*; Elliott, M. A. ed; Wiley: New York, 1981, pp. 369-424.

[15]   Speight, J. G. *Handbook of coal analysis. Chemical analysis: A series of monograph on analytical chemistry and its applications. Vol. 182*, 2ed.; Wiley: Hoboken, New Jersey, 2015.

[16]   Speight, J. G. *The chemistry and technology of coal,* 3rd ed.; CRC Press: Boca Raton, 2012.

[17]   Mraw, S. C.; De Neufville, J. P.; Freund, H.; Baset Z.; Gorbaty, M. L.; Wright, F. J. The science of mineral matter in coal. *Coal Science* **1983**, *2*, 1-63.

[18]   Shirazi, A. R.; Börtin, O.; Eklund, L.; Lindqvist, O. The impact of mineral matter in coal on its combustion, and a new approach to the determination of the calorific value of coal *Fuel* **1995**, *74* (2), 247-251.

[19]   Wang, W.; Hou, Y.; Wu, W.; Niu, M.; Liu, W. Production of benzene polycarboxylic acids from lignite by alkali-oxygen oxidation. *Ind. Eng. Chem. Res.* **2012**, *51*, 14994-15003.

[20]   Liu, Z. -X.; Liu, Z. -C.; Zong, Z. -M.; Wei, X.-Y.; Wang, J.; Lee, C. W. GC/MS Analysis of water-soluble products from the mild oxidation of Longkou brown coal with H_2O_2. *Energy & Fuels* **2003**, *17*, 424-426.

[21]   Pan, C.-X.; Wei, X.-Y.; Shui, H.-F.; Wang, Z.-C.; Gao, J.; Wei, C.; Cao, X.-Z.; Zong, Z.-M. Investigation on the macromolecular network structure of Xianfeng lignite by a new two-step depolymerization. *Fuel* **2013**, *109*, 49-53.

[22]   Stock, L. M.; Obeng, M. Oxidation and decarboxylation. A reaction sequence for the study of aromatic structural elements in Pocahontas No. 3 coal. *Energy Fuels* **1997**, *11*, 987-997.

[23]   Liu, F. J.; Wei, X.-Y.; Zhu, Y.; Gui, J.; Wang, Y.-G.; Fan, X.; Zhao, Y.-P.; Zong, Z.-M.; Zhao, W. Investigation on structural features of Shengli lignite through oxidation under mild conditions. *Fuel* **2013**, *109*, 316-324.

[24]   Wender, I.; Heredy, L. A.; Neuworth, M. B.; Dryden, I. G. C. Chemical reactions and the constitution of coal. In *Chemistry of coal utilization, Second Supplementary Volume*; Elliott, M. A. ed; Wiley: New York, 1981, pp. 425-521.

[25]   Liu, K.; Yang, J.; Jia, J.; Wang, Y. Desulphurization of coal via low temperature atmospheric alkaline oxidation. *Chemosphere* **2008**, *71*, 183-188.

[26]   Liu, F. J; Wei, X. Y.; Fan, M.; Zong, Z. M. Separation and structural characterization of the value-added chemicals from mild degradation of lignites: a review. *Applied Energy* **2016**, *170*, 415-436.

[27]   Miura, K.; Mae, K.; Okutsu, H.; Mizutani, N. New oxidative degradation method for producing fatty acids in high yields and high selectivity from low-rank coals. *Energy Fuels* **1996**, *10*, 1996-1201.

[28]   Wang, W.; Hou Y.; Wu W.; Niu M. Simultaneous production of small-molecule fatty acids and benzene polycarboxylic acids from lignite by alkali-oxygen oxidation. *Fuel Processing Technology* **2013**, *112*, 7-11.

[29]   Montoya, N.; De Klerk, A. Autoxidation of aromatics. *Applied petrochemical research* **2018**, *8*, 55-78.

[30]   Yao, Z.-S.; Wei, X.-Y.; Lv, J.; Liu, F.-J.; Huang, J.-G.; Xu, J.-J.; Chen, F.-J.; Huang, Y.; Li, Y.; Lu, Y.; Zong, Z.-M. Oxidation of shenfu coal with RuO_4 and NaOCl *Energy Fuels* **2010**, *24*, 1801-1808.

[31]   Clemens, A. H.; Matheson, T. W.; Rogers, D. E. Low temperature oxidation studies of dried New Zealand coals. *Fuel* **1991**, *70* (2), 215-221.

[32]   Hayashi, J.; Matsuo, Y.; Kusakabe, K.; Morooka, S. Depolymerization of lower rank coals by low-temperature O_2 oxidation. *Energy Fuels* **1997**, *11*, 227-235.

[33]   Kapo, G.; Calvert, S. Liquid phase oxidation of coal in alkali. *Ind. Eng. Chem. Proc. Des. Dev.* **1966**, *5*, 97-104.

[34]   Wang, W.; Hou Y.; Wu W.; Niu M.; Wu, T. High-temperature alkali-oxygen oxidation of lignite to produce benzene polycarboxylic acids. *Ind. Eng. Chem. Res.* **2013**, *52*, 680-685.

[35]   Yang, S.; Liu, D.; Li, Y.; Yang, C.; Yang, Z.; Chen, X.; Li, H.; Tang, Z. Experimental study on the oxidative dissolution of carbonate-rich shale and silicate-rich shale with H_2O_2, $Na_2S_2O_8$ and $NaClO$: Implication to the shale gas recovery with oxidation stimulation. *Journal of Natural Gas Science and Engineering* **2020**, *76*, 103207.

[36]   Chakrabartty, Sujit K. Oxidation of coal by alkaline sodium hypochlorite. In *Organic chemistry of coal*, Larsen, J. W. ed; American Chemical Society: Washington, 1978, pp. 100-107.

[37]   Chakrabartty, S. K.; Kretschmer, H. O. Studies on the structure of coals. 2. The valence state of carbon in coal. *Fuel* **1974**, *53* (2), 132-135.

[38]   Chakrabartty, S. K.; Kretschmer, H. O. Sodium hypochlorite as a selective oxidant for organic compounds. *Journal of the Chemical Society, Perkin Transactions* **1974**, *1*, 222-228.

[39]   Gong, G.-Z.; Wei, X.-Y.; Zong, Z.-M. Separation and analysis of the degradation products of two coals in aqueous NaOCl solution. *Journal of fuel chemistry and technology* **2012**, *40* (1), 1-7.

[40]   Maximov, O. B.; Schapovalov, V. E.; Shvets, T. V. Alkaline permanganate oxidation of methylated humic acids. *Fuel* **1972**, *51* (3), 185-189.

[41]   Tarafdar, M. N.; Guha, D. Application of wet oxidation processes for the assessment of the spontaneous heating of coal. *Fuel* **1989**, *68* (3), 315-317.

[42]   Lalvani, S.; Pata, M.; and Coughlin, R. W. Electrochemical oxidation of lignite in basic media. *Fuel* **1986**, *65*, 122-128.

[43]   Mae, K.; Maki, T.; Araki, J.; Miura, K. Extraction of low-rank coals oxidized with hydrogen peroxide in conventionally used solvents at room temperature. *Energy Fuels* **1997**, *11*, 825-831.

[44]   Mae, K.; Shindo, H.; Miura, K. A new two-step oxidative degradation method for producing valuable chemicals from low rank coals under mild conditions. *Energy Fuels* **2001**, *15*, 611- 617.

[45]   Chen, Q.; Kang, Y.; You, L.; Yang, P.; Zhang, X.; Cheng, Q. Change in composition and pore structure of Longmaxi black shale during oxidative dissolution. *International Journal of Coal Geology* **2017**, *172*, 95-111.

[46]   Sabar, M. A.; Ali, M. I.; Fatima, N.; Malik, A. Y.; Jamal, A.; Liaquat, R.; He, H.; Liu, F.-J.; Guo, H.; Urynowicz, M.; Huang, Z. Evaluation of humic acids produced from Pakistani subbituminous coal by chemical and fungal treatments. *Fuel* **2020**, *278*, 118301.

[47]   Pan, C.-X.; Liu, H.-L.; Liu, Q.; Shui, H.-F.; Wang, Z.-C.; Lei, Z.-P.; Kang, S.-G; Wei, X.-Y. Oxidative depolymerization of shenfu subbituminous coal and its thermal dissolution insoluble fraction. *Fuel Processing Technology* **2017**, *155*, 168-173.

[48]   Zhou, L.; Yuan, L.; Zhao, B.; Li, Y.; Lin, Z. Structural characteristics of humic acids derived from chinese weathered coal under different oxidizing conditions. *Plos one* **2019**, *14* (5), e0217469.

[49]   Chen, S.; Zhou, W.; Liu, M.; Zhao, G.; Cao, Q.; Zhao, B.; Kou, K.; Gao, J. Oxidation of zhundong subbituminous coal by Fe^{2+}/H_2O_2 system under mild conditions. *Korean J. Chem. Eng.* **2020**, *37* (4), 597-603.

[50]   Mae, K.; Maki, T.; Okutsu, H; Miura, K. Examination of relationship between coal structure and pyrolysis yields using oxidized brown coals having different macromolecular networks. *Fuel* **2000**, *79*, 417-425.

[51]   Carrillo-Pedroza, F. R.; Dávalos Sánchez, A.; Soria-Aguilar, M; Pecina Trevino, E.T. Coal desulfurization in oxidative acid media using hydrogen peroxide and ozone: A kinetic and statistical approach. *Energy Fuels* **2009**, 3703-3710.

[52]   Savich; T. R.; Howard, H. C. Oxidation of bituminous coal to organic acids by nitric acid and oxygen. *Ind. Eng. Chem.* **1952**, *44* (6), 1409-1411.

[53]   Alvarez, R.; Clemente, C.; Gomez-Limon, D. 2003. The influence of nitric acid oxidation of low rank coal and its impact on coal structure. *Fuel* **2003**, *82*, 2007-2015.

[54] Zhumanova, M. O.; Usanboev, N.; Namazov, S. S.; Beglov, B. M. Oxidation of brown coal of Angren deposit with a mixture of nitric and sulfuric acids. *Russian Journal of Applied Chemistry* **2009**, *82* (12), 2223-2229.

[55] Honda, H.; Hirose, Y. Wet oxidizability of coal using phosphoric acid-potassium dichromate solution. *Fuel* **1958**, *37* (3), 323-331.

[56] Yang, F.; Hou, Y.; Niu, M.; Lu, T.; Wu, W.; Liu, Z., Catalytic oxidation of lignite to carboxylic acids in aqueous H5PV2Mo10O40/H2SO4 solution with molecular oxygen. *Energy Fuels* **2017**, *31*, 3830-3837.

[57] De Abreu, Y.; Patil, P.; Marquez, A. I.; Botte, G. G.; Characterization of electrooxidized Pittsburgh No. 8 coal. *Fuel* **2007**, *86* (4), 573-584.

[58] Stephens, J. F.; Leow, H. M.; Gilbert, T. D.; Philp, R. P. Aqueous sodium dichromate oxidation of australian vitrinite concentrates. *Fuel* **1985**, *64* (11), 1531-1536.

[59] Ahmed, M. D; Kinney, C. R. Ozonization of humic acids prepared from oxidized bituminous coal. *Journal of the American Chemical Society* **1950**, *72*, 559-561.

[60] Wang, Y.; Chen, S.; Ding, M.; Xu, Z. Study of oxidization of coal–pitch by O3. *International Journal of Mining Science and Technology* **2016**, *26*, 677-681.

[61] Mackowsky, M.-TH. The application of coal petrography in technical processes. In *Coal Petrology third revised and enlarged edition*; Stach, E., Mackowsky, M.-TH., Teichmüller, M., Taylor, G. H., Chandra, D., Teichmüller, R. eds.; Gebrüder Borntraeger: Berlin, 1982, pp413-474.

[62] Schmidt, L.D. and Elder, J.L., 1940. Atmospheric oxidation of coal at moderate temperatures. *Industrial & Engineering Chemistry* **1940**, *32* (2), 249-256.

[63] Siddiquee, M. N.; De Klerk, A.; Nazemifard, N. Application of microfluidics to control product selectivity during non-catalityc oxidation of naphthenic-aromatic hydrocarbons. *Reaction Chemistry & Engineering* **2016**, *1*, 418-435.

[64] Taraba, B; Kupka, J. Subaquatic oxidation of coal by water-dissolved oxygen. *Fuel* **2010**, *89*, 3598-3601.

[65] Wang, H.; Dlugogorski, B. Z.; Kennedy, E. M. Coal oxidation at low temperatures: oxygen consumption, oxidation products, reaction mechanism and kinetic modelling. *Progress in Energy and Combustion Science* **2003**, *29*, 487-513.

[66]   Carras, J. N.; Young, B. C. Self-heating of coal and related materials: models, application and test methods. *Progress in Energy and Combustion Science* **1994**, *20*, 1-15.

[67]   Itay, M.; Hill, C. R.; Glasser, D. A study of the low temperature oxidation of coal. *Fuel Processing Technology* **1989**, *21*, 81-97.

[68]   Akgün, F.; Arisoy, A. Effect of particle size on the spontaneous heating of a coal stockpile. *Combustion and Flame* **1994**, *99*, 137-146.

[69]   Kaji, R.; Hishinuma, Y.; Nakamura, Y. Low temperature oxidation of coals: effects of pore structure and coal composition. *Fuel* **1985**, *64*, 297-302.

[70]   Mishra S. K.; Kanungo, S. B. Factors affecting the preparation of highly concentrated coal-water slurry (HCCWS). *Journal of scientific & industrial research* **2000**, *59*, 765-790.

[71]   Singh, H.; Kumar, S.; Mohapatra, S. K.; Prasad, S. B.; Singh, J. Slurryability and flowability of coal water slurry: Effect of particle size distribution. *Journal of Cleaner Production* **2021**, *323*, 129-183.

[72]   Chen, R.; Wilson, M.; Leong, Y.K.; Bryant, P.; Yang, H.; Zhang, D.K. Preparation and rheology of biochar, lignite char and coal slurry fuels. *Fuel* **2011**, 90, 1689-1695.

[73]   Peña-Méndez, E. M.; Havel, J.; Patočka, J. 2005. Humic substances-compounds of still unknown structure: applications in agriculture, industry, environment, and biomedicine. *Journal of Applied Biomedicine* **2005**, *3*,13-24.

[74]   Raj, S. S. *A study of some chemical structural parameters of coal*; Ph.D. Thesis, Pennsylvania State University, 1976.

[75]   Roy, A. N.; Howard, H. C. Solvent Fractionation of Polycarboxylic Acids from Oxidation of Coal. *Journal of the American Chemical Society* **1952**, *74*, 3239-3242.

[76]   Murata, S.; Hosokawa, M.; Kidena, K.; Nomura, M. Analysis of oxygen-functional groups in brown coals. *Fuel Processing Technology* **2000**, *67* (3), 231-243.

[77]   Attar, A.; Hendrickson, G. G. Functional groups and heteroatoms in coal. In *Coal Structure*; Meyers, R. A., Ed.; Academic Press: New York, 1982; pp 131−198.

3.   Oxidative coal dissolution: coal characterization

Abstract

This study focuses on the characterization of coal provided by Mancal Coal Inc., with the objective of understanding the structural groups and fundamental properties of the coal to enhance value addition through oxidative coal dissolution reaction. The coal is classified as low-rank subbituminous coal, and its characterization is done through various analytical techniques such as proximate and elemental analysis, Van Krevelen diagrams, diffuse reflectance infrared Fourier spectroscopy, and scanning electron microscopy with energy dispersive X-ray spectroscopy.

The chemical composition of Mancal's coal is complex and shows properties associated with lignite, subbituminous, and bituminous coal. The Van Krevelen H/C versus O/C diagram confirms that Mancal's coal falls between lignite/subbituminous coal and low-rank bituminous coal, containing aromatic clusters in its molecular makeup. The difference in the total ash content obtained through SEM-EDS analysis and proximate analysis can be attributed to the heterogeneity of coal and the different analysis methods used.

Overall, the study demonstrates the importance of proper coal characterization to enhance value addition through oxidative coal dissolution reaction, and the need to use multiple analytical techniques to obtain a comprehensive understanding of coal's structural groups and fundamental properties. The study also highlights the limitations of existing coal structure models and the complexity of coal as a mixture.

Keywords: Coal, Proximate analysis, Elemental analysis, SEM-EDS, DRIFT

3.1   Introduction

As described in chapter 1, section 1.1, coal reserves in Canada are vast. Most of the coal deposits are located in western provinces where Mancal Coal Inc. has various holdings and they have an interest in adding value to it. This project's approach to value addition is through oxidative coal

dissolution reaction, and the outcome is expected to be directly related to the feed composition and feed properties. Therefore, proper coal characterization is necessary.

According to *Van Krevelen* [1], coal characterization can be classified from two perspectives based on their purpose. From a commercial perspective, it deals with aspects such are comercial value, utilization, technological properties and suitability for certain end uses. From a research perspective, which is our focus in this project, systems of classification are concerned with the origin, constitution, and fundamental properties.

Chapter 2, section 2.2 presents a general scientific description of coal based on macerals groups, chemical composition, rank classification and mineral matter.

Previous work performed in our research group on coal samples provided by Mancal[2], classified the coal as low-rank subbituminous coal. In order to understand Mancal's coal characteristics, and structural groups, the coal was further characterized.

A chemical analysis, including both proximate and elemental analysis, provides coal's composition and allows the calculation of some physical properties. Additionally, as it was described in Chapter 2, with additional parameters such as those given in *Van Krevelen* [1] diagrams, it is possible to have a general idea of the coal skeleton or the macerals group to which it belongs. Furthermore, infrared spectroscopy is practical in particular fields of coal research, such as oxidative coal dissolution. This technique gives possibilities for structural group analysis of coal which are not achievable by classification chemical analysis [1]. Specifically, Diffuse Reflectance Infrared Fourier (DRIFT) spectroscopy is commonly used for powders, and rough surfaces such as ground coal, providing information from the bulk matrix. Finally, the specific coal micromorphology and mineral distribution from feed is identified by the Scanning electron microscope (SEM) with the help of a coupled energy dispersive X-ray spectroscopy (EDS).

3.2 Experimental

3.2.1 Materials

Coal from the northwest area of Canada (Alberta and Saskatchewan) was used for the oxidative coal dissolution process. Mancal Coal Inc provided the sample to the University of Alberta. Before each analysis, the coal samples were stored in an airtight plastic bag at -4 °C after being grinded to less than 0.1 mm (mesh 140 ASTM E-11 Standard Cole-Palmer) in a Disk Miller Bico UA Pulverizer. This was necessary to limit autoxidation of the coal.

Chemicals, cylinders and calibration substances employed in this study are shown in Table 3-1

Table 3-1 Materials employed in Coal Characterization.

Compound	Formula	CASRN [a]	Mass fraction purity [b]	Supplier
Chemicals				
Potassium Bromide	KBr	7758-02-3	>99%	Thermo Scientific
Cylinder gases				
Nitrogen	N_2	7727-37-9	>99%[c]	Linde
Oxygen	O_2	7782-44-7	>99%[c]	Linde
Calibration materials				
BBOT 2,5-Bis(5-tert-butyl-2-benzo-oxazol-yl)thiophene.	$C_{26}H_{26}N_2O_2S$	7128-64-5	95%[d]	OEA Labs

[a] CASRN = Chemical Abstracts Services Registry Number
[b] This is the purity of the material guaranteed by the supplier; material was not further purified.
[c] Mole fraction purity.
[d] Expressed as percentage of confidence in accordance with ISO/IEC17025

3.2.2 Analyses

Elemental Analysis of grinded coal is performed by the Chemistry department of the University of Alberta with a Thermo Fisher Flash 2000 Organic Elemental Analyzer (Cambridge UK). The autosampler, which is continuously swept with a carrier gas, drops the sample contained within a tin (Sn) cup into a vertical quartz tube called the combustion reactor that is maintained at 1000 °C. The upper portion of the combustion reactor is filled with tungstic oxide (WO_3) as the oxidation

catalyst, and the lower portion is filled with pure reduced copper wires. Once the sample enters the combustion reactor, a small, fixed volume of pure oxygen is added to the helium carrier gas. The added oxygen creates a highly oxidizing atmosphere, which completely burns the sample and tin cup container. The carbon, hydrogen, nitrogen, and sulfur present in the samples are quantitatively converted to carbon dioxide (CO_2), water (H_2O), nitrogen oxides (NO_x), and sulfur dioxide (SO_2), respectively. Excess oxygen is removed in the copper reduction portion of the combustion chamber, and NO_x is reduced to nitrogen (N_2). The carrier gas sweeps the combustion products onto the chromatographic column (Porapak QS, 4 mm ID, 2 m long), where the gases are separated. The detection of the individual gases is achieved with a thermal conductivity detector. The Eager Xperience software program converts the output signal from the thermal conductivity detector into a chromatogram that displays the nitrogen, carbon dioxide, water and sulfur dioxide peaks. The software generates the area count data used to calculate the percentage of nitrogen, carbon, hydrogen and sulfur present in the sample. The analytical run lasts for 11 minutes.

The proximate Analysis of the as received grinded coal feed was performed using a thermogravimetric analyzer. A Leco TGA-701 available in the Coal Laboratory was used. The TGA can accommodate multiple crucibles, allowing for continuous analysis with one crucible reserved for the blank or reference crucible. The furnace can be heated rapidly 30-45 °C/min from ambient to 1000 °C. The temperature is monitored and maintained at values specified for each determination. The system has an integrated balance capable of repeatedly weighing the crucibles and test specimens throughout the analysis. All mass measurements are conducted and recorded by the system. Analyses were carried out with about 1g of sample and were determined following the standard test method ASTM D7582 [3] for determining moisture, volatiles and ash in coal. The specific programmable conditions configured in the TGA for each determination are as follows: For Moisture, Temperature: 107 °C. Gas: N_2, 310.3 kPa (45 psi gauge), 7.0 L.min^{-1}. Time: until constant mass or 1 hour. For Volatile matter, Temperature: 950 °C. Gas: N_2, 310.3 kPa (45 psi gauge), 7.0 L.min^{-1}. Time: ramp up 19 min and hold for another 7 min. For Ash, Temperature: 750 °C. Gas: O_2, 241.3 kPa (35 psi gauge), 7.0 L.min^{-1}. Time: 2 hours.

The solid ground coal was analyzed using an ABB MB3000 Fourier transform infrared (FT-IR) spectrometer instrument equipped with a Diffuse Reflectance (DRIFT) attachment at 22 °C with

nitrogen flow at 15 mL.s^{-1}. The spectra were obtained at a resolution of 4 cm^{-1} as the average of 120 scans over the spectral region 4000-600 cm^{-1}.

A Scanning Electron Microscope Zeiss Sigma 300 VP-FESEM with a resolution of ~10 nm was used to obtain the solid grinded coal feed images. I was physically present during the analyses but did not perform the analyses myself. The analyses were performed at the Earth & Atmospheric Science department in the Scanning Electron Microscope Laboratory. The equipment includes a Bruker energy dispersive X-ray spectroscopy (EDS) system with dual silicon drift detectors, each with a resolution of 123 eV and a 60 mm^2 window area. The acceleration voltage used for the EDS analysis was 15 keV. It could work at variable pressure and environmental mode. Samples were coated with carbon to prevent image disruption due to conductance during the analysis of the samples in the presence of a secondary electron gun beam.

3.2.3 Calculations

As grinded coal is used as the feed for the oxidative coal dissolution process, calculations are necessary to accurately interpret the elemental analysis by converting the CHNS elemental values to CHNSO values, which are corrected for the presence of both moisture and ash in the coal sample.

Once the weight percentage of ash is provided from the proximate analysis, and carbon, hydrogen, sulfur and nitrogen weight composition are obtained from the elemental analysis. The oxygen weight composition is calculated by difference as follows:

$$O\% = 100 - [C\% + H\% + S\% + N\% + ash] \tag{3-1}$$

The method from equation 3-1 estimates oxygen value by subtracting the determined weight percentages of all other constituents from 100. The errors in the determined values are reflected in the estimated oxygen value. These errors may be partially compensating or may be additive [4]. The uncertainty associated with the oxygen content determined by difference is therefore larger than that of the other elements in the CHNSO elemental analysis.

ASTM D3174 [5] and ASTM D3173 [6] are used for converting the data on as-received basis to moisture, ash-free basis. Moisture in coal according to the definition by *Allardice & Evans* [7] is used in this research thesis. It refers to moisture as the presence of water molecules within the coal structure and its pores. This water can be released at temperatures from 105-100 °C at atmospheric pressure. It should be noted that this definition does not encompass water derived from the breakdown of functional groups or water that is strongly chemically bound within the coal matrix.

First, ash-free basis weight percentage is calculated with equation 3-2. For oxygen, the weight concentration calculated by equation 3-1 was used as the as-received value.

$$\textbf{Ash free element \%} \ = \frac{\textbf{Element\% as received} * \textbf{100}}{\textbf{100} - \textbf{\textit{ash}\%}} \tag{3-2}$$

Equations 3-3 and 3-4 apply to hydrogen and oxygen in converting to the moisture, ash-free basis (maf). The ash free weight percentage of each element is the value calculated in equation 3-2. Moisture, volatile material (VM) and fixed carbon are obtained from the proximate analysis.

$$\textbf{moisture, ash} - \textbf{free H\%} \ = \textbf{ash free H\%} - \frac{\textbf{Moisture\%}}{\textbf{(Moisture+VM+Fixed Carbon)}} * \textbf{100} * \frac{\textbf{2}}{\textbf{18}} \tag{3-3}$$

$$\textbf{moisture, ash} - \textbf{free O\%} \ = \textbf{ash free O\%} - \frac{\textbf{Moisture\%}}{\textbf{(Moisture+VM+Fixed Carbon)}} * \textbf{100} * \frac{\textbf{16}}{\textbf{18}} \tag{3-4}$$

Once moisture, ash-free weigth percentages of hydrogen and oxygen are calculated, all elements compositions are normalized using the data from equation 3-2 for carbon, nitrogen and sulfur, equation 3-3 for hydrogen and equation 3-4 for oxygen.

The gross heating value (GHV) of coal on a moisture, ash-free basis is calculated with the weight percentages of oxygen, carbon, hydrogen and sulfur using Dulong's correlation [8] in BTU/lb (430 BTU/lb =1 MJ/kg) units as it is shown in equation 3-5.

$$\textbf{GHV} = \textbf{145.44} * \textbf{C\%} + \textbf{620.28} * \textbf{H\%} + \textbf{40.5} * \textbf{S\%} - \textbf{77.54} * \textbf{O\%} \tag{3-5}$$

3.2.4 Calibrations

The Thermo Fisher Flash 2000 Organic Elemental Analyzer is calibrated using at least three samples of an organic analytical standard (OAS) at the start of each analysis day. The standard used for coal samples is BBOT 2,5-Bis(5-tert-butyk-2-benzo-oxazol-yl)thiophene. It is accurately weighed directly into tin cups using a Mettler XP2U microgram balance, which is readable to 0.1 micrograms. The standards span the range from ~0.5 to ~3 mg. Once the standard runs are finished, linear regression analysis is performed on the peak areas for each of the elements (C, H, N, S) versus the milligrams of each element contained in the standards. The amount of each element is calculated by multiplying the known proportion of each element in the standards by the amount of sample. The equation of the regression line that fits these points is used to calculate the amount of C, H, N, and S in the samples. An acceptable regression line for each element has a coefficient of determination (R^2) value of at least 0.999. For R^2 values less than these, another set of standards are run, and a new calibration curve is obtained. To monitor the accuracy of the instrument, a sample of the OAS is used as a calibration check every 4 test samples. The calibration check is treated as an unknown. The check samples are weighed such that they are within the calibration range of the standards used. The measured values for these standards should produce results that are within ±0.3% of the theoretical values. If they do not agree within ±0.3%, the system is inspected for possible malfunction, and, if necessary, repairs are performed on the instrument and the samples are re-analyzed.

Thermogravimetric analysis is primarily a method that determines absolute weight loss. Therefore, the calibration procedure is used to compensate for the differences between the measured and certified results of specific standards when they are required. Standards are certified reference materials with known concentration and uncertainty levels, typically required for analyzing the volatile matter. As the measurements scope of Mancal coal with test method ASTM D7582 does not require a specific reference material, this calibration is unnecessary.

For the Scanning Electron Microscope Zeiss Sigma 300 VP-FESEM, the vendor performs all setting conditions, control elements, operation systems and maintenance or repair. Operators can adjust the extractor voltage in the SEM control system with certain limits to optimize the proven

current for particular applications. This particular adjustment was not performed for the images taken of coal.

3.3 Results

3.3.1 Proximate and Elemental Analysis

The proximate and elemental analyses of coal provide a broad understanding of its characteristics. General parameters such as moisture, fixed carbon, volatile matter, and ash concentration, combined with the chemical composition of coal, are used not only to classify coal but also as a measure to understand the OCD process. Characterization of the Mancal coal is provided in Table 3-2. Proximate and elemental analyses were performed in duplicate, and the average values are reported.

Table 3-2 Characterization of Mancal coal

Description	Mancal Coal	
Proximate Analysis (wt%)[a]	x	s
Moisture	26.5	0.02
Volatile matter	30.5	0.32
Fixed Carbon	32.8	0.25
Ash	10.2	0.59
Elemental Analysis (wt%, maf)[b]		
Carbon	71.7	0.17
Hydrogen	4.1	0.22
Nitrogen	1.3	0.01
Sulfur	0.8	0.01
Oxygen[c]	22.0	-
H/C molar ratio (mol/mol)	0.69	-
O/C molar ratio (mol/mol)	0.23	-
Gross heating value[d] (MJ/kg)	26.3	-

[a]Averages (x) and sample standard deviations (s) of duplicate analyses
[b]Calculated on a moisture, ash-free basis using elemental and proximate Analysis
[c]Oxygen was determined by difference
[d]Calculated on the basis of Dulong's correlation (Eq. 3-5)

From proximate analysis, moisture value is very important due to its influence on other measured and calculated values used in coal analysis, such as the elemental analysis on a moisture, ash-free basis. It is also important for coal trading processes. The ash is composed primarily of oxides and

sulfates as a result of chemical changes in the mineral matter at high temperatures, as described in Chapter 2 and tables 2.4 and 2.5. Volatile matter in coal refers to the components of coal, except for moisture, which is liberated at high temperatures in the absence of air. Finally, Fixed carbon is the material remaining after the determination of moisture, volatile matter, and ash. It differs from the carbon content of coal as determined by ultimate analysis since some carbon is lost in hydrocarbons with volatile matter and the carbon-rich material that remains is not devoid of hydrogen, nitrogen, sulfur, or oxygen [9].

The elemental analysis of coal described in Table 3-1 involves the determination of the weight percent carbon as well as sulfur, nitrogen, and oxygen estimated by difference. Carbon includes carbon present as organic carbon occurring in the coal substance and any carbon present as mineral carbonate. Hydrogen determination includes mainly hydrogen present in the organic materials. Nitrogen is assumed to occur within the organic matrix of coal. On the other hand, The amount of sulfur detected is mostly from the organically bound sulfur, but some sulfide minerals can react with the organic matter to transfer sulfur that will be detected as SO_2 and increase the sulfur content.

3.3.2   Diffusive Reflectance Infrared Fourier (DRIFT)

Infrared radiation, which is part of the electromagnetic spectrum between the visible and microwave regions, is absorbed and converted by an organic molecule into energy of molecular vibration. The frequency or wavelengths of absorption depends on the relative masses of the atoms, the force constants of the bonds and the geometry of the atoms [10]. Infrared spectrometry is a technique used to determine a compound's structure by studying the interaction between infrared radiation and matter. Therefore, it is one of the most valuable techniques for identifying different chemical groups into coal.

Diffuse Reflectance Infrared Fourier (DRIFT) spectroscopy is commonly used for powders and rough surfaces since it provides information from the bulk matrix. The IR radiation interacts with the particles and then reflects off their surfaces, causing the light to diffuse or scatter as it moves throughout the sample. The coal solid sample was mixed at a similar weight percentage with

Potassium Bromide, and then pressed into the crucible for the measurement. DRIFT spectrum for Mancal's coal is shown in Figure 3-1.
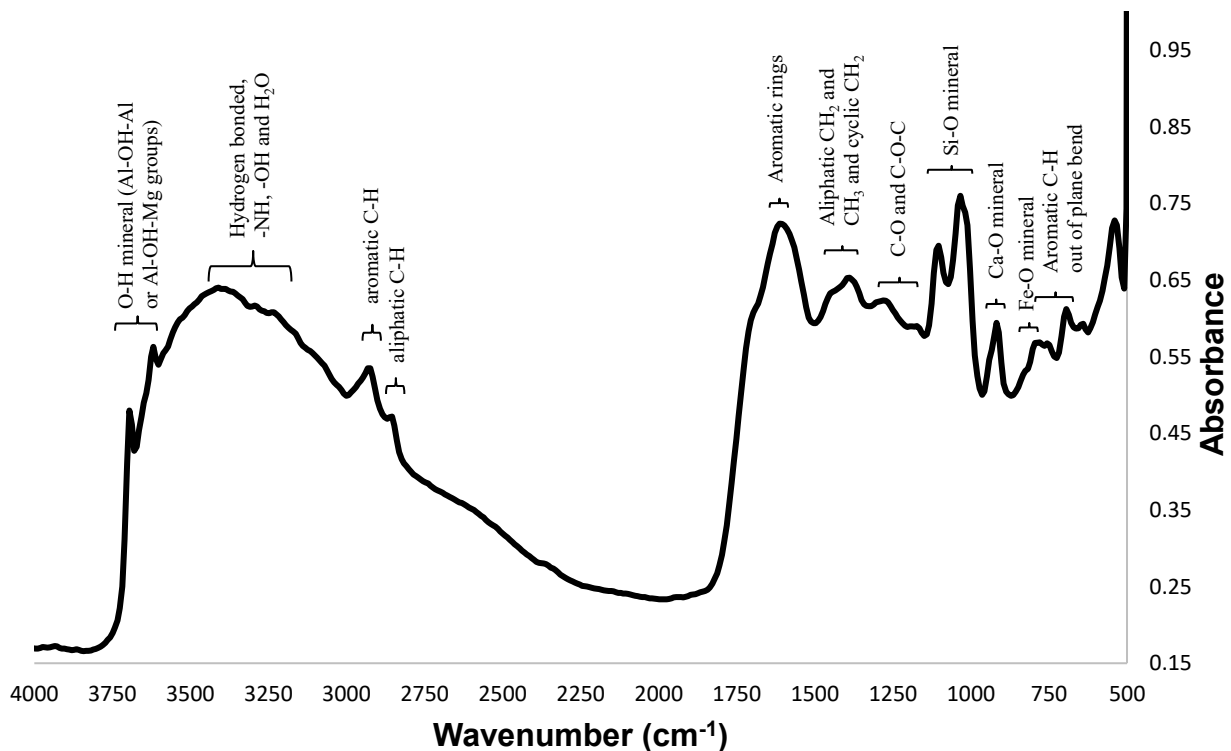
Figure 3-1 Mancal Coal DRIFT Spectrum

Figure 3-1 exhibits the peaks identified in the Mancal coal DRIFT spectrum, with possible corresponding chemical functional groups attributed based on literature references on coal [1][11][12][13]. The description and specific wavenumber values found for each peak, presented in parentheses, are detailed below.

First, there is a rather broad band that goes from approximately 3700 to 2100 cm^{-1}. This energy is caused by the stretching of the O-H bonds in water and other hydrogen-containing substances in the coal. These substances are bonded together in various ways, which causes them to vibrate differently. The energy band also includes vibrations from the C-H bonds in the organic components of the coal, such as aromatic and aliphatic compounds [14].

The aromatic hydrogen contents are determined from the bands of the aromatic C-H stretching modes between 3100 and 3000 cm^{-1} (~3052) and from the aromatic C-H out of plane bending

58

modes between 900 and 6750 cm^{-1} (~795 ~779, ~756, ~694 cm cm^{-1}). The aliphatic hydrogen contents are derived from the aliphatic C-H stretching modes between 3000 and 2800 cm^{-1} (~2854 cm^{-1}). The Hydrogen bonded, -NH -OH and H$_2$O groups are present in the band position between 3600 and 3200 cm^{-1} (~3410, ~3294, ~3232 cm^{-1}). Between 1615 and 1590 cm^{-1} (~1612) there are some peaks associated with coal to polynuclear aromatic ring stretch. Aliphatic CH$_2$ and CH$_3$ and cyclic CH$_2$ functional groups are present between 1460 and 1370 cm^{-1} (~1466 and ~1389 cm^{-1}). There are also peaks assigned to phenolic and alcoholic C-O and C-O-C bending between 1300 and 1100 cm^{-1} (~1281 and ~1173 cm^{-1}). Regarding to mineral matter content in feed coal, sharp peaks within the ranges 3700-3600 cm^{-1} (~3695 and ~3618 cm-^{1}) are associated with Al-OH-Al or Al-OH-Mg groups. Si-O minerals might generate the peak from 1100 cm^{-1} -1000 cm^{-1} (~1103 and ~1034 cm^{-1}) and peaks of Ca-O and Fe-O can be traced with the peaks at approximately 916 cm^{-1} (~918 cm^{-1}) and between 870 cm^{-1} and 790 cm^{-1} (~795 cm^{-1}) respectively. These are tentative assignments, since more than one group may absorb at a wavenumber. For example, the peaks tentatively identified as Ca-O and Fe-O may also be indicative of different methyl substitution patterns on benzene-rings.

3.3.3 Scanning electron microscope with energy dispersive X-ray spectroscopy SEM-EDS

Studies such as Scanning electron microscope (SEM) coupled with energy dispersive X-ray spectroscopy (EDS) are important to understand solid coal micromorphology and mineral distribution. Some secondary electron images were of Mancal's coal, previously grinded to less than 0.1 mm. Figure 3-2 shows coal particles with distributed minerals in the surface. The SEM uses a beam of high-energy electrons to scan the surface of the coal sample. This produces a high-resolution image of the sample's surface, which can reveal the texture and morphology of the coal and minerals.
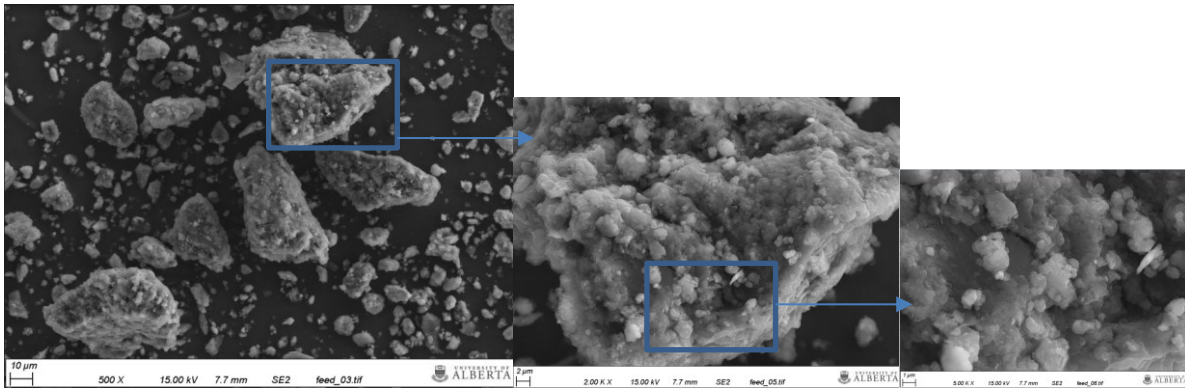
Figure 3-2 Secondary electron images taken to Mancal Coal in SEM-EDS

While the SEM is scanning the sample, the EDS system detects and analyzes the X-rays emitted from the sample's surface. These X-rays are generated by the interaction of the high-energy electrons from the SEM with the atoms in the sample. Each element in the coal sample produces a unique X-ray spectrum, which can be used to identify the element. By comparing the X-ray spectra of the sample to a database of known element spectra, the EDS system can identify the element present in the sample and determine their relative abundance. Figure 3-3 show the main elements identified in Mancal's coal and their distribution. In Figure 3-3 and various bright sites can be identified which are characteristic of some element shown in Figure 3-1, such are Silicon and Aluminium.

Figure 3-3 Secondary Electron **SE** image from Mancal's Coal elemental distribution in SEM-EDS (Map/Spectrum)

From Figure 3-3, apart from carbon and oxygen, which are presented at higher concentrations, major metals seem to be finely dispersed. Also, reviewing the elements that constituted the major mineral associated with coal in chapter 2, section 2.2.3 (Al/Na/Si/Mg-Clay, Ca-carbonates, Si-Silicates, Fe-sulfides), all of the elements associated with them are present in all coal samples.

Once the elements have been identified, the EDS system can calculate the percentage of each mineral in the sample based on the intensity of the X-ray peaks. A sample excited by an energy source dissipates some of the absorbed energy by ejecting a core-shell electron. A higher energy outer-shell electron then proceeds to fill its place, releasing the difference in energy as an X-ray that has a characteristic spectrum based on its atom of origin. This allows for the compositional analysis of a given sample volume that has been excited by the energy source. As the electron probe is scanned across the sample, characteristic X-rays are emitted and measured; each recorded EDS spectrum is mapped to a specific position on the sample through the characteristic x-ray (K_α line) in the EDX spectrum for the element in question and therefore the electron transition in the emission energy spectrum. The position of the peaks in the spectrum identifies the element, whereas the signal's intensity corresponds to the element's concentration. This is a semi-quantitative value, although with proper calibration (not done for this sample) it can yield quantitative values.

Table 3-3 presents the weight percentages of each element identified in the sample using EDS analysis. The coal sample was analyzed in five specific areas. The table provides the average weight percentages and standard deviation for each element based on multiple measurements taken in each area.

In addition to the mineral related elements presented in Table 3-3, repeated detection of oxygen and carbon was observed during the analysis, although these elements were not reported in Table 3-3 since most of its composition is representative of the organic structure of coal. Sulfur, on the other hand, is also a component of the organic structure of coal, but as it was explained in Chapter 2, Section 2.4.5, a significant portion of total sulfur (30-50%) is present in the form of sulfur-containing minerals, which significantly influence the mineral matter content of the coal sample.

Therefore, the presence of sulfur-containing minerals should be taken into account when analyzing the mineralogy and chemical composition of coal.

Table 3-3 Main mineral elements identified in Mancal's coal with SEM-EDS

Element	K_α (keV)	Wt Percentage in coal (%)	
		x	s
Si	1.7	1.92	0.55
Al	1.5	1.87	0.25
Ca	3.7	1.61	0.16
Na	1.0	0.68	0.09
Fe	6.4	0.62[a]	-
S	2.3	0.48	0.10
P	2.0	0.27[a]	-
Mg	1.2	0.20	0.04

Averages (x) and sample standard deviations (s) of five diferent measures
[a]Those elements were only detected in one of the areas mapped

3.4   Discussion

3.4.1   Mancal's coal rank

Based on the proximate and elemental analysis results for Mancal's coal presented in Table 3-1, as well as the typical composition and physical property ranges of coal outlined in Table 2-2 of Chapter 2, Mancal's coal has a moisture value falling within the lignite coal range. The volatile matter and fixed carbon content, on the other hand, fall within the subbituminous coal region. Additionally, the ash content is found to be at the upper limit of subbituminous coal, while still being within the range observed for lignite coal.

Regarding the elemental analysis results, it can be observed that the oxygen content of the coal falls within the range typically observed for subbituminous coals. Hydrogen content, on the other hand, falls within the range typical for bituminous coals, while nitrogen content is found in both the bituminous and subbituminous coal ranges. The sulfur content of the coal is relatively low compared to the upper limit typically observed for bituminous coal, yet it is still within the range observed for all coal ranks.

However, as evidenced in Chapter 2, Table 2.2, sulfur and nitrogen show no clear association with coal rank and therefore, are not necessarily rank indicators. The ranges of these properties overlap across different coal ranks, and certain coals display notable deviations, for example from the typical sulfur content the variations are predominantly attributed to specific geographical locations [15]. It is believed that the original decaying plant matter, which underwent coalification, contained sulfur levels of up to 0.5%. Any sulfur content exceeding this threshold is believed to be influenced, in part, by the composition of dissolved salts present in the specific deposit [16].

For coals with heating values below 32.6 MJ/kg (14000 Btu/lb) and fixed carbon content on a moisture, ash-free basis lower than 69% (Mancal's coal fixed carbon on a moisture, ash-free basis is 51.3 wt%), the primary classification for coal rank is determined based on the heating value [4]. In the case of Mancal's coal, the calculated heating value is 26.3 MJ/kg (11324 Btu/lb). Referring to Chapter 2, Table 2.2, this heating value falls near the threshold between subbituminous and bituminous coal ranks. Consequently, the specific classification of Mancal's coal based on heating value may vary depending on the specific characteristics of the sample as either subbituminous or high-volatile C bituminous coal.

As previously mentioned in Chapter 2, Section 2.2, Van Krevelen's H/C and O/C diagrams [1] not only serve as a means of graphically representing reaction processes, but also provide insight into the carbon skeleton and rank of a given sample. In line with this, Figure 3-4 illustrates Van Krevelen's diagram, highlighting Mancal's coal H/C versus O/C molar ratio identification. According to Figure 3-4, Mancal's coal appears to fall between (V) lignite/Subbituminous coal and (VI) Low-rank Bituminous coal. Additionally, the structure of the coal appears to include aromatic clusters within its molecular makeup. The last is confirmed by the DRIFT results which show aromatic bonding in coal structure. The presence of aromatic bonds in the coal structure is also supported by the DRIFT results with aromatic stretching modes showed in form of peaks to the specific wavenumber associated to those groups.
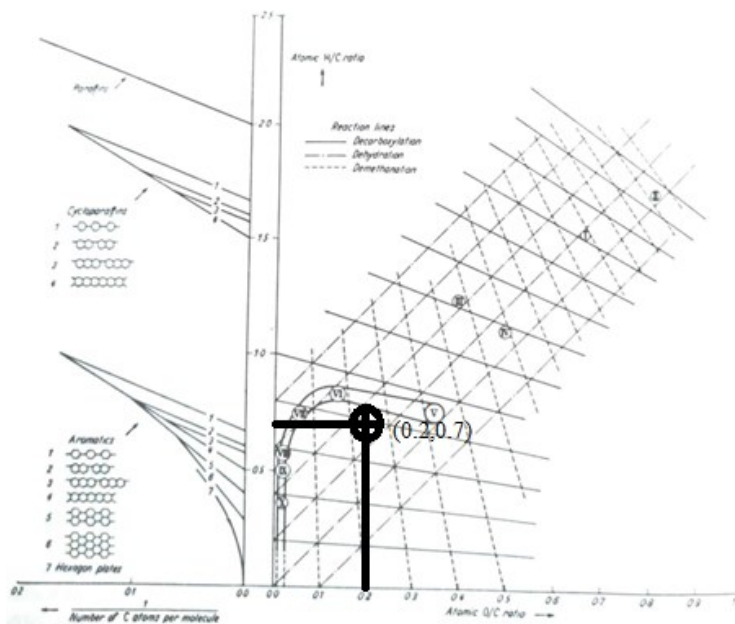
Figure 3-4 Van Krevelen H/C versus O/C diagram for different coal ranks: (I) Wood, (II) Cellulose, (III) Lignin, (IV) Peat, (V) lignite/Subbituminous coal, (VI) Low rank Bituminous coal, (VII) medium rank bituminous coal, (VIII) high rank bituminous coal, (IX) semi-antracite, (X) Antracite. With Mancal's coal H/C versus O/C molar ratio identification Modified from [1]

Based on the previous description, Mancal's coal has chemical properties associated with lignite, bituminous and subbituminous coals. However, most of the properties and compositions are related to subbituminous rank more than the others. Nevertheless, coal composition changes not only according to the rank but also due to the source from which it comes. As previously mentioned, coal is not structurally dependent on a single molecule but a complex mixture of molecules. Coal is also known only as a series of parameters and a few identified "building blocks" [17]. Based on that, model structures are interpretations of possible combinations of these factors, and they play a key role in understanding the reactions and mechanism of oxidative coal dissolution.

There is a large number of coal structure representations in literature. Most of the investigation focuses on bituminous coal, but some subbituminous coal structures have been proposed. Models differ because of the specifics of the chemical data used as well as analytical techniques. Figure 3-5 shows four molecular representations of subbituminous coals that give an idea about the configuration and distribution of organic groups.

64
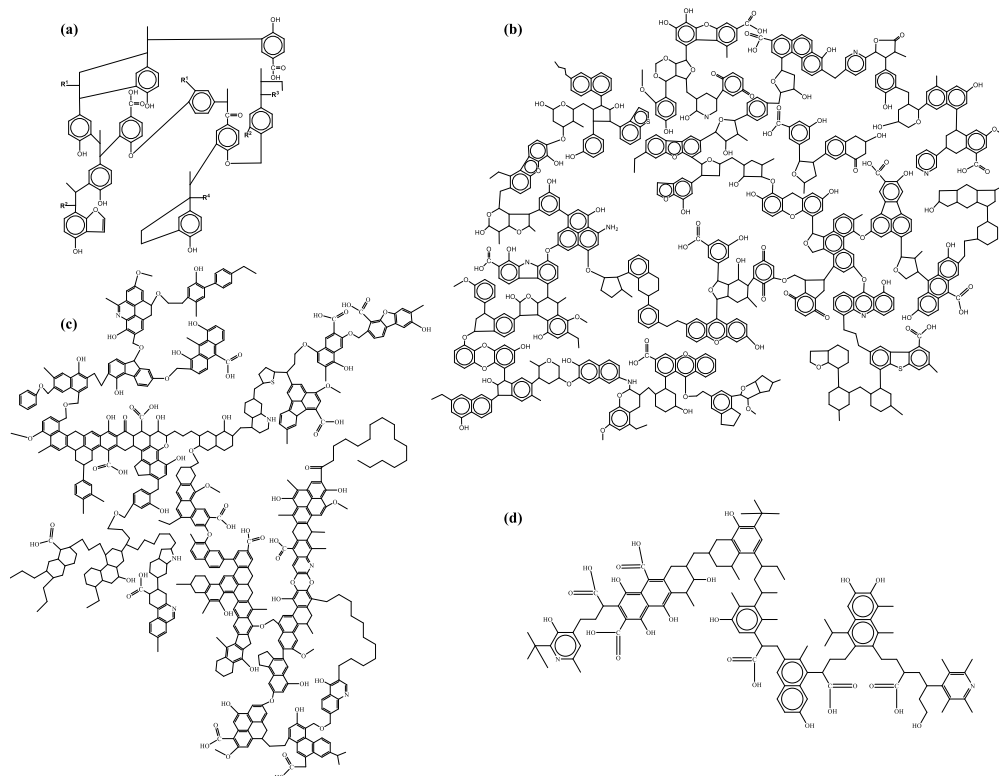
Figure 3-5 Molecular representation of subbituminous Coal (a) [18], (b) [19], (c) [20], (d) [21]

Structure from Hatcher [18] has individual aromatic rings where the average aryl-O contents are consistent with the average structure being monohydric phenols. There is also an average of about one hydroxyl group per ring. The (R) indicate cross-link sites to other (R) letters. Sites R3 and R4 are cross-links to the coal macromolecules. The model from Shinn [19] contains up to three-ring structures with different oxygen groups. Some nitrogen groups are evident. The structure unit from Nomura et al. [20] has various polyaromatic structures, some of them containing nitrogen and sulfur. The last model from Liu et al. [21] is in the same trend as the previous two models, with aromatic rings, primarily benzene and naphthalene, and all nitrogen atoms exit only in the pyridine form. A feature in all models is the abundance of hydroxyl and carboxylic groups.

Table 3-4 provides a comparison of the different molecular representations of subbituminous coal with Mancal's coal. The aim is to evaluate how well each representation accurately reflects the ultimate analysis of the Mancal coal. This evaluation is done by calculating the CHNSO composition (in weight percentages) of the four structures and comparing them to the composition of the Mancal coal.

Table 3-4 CHNSO Calculation for molecular representations of subbituminous coal

CHNSO Analysis (wt%)	Hatcher [18] $C_{89}H_{80}O_{14}$	Shinn [19] $C_{617}H_{590}N_7S_2O_{112}$	Nomura et al. [20] $C_{525}H_{536}N_6SO_{75}$	Liu et al. [21] $C_{111}H_{136}N_2O_{23}$	Mancal Coal[a]
Carbon	77.8	74.4	72.2	71.5	71.7
Hydrogen	5.8	5.9	6.6	7.3	4.1
Nitrogen	0.0	1.0	1.0	1.5	1.3
Sulfur	0.0	0.6	0.4	0.0	0.8
Oxygen	16.3	18.0	14.7	19.7	22.0[c]
H/C molar ratio (mol/mol)	0.89	0.95	1.02	1.22	0.69
O/C molar ratio (mol/mol)	0.16	0.18	0.14	0.21	0.23

[a]Calculated on a moisture, ash-free basis using elemental and proximate Analysis
[c]Oxygen was determined by difference

Analyzing the molecular representations of subbituminous coal, regarding carbon content, the molecular representations of Hatcher, Shinn, and Nomura et al. exhibit slightly higher percentages than the Mancal coal but with close values. while Liu et al.'s representation shows a slightly lower carbon content compared to Mancal's coal. All the molecular representations generally display higher percentages of hydrogen than the Mancal coal and Hatcher model does not include sulfur or nitrogen in its representation. However, sulfur and nitrogen are typically present in real coal samples across different ranks. This indicates that the Hatcher model lacks the inclusion of these essential elements, making it less representative of actual coal compositions.

The H/C molar ratio reflects the hydrogen content relative to the carbon content. A lower H/C ratio is typically associated with higher coalification levels and more mature coal, indicating a higher carbon content relative to hydrogen. In this case, the Mancal coal has the lowest H/C ratio of 0.69, suggesting a higher degree of coalification compared to the molecular representations.

The O/C molar ratio provides insights into the oxygen content relative to the carbon content. A higher O/C ratio generally indicates a higher oxygen content and a lower degree of coalification. In this comparison, the O/C ratios for the molecular representations range from 0.14 to 0.21, whereas the O/C ratio for the Mancal coal is 0.23. This suggests that the molecular representations,

on average, have slightly lower oxygen contents compared to the Mancal coal, indicating a relatively lower degree of coalification in the Mancal coal.

The findings from the molecular representations suggest that the classification of the Mancal coal's rank may exhibit variation, ranging from more coalified to less coalified coal, depending on the specific model chosen. However, it is important to recognize that ultimately these are all only mental models of an average coal structure and despite the value of capturing the nature of coal composition in this way, coal is a complex mixture. These models are therefore just simplifications to aid understanding of the molecular complexity.

3.4.2   Mineral Matter in Mancal's Coal

The results from Table 3-3 show that the mineral elements found with the SEM-EDS are similar to those associated with coal in Chapter 2, Table 2-3. Regarding the consistency of the results from Table 3-3 with respect to the ash percentage calculated with the proximate analysis and described in Table 3-2, it is necessary to associate those elements with the major inorganic constituents of coal ash that are generated after the reaction of mineral matter on the heating process. This is because ash is, in reality, the residue remaining after the complete combustion of the organic portion of the coal matrix. Thus, the constituents of ash do not occur as such in coal but are formed as a result of chemical changes which take place in the mineral matter during the combustion (ashing) process [9]. These changes usually involve the breakdown of complex chemical structures (such as can occur in clays and many minerals) with the formation of metal oxides which are identified in Chapter 2, Table 2-5.

By utilizing SEM-EDS to identify the mineral elements present in Mancal's coal, it is conceivable to assume that these elements may be associated with the metal oxides formed during the ashing process. Thus, it is possible to estimate the weight percentage of each metal oxide in the ash constituents of the coal by considering the atomic weight of each element and its stoichiometric bonding with oxygen. The estimates of the major inorganic constituents of Mancal's coal ash are presented in Table 3-5. Despite sulfur not being a metallic element, minerals containing sulfur play a significant role in the mineral structure as previously explained. Therefore, taking into

67

account that 30-50% of total sulfur is present in the form of sulfur-containing minerals [77], 40%wt of the total sulfur identified on SEM-EDS is encompassed in the analysis.

Table 3-5 Major inorganic constituents of Mancal's coal ash

Compounds	Wt Percentage of each element in the metal oxide (%)		Wt Percentage of each constituent in ash (%)
	metal	Oxygen	
SiO_2	1.92	2.20	4.12
Al_2O_3	1.87	1.67	3.54
CaO	1.61	0.64	2.25
Na_2O	0.68	0.24	0.92
Fe_2O_3	0.62	0.27	0.89
SO_3	0.19[a]	0.29	0.48
P_2O_5	0.27	0.35	0.62
MgO	0.20	0.13	0.33
			Total ash: 13.18

[a]40%wt of the total sulfur identified on SEM-EDS

Table 3-5 provides valuable information regarding the mineral matter in Mancal's coal. The total ash content of the coal was found to be 13.18% by SEM-EDS analysis, which is higher than the ash content obtained by proximate analysis (10.2%). The difference in the results can be attributed to various factors.

Firstly, coal is a heterogeneous material, meaning that even if the coal samples are taken from the same batch that was ground and sieved, there is no guarantee that each individual sample will provide a homogeneous representation of the coal as a whole. This heterogeneity can result in different results in SEM-EDS.

Secondly, the ash determination procedure in TGA analysis is based on ASTM standards and involves analyzing the entire sample, whereas SEM-EDS analysis is reliant on the selection of specific areas of interest for analysis, which may not be representative of the entire sample. However, SEM-EDS analysis enables the identification of individual mineral elements, a capability not available in TGA analysis. Based on the specific regions evaluated in SEM-EDS analysis, it was possible to validate the presence of major inorganic components in coal, such as

silicon and aluminium oxides, which aligns with the findings reported in Chapter 2, Table 2-5 of the literature. Lastly, SEM-EDS as employed in this study was a semi-quantitative analysis, since no matrix specific calibration was performed.

3.5   Conclusions

- Based on the calculated heating value, Mancal's coal falls near the threshold between subbituminous and bituminous coal ranks, suggesting that its classification may vary depending on the specific sample characteristics, potentially placing it as either subbituminous or high-volatile C bituminous coal.

- The comparison of ash content values in Mancal's coal determined by SEM-EDS analysis and TGA reveals that they are generally comparable but not identical. SEM-EDS analysis provides detailed information on the specific mineral elements present in the coal, enabling insights into the composition of the mineral matter through the potential association of elements with metal oxides formed during ashing. In contrast, TGA, following ASTM standards, analyzes the entire sample and provides a more comprehensive assessment of the coal's overall ash content.

3.6   References

[1]   Van Krevelen, D. W. *Coal. Typology-Physics-Chemistry-Constitution*, 3rd ed.; Elsevier: Amsterdam, 1993.

[2]   Siddiquee, M. N.; De Klerk, A. Heteroatom removal as pretreatment of boiler fuels. *Energy Fuels* **2019**, *33*, 5790-5801.

[3]   ASTM International. ASTM D7582, *Standard Test Methods for Proximate Analysis of Coal and Coke by Macro Thermogravimetric Analysis*; ASTM International: West Conshohocken, PA, 2010.

[4]   Riley, J. T. *Routine coal and coke analysis: collection, interpretation, and uses of analytical data*, 2nd ed.; ASTM International: West Conshohocken, 2014.

[5]   ASTM International. ASTM D3174, *Standard Test Methods for Ash in the Analysis sample of Coal and Coke from Coal*; ASTM International: West Conshohocken, PA, 1997.

[6]   ASTM International. ASTM D3173, *Standard Test Methods for Moisture in the Analysis sample of Coal and Coke*; ASTM International: West Conshohocken, PA, 1997.

[7]   Allardice, D. J.; Evans, D. G. Moisture in coal. In *Analytical methods for coal and coal products, Volume 1*; Karr, C. Jr. ed.; Morgantown, West Virginia, 1978, p. 247-262.

[8]   Mason, D. M.; Gandhi, K. Formulas for calculating the heating value of coal and coal char: Development, tests and uses. *Prepr. Pap.−Am. Chem. Soc., Div. Fuel Chem*. **1980**, 25 (3), 235−245.

[9]   Speight, J. G. *Handbook of coal analysis. Chemical analysis: A series of monograph on analytical chemistry and its applications. Vol. 182*, 2ed.; Wiley: Hoboken, New Jersey, 2015.

[10]   Silverstein, R. M.; Bassler, G.C; Morrill, T.C. *Spectrometryc identification of organic compounds* 4th ed.; John Wiley & Sons Ltda: New York, 1981.

[11]   Sharma, D.K.; Singh, S. K. Advanced process for the production of clean coal by chemical leaching technique. *Energy sources* **1995**, 17(4):485-493.

[12]   Yoshida, T.; Takanohashi, T.; Sakanishi, K.; Saito, I.; Fujita, M.; Mashimo, K. The effect of extraction condition on HyperCoal production (1) -under room temperature filtration. *Fuel* **2002**, 81(11):1463-1469.

[13]   Rahman, M.; Samanta, A.; Gupta, R. Production and characterization of ash-free coal from low-rank Canadian coal by solvent extraction. *Fuel Processing Technology* **2013**, 115, 88-98.

[14]   Smyrl, N. R.; Fuller, E. L. Chemistry and structure of coals: Diffuse reflectance IR Fourier transformation (DRIFT) spectroscopy of air oxidation. In *Coal and coal products: Analytical characterization techniques*; Fuller, E. L. ed.; Washington, D.C, 1982, p. 133-145.

[15]   Stach, E. The microlithotypes of coal and their strength. In *Coal Petrology third revised and enlarged edition*; Stach, E., Mackowsky, M.-TH., Teichmüller, M., Taylor, G. H., Chandra, D., Teichmüller, R. eds.; Gebrüder Borntraeger: Berlin, 1982, p140-150.

[16]   Speight, J. G. *The chemistry and technology of coal,* 3rd ed.; CRC Press: Boca Raton, 2012

[17]   Davidson, R. M. Molecular structure of coal. In *Coal science Vol. 1*; Gorbaty, M. L., Larsen, J. W., Wender, I. eds.; Academic Press: Orlando, 1982, pp.83-160.

[18]   Hatcher, P. G. Chemical structural models for coalified wood (vitrinite) in low rank coal. *Organic Geochemistry* **1990**, *16*, 959-968.

[19]   Shinn, J. H. Visualization of complex hydrocarbon reaction systems. *Prepr. Pap. - Am. Chem. Soc., Div. Fuel Chem.* **1996**, *41*, 510-515.

[20]   Nomura, M.; Pugmire, R. J.; Moro-Oka, S. Fletcher, H. T.; Ye, C. *Personal communication report: molecular level characterization of carbonaceous resources of advanced utilization technologies*; *Preprints of Papers,* New Energy, and Industrial Technology Development Organization (NEDO): Japan, 1999.

[21]   Liu, Y.; Zhu, Y.; Li, W.; Zhang, C.; Wang, Y. Ultra micropores in macromolecular structure in subbituminous coal vitrine. *Fuel* **2017**, *210*, 298-306.

[22]   Attar, A.; Hendrickson, G. G. Functional groups and heteroatoms in coal. In *Coal Structure*; Meyers, R. A., Ed.; Academic Press: New York, 1982; pp 131−198.

4.   Oxidative coal dissolution: scoping experiments with OCD

Abstract

Oxidative coal dissolution (OCD) was studied through scoping experiments and oxidation was conducted under atmospheric conditions. The primary objective is to assess the impact of temperature and time on the oxidation conversion and product yields.

The comprehensive material balance of the OCD reactions ensures that the inputs and outputs of the system are properly accounted for. The experiments conducted at different temperatures and times showed an average material balance that closed within 2-3 %. Gas analysis was performed for feed air and gas products, focusing on the quantification of oxygen consumption and carbon dioxide production during the OCD reactions. The experiments conducted at different temperatures and times demonstrate that as these variables increase, oxygen consumption and carbon dioxide production also increase.

This chapter analyzed the yield to carbon as a measure of liquid product yield, focusing on the total carbon content in the obtained liquid extract. The findings indicated that based on the experiments developed at atmospheric pressure, within a temperature range of 65 °C to 95 °C, and with a reaction time span of 15 minutes to 4 hours, the higher temperatures and longer reaction time increase the oxidation conversion and product yields in OCD. However, the carbon yield from OCD leading to liquid product production is exceedingly low, with less than 1% in most cases. This low carbon yield has significant economic implications for large-scale applications, as the associated equipment costs would substantially increase, and operating expenses, particularly utilities costs, would represent a considerable portion of the overall expenses. Consequently, the process of oxidative coal dissolution at these specific conditions is unlikely to be economically viable for generating high-value products.

Keywords: Temperature, Oxidation, Time, OCD

4.1   Introduction

Coal oxidation at mild conditions, was first investigated to elucidate spontaneous combustion of coal during storage, and specifically oxidative coal dissolution, was mainly used looking to understand coal constitution [1][2][3]. Later, it was considered a potentially effective method for converting low rank coal into small molecules to produce commercial value-added chemicals in high yields. However, as it is presented in Chapter 2, Section 2.3.3 typical work reported for oxidative coal dissolution (OCD) has been developed in alkaline or acid media, with alkaline media being the most widely used method, including when oxygen is used as the oxidant. The importance, possible advantages, and challenges of pH changes have been described in the same section. Some of the most characteristic products obtained after coal oxidation at mild conditions and changing operating variables such as oxidant and pH are described in Chapter 2, Section 2.4 and divided by functional groups.

Previous studies on coal oxidation in aqueous media have not considered the economic and environmental impact of scaling the conversion process to an industrial level. As the amount of reactants increases, the cost of oxidants and alkalis becomes increasingly significant. Furthermore, the reaction conditions, such as temperature and pressure, impact the cost of construction materials (Capital Expenditures) and utilities (Operational Expenditures). Additionally, the utilization of alkalis would necessitate the implementation of specific units for water treatment (Capital Expenditures) and the ongoing use of additives (Operational Expenditures) for neutralization prior to final disposal.

In this chapter, an initial set of experiments for OCD is developed at atmospheric conditions, with temperatures up to 95 °C, where it is not necessary to make use of a pressurized system to maintain the reaction in liquid phase. The initial scope includes changes in temperature and time to mainly evaluate the impact on oxidation conversion and products yield.

4.2   Experimental

4.2.1   Materials

Coal from the northwest area of Canada (Alberta and Saskatchewan) was utilized as the feedstock for the oxidative coal dissolution process, which is the focus of this study. The coal's characterization is provided in Chapter 3. Table 4-1 presents the proximate and elemental analysis of the samples used in the experiments conducted in this chapter at different temperatures (same sample used for characterization in Chapter 3) and different times (sample from same batch of coal and characterization presented here).

Table 4-1 Characterization of Mancal coal for reactions at atmospheric pressure at different temperature and different time periods

Description	Feed OCD Temperatures		Feed OCD Time	
Proximate Analysis (wt%)[a]	**x**	**s**	**x**	**s**
Moisture	26.5	0.02	25.8	0.02
Volatile matter	30.5	0.32	30.4	0.32
Fixed Carbon	32.8	0.25	30.6	0.33
Ash	10.2	0.59	13.2	0.01
Elemental Analysis (wt%, maf)[b]				
Carbon	71.7	0.17	72.3	0.31
Hydrogen	4.1	0.22	4.4	0.29
Nitrogen	1.3	0.01	1.4	0.01
Sulfur	0.8	0.01	0.3	0.00
Oxygen[c]	22.0	-	21.5	-
H/C molar ratio (mol/mol)	0.69	-	0.73	-
O/C molar ratio (mol/mol)	0.23	-	0.22	-
Gross heating value[d] (MJ/kg)	26.3	-	27.0	-

[a]Averages (x) and sample standard deviations (s) of duplicate analyses
[b]Calculated on a moisture, ash-free basis using elemental and proximate Analysis
[c]Oxygen was determined by difference
[d]Calculated on the basis of Dulong's correlation

The elemental distribution of Mancal's Coal feed, employed in experiments conducted at various time intervals, is presented in Figure 4-1. Additionally, Table 4-2 presents the weight percentages corresponding to individual mineral elements detected in the sample through SEM-EDS analysis. The coal sample underwent analysis in five distinct regions, with the table providing the mean

weight percentages and standard deviations for each element, based on multiple measurements taken within each region. While the majority of metals are evenly distributed throughout the sample, the presence of conspicuous bright sites or mineral chunks, such as silicon and aluminum, notably increased in comparison to the feed employed in experiments conducted at different temperatures. This observation may elucidate the observed rise in weight percentages for these elements, as depicted in Table 4-2.
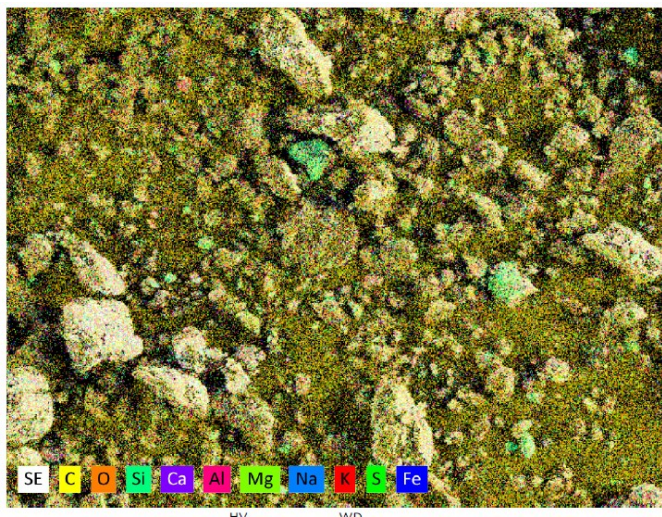
Figure 4-1 Secondary Electron image from Mancal's Coal elemental distribution in SEM-EDS (Map/Spectrum) for feed to OCD with changes on time.

Table 4-2 Main mineral elements identified in Mancal's coal for feed to OCD to study changes with oxidation time.

Element	Wt Percentage in coal (%)[a]	
	x	**s**
Si	3.37	1.66
Al	3.05	1.37
Ca	1.37	0.52
Na	0.76	0.21
Fe	0.38[b]	-
S	0.25	0.07
Mg	0.24	0.07

[a]Averages (x) and sample standard deviations (s) of five different measures
[b]Those elements were only detected in one of the areas mapped

Chemicals, cylinders and calibration substances employed in this study are shown in Table 4-3. Milli-Q water was prepared using a Millipore water purification system.

Table 4-3 Materials employed in Oxidative coal dissolution at different operating conditions

Compound	Formula	CASRN [a]	Mass fraction purity [b]	Supplier
Chemicals				
Calcium Chloride Anhydrous	$CaCl_2$	10043-52-4	-	Fisher Chemical
Toluene	C_7H_8	108-88-3	0.999	Fisher Chemical
Cylinder gases				
Air	N_2/O_2	132259-10-0	>99%[c]	Linde
Calibration materials				
Buffer Solution pH 10:				Fisher Chemical
▪ Water	H_2O	7732-18-5	0.9780	
▪ Potassium Carbonate	K_2CO_3	584-08-7	0.006	
▪ Potassium Borate	$B_4K_2O_7$	1332-77-0	0.004	
▪ Potassium Hydroxide	KOH	1310-58-3	0.002	
▪ Disodium EDTA Dihydrate	$C_{10}H_{18}N_2Na_2O_{10}$	6381-92-6	0.010	
Buffer Solution pH 7:				
▪ Water	H_2O	7732-18-5	0.9918	Fisher Chemical
▪ Dihydrogen potassium phosphate	KH_2PO_4	7778-77-0	0.007	
▪ Sodium Hydroxide	NaOH	1310-73-2	0.001	
▪ FD&C Yellow No. 5	$C_{16}H_9N_4Na_3O_9S_2$	1934-2-0	0-0.0002	
Buffer Solution pH 4:				
▪ Water	H_2O	7732-18-5	0.9891	
▪ 1,2-Benzenedicarboxylic acid, monopotassium salt	$C_8H_5KO_4$	877-24-7	0.0010	Fisher Chemical
▪ Formaldehyde	CH_2O	50-00-0	0.0005	
▪ Methyl alcohol	CH_3OH	67-56-1	0.0002	
▪ Fluorescein, 2',4',5',7'-tetraiodo, disodium salt	$C_{20}H_6I_4Na_2O_5$	16423-68-0	0.0002	

[a] CASRN = Chemical Abstracts Services Registry Number
[b] This is the purity of the material guaranteed by the supplier; material was not further purified
[c] Mole fraction purity

4.2.2 Equipment and procedure

Grinding Coal

To conduct each experiment, a modification was made to the grinding procedure described in Chapter 3. The original grinding process, which utilized the Disk Miller Bico UA, was replaced with a Rest Ball Miller. This substitution was implemented due to the use of the disk miller which

belongs to the faculty of science-Earth & atmospheric Sciences was temporary while procuring a permanent miller in our facilities. As a result, the ball miller became accessible and available for use in the coal laboratory.

The primary distinction between the disk miller and the ball miller lies in their respective principles of operation. The disk miller operates by grinding coal through the interaction of two rotating discs. Coal is introduced between the discs, and the combined rotational motion and applied pressure facilitate the crushing and grinding of the coal. On the other hand, the ball miller employs a bowl containing stainless steel balls. As the container rotates, the balls cascade and collide with the coal, crushing it. The grinding of coal in the ball miller occurs due to the impact and friction generated by the collisions between the balls and the coal particles.

In this case, Mancal's coal sample was grinded using a Retsch Ball Mill type PM100. The grinding bowl was filled with approximately 80 g of coal and stainless steel balls. Specifically, the bowl contained 7 large balls with a diameter of 20 mm and 27 small balls with a diameter of 10 mm. The grinder was set to run for 5 minutes at 500 rpm to ensure thorough grinding of the coal particles.

After grinding, the coal particles were separated by size in a Ro-Tap sieve shaker for approximately 5 minutes with the objective to obtain a coal particle size of less than 0.1 mm, which corresponds to mesh 140 according to the ASTM E-11 Standard Cole-Palmer. Any coal particles that did not pass through mesh 140 was grinded and separated again one more time using the same conditions.

This process was repeated for each oxidation experiment to ensure consistency in the particle size of the Mancal's coal sample used. The resulting grinded and sieved coal particles were then stored in an airtight plastic bag at 4 °C before they are used as the starting material for each experiment.

Reaction setup

Oxidative coal dissolution at different temperatures (65 to 95 °C for 4 hours) and time (15 to 120 minutes at 95 °C) conditions was carried out in a batch reaction system. The first step was to

measure 500 mL of Milli-Q water using two Fisherbrand volumetric flasks of 250 mL each with ±0.12 mL tolerance. The pH of Milli-Q water was measured using an Oakton PC700 pH/mV/Conductivity/°C/°F meter. 0.25 L of water was then added to a 2 L three neck round bottom flask (reactor) followed by the addition of approximately 20 g of coal and then the three neck round bottom flask was filled with the remaining 0.25 L of Milli-Q water.

To control the reaction temperature, a Fischer Scientific Isotemp heater plate was used. The flask was stirred at 300 RPM using an octagonal magnetic Fisherbrand Stir Bar 2X3/8. The three-neck round bottom flask was equipped with a reflux condenser to condense volatile products from the reaction system. The chilled water supply to the condenser was maintained at 5 °C.

Once the heating started and the target temperature was reached, the system was allowed to stabilize for 10 minutes before the reaction started. Oxidation of coal was conducted with extra-dry air from a Praxair cylinder. The air stream flow was measured and controlled through an Airgas112-02-N flowmeter, with a flow rate of 348.7 mL.min^{-1} into the reactor. The stirring mechanism was simultaneously activated.

The gas stream going out the reactor and reflux condenser flowed through a cold trap to ensure liquid-free off-gas. The liquid-free off-gas then passed through a gas washing bottle with a calcium chloride ($CaCl_2$) bed to absorb any additional water vapor. The off-gas flow was measured in an Airgas 112-02-N flowmeter before it was analyzed online with a series 9600 oxygen and carbon dioxide gas analyzer from Alpha Omega Instruments and a Extorr mass spectrometer.

For oxidative coal dissolution at different temperatures, the experiments were carried out at 65 °C, 75 °C, 85 °C and 95 °C for 4 hours. When the reaction time changed, experiments were carried out at 15, 30, 60, and 120 minutes at 95 °C. After the 4-hour reaction time, the air supply, stirring, and heat supply were stopped, and the resultant mixture was allowed to reach room temperature. A diagram of the equipment employed is shown in Figure 4-2.
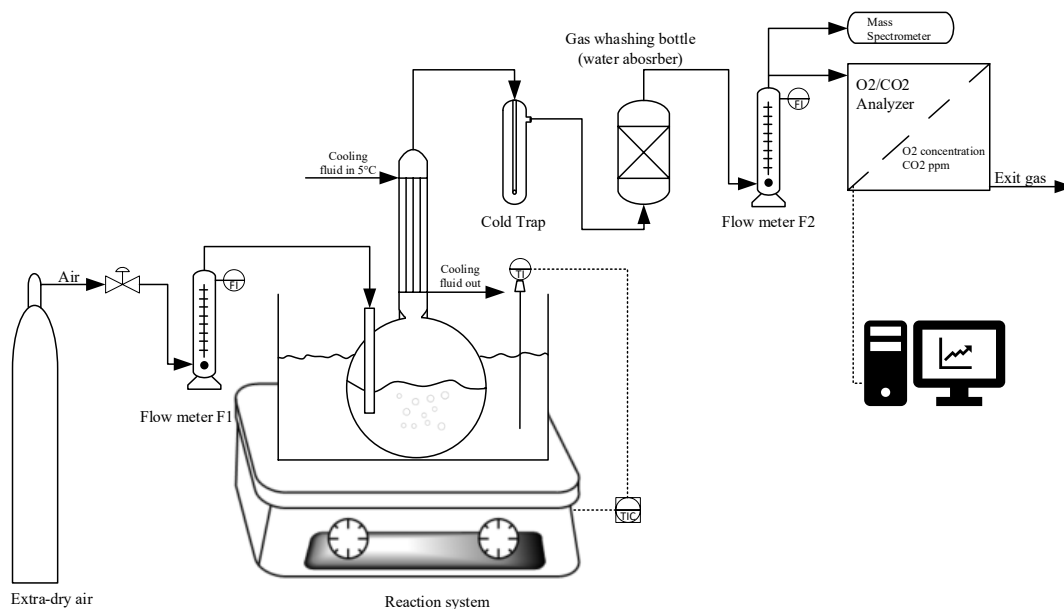
Figure 4-2 Experimental Setup for oxidative coal dissolution at ambient pressure

Residue and extract recovery

The resulting mixture obtained from the reaction process was first transferred to 50 mL corning centrifuge tubes with the addition of 50 mL of Milli-Q water by a Fisherbrand volumetric flask of 50 mL with ±0.05 mL tolerance. The purpose of adding water was to collect any solid remnant that might be present in the 2 L three-neck round bottom flask. The mixture was then centrifuged in a Eppendorf 5430 centrifuge at 6000 rpm for 15 minutes. The supernatant was collected, and the residue is centrifuged one more time at 6000 rpm for 15 minutes.

Most of the residue was then collected in pre-weighted aluminum foil weighing dishes, while part of it remained stuck at the bottom and surface of the corning centrifuge tubes. The aluminum foil weighing dishes and corning centrifuge tubes were then placed in a fume hood for 24 hours to facilitate the collection of the remaining coal from the tubes. The additional coal was then collected in another pre-weighted aluminum foil weighing dish. The collected residue was dried in a Temp Cole-Parmer vacuum oven for 2 hours at 6 kPa (60 mbar) absolute pressure and a temperature ramp from 20 °C to 73 °C to remove any remaining water content. Finally, the residue was left in a fume hood for 2-3 days to attain a constant weight. A Mettler Toledo XS105 balance, with an readability of 0.01 mg, was used to weigh the samples.

The resulting supernatant (extract) was collected and combined in an Erlenmeyer flask . The extract was then filtered using a vacuum filtration system with pre-weighted 1.5 μm glass microfiber filter and 0.22 μm membrane filter paper (Millipore). The filters were then dried in the fume hood for 2-3 days before final weighing. To measure the final extract pH, an Oakton PC700 pH/mV/Conductivity/°C/°F meter was used. A process flow diagram with the main steps of the procedure developed in the laboratory is shown in Figure 4-3. This diagram provides a clear picture of the steps and the operating conditions involved in the process, starting from the grinding process to the final solid and liquid products.
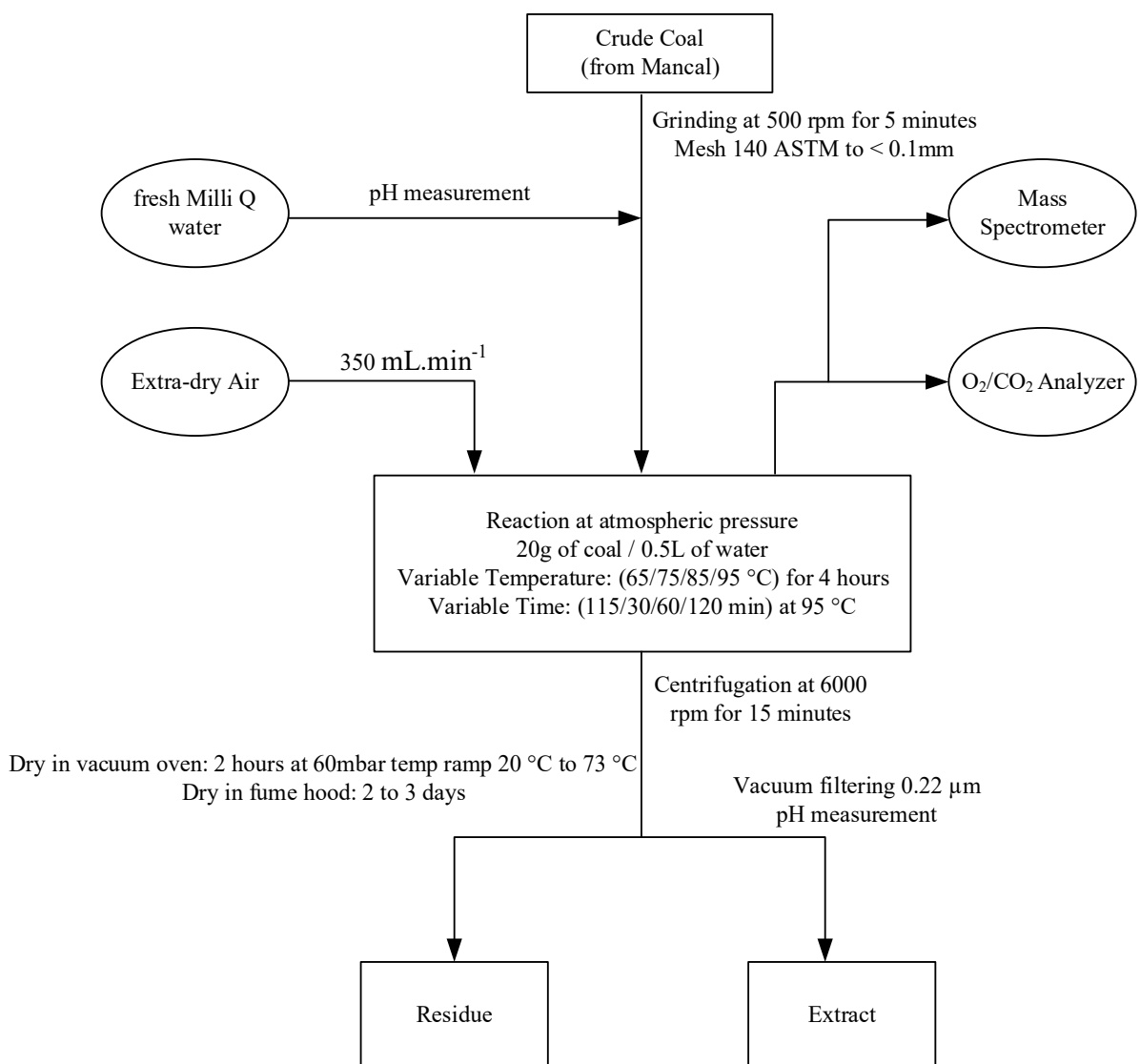
Figure 4-3 Laboratory Process Flow diagram

4.2.3 Analyses

Proximate and elemental analyses and scanning electron microscope (SEM) coupled with energy dispersive X-ray spectroscopy (EDS) performed in this set of experiments was described in Chapter 3.

The gaseous product of the reaction system was directed through an Alpha Omega Instruments Series 9600 A oxygen and carbon dioxide analyzer. The analyzer was equipped with an electrochemical sensor utilizing an Enhanced Electrolyte System (EES), which employed a weak acid electrolyte to generate an electrical signal proportional to the concentration of oxygen in the gas sample. The sensor had a measurement range spanning from 0 to 100%. To detect the concentration of carbon dioxide in the gas sample, the analyzer utilized a non-dispersive infrared (NDIR) sensor which did not undergo any chemical reaction with the gas. The NDIR sensor had a measurement range of 0 to 5000 parts per million (ppm) for carbon dioxide.

The gaseous product from the reaction system was analyzed by directing it through an Extorr mass spectrometer. This type of mass spectrometer is commonly used to analyze gases and vapors by ionizing the sample molecules, separating them based on their mass-to-charge ratio, and detecting these ions. The operational process of the Extorr mass spectrometer involves introducing the sample into a vacuum system, ionizing the sample molecules using an ion source, accelerating the ions into the mass analyzer, which separates the ions based on their mass-to-charge ratio, detecting the ions that pass through the mass analyzer using a detector, and analyzing the resulting mass spectrum to identify the different types of ions present in the sample and their relative abundances. This provides detailed information about the composition of the sample.

The Total Organic Carbon (TOC) content of liquid samples was determined by the Natural Resources Analytical Laboratory at the University of Alberta using a Shimadzu TOC-L CPH Model Total Organic Carbon Analyzer equipped with an ASI-L autosampler. The TOC analyzer is based on a method that measures the quantity of non-purgeable organic carbon (NPOC) in water and soil extracts. The NPOC is measured by adding 1M HCl to an aliquot of the water or soil extract to acidify it, then sparging the sample to remove any purgeable organic and inorganic

carbon. The resulting sample is then injected into a combustion tube that contains platinum catalyst beads and is maintained at a temperature of 720 °C. This causes an oxidation reaction to occur that generates carbon dioxide gas (CO_2), which is detected by a non-dispersive infrared (NDIR) detector to determine the NPOC concentration. To determine the Total Inorganic Carbon (TIC) content of the sample, an aliquot of the sample is injected into a bubble chamber. Then, phosphoric acid (25%) is added to the sample, which reacts with any inorganic carbon present to generate CO_2. The CO_2 generated is then passed through the NDIR detector for TIC analysis.

The density of liquid feed water and the aqueous phase of the extract is measured using the Anton Paar 4500M digital density meter. This device utilizes a U-shaped glass tube that undergoes oscillation at a specific frequency determined by the sample being analyzed. By analyzing the frequency of oscillation, the density of the sample can be accurately determined. Prior to each measurement, the density meter is thoroughly cleaned using toluene and subsequently dried with air for 5 minutes. For every sample, three measurements were taken at a temperature of 20 °C.

4.2.4 Calculations

Calculations for oxygen weight composition, moisture, ash-free basis elements compositions and heating values based on proximate and elemental analyses results of solid coal were described in Chapter 3. In this chapter the same calculations were applied to the coal residue after OCD.

The quantification of O_2 consumption and CO_2 production involves a numerical integration applied to the recorded data obtained from the oxygen and carbon dioxide analyzer. The integration method allows for the calculation of the total amount of O_2 consumed and CO_2 produced throughout the reaction period. This is achieved by summing up the values computed using equations 4.1 and 4.2, which determine the sum of oxygen consumption and carbon dioxide production rates every 10 seconds for a range from zero seconds to the time of each reaction duration.

Considering that the flowmeters were initially calibrated in milliliters per minute ($mL.min^{-1}$), the recorded readings for both the feed air and product gas flows are divided by six. This conversion

is necessary to obtain the flow rate per 10-second interval, which aligns with the reading range of the oxygen and carbon dioxide analyzer and matches the time subinterval length required for the numerical integration process.

$$O_2\text{consumed(g)} = \delta_{O2} * \left(\sum_{i=0}^{n}\left(\frac{1}{6}F_{in(i)} * O_{2in(i)} - \frac{1}{6}F_{out(i)} * O_{2out(i)}\right)\Delta x\right) \tag{4.1}$$

Where:

δ_{O2} = Density of O_2 calculated with the ideal gas equation at the reaction conditions (g.mL^{-1})

i = Time subinterval at which flows and fractions are measured

n = Number of time subintervals at which flows and fractions are measured

Δx = Each time subinterval length at which flows and fractions were measured (10 sec).

$F_{in(i)}$ = Flow of air coming into the reaction in at the specific time subinterval 'i' (mL.min^{-1})

$O_{2in(i)}$ = O_2 in air coming into the reaction at the specific time subinterval 'i' (Volume fraction)

$F_{out(i)}$ = Flow of gas product coming out of the reaction at the specific time subinterval 'i' (mL. min^{-1})

$O_{2out(i)}$ = Volume fraction of O_2 in gas product coming out of the reaction at the specific time subinterval 'i' measured in the oxygen and carbon dioxide analyzer

In the absence of a reaction, when the feed air is directly introduced into the oxygen and carbon dioxide analyzer, the concentration of CO_2 initially present and measured in the oxygen and carbon dioxide analyzer begins to decline. It takes approximately 30 seconds for the measured CO_2 concentration to reach zero, and it remains at zero indicating that the CO_2 content in the feed air is negligible and goes undetected by the oxygen and carbon dioxide analyzer. Therefore, for calculations involving equation 4.2, the "in" flow of CO_2 from feed air is assumed to be zero. CO_2 coming out of the reaction is divided by 1000000 to convert the ppm units to volume fraction.

$$CO_2\text{ produced(g)} = \delta_{CO2} * \left(\sum_{i=0}^{n}\left(\frac{1}{6}F_{out(i)} * \frac{CO_{2out(i)}}{1000000}\right)\Delta x\right) \tag{4.2}$$

Where:

δ_{CO2} = Density of CO$_2$ calculated with the ideal gas equation at the reaction conditions (g.mL^{-1})

i = Time subinterval at which flows and fractions are measured

n = Number of time subintervals at which flows and fractions are measured

Δx = Each time subinterval length at which flows and fractions were measured (sec). It is a 10 seconds subinterval

$F_{out(i)}$ = Flow of gas product coming out of the reaction at the specific time subinterval 'i' (mL. min^{-1})

$CO_{2out(i)}$ = CO$_2$ in gas product coming out of the reaction at the specific time subinterval 'i'(ppm) measured in the oxygen and carbon dioxide analyzer

The quantities of feed air and gas product, measured in grams, are also determined using a numerical integration technique. This method relies on computing the weighted average molecular mass with flow, considering the inlet and outlet flow rates at 10-second intervals, spanning from the beginning of the reaction to its completion. Specifically, Equation 4.3 is employed to calculate the total mass of feed air participating in each oxidative coal dissolution reaction. It assumes that the composition of the feed air remains constant throughout the process, with 21% oxygen (O$_2$) and 79% nitrogen (N$_2$)

$$Feed\ Air\ (g) = \left(\sum_{i=0}^{n} \frac{1}{6} F_{in(i)} \left(\delta_{O2} * O_{2in(i)} + \delta_{N2} * N_{2in(i)}\right)\Delta x\right) \tag{4.3}$$

Where:

i = Time subinterval at which flows and fractions are measured

n = Number of time subintervals at which flows and fractions are measured

Δx = Each time subinterval length at which flows and fractions were measured (sec). It is a 10 seconds subinterval

δ_{O2} = Density of O$_2$ calculated with the ideal gas equation at the reaction conditions (g.mL^{-1})

δ_{N2} = Density of N$_2$ calculated with the ideal gas equation at the reaction conditions (g.mL^{-1})

$F_{in(i)}$ = Flow of air coming into the reaction in at the specific time subinterval 'i' (mL.min^{-1})

$O_{2in(i)}$ = O_2 in air coming into the reaction at the specific time subinterval 'i' (Volume fraction)

$N_{2in(i)}$ = N_2 in air coming into the reaction at the specific time subinterval 'i' (Volume fraction)

Equation 4.4 is utilized to compute the overall mass of gas product generated by each oxidative coal dissolution reaction. Some assumptions are considered. Firstly, N_2 from the feed air is considered inert and does not actively participate in the reaction. Therefore, the N_2 content in the gas product is assumed to be the same as that in the feed air. Additionally, apart from carbon CO_2, no other gas products are generated, as discussed in the context of carbon yield to gases in Equation 4.9 and Section 4.3.4. Finally, the concentrations of oxygen O_2 and carbon dioxide CO_2 are measured at 10-second intervals using an oxygen and carbon dioxide analyzer.

$$Product\ Gas\ (g) = \left(\sum_{i=0}^{n}\left(\frac{1}{6}F_{in(i)} * \delta_{N2} * N_{2in(i)} + \frac{1}{6}F_{out(i)} * \delta_{O2} * O_{2out(i)} + *\frac{1}{6}F_{out(i)} * \delta_{CO2} * \frac{CO_{2out(i)}}{1000000}\right)\Delta x\right) \quad (4.4)$$

Where:

i = Time subinterval at which flows and fractions are measured

n = Number of time subintervals at which flows and fractions are measured

Δx = Each time subinterval length at which flows and fractions were measured (sec). It is 10 seconds subinterval

δ_{O2} = Density of O_2 calculated with the ideal gas equation at the reaction conditions (g.mL^{-1})

δ_{N2} = Density of N_2 calculated with the ideal gas equation at the reaction conditions (g.mL^{-1})

δ_{CO2} = Density of CO_2 calculated with the ideal gas equation at the reaction conditions (g.mL^{-1})

$F_{in(i)}$ = Flow of air coming into the reaction in at the specific time subinterval 'i' (mL.min^{-1})

$N_{2in(i)}$ = N_2 in air coming into the reaction at the specific time subinterval 'i' (Volume fraction)

$F_{out(i)}$ = Flow of gas product coming out of the reaction at the specific time subinterval 'i' (mL.min^{-1})

$O_{2out(i)}$ = Volume fraction of O_2 in gas product coming out of the reaction at the specific time subinterval 'i' measured in the oxygen and carbon dioxide analyzer

$CO_{2out(i)}$ = CO_2 in gas product coming out of the reaction at the specific time subinterval 'i' (ppm) measured in the oxygen and carbon dioxide analyzer

The weight of carbon or oxygen in feed and residue is calculated with equations 4.5 and 4.6. Feed(g) represents the Mancal coal previously grinded and used as feed in each OCD reaction. Residue(g) is the solid product after each reaction at different temperatures or time. The weight percentage of moisture (moisture%) and ash (ash%) are obtained from the proximate analysis, and the weight percentage of each carbon(carbon%) is acquired from the elemental analysis. The methodology used for determining the increase in oxygen content of a residue as compared to the oxygen content of the feed involves the application of identical equations and analytical techniques.

$$\textit{Carbon in } \textbf{feed(g)} = \frac{\textbf{feed(g)}*(\textbf{100}-\textbf{moisture}\%-\textbf{ash}\%)*\textit{carbon}\%_{in\,feed}}{\textbf{10000}} \tag{4.5}$$

$$\textit{Carbon in } \textbf{residue(g)} = \frac{\textbf{residue(g)}*(\textbf{100}-\textbf{moisture}\%-\textbf{ash}\%)*\textit{carbon}\%_{in\,residue}}{\textbf{10000}} \tag{4.6}$$

Once carbon weight in feed and residue is calculated on moisture-ash-free basis, carbon yield to residue products (unconverted carbon) is calculated dividing the carbon weight of residue by the carbon weight present in the feed. Carbon's yield to residue is calculated by equation 4.7.

$$\textbf{Carbon Yield \% (residue)} = \frac{\textit{Carbon in residue(g)}}{\textbf{Carbon in feed(g)}} * \textbf{100} \tag{4.7}$$

The calculation of carbon yield to liquids involves dividing the organic carbon content obtained from total organic carbon (TOC) analysis and reaction liquid volume by the carbon weight present in the feed, which is determined on a moisture-ash-free basis. This calculation is expressed in Equation 4.8.

$$\textbf{Carbon Yield \% (Liquids)} = \frac{\textit{carbon in liquid(g)}}{\textbf{Carbon in feed(g)}} * \textbf{100} \tag{4.8}$$

Based on the findings from the mass spectrometer analysis of the product gas, there are signals that may suggest the presence of carbon in the gas products in the form of methane (CH_4), carbon monoxide (CO), or carbon dioxide (CO_2). However, the presence of signals at specific mass-to-charge ratios (amu) such as 14, 16, and 28 are not conclusive about the identification of CH_4 or

CO due to the same signals are also observed in the spectrum of the air feed. These signals may originate from compounds and ions present in the feed air, as discussed in Section 4.3.4 of the study. Therefore, while the presence of CH_4 and CO cannot be entirely ruled out in the gas product, they are not considered in the calculations for carbon yield to gases.

On the other hand, the presence of a CO_2 signal at amu 44 exclusively in the gas product confirms the production of this compound. This is supported by measurements obtained from the oxygen and carbon dioxide analyzer. The distinct presence of CO_2 at amu 44 in the gas product validates its production during the reaction. Carbon yield to gases calculation includes dividing the mass of carbon present in the carbon dioxide (CO_2) as calculated in equation 4.2, by the mass of carbon in the feed material. This calculation is expressed in Equation 4.9.

$$\textbf{Carbon Yield \% (gases)} = \frac{carbon\ in\ gases(g)}{\textbf{Carbon in feed}(g)} * \textbf{100} \tag{4.9}$$

To determine the increase in oxygen content of residue as compared to the oxygen content of the feed involves the application of identical equations and analytical techniques than those applied for carbon content in feed and residue. The calculations are shown in equations 4.10 and 4.11.

$$\textit{Oxygen in }\textbf{feed}(g) = \frac{\textbf{feed}(g)*(\textbf{100}-\textbf{moisture\%}-\textbf{ash\%})*oxygen\%_{in\ feed}}{\textbf{10000}} \tag{4.10}$$

$$\textit{Oxygen in }\textbf{residue}(g) = \frac{\textbf{residue}(g)*(\textbf{100}-\textbf{moisture\%}-\textbf{ash\%})*oxygen\%_{in\ residue}}{\textbf{10000}} \tag{4.11}$$

4.2.5 Calibrations

Oakton PC700 pH/mV/Conductivity/°C/°F meter

pH calibration was performed with known accurate standards, buffer solutions of pH 4.01, 7.00 and 10.01 (Thermo Scientific) according to the equipment manual procedure.

Alpha Omega Instruments Series 9600 A oxygen and carbon dioxide analyzer

Oxygen calibration was performed with Extra-dry Praxair Air regulated at 200 kPa. An additional ball valve was installed after the regulator for safety reasons to avoid any possibility of pressure changes downstream. Power was applied to the Series 9600 Oxygen and Carbon Dioxide Analyzer and, there was a waiting time of 20 minutes to allow the instrument to warm up. The calibration gas flow rate was set to a nominal 0.25 standard $L.min^{-1}$. Then, there was an additional waiting time of at least 5 minutes until a stable reading had been established and the value of the oxygen reading was adjusted as required. The reading from the LCD should reflect the oxygen concentration of the calibration gas. Therefore, adjustments were performed on the instrument board accordingly, so the value displayed in the LCD is identical to that of the value of the calibration gas.

For the Carbon dioxide analyzer, factory calibration was maintained with a concentration range between 250 and 450 ppm under room conditions.

Airgas 112-02-N Flowmeters

The flowmeters used for calibration were rotameters which consists of a conical tube with a float inside. The operating principle of this rotameter involves the measurement of the flow rate based on the height of the float within the meter. As the fluid passes through the conical tube, the float rises. When there is no flow, the float stays at the bottom. The scale on the flow meter is calibrated in millimeters (mm) to indicate the position of the float.

Flowmeters were calibrated with Extra-dry Praxair Air regulated at 200 kPa. An additional ball valve was installed after the regulator for safety reasons to enable shutoff of the air flow. Air flowed to the inlet of the flowmeter and the flow rate of the outlet line was controlled within the flowmeter using a needle control valve. Discharge air volume was transferred and recorded in a 0.5L Ritter Flowmeter during different periods of time (2, 5 and 10 minutes). The Ritter Flowmeter works on the principle of positive displacement. The sample gas flow turns the measuring cylinder that is usually placed in water or low viscosity white oil. A dial gauge and a counter connected to

the cylinder measures and records the gas flow rate of the sample as it fills and pours out of fixed volume measurement partitions.

The measurement scale of the flow meter ranges from 0 to 160 mm, and calibration was performed at intervals of 10 mm. The resulting calibration curves for both flow meters were analyzed using linear regression, and the coefficient of determination (R^2) was found to be greater than 0.99 for both cases.

4.3   Results

4.3.1   Material balance

The products resulting from the oxidative coal dissolution reaction can be considered as a multiphase system containing gaseous, liquid, and solid components. In Table 4-4 and Table 4-5, the measured values to calculate the material balance of the reactants entering the system "in" and the products exiting the system "out" is presented for the 4-hour reaction conducted at temperatures ranging from 65 to 95 °C and for the 95 °C reactions conducted for durations ranging from 15 to 120 minutes, respectively.

The mass balance determination involves various procedures and instruments to ensure accurate measurements. The mass of the feed coal is determined by weighing the coal sample after the grinding process, prior to its introduction into the reaction system. For the mass determination of the feed and washing water, the volume of the feed water is determined with two volumetric flasks of 250 mL with ±0.12 mL tolerance and a for the washing water a volumetric flask of 50 mL with ±0.05 mL tolerance is used. The density of water is determined using a density meter, allowing for the calculation of the corresponding mass.

The mass of the residue is determined by weighing the remaining coal after the completion of the reaction and subsequent drying process. To determine the mass of the extract, a similar procedure to the mass of water is followed. The volume of the first 500 mL of extract is experimentally determined with two volumetric flasks of 250 mL with ±0.12 mL tolerance. Once the 500 mL

89

mark is reached, any additional volume of extract is measured using a 100 mL capacity graduated cylinder with a readability of ±1.0 mL. The density is measured to a sample of the aqueous phase of the extract using a density meter and assuming it as representative of the whole extract sample. This information is used to estimate the mass of the entire sample. The water content in the residue represents the loss of water from the residue from the time it is collected from the centrifuge tubes until it is completely dried, and it is calculated by difference in the weight measured. This allows for the quantification of the water removed from the residue in the vacuum oven and the fume hood.

The calculation of water absorbed in $CaCl_2$ involves measuring the difference in mass of the absorber bed before and after each reaction. This change in mass indicates the amount of water absorbed by the $CaCl_2$ drying agent.

The quantities of feed air and gas product, measured in grams, are determined using a numerical integration of the weighted average molecular mass with the flow, considering the inlet and outlet flow rates at 10-second intervals, spanning from the beginning of the reaction to its completion as it is explained in Section 4.2.4 Calculations, Equations 4.3 and 4.4.

Table 4-4 Measurements used in material balance of OCD during 4 hours from 65 to 95 °C

Reaction Temperature (°C)	'In' (g)				'Out' (g)				
	Feed coal	Water		Feed air	Residue	Extract	Water from residue	Water absorbed in $CaCl_2$	Product gas
		Initial water	Washing water						
65	20.24	499.08	49.91	100.36	16.91	535.11	6.32	1.64	100.10
75	21.71	499.08	49.91	99.60	18.13	533.11	5.24	1.74	99.24
85	20.65	499.08	49.91	100.29	16.97	533.17	4.18	3.44	99.96
95	21.04	499.08	49.91	100.50	17.35	525.16	7.13	8.86	100.15

Table 4-5 Measurements used in material balance of OCD at 95 °C from 15 to 120 minutes

Reaction Time (min)	'In' (g)				'Out' (g)				
	Feed coal	Water		Feed air	Residue	Extract	Water from residue	Water absorbed in $CaCl_2$	Product gas
		Initial water	Washing water						
15	20.06	499.08	49.91	6.53	16.34	535.18	7.92	0.34	6.47
30	20.61	499.08	49.91	12.71	16.83	534.15	5.98	0.78	12.62
60	20.08	499.08	49.91	25.14	16.27	529.18	6.55	1.76	25.02
120	20.16	499.08	49.91	50.29	16.09	528.19	6.27	4.01	50.07

Table 4-6 presents the material balance, encompassing the conversion from reactants to products. The calculation takes into account the masses of coal, initial water, washing water and feed air as reactants coming 'in'. Additionally, it incorporates the masses of residue, extract, water from residue, water absorbed in $CaCl_2$ and product gas as products coming 'out'. Under those assumptions, experiments performed under different temperature and pressure conditions showed an average material balance that closed within 2-3 %.

Table 4-6 Material balance of OCD during 4 hours from 65 to 95 °C and at 95 °C from 15 to 120 minutes

Description	Total mass coming 'in'	Total mass going 'out'	Yield to products (%)
Reaction Temperature (°C)			
65	669.59	660.08	98.58
75	670.30	657.46	98.08
85	669.93	657.72	98.18
95	670.53	658.65	98.23
Reaction Time (min)			
15	575.58	566.25	98.38
30	582.31	570.36	97.95
60	594.21	578.78	97.40
120	619.44	604.63	97.61

4.3.2 Proximate and elemental analysis

In this study, proximate and elemental analyses were performed on the solid OCD products (residue) generated by reactions at different temperatures and reaction times. The results of these analyses are presented in Table 4-7 and Table 4-8 for reactions with varying temperatures and in Table 4-10 and Table 4-11 for reactions with varying times.

Table 4-7 Proximate Analysis of residue product from OCD during 4 hours from 65 to 95 °C

Description	Reaction temperature							
	65 °C		75 °C		85 °C		95 °C	
Proximate Analysis (wt%)[a]	X	S	X	S	X	S	X	S
Moisture	12.6	0.07	13.6	0.03	13.7	0.02	13.9	0.01
Volatile matter	37.1	0.27	36.6	0.14	36.9	0.01	36.7	0.21
Fixed Carbon	39.8	0.20	39.2	0.13	39.4	0.04	39.1	0.26
Ash	10.5	0.13	10.6	0.01	10.1	0.00	10.2	0.06

[a]Averages (x) and sample standard deviations (s) of duplicate analyses

Table 4-8 Elemental Analysis of residue product from OCD during 4 hours from 65 to 95 °C

Description	Reaction temperature							
	65 °C		75 °C		85 °C		95 °C	
Elemental Analysis (wt%, daf)[a]	X	S	X	S	X	S	X	S
Carbon	71.5	0.09	71.3	0.02	70.4	0.16	71.5	0.05
Hydrogen	3.5	0.04	3.2	0.02	3.1	0.02	3.3	0.03
Nitrogen	1.3	0.00	1.3	0.00	1.3	0.01	1.3	0.01
Sulfur	0.5	0.02	0.5	0.03	0.5	0.00	0.6	0.08
Oxygen[b]	23.1	-	23.7	-	24.7	-	23.3	-
H/C molar ratio (mol/mol)	0.59	-	0.54	-	0.53	-	0.54	-
O/C molar ratio (mol/mol)	0.24	-	0.25	-	0.26	-	0.24	-
Gross heating value[c] (MJ/kg)	25.2	-	24.6	-	23.9	-	24.7	-

[a]Averages (x) and sample standard deviations (s) of duplicate analyses. Calculated on a dry and ash-free basis using elemental and proximate Analysis
[b]Oxygen was determined by difference
[c]Calculated on the basis of Dulong's corelation

For reactions changing temperature, in the proximate analysis Table 4-7, the results show that at 65 °C moisture content is a little lower than for the other reaction temperatures, while the volatile matter, fixed carbon and ash remain relatively constant. The sample standard deviations for each analysis are relatively small, indicating good precision and reproducibility of the analytical results.

To assess the internal consistency of the analytical results, a comparison of the ash content from the coal feed to the ash content in the residue product was performed. Table 4-9 shows the change in ash content from the feed to the residue product at different reaction temperatures and sub-section 4.4.1 discuss the results.

Table 4-9 Change in ash content from feed to residue product from OCD during 4 hours from 65 to 95 °C

Description	Reaction temperature			
	65 °C	75 °C	85 °C	95 °C
Total ash in feed (g)	2.07	2.22	2.11	2.15
Total ash in residue (g)	1.78	1.92	1.71	1.79
Change in ash from feed to residue (g)	0.29	0.31	0.40	0.37
Change in ash from feed to residue (%)	14.0	13.7	19.1	17.0

In the elemental analysis Table 4-8, the results show that as the reaction temperature increases, for the residue there is a slight decrease in carbon and hydrogen content at temperatures up to 85 °C, while nitrogen, and sulfur remain relatively constant. Furthermore, the oxygen content and the O/C (oxygen-to-carbon) molar ratio display a slight increase as the temperature rises, specifically up to 85 °C. In contrast, the H/C (hydrogen-to-carbon) molar ratio exhibits a slight decrease with increasing temperature, again up to 85 °C.

Comparing the feed properties (Table 4-1) with the residue product properties (Table 4-7), there is a decrease in moisture and an increase in volatile matter and fixed carbon content, while ash content remains relatively constant. The carbon and nitrogen content remain relatively constant, while hydrogen, and sulfur content are lower in the residue products. The oxygen content is slightly higher in the residue product, consequently the H/C molar ratio is lower in the residue product while O/C molar ratio is higher.

Table 4-10 Proximate Analysis of residue product from OCD at 95 °C from 15 to 120 min

Description	Reaction time							
	15 min		30 min		60 min		120 min	
Proximate Analysis (wt%)[a]	x	s	x	s	x	s	x	s
Moisture	11.4	0.02	9.7	0.01	9.8	0.01	9.4	0.01
Volatile matter	36.1	0.32	36.7	0.02	36.4	0.06	36.6	0.21
Fixed Carbon	38.3	0.28	38.4	0.11	38.6	0.11	39.0	0.30
Ash	14.2	0.02	15.2	0.07	15.2	0.06	15.0	0.09

[a]Averages (x) and sample standard deviations (s) of duplicate analyses

Table 4-11 Elemental Analysis of residue product from OCD at 95 °C from 15 to 120 min

Description	Reaction time							
	15 min		**30 min**		**60 min**		**120 min**	
Elemental Analysis (wt%, daf)[a]	**x**	**s**	**x**	**s**	**x**	**s**	**x**	**s**
Carbon	71.8	0.71	71.5	0.75	72.0	0.28	71.5	0.04
Hydrogen	3.8	0.10	3.9	0.09	4.0	0.03	3.9	0.03
Nitrogen	1.3	0.01	1.4	0.01	1.4	0.02	1.4	0.02
Sulfur	0.3	0.02	0.3	0.03	0.4	0.00	0.3	0.03
Oxygen[b]	22.7	-	22.9	-	22.3	-	22.9	-
H/C molar ratio (mol/mol)	0.63	-	0.66	-	0.65	-	0.66	-
O/C molar ratio (mol/mol)	0.24	-	0.24	-	0.23	-	0.24	-
Gross heating value[c] (MJ/kg)	25.7	-	25.7	-	26.1	-	25.8	-

[a]Averages (x) and sample standard deviations (s) of duplicate analyses. Calculated on a dry and ash-free basis using elemental and proximate Analysis
[b]Oxygen was determined by difference
[c]Calculated on the basis of Dulong's corelation

For reactions changing time, In the proximate analysis Table 4-10, moisture content is a little higher at 15 minutes, than for the other reaction times, which is reflected in a lower ash contend while the volatile matter and fixed carbon remain relatively constant. With respect to the elemental analysis Table 4-11, there is not a specific trend to increase or decrease for elements with changes on time.

Regarding the feed properties with respect to the residue product, there is also a decrease in moisture and an increase in volatile matter, fixed carbon content and ash. On the other hand, only hydrogen shows a notable decrease in the residue products while oxygen content increase. Therefore, as in the reactions at different temperatures the H/C molar ratio is lower in the residue product while O/C molar ratio is higher.

Table 4-12 shows the changes in ash content which ranges from 6.3 % to 12.8 % for the varying reaction times studied. Sub-section 4.4.1 discusses the results.

Table 4-12 Change in ash content from feed to residue product from OCD at 95 °C from 15 to 120 min

Description	Reaction time			
	15 min	**30 min**	**60 min**	**120 min**
Total ash in feed (g)	2.65	2.73	2.66	2.67
Total ash in residue (g)	2.31	2.56	2.47	2.41
Change in ash from feed to residue (g)	0.34	0.17	0.18	0.26
Change in ash from feed to residue (%)	12.8	6.3	6.9	9.7

4.3.3 Total carbon to liquid extract

In the context of the analytical procedure for Total Carbon, during the TOC analysis, the non-purgeable organic carbon (NPOC) in the liquid extract is measured, which includes various organic carbon compounds present in the sample. Organic carbon compounds derived from coal dissolution may include a wide range of molecules that originate from the organic components of coal as it was presented in Chapter 2 section 2.4. These components may consist of aromatic and aliphatic hydrocarbons, as well as other organic functional groups like oxygenated compounds, nitrogen-containing compounds, and sulfur-containing compounds present in the coal.

During the TIC analysis, any inorganic carbon present in the liquid extract reacts with phosphoric acid, leading to the generation of CO_2. Inorganic carbon compounds originating from coal dissolution encompass carbon species that are not directly linked to the organic structure of coal but rather arise from mineral components present in the coal. These inorganic carbon compounds typically include carbonates and bicarbonates, which can be generated from the release of carbonates or other inorganic carbon sources during the dissolution process.

Table 4-13 and Table 4-14 show the total carbon content in the liquid extract obtained from the Total carbon analysis performed to the liquid extract product of the 4 h reactions conducted at temperatures ranging from 65 to 95 °C and the reactions at 95 °C from 15 to 120 minutes respectively.

Table 4-13 Total carbon in liquid extract at 4 hours reaction and temperatures from 65 to 95°C

Reaction temperature (°C)	TOC (g)	TIC (g)	TC (g)
65	0.037	0.019	0.056
75	0.038	0.017	0.055
85	0.045	0.022	0.067
95	0.049	0.023	0.072

Table 4-14 Total carbon in liquid extract at 95 °C reaction and times from 15 to 120 minutes

Reaction time (min)	TOC (g)	TIC (g)	TC (g)
15	0.062	0.017	0.079
30	0.063	0.016	0.079
60	0.069	0.016	0.085
120	0.078	0.015	0.094

Table 4-13 shows that as the reaction temperature increases from 65 to 95 °C, the total organic carbon (TOC) values show a more pronounced increase than the total inorganic carbon (TIC) which values exhibit relatively minor variations, suggesting a more stable level of inorganic carbon content. Similarly, in Table 4-14 extending the reaction time from 15 to 120 minutes results in a consistent increase in TOC content, indicating the generation of organic carbon compounds over time. In contrast, the TIC values remain relatively constant, indicating a consistent level of inorganic carbon content.

4.3.4 Gases analysis

The oxygen (O_2) and carbon dioxide (CO_2) analyzer was able to detect the production of CO_2 and the changes in O_2 concentration from the gas stream going out the reactor every 10 seconds. Figure 4-4 and Figure 4-5 show the changes in O_2 percentage and CO_2 concentration from the recorded data during the 4-hour reaction at temperatures ranging from 65 to 95 °C. Between 12,000 and 12,100 seconds after the reactions started, the generation of CO_2 shows a relatively constant pattern at all temperatures, reaching a state of equilibrium. The concentration of CO_2 at this steady state for each temperature is noted in Figure 4-5.

As evidenced in Figure 4-4 and Figure 4-5, during the initial 10 minutes of the reaction (as shown in the zoomed-in graphs from 0 to 600 minutes), there was a marked increase in CO_2 concentration

as the reaction temperature increased. This increase in CO_2 production was accompanied by a concurrent decrease in O_2 percentage in the gas product at the outlet.
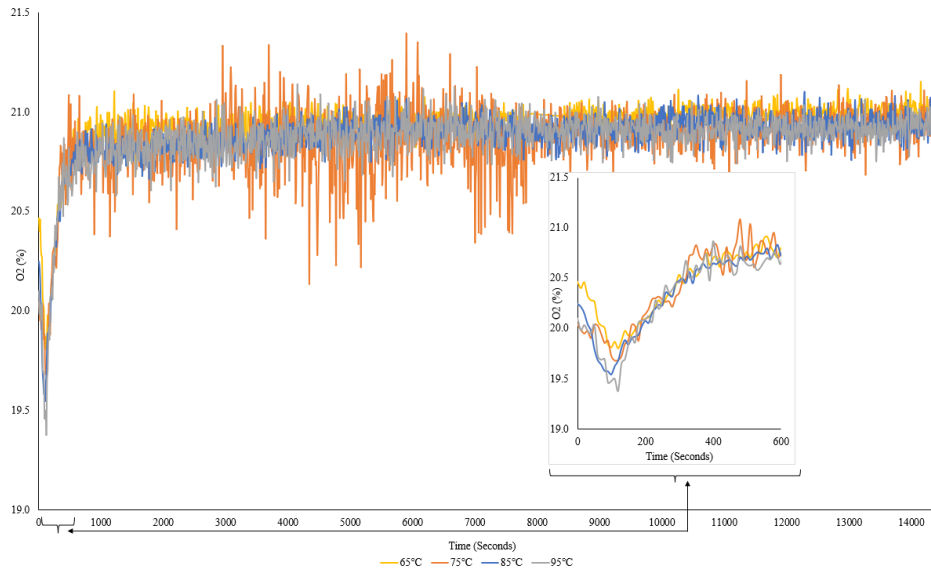
Figure 4-4 O_2 Percentage in gas product during OCD reaction at 4 h and temperatures from 65 to 95 °C.
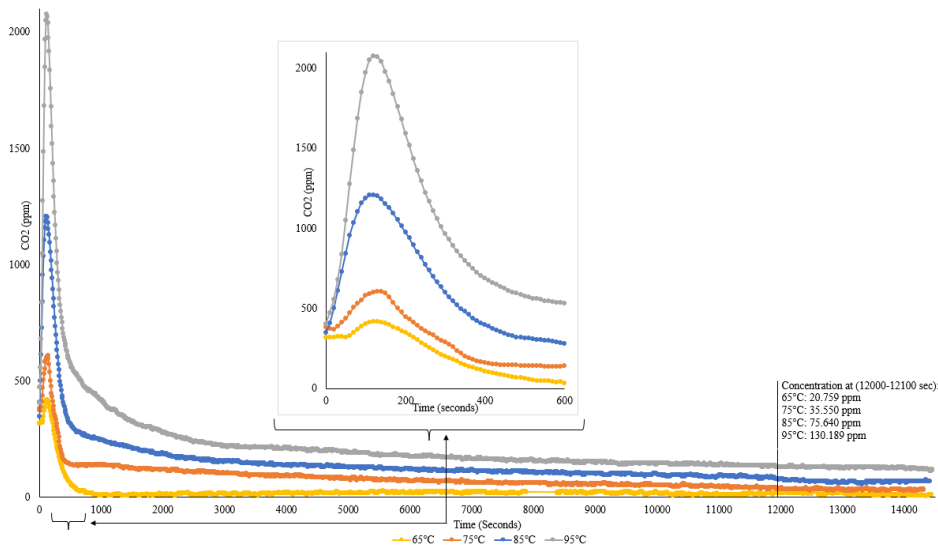
Figure 4-5 CO_2 concentration in gas product during OCD reaction at 4 h and temperatures from 65 to 95 °C.

Figure 4-6 and Figure 4-7 show the changes in O_2 percentage and CO_2 concentration from the recorded data during the reaction at 95 °C and times from 15 to 120 minutes.
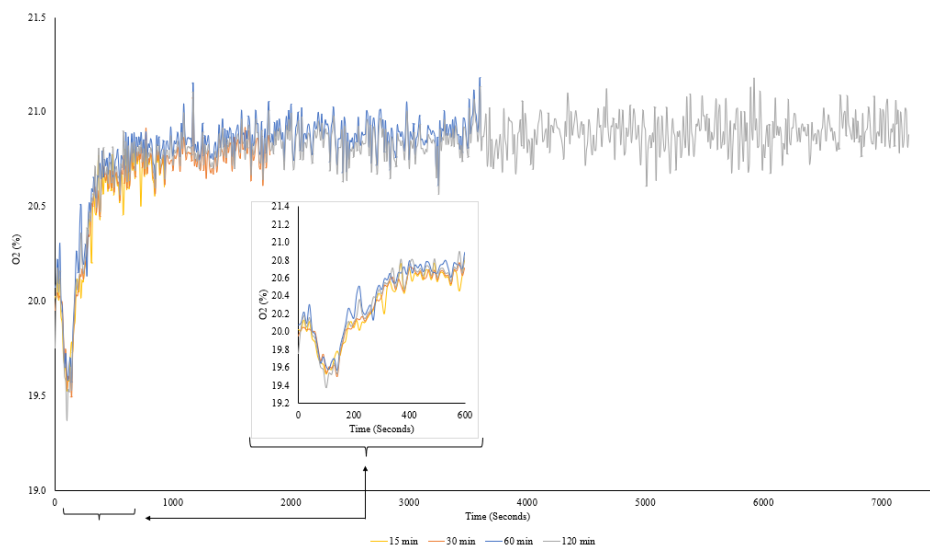
Figure 4-6 O_2 percentage in gas product during OCD reaction at 95 °C reactions from 15 to 120 minutes
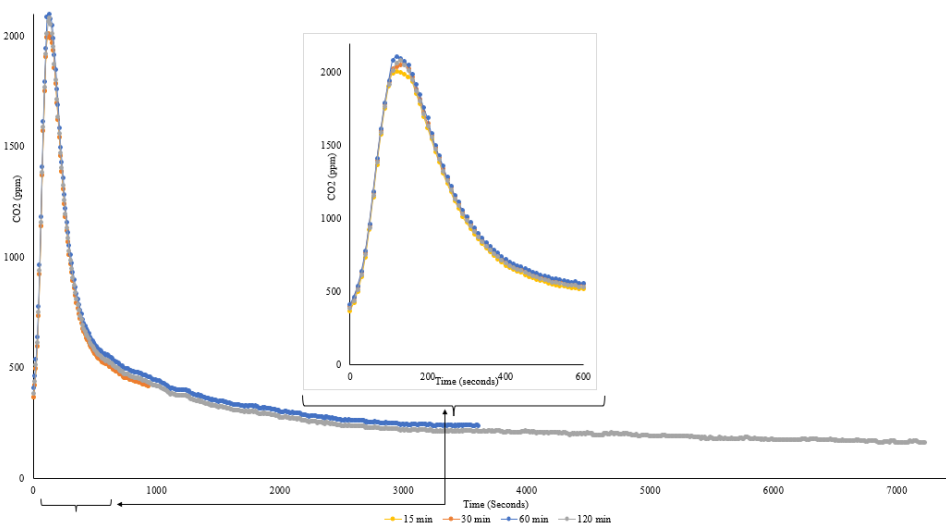
Figure 4-7 CO_2 concentration in gas product during OCD reaction at 95 °C reactions from 15 to 120 minutes.

Table 4-15 and Table 4-16 present the quantification of O_2 consumption and CO_2 production during the 4 h reaction conducted at temperatures ranging from 65 to 95 °C and at 95 °C reactions from 15 to 120 minutes respectively. The variations observed in the oxygen coming "in" to the 4 h reactions can be attributed to slight disparities in reaction time since the flow rate was always the same. The CO_2 coming "in" to the reaction is assumed as zero. This assumption is made based on the absence of measurable CO_2 concentrations if only feed air flows into the oxygen and carbon dioxide analyzer.

Table 4-15 O_2 consumed and CO_2 produced at 4 h reaction and temperatures from 65 to 95 °C.

Reaction temperature (°C)	Reaction time (min)	Oxygen O_2 (g)			CO_2 (g)		
		'In'	'Out'	consumed	'In'	'Out'	Produced
65	240.7	23.39	23.12	0.27	0	$3.75*10^{-3}$	$3.75*10^{-3}$
75	238.7	23.19	22.84	0.35	0	$1.21*10^{-2}$	$1.21*10^{-2}$
85	240.3	23.35	23.02	0.34	0	$2.15*10^{-2}$	$2.15*10^{-2}$
95	241.0	23.42	23.03	0.39	0	$3.37*10^{-2}$	$3.37*10^{-2}$

Table 4-16 O_2 consumed and CO_2 produced at 95 °C reactions from 15 to 120 minutes.

Reaction temperature (°C)	Reaction time (min)	Oxygen O_2 (g)			CO_2 (g)		
		'In'	'Out'	consumed	'In'	'Out'	Produced
95	15.5	1.52	1.46	0.07	0	$8.00*10^{-3}$	$8.00*10^{-3}$
95	30.3	2.96	2.86	0.10	0	$1.17*10^{-2}$	$1.17*10^{-2}$
95	60.2	5.86	5.72	0.14	0	$1.69*10^{-2}$	$1.69*10^{-2}$
95	120.5	11.72	11.48	0.24	0	$2.31*10^{-2}$	$2.31*10^{-2}$

From the Extorr mass spectrometer, online measurements of the mass-to-charge ratio were obtained for each gas product and reaction. Data points were collected at intervals of 5 minutes, and after the first 30 minutes, the interval was extended to 10 minutes. The online data revealed fluctuations in the peak intensities over time. However, the spectrum consistently exhibited specific peaks at particular mass-to-charge ratios throughout the reactions. Figure 4-8 presents the spectrum derived from the reaction conducted at a temperature of 95 °C after a duration of 5 minutes.

From the Extorr mass spectrometer, the mass-to-charge ratio at different counts per second from each gas product of each reaction was measured online and the data from specific points of the reaction (initially each 5 minutes, and after the first 30 minutes, each 10 minutes). The data online showed variations in the intensity of the peaks over time, but the spectrum consistently exhibited the same peaks at specific mass-to-charge ratios during the reaction. The spectrum displayed in Figure 4-8 was obtained from the product gas reaction at 95 °C and after 5 minutes. The signal intensities in the spectrum are represented on a logarithmic scale with a base of 10. To provide a reference for comparison, the spectrum for the feed air was also included. It is important to acknowledge that during the data acquisition process, there were indications of background noise

in the signal range between 1E-11 and 1E-10 counts per second. Therefore, in order to present a clear and meaningful representation of the data the diagram was plotted starting from 1E-11 counts per second, thereby excluding the potentially unreliable noise range.
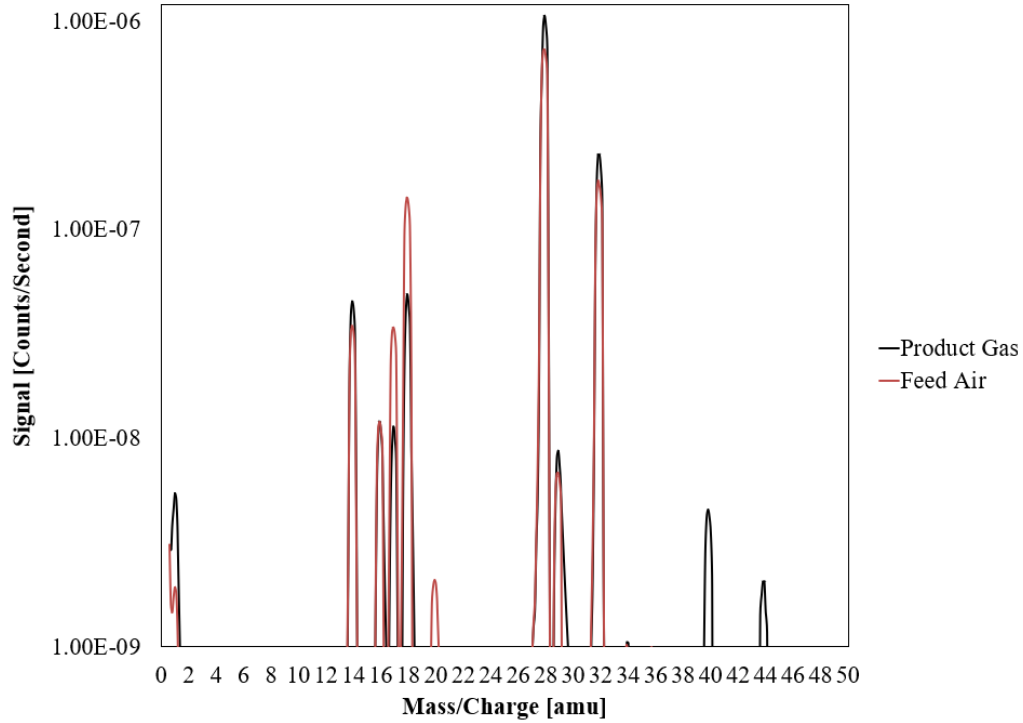
Figure 4-8 Feed air and reaction product gas gases mass spectrum

Table 4-17 shows the specific signal in counts per second at the mass-to-coal ratio for the peaks identified in Figure 4-8.

Table 4-17 Mass-to-charge ratio versus signal

Mass-to-charge ratio (amu)	Signal (counts.second^{-1})	
	Feed Air	**Product gas**
1	1.93E-9	5.43E-9
14	3.23E-8	4.19E-8
16	1.09E-8	1.06E-8
18	1.31E-7	4.40E-8
28	6.68E-7	9.51E-7
32	1.44E-7	1.95E-7
40	-	3.53E-9
44	-	1.46E-9

Comparing both lines in the Figure 4-8 and Table 4-17 they show that most of the compounds or ions identified in the product gas are also present in the feed air. The peak observed at mass-to-charge ratio (amu) 1 may represent hydrogen ions and hydrogen molecules originating from ionized water. These ions may have resulted from residual moisture that remained in the system after the reaction process, as indicated by the more pronounced peak intensity in the product gas line compared to the feed air, where water content should be minimal.

The peak at amu 14 in feed air and most probably in product gas may correspond to the presence of ionized nitrogen, which is a prevalent component of air and serves as the oxidizing component of the reaction. The peak at amu 16 may correspond to ionized oxygen, another common component of air. This peak may also represent other ionized molecules, such as oxygen derived from compounds like water, or carbon monoxide and carbon dioxide that could have been generated during the reaction. However, for these compounds to be responsible for the observed peak, a corresponding peak at amu 12, corresponding to the carbon ion, would also be expected. Yet, no such peak is evident in the mass spectrum, indicating that the carbon-containing compounds mentioned above are unlikely to be the source of the observed peak at mass-to-charge ratio 16. Another possible compounds present in the product gas and represented at the peak at amu 14 or 16 are those that derivate from methane that could be generating during the oxidation of coal.

The peak at mass-to-charge ratio 18 could indicate the presence of water, which may have resulted from residual moisture that could not be removed in the preceding process steps. However, the feed air which has no moisture also presents the same peak. The peaks at amu of 28 and 32 are likely attributed to larger molecules that are not ionized from the ambient air, such as molecular nitrogen, carbon monoxide and molecular oxygen. These molecules have molecular masses of approximately 28 amu and 32 amu, respectively, which coincide with the detected peaks.

In addition to the previous observations, the mass spectrum reveals two peaks exclusively associated with the product gas at amu 40 and 44. The peak observed at amu 40 could be attributed to ionized calcium derived from the calcium chloride bed utilized to remove any residual water vapor post reaction and prior to entering the mass spectrometer, However, there is not a counter

ion for Ca shown in the spectrum. Instead, it is more plausible that the peak observed at amu 40 belongs to argon (Ar) which ingress from air due to the high vacuum environment intrinsic to the mass spectrometer and incompletely sealed connections. This would also explain why N2 (28 amu) and O2 (32 amu) in the product gas is higher than in the feed. On the other hand, the peak at amu 44 suggests the potential presence of carbon dioxide, indicating that this peak likely represents carbon dioxide generated during the reaction.

4.3.5 Carbon balance

Carbon content in coal is an essential indicator of the reaction yield for oxidative coal dissolution. Since coal is the only feed reactant with carbon in its structure, all the possible valuable products obtained after the reaction, including carboxylic acids and other products, as explained in Chapter 2 section 2.4 on products of coal oxidation, contain this element. Therefore, the presence of carbon serves as a crucial factor for assessing the effectiveness and efficiency of the OCD reaction.

The tabulated data in Table 4-18 and Table 4-19 represent the carbon balance for the reactions at atmospheric pressure, as a function of temperature and time. It details the quantities of carbon present in the coal feed before the reaction 'in', as well as in the residue, extract (liquid product) and gases 'out' after the reaction has taken place. The carbon coming 'in' to the reaction refers to the carbon content present in the coal feed. This carbon content is determined by conducting proximate and elemental analyses, considering a moisture and ash-free basis.

Regarding the carbon coming 'out' of the reaction, the carbon in the resulting residue represents the carbon content in the solid residue obtained after the reaction. This carbon content is also calculated by conducting proximate and elemental analyses, considering a moisture and ash-free basis. The carbon content in the liquid extract is measured by performing total organic carbon (TOC) and total inorganic carbon (TIC) analyses at a specific volume of extract obtained from the reaction. The quantity of carbon released in the form of carbon CO_2 gas during the reaction is calculated based on the percentage of carbon present in the CO_2 produced and calculated in the gas analysis section.

Table 4-18 Carbon balance at 4 hours reaction and temperatures from 65 to 95 °C.

Reaction temperature (°C)	In (g)	Out (g)		
	Carbon in feed	Carbon in residue[a]	Carbon in extract	Carbon in CO_2
65	9.18	9.30	0.056	$1.02*10^{-3}$
75	9.85	9.80	0.055	$3.30*10^{-3}$
85	9.37	9.11	0.067	$5.87*10^{-3}$
95	9.55	9.40	0.072	$9.19*10^{-3}$

Table 4-19 Carbon balance at 95 °C reaction and times from 15 to 120 minutes.

Reaction time (min)	In (g)	Out (g)		
	Carbon in feed	Carbon in residue	Carbon in extract	Carbon in CO_2
15	8.85	8.74	0.079	$2.18*10^{-3}$
30	9.09	9.04	0.079	$3.19*10^{-3}$
60	8.86	8.78	0.085	$4.60*10^{-3}$
120	8.89	8.70	0.094	$6.29*10^{-3}$

From the carbon balance in Table 4-19 and Table 4-20 carbon yield to products can be calculated. Table 4-20 and Table 4-21 provide information on the product yield for carbon balance in the different products, which serves as a quantitative measure of the efficiency of the process in terms of converting reactants into desired products.

Table 4-20 Carbon Yield at 4 hours reaction and temperatures from 65 to 95 °C.

Reaction temperature (°C)	Carbon Yield (%)		
	Solid	Liquid	Gas
65	101.26	0.61	0.11
75	99.45	0.56	0.33
85	97.23	0.72	0.63
95	98.52	0.76	0.96

Table 4-21 Carbon Yield at 95 °C reaction and times from 15 to 120 minutes.

Reaction time (min)	Carbon Yield (%)		
	Solid	Liquid	Gas
15	98.73	0.89	0.25
30	99.45	0.87	0.35
60	99.15	0.96	0.52
120	97.86	1.05	0.71

Experiments performed under different temperature conditions showed an average material balance that closed within 4 %. The material balance was between 98 and 102 %. For the experiments performed at different times, the average material balance closed within 2% with a material balance between 99 and 101 %.

4.3.6   Oxygen change from coal feed to residue

The assessment of oxygen change from the solid to the residue product also serves to identify the portion of oxygen consumption by the solid residue in the reaction. Table 4-22 and Table 4-23 show the quantitative measurement of oxygen change from solid feed to residue varying reaction conditions.

Table 4-22 Oxygen change in coal from feed to residue at 4 hours reaction and temperatures from 65 to 95 °C

Reraction temperature (°C)	Oxygen in feed[a] (g)	Oxygen in residue[a] (g)	change in oxygen (g)
65	2.82	3.00	0.18
75	3.03	3.25	0.23
85	2.88	3.20	0.32
95	2.93	3.07	0.13

[a] Calculated on a moisture, ash-free basis as a difference between the weight of feed and residue

Table 4-23 Oxygen gain in coal from feed to residue at 95 °C reaction and times from 15 to 120 minutes.

Reraction time (min)	Oxygen in feed[a] (g)	Oxygen in residue[a] (g)	Gain in oxygen (g)
15	2.63	2.77	0.13
30	2.70	2.90	0.19
60	2.63	2.72	0.09
120	2.65	2.78	0.14

[a] Calculated on a moisture, ash-free basis as a difference between the weight of feed and residue

The results show that there is a gain in oxygen with all reactions, regardless of the specific reaction condition. This is evident from the positive values of the oxygen change reported. However, the data also indicates no clear or direct relationship between the gain in oxygen and any specific reaction condition, such as temperature or reaction time.

4.3.7 pH

To ascertain the level of acidity of the liquid products and the extent of its alteration from the initial state of fresh milli Q water, pH measurement was carried out after the reaction and successive extraction. The results obtained are presented in Table 4-24 and Table 4-25.

Table 4-24 pH of liquid products at temperatures from 65 to 95 °C.

Description	Reaction temperature							
	65 °C		75 °C		85 °C		95 °C	
pH[a]	X	S	X	S	X	S	X	S
Fresh Milli Q water	7.98	0.04	8.10	0.30	7.83	0.01	7.89	0.03
Extract	7.19	0.01	7.37	0.01	7.18	0.02	7.13	0.04

[a]Averages (x) and sample standard deviations (s) of duplicate analyses

Table 4-25 pH of liquid products at time from 15 to 120 minutes.

Description	Reaction time							
	15 min		30 min		60 min		120 min	
pH[a]	X	S	X	S	X	S	X	S
Fresh Milli Q water	7.63	0.03	7.13	0.01	6.67	0.02	6.83	0.01
Extract	7.25	0.01	7.01	0.01	6.59	0.01	6.42	0.01

[a]Averages (x) and sample standard deviations (s) of duplicate analyses

In certain measurements, fresh Milli-Q water exhibits a higher pH value than the anticipated neutral pH. There are some potential reasons for this observation. On the one hand is the possible presence of certain water-soluble minerals, such as sodium, potassium, magnesium and calcium carbonate and bicarbonate minerals [4], which have the potential to elevate the pH of water. However, it is highly unlikely for these minerals to be present in Milli Q water, as the water purification system employs a range of purification techniques specifically designed to eliminate such contaminants.

On the other hand, prior to each measurement of the pH for the fresh Milli-Q water and the extract there was a calibration procedure conducted there was a calibration process performed every time before the fresh Milli Q water and extract pH were measured. The calibration protocol started with the solution buffer pH 7 as it is recommended by the equipment vendor. Then, the calibration

proceeded with the buffer pH 4.01 and finally with the buffer 10.01. After each calibration step, the electrode was rinsed with fresh Mili Q water, and dried with a soft tissue, and then the actual pH measurement was performed. However, considering that the most recent calibration involved the alkaline buffer, it is possible that the electrode might not have been entirely clean, potentially retaining alkali contaminants that could have contributed to the observed variation in the pH measurements.

To prove the aforementioned hypothesis, a new calibration protocol was conducted, starting with the solution buffer with a pH 7 and switching following the buffer calibrations with the buffer pH 10.01 first, and finally with the buffer pH 4.01. Following the completion of this protocol, the pH of the Milli-Q water was measured, yielding results within the range of 6 to 6.5 in four separate measurements. This finding supports the hypothesis that the most probable cause of contamination is associated with the final buffer calibration solution.

Regarding the extract pH measurement, if it is considered that the alkali contamination due to the calibration process of the pH meter was the reason for an increase in the pH of fresh milli Q water, it also affects the extract pH value since the same calibration procedure was also performed prior to measuring the extract pH. Table 4-24 and Table 4-25 show that the pH values of all the liquid products indicate an increase in acidity when compared to the initial Milli-Q water for reactions temperature and time. This deviation in pH before and after the reaction suggests the presence of acidic components in the liquid extracts.

4.3.8 Scanning electron microscope with energy dispersive X-ray spectroscopy SEM-EDS

Some secondary electron images were taken using Scanning Electron Microscopy SEM to examine potential variations in residue products resulting from OCD under different temperature and time conditions. The resulting SEM images, as depicted in Figure 4-9 and Figure 4-10, illustrate the residue morphology observed under these conditions. Based on the analysis of these images, it appears that any changes in texture or morphology of the coal and minerals present are negligible.
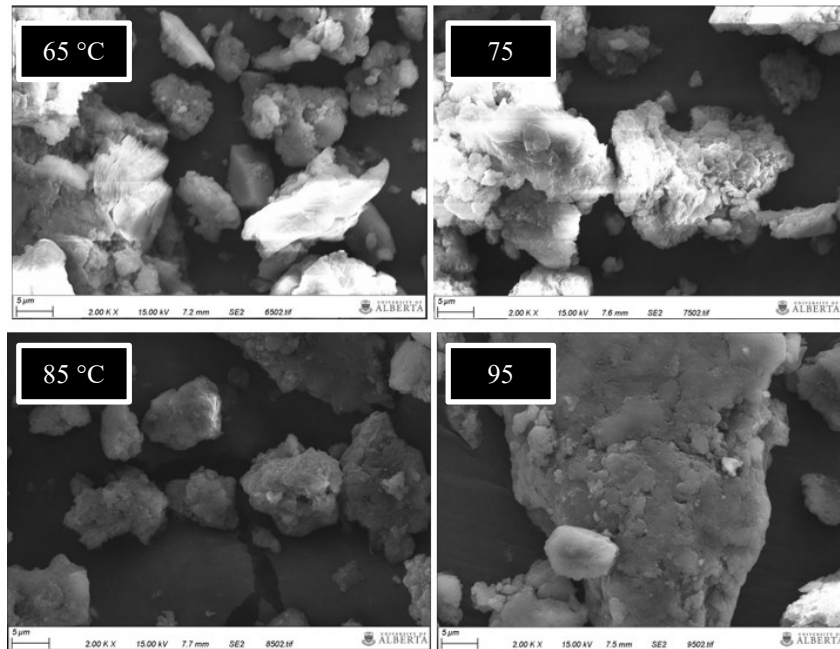
Figure 4-9 Secondary electron images taken to residue after reaction temperatures from 65 to 95 °C during 4 hours in SEM-EDS
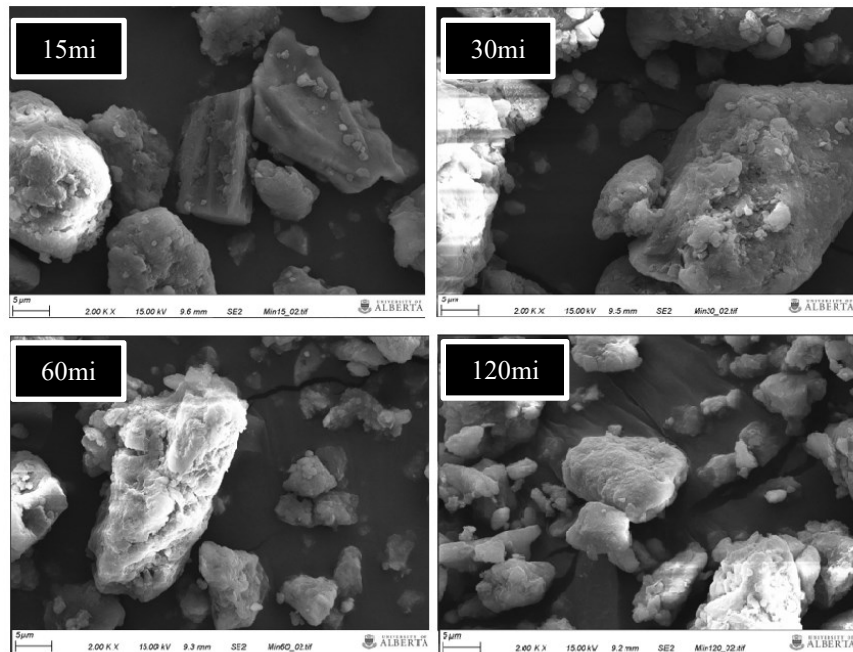
Figure 4-10 Secondary electron images taken to residue after reaction times from 15 to 120 minutes at 95 °C in SEM-EDS

To the residue product of each specific reaction, secondary electron images from elemental distribution in SEM-EDS (Map/Spectrum) were also taken. The results showed that as the

Mancal's coal characterization in chapter 3 section 3.3.3 major metals identified seemed to be finely dispersed in the samples. The percentage of each mineral in the sample based on the intensity of the X-ray peaks was also quantified and the results are present in Table 4-26 and Table 4-27. Each sample was analyzed between five and seven specific areas. The results provide the average weight percentages for each element based on the multiple measurements taken.

Table 4-26 Main mineral elements identified in Mancal's coal after reactions at 4 hours reaction and temperatures from 65 to 95 °C with SEM-EDS

Element	Wt Percentage in coal (%)[a]							
	65 °C		75 °C		85 °C		95 °C	
	x	s	x	s	x	s	x	s
Si	1.46	0.46	2.18	2.79	2.22	2.33	1.40	1.53
Al	1.09	0.14	1.34	1.71	1.46	1.53	0.95	0.75
Ca	1.97	0.21	1.82	0.68	2.16	0.79	2.44	1.24
Na	0.60	0.12	0.62	0.22	0.63	0.18	0.63	0.24
Fe	0.43	0.07	0.54	0.23	0.77	0.50	0.72	0.37
S	0.38	0.10	0.38	0.12	0.39	0.16	0.36	0.26
Mg	0.19[b]	-	0.40	0.11	0.43	0.07	0.28	0.19

[a]Averages (x) and sample standard deviations (s) of five different measures
[b]Those elements were only detected in one of the areas mapped

Table 4-27 Main mineral elements identified in Mancal's coal after reactions at 95 °C and times from 15 to 120 minutes with SEM-EDS

Element	Wt Percentage in coal (%)[a]							
	15 min		30 min		60 min		120 min	
	x	s	x	s	x	s	x	s
Si	2.89	2.15	0.99	0.42	1.95	2.23	1.30	0.95
Al	2.37	1.57	1.05	0.27	1.83	2.05	1.44	0.61
Ca	1.55	0.44	1.61	0.60	1.84	0.86	1.26	0.43
Na	0.86	0.18	0.85	0.12	0.73	0.27	0.61	0.24
Fe	0.46	0.06	0.59	0.23	0.32[b]	-	0.35[b]	-
S	0.50	0.26	0.34	0.15	0.31	0.11	0.27	0.10
Mg	0.25	0.04	0.25	0.05	0.26	0.08	0.24	0.04

[a]Averages (x) and sample standard deviations (s) of five different measures
[b]Those elements were only detected in one of the areas mapped

The results indicate that the residue samples contain the major minerals associated with coal in chapter 2, section 2.2.3 (Al/Na/Si/Mg-Clay, Ca-carbonates, Si-Silicates, Fe-sulfides) and those found in feed characterization in chapter 3 section 3.3.3, Among these minerals, Si, Al, and Ca are identified as the most abundant metals, with a weight percentage ranging from 1 to 3 in coal. This results also exhibit coal heterogeneity, since, for some metals there is a noticeable variation in element composition between residual samples with different reaction times. As an example, the weight percentage of Si in the residual sample with a reaction time of 15 minutes is approximately 3%, whereas in the residual sample with a reaction time of 30 minutes, it is less than 1%.

4.4   Discussion

4.4.1   Change in ash content from coal feed to residue

Through the analytical comparison, it is observed that the ash content in the residue product showed a decrease compared to that in the feed coal across all reaction temperatures and times. While this trend does not adhere to the assumption of ash conservation, the percentage changes in ash content remained relatively moderate. The apparent decrease in ash content indicates that certain transformations, loss, or removal of ash may occur during the reaction process.

Taking into account the information presented in Table 4-2 regarding the notable metal content, specifically sodium (Na), calcium (Ca), and magnesium (Mg) concentrations in the feed coal, as well as the data shown in Table 4-13 and Table 4-14 indicating the presence of total Organic Carbon (TOC) and some total Inorganic carbon (TIC) in the liquid extract, and the pH measurements provided in Table 4-24 and Table 4-25 which show the pH of the liquid extract, it is reasonable to contemplate the potential formation of carboxylate salts involving Na, Mg, and Ca in the liquid extract and also carbonates or bicarbonates, which can be generated from the release of carbonates or other inorganic carbon sources of coal during the dissolution process in the liquid extract.

Given the pH conditions in the liquid extracts (pH 6-8), it is more likely the formation of metal carboxylates in the aqueous phase, resulting from the transformation of carboxylic acids, and it becomes the most pertinent consideration. As the pH is higher than the pKa value for most of the carboxylic acids [5], the solution is relatively basic. Therefore, the concentration of H^+ ions is lower, favoring the deprotonation of the carboxylic acid. The carboxylate ion ($RCOO^-$) is more prevalent in solution to form the metal carboxylates, contributing to the shift in ash content from coal feed to residue. Consequently, it is conceivable that metal carboxylates are present in the liquid extract (aqueous phase), potentially accounting for the reduction of ash in the solid residue.

4.4.2 Oxygen consumed and Carbon dioxide produced

The consumption of O_2 in the process is significantly higher than the production of CO_2. This observation can be attributed to the role of molecular oxygen O_2 as the primary oxidant in the reaction. O_2 functions as a reactant during the oxidative coal dissolution process, leading to the formation of liquid products. Furthermore, O_2 is also responsible for incorporating oxygen into the resulting extract and residue product. Consequently, the consumption of O_2 is considerable due to its involvement in various reaction pathways, as presented in Chapter 2, Section 2.3.3, and its substantial contribution to the overall oxidation process.

Also, as presented in the reaction mechanism discussed in Chapter 2 and proposed by *Clements et al* [6] the gas product stream does not exclusively consist of CO_2 as the product. It may also contain at least CO as another gaseous product which is also formed during the oxidation of coal. The generation of CO can be a product of the partial oxidation of carbonaceous compounds in coal where even if there is not a deficiency of oxygen (there is plenty of oxygen bubbling in the reaction system) it may require other conditions such are more solubility of the oxygen in the liquid phase by increasing pressure and/or more energy to facilitate the complete oxidation of coal by increasing temperature. In previous investigations related to coal oxidation, CO/CO_2 show a shifting ratio across distinct temperature ranges. Specifically, those findings denote a ratio of 1.3 at 65 °C, a reduction to 0.6 within the temperature ambit of 125-150 °C, and a further decline to 0.4 at 300 °C [6].

4.4.3 Carbon balance and yield

The yield in oxidative coal dissolution described in this chapter, intent to identify the amount of desired products obtained from the reaction, compared to the amount of coal feed used as the reactant. In this case, the desired products are carboxylic acids and other valuable products, which contain carbon from the coal feed and are described in Chapter 2, section 2.4.

The total carbon to liquid data in Table 4-13 and Table 4-14, carbon balance data in Table 4-18, Table 4-19 and carbon yield in Table 4-20 and Table 4-21 provide an insight into the effectiveness and efficiency of the OCD reaction in terms of carbon utilization. On the one hand, from the results on the total organic carbon dissolved in the liquid extract, it is confirmed that organic carbon is present in the liquid extract and tends to increase as the reaction temperature and time increase. This indicates that higher temperatures and longer reaction times favor the conversion of coal into liquid products with the expected functional groups from coal oxidation, which is desirable in terms of maximizing the yield of the reaction. However, the maximum yield to liquids is less than 1% at almost all the experimental conditions. This could be an indication that the reaction conditions may not be very effective in terms of producing the desired products from the feed coal.

The observation of concentration of total inorganic carbon (TIC) in the liquid product of oxidative coal dissolution provides insights into the interaction dynamics of mineral matter and liquid extract during the OCD and at the same time strengthen the hypothesis of the decrease in ash content in residue due to the dissolution of mineral matter in liquid extract. The identification of TIC content suggests that there is a transfer of mineral matter from the coal feed to the liquid extract, specifically in the form of carbonates and bicarbonates. With changes in temperatures, there is an increase in mineral matter content in the liquid extract as the temperature increases to 85 °C and 95 °C. This increase in mineral matter concentration may be attributed to enhanced reactivity and higher rates of coal dissolution at higher temperatures, leading to a more substantial release of carbonates and bicarbonates into the liquid phase. However, in the reactions conducted at a constant temperature of 95°C with varying reaction times, the total mineral matter content tends to stabilize and remain relatively constant. This finding may indicate that at the temperature of 95 °C, the release of mineral matter from the coal is not sensitive with changes in reaction time.

111

In reference to the aggregate content of total organic carbon (TOC) within the liquid extract, its concentration is attributed to the presence of salts originating from carboxylates, as expounded upon in section 4.4.1. These carboxylate salts are generated from precursor compounds of carboxylic acids generated from OCD, which encompass formates, acetates, oxalates, and comparable chemical species.

Regarding carbon balance analysis for gas products, the determination of carbon is solely on carbon dioxide (CO_2) generation. The consideration is specifically limited to the quantification of CO_2 gas produced during the oxidative coal dissolution (OCD) reaction. The carbon balance calculation does not account for the generation of carbon from carbon monoxide (CO) in the gaseous product, even though, as it was discussed in section 4.4.2 it is produced during the oxidation of coal [7]. While the exact mechanisms can depend on the specific conditions and compounds involved, a few general factors could potentially lead to decarbonylation without CO oxidation during oxidative coal dissolution, the intermediate species formed during coal dissolution which can interact with the carbonyl groups, promoting decarbonylation as shown in the mechanism proposed by *Clements et al* [6], and the temperature conditions due to, decarbonylation reactions might be favored over CO oxidation due to differences in energy barriers. However, for the purpose of the carbon balance analysis presented here, the assessment focuses only on CO_2. While this approach allows for quantifying the carbon content released as CO_2 gas, it may result in an underestimation of the overall carbon yield. This is particularly relevant considering that the carbon yield is observed to be low under the studied reaction conditions.

On the other hand, carbon balance results also indicate an increase of carbon from feed to residue at 65 °C, which is physically impossible since even at zero conversion to gas or liquid products, the quantity of carbon present in the solid residue cannot exceed that which was present in the initial feed coal. But it could indicate no conversion of carbon to liquid or gas products at those specific conditions. However, results also show conversion to liquids and gases products in the reaction at 65 °C. This implies that some degree of conversion takes place at this specific temperature despite the lower conversion observed in the liquid and gas products.

The pH values of the resulting liquid product at 65 °C decreases compared to the original milli Q water used in the reaction. In the context of the discussion presented in section 4.4.1 and according to the Table 4-28 that shows the typical pK_a of some of the expected carboxylic acids product of OCD, it exhibit that the pK_a of all those carboxylic acids is lower than the pH of liquid extract. Despite the anticipated pK_a values of the carboxylic acids, a fraction of TOC is indeed identified within the liquid extract resulting from the reaction at 65 °C. This observation suggests the potential formation of carboxylic acids in the form of carboxylates products and provides further confirmation that oxidation indeed occurred at 65 °C.

Table 4-28 pK_a values of some of the expected carboxylic acids product of OCD [5][8][9]

Carboxylic acid	pK_a
Formic acid	3.75
Acetic acid	4.76
Oxalic acid	4.28
Propionic acid	4.87
Adipic acid	4.43
Butyric acid	4.82
Succinic acid	4.19
Benzoic acid	4.37

One possible explanation for the negative carbon balance at 65 °C could be the deviation error in the data due to the low yield. The small yield of desired products obtained from the reaction could be responsible for the relatively high standard deviation in the experimental results. Therefore, a higher number of replicates could potentially reduce the standard deviation and help to establish a more accurate carbon balance for the OCD reaction. Nevertheless, the data already available from the experiments performed and the literature reviewed in Chapter 2 section 2.3.4 suggest that higher temperatures will favor the conversion of coal into liquid products in the OCD reaction.

4.4.4 Economic viability of low yields in oxidative coal dissolution

The low yield in oxidative coal dissolution has significant economic implications in large-scale applications. Low carbon yield implies that a considerable amount of coal feed may be required to

generate a desirable amount of products. Consequently, the capital and operational costs associated with large-scale equipment needed for the process would increase significantly.

The economic feasibility of oxidative coal dissolution can be compared to processes associated at large scale such as mining, leaching and flocculation. For processes with hypothetical operations in common at large scale such as a gold plant, comminution (Crushing and milling) makes up to 21 % and leaching makes 7.5 % of the capital cost [10]. It means that with low carbon yields, the comminution equipment, the stirring motor, and the pump required for pumping air to the reaction will also increase exponentially, and that is just for mentioning some. Regarding operational costs, utilities represent over one-quarter of the total expenses [10]. Output energy requirements would be much higher. i.e. the energy required to pressurize and pump air or to stir the reactants in the reaction system due to the low yield of products would increase exponentially. The amount of air needed can vary depending on the size of the operation and other factors. The low yields mean that the process requires more inputs and energy to produce a given amount of output, including the cost of pumping air into the reactor. This process requires significant energy, and the cost of electricity can account for a significant portion of the operational costs.

The cost of mining coal can vary widely depending on the type of deposit, mining method, and other factors. However, *Winter et al*. [11] estimated that the capital cost for a surface mine including surface pits, waste rock disposal areas, a coal handling and processing plant and water management structures in about $800 million CAD, with operating costs of $90 CAD per ton of ore mined. In comparison, the comminution equipment alone for a large-scale oxidative coal dissolution process can make up to 21% of the capital cost, as mentioned in the previous paragraph. This means that a low yield of desirable products can significantly impact the economic feasibility of the process, as the necessary equipment costs would increase exponentially.

In consideration of the low carbon yield to liquid extract and the economic implications outlined, it is necessary to study the impact of higher reaction temperatures but keeping mild conditions within the range of 90 to 180 °C, along with elevated pressures of 5 MPa on the oxidative coal dissolution (OCD) process as presented in the next chapter. The fundamental premise underlying these operational changes implies that the application of elevated temperature and pressure

conditions will have notable modifications to carbon conversion and product distribution within the OCD.

4.5   Conclusions

- According to the carbon yield of liquid to liquid products resulting from the oxidative dissolution of coal, conducted within a temperature range of 65 °C to 95 °C for a duration of 4 hours, and at varying time intervals between 15 minutes to 120 minutes at a temperature of 95 °C, it can be inferred that even though the yield is very low, higher temperatures and prolonged reaction times tend to increase the transformation of carbon in coal to liquid products.

- The carbon yield from oxidative coal dissolution leading to the production of liquid products at atmospheric pressure, within a temperature range of 65 °C to 95 °C, and with a reaction time span of 15 minutes to 4 hours, is exceedingly low with less than 1% in most of the cases.

- The low carbon yield in this oxidative coal dissolution approach has significant economic implications for larger-scale applications due to high equipment and utility costs. Consequently, the process is economically unfeasible for generating valuable products. These results lead to the exploration of strategies to enhance carbon yield by increasing reaction temperature and therefore oxygen in air pressure.

4.6   References

[1]   Howard, H. C. Chemical constitution of coal: as determined by oxidation reactions. In *Chemistry of coal utilization. Vol.1*; Lowry, H. H. ed; Wiley: New York, 1945, pp.346-376.

[2]   Dryden, I. G. C. Chemical constitution and reactions of coal. In *Chemistry of coal utilization, Supplementary Volume*; Lowry, H. H. ed.; Wiley: New York, 1963, p. 232-295.

[3]   Francis, W. *Coal. Its formation and composition*, 2ed.; Edward Arnold: London, 1961.

[4]   Marion, M. G. Carbonate mineral solubility at low temperatures in the Na-K-Mg-Ca-H-Cl-SO$_4$-OH-HCO$_3$-CO$_3$-CO$_2$-H$_2$O system. *Geochimica et Cosmochimica* **2001**, *65* (12), 1883-1896.

[5]   Zeng, Y.; Chen, X.; Zhao, D.; Li, H.; Zhang, Y.; Xiao, X. Estimation of pK$_a$ values for carboxylic acids, alcohols, phenols and amines using changes in the relative Gibbs free energy. *Fluid Phase Equilibria* **2012**, 148-155.

[6]   Clemens, A. H.; Matheson, T. W.; Rogers, D. E. Low temperature oxidation studies of dried New Zealand coals. *Fuel* **1991**, *70* (2), 215-221.

[7]   Van Krevelen, D. W. *Coal. Typology-Physics-Chemistry-Constitution*, 3rd ed.; Elsevier: Amsterdam, 1993.

[8]   Parthasarathi, R.; Padmanabhan, J.; Elango, M.; Chitra, K.; Subramanian, V.; Chattaraj, P. K. pK$_a$ prediction using group philicity. *The Journal of Physical Chemistry* **2006**, 110(20), 6540-6544.

[9]   Tao, L.; Han, J.; Tao, F. M. Correlations and predictions of carboxylic acid pK$_a$ values using intermolecular structure and properties of hydrogen-bonded complexes. *The Journal of Physical Chemistry* **2008,** 112(4), 775-782.

[10]   Stange, W. The process design of gold leaching and carbon-in-pulp circuits. *The Journal of The South African Institute of Mining and Metallurgy* **1999**, 13-26.

[11]   Winter, J.; Bailey, M.; Galley, E.; Joseph, C.; Shaffer, B. A multiple account benefit-cost analysis of coal mining in Alberta. *The school of public policy publications* University of Calgary **2021**, 14, 32

5. Oxidative coal dissolution at 5 MPa and different temperatures

Abstract

This study aimed to explore the influence of temperatures (90 to 180 °C) and pressures (5 MPa) on OCD to obtain a comprehensive understanding of carbon conversion, product distribution, and economic feasibility. It is developed with the hypothesis that elevated temperature and pressure conditions would significantly affect carbon conversion and product distribution in OCD. Experiments were conducted in a Parr batch reactor, and the carbon balance and yield were analyzed for residue, extract, and gases generated at different temperatures. Gas composition and oxygen content changes were also examined.

The findings revealed that pressurizing the reaction system at 5 MPa substantially increased the yield of liquid products compared to atmospheric pressure experiments (Chapter 4) at similar temperatures. Higher oxygen concentration and improved mass transfer into the coal matrix contributed to enhanced oxidation. The yield of liquid products increased with higher temperatures, reaching 13.8 % in liquid extract at 180 °C and 5 MPa after 4 hours of reaction. However, carbon yield to gases consistently exceeded carbon yield to liquids at all reaction temperatures at 5 MPa, indicating a preference for gaseous products during coal dissolution. The highest selectivity to liquid products was observed at 150 °C, suggesting challenges in achieving higher selectivity due to over-oxidation to gaseous products. Metal concentrations in the liquid extract increased with higher reaction temperatures at 5 MPa and 4 hour reaction time, with certain metals showing lower concentration at 180 °C compared to 150 °C.

These findings contribute to a deeper understanding of OCD under elevated temperature and pressure conditions and highlight the potential for improved carbon conversion and product distribution. However, challenges related to over-oxidation and metal release require further investigation.

Keywords: Yield, reaction temperature, carbon conversion, overoxidation, OCD

5.1   Introduction

In Chapter 4, an initial set of experiments for oxidative coal dissolutions (OCD) was carried out under atmospheric conditions, assessing a temperature range of 65 °C to 95 °C for 4 hours, and at 95 °C with a reaction time span of 15 minutes to 4 hours. These experiments aimed to evaluate the impact of temperature and time on oxidation conversion and product yield.

Although the results on Chapter 4 shed light on the behavior of OCD at atmospheric conditions, there are several knowledge gaps that need to be addressed. Firstly, the carbon yield from oxidative coal dissolution to liquid products under these conditions is exceedingly low, with less than 1 % in most cases. This low carbon yield raises concerns about the economic viability of the process for large-scale applications. The necessary equipment and utilities costs become substantial, jeopardizing the feasibility of generating high-value products.

To overcome these limitations, it is imperative to explore the influence of higher temperatures and changes in oxygen availability on OCD. By assessing the process at elevated pressures of 5 MPa and temperatures ranging from 90 to 180 °C, a more comprehensive understanding of carbon conversion, product distribution, and economic viability can be obtained.

In this study, I postulated that elevated temperature and pressure conditions will have a substantial effect on carbon conversion and product distribution in oxidative coal dissolution. To test this hypothesis, a series of experiments was conducted in a Parr batch reactor, operating at a pressure of 5 MPa since in this initial pressure in the oxidant gas was found as the more ideal to get high yield of valuable liquid products from oxidative coal dissolution [1]. Temperatures of 90, 120, 150, and 180 °C were chosen based on their relevance to coal conversion processes and their potential to yield valuable insights into the efficiency and distribution of carbon during the reaction process at mild conditions [2][3].

The investigation involved analyzing the carbon balance and yield from residue, extract, and gases generated at different temperatures. It enabled us to assess the overall efficiency of carbon conversion and the relative distribution of carbon among the various product streams.

5.2   Experimental

5.2.1   Materials

Coal from the northwest area of Canada (Alberta and Saskatchewan) was utilized as the feedstock for the oxidative coal dissolution process, which is the focus of this study. The entire coal's characterization is provided in Chapter 3. Table 5-1 presents the proximate and elemental analysis results of the sample feed for experiments under a pressure of 5 MPa, at different temperatures in the autoclave reactor. Additionally, as a reference, it also shows the results of proximate and elemental analyses conducted on the feed samples utilized in the experiments outlined in Chapter 4, at atmospheric pressure (0.1 MPa) varying temperatures (same sample used for characterization in Chapter 3) and time periods.

Table 5-1 Characterization of Mancal coal feed for reactions at 5 MPa

Description	Feed OCD Temperatures at 0.1 MPa		Feed OCD Time at 0.1 MPa		Feed OCD Temperatures at 5 MPa	
Proximate Analysis (wt%)[a]	x	s	x	s	x	s
Moisture	26.5	0.02	25.8	0.0	18.0	0.02
Volatile matter	30.5	0.32	30.4	0.3	33.9	0.32
Fixed Carbon	32.8	0.25	30.6	0.3	35.2	0.30
Ash	10.2	0.59	13.2	0.0	13.0	0.03
Elemental Analysis (wt%, maf)[b]						
Carbon	71.7	0.17	72.3	0.31	71.1	0.36
Hydrogen	4.1	0.22	4.4	0.29	2.7	0.41
Nitrogen	1.3	0.01	1.4	0.01	1.3	0.01
Sulfur	0.8	0.01	0.3	0.00	0.4	0.00
Oxygen[c]	22.0	-	21.5	-	24.5	-
H/C molar ratio (mol/mol)	0.69	-	0.73	-	0.45	-
O/C molar ratio (mol/mol)	0.23	-	0.22	-	0.26	-
Gross heating value[d] (MJ/kg)	26.3	-	27.0	-	23.5	-

[a]Averages (x) and sample standard deviations (s) of duplicate analyses
[b]Calculated on a moisture, ash-free basis using elemental and proximate Analysis
[c]Oxygen was determined by difference
[d]Calculated on the basis of Dulong's correlation

The elemental distribution of Mancal's Coals feed, employed in experiments conducted in this Chapter, is presented in Figure 5-1. Additionally, Table 5-2 presents the weight percentages

corresponding to individual mineral elements detected in the sample through SEM-EDS analysis. The analysis was conducted utilizing the identical methodology employed in the preceding Chapters. Conspicuous bright sites or mineral chunks, such as silicon (like present as quartz) [4][5] and aluminum (like present as alumina-rich-clays) [4][5][6] were also in the feed as in the feed samples used for experiments in Chapters 3 and 4.

Figure 5-1 Secondary Electron **SE** image from Mancal's Coal elemental distribution in SEM-EDS (Map/Spectrum) for feed to OCD with changes on temperature at 5 MPa.

Table 5-2 Main mineral elements identified in Mancal's coal for feed to OCD with changes on temperature at 5 MPa.

Element	Wt Percentage in coal (%)	
	x	s
Si	1.78	0.95
Al	1.43	0.75
Ca	2.46	1.65
Na	0.70	0.43
Fe	0.44	0.14
S	0.56	0.17
Mg	0.28	0.18

Averages (x) and sample standard deviations (s) of five different measures

Air cylinder, pH buffer solutions and Milli-Q water utilized in this Chapter were the same as described in Chapter 4. Additional chemicals, cylinder gases and calibration substances employed in this study are shown in Table 5-3.

Table 5-3 Materials employed in Oxidative coal dissolution at different operating conditions.

Compound	Formula	CASRN [a]	Mass fraction purity [b]	Supplier
Chemicals				
Cylinder gases				
Argon 4.8	Ar	7440-37-1	99.99%[c]	Linde
Hydrogen	H_2	1333-74-0	99.99%[c]	Linde
Oxygen	O_2	7782-44-7	99.99%[c]	Linde
Nitrogen	N_2	7727-37-9	99. 99%[c]	Linde
Certified Standard Mix 1				Praxair
▪ Carbon dioxide	CO_2	124-38-9	10.05%[c]	
▪ Carbon Monoxide	CO	630-08-0	15.04%[c]	
▪ Methane	CH_4	74-82-8	1.00%[c]	
▪ Oxygen	O_2	7782-44-7	0.969%[c]	
▪ Nitrogen	N_2	7727-37-9	10.03%[c]	
▪ Hydrogen	H_2	1333-74-0	Balance	
Certified Standard Mix 2				Linde
▪ Carbon dioxide	CO_2	124-38-9	40%[c]	
▪ Methane	CH_4	74-82-8	40%[c]	
▪ Nitrogen	N_2	7727-37-9	Balance	
ICP-OES Calibration Standards[d]				
Silicon Standard:	Si		1000 µg. mL^{-1}	Agilent
Calibration mix majors Standard:			500 µg.L^{-1}	Agilent
▪ Calcium	Ca			
▪ Magnesium	Mg			
▪ Sodium	Na			
▪ Iron	Fe			
▪ Potassium	K			
Calibration mix 2 majors:			100 mg.L^{-1}	Agilent
▪ Silver	Ag			
▪ Arsenic	As			
▪ Barium	Ba			
▪ Beryllium	Be			
▪ Cadmium	Cd			
▪ Cobalt	Co			
▪ Chromium	Cr			
▪ Copper	Cu			
▪ Manganese	Mn			
▪ Nickel	Ni			
▪ Lead	Pb			
▪ Selenium	Se			
▪ Thallium	Tl			
▪ Thorium	Th			
▪ Uranium	U			
▪ Vanadium	V			
▪ Zinc	Zn			

5.2.2   Equipment and procedure

The coal grinding process and residue and extraction recovery were the same as used in Chapter 4. With the only difference that the additional 50 mL of Milli-Q water used in residue and extraction recovery were used to collect any solid in the Parr 4572 HP/HT 1.8 L Reactor instead than in the 2L three neck round bottom flask.

Reaction Setup

A diagram of the equipment employed in the process is shown in Figure 5.2, which illustrates the connection between the Parr 4572 HP/HT 1.8 L Reactor and the Parr 4848 controller, as well as the cooling system, gas inlet/outlet lines, and pressure transducer and thermocouple. All valves and instruments are labeled with numbers and indicated accordingly in the procedure.
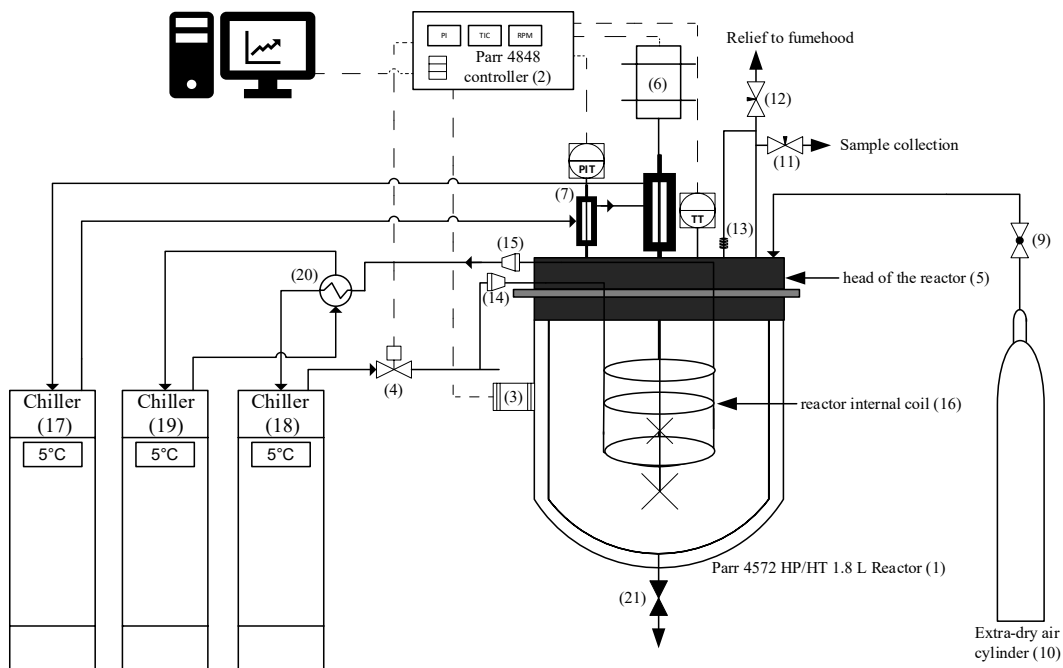
Figure 5.2 Experimental Setup for oxidative coal dissolution at 5 MPa in Parr Reactor
Abbreviations: PI=pressure indicator, TIC= temperature indicator and controller, RPM=rotation per minute, PIT=pressure indicator and transmitter, TT= temperature transmitter.

The oxidative coal dissolution experiments were conducted in a continuous stirred tank reactor. The Parr 4572 HP/HT 1.8 L Reactor (1) shown in Figure 5.2 is designed to hold pressure up to 3447.4 kPa (5000 psi) at 500 ºC and is connected to a Parr 4848 controller (2), which controls temperature and stirring and monitors pressure. To control temperature, the controller is connected to a 230 VAC, 15 Amps, 50/60 Hz power outlet (3) to heat and a solenoid valve (4) that allows the flow of refrigerant to the reactor to cool it down. The temperature controller includes on/off and PID modes.

The head of the reactor (5) has a magnetic stirrer (6) that is connected to the controller through an overarm. There is a pressure transducer (7) that measures, indicate and transmit pressure and a thermocouple (8) that measures and transmit temperature to the Parr 4848 controller (2). There is an inlet gas line connected to a shut-off valve (9) for the compressed air that comes from the extra

dry air cylinder (10) and an outlet gas line for sample collecting with a needle valve (11) and relief with needle valve (12). A rupture disk (13) is installed to prevent the reactor from going beyond its temperature and pressure limits, and it is connected to tubing leading to a fume hood. There are also two connections (Swagelok quick connectors) for inlet (14) and outlet (15) of the cooling water that flows through the reactor internal cooling coil (16).

The cooling system consists of three Fisher Scientific Isotemp 5150 R28 Recirculating Chillers using water as the cooling fluid. The first chiller (17) is connected to the pressure transducer and the magnetic drive cooling mantle. Cooling tubes are connected from the chiller to the pressure transducer (7) sleeve and the magnetic stirrer (6) cooling sleeve. These sleeves are mounted in series and are needed to protect the pressure transducer and magnetic stirrer from the heat of the reactor. The second chiller (18) is used for internal cooling of the reactor. A solenoid valve (4) controls the flow of refrigerant to the reactor through the controller. The last chiller (19) is used to control the temperature of the refrigerant water coming out from the reactor using a shell and tube heat exchanger (20). The internal cooling flow is cooled for two reasons. Firstly, due to the high operating temperatures for most of the reactions (exceeding 100 °C), the water from the reactor cooling system undergoes evaporation, necessitating condensation before coming back to the internal cooling chiller. Secondly, the cooling chiller itself has a maximum capacity of 150 °C, which is lower than the higher reaction temperature. At the bottom of the reactor there is a bottom drain valve (21) which is open to collect the products at the end of the reaction.

To start the oxidative coal dissolution process, 0.5L of Milli-Q water were measured using two Fisherbrand volumetric flasks of 250 mL each with ±0.12 mL tolerance. The pH of Milli-Q water was measured using an Oakton PC700 pH/mV/Conductivity/°C/°F meter. 0.25 L of water was then added to the Parr 4572 HP/HT 1.8 L Reactor (1) vessel followed by the addition of approximately 20 g of coal and then the Parr 4572 HP/HT 1.8 L Reactor (1) vessel was filled with the remaining 0.25 L of Milli-Q water. The head of the reactor (5) is placed on the vessel, the reactor is closed, and all connections are verified.

Oxidation of coal was conducted with extra-dry air from a Praxair cylinder (10). The air stream pressure in the reactor was measured in the Parr 4848 controller (2) and controlled through the

extra-dry air cylinder (10) regulator. Once the system achieved the reaction pressure of 5 MPa (725 psi), the reactor (1) was tested for leaks by leaving it pressurized for 10 minutes. Air was shut off (9) after leak test and the heating process started. Once the heating started and the target temperature was reached, the system was allowed to stabilize for 10 minutes before the reaction started. For heating, the control system was set in mode on/off and heated up to 30 °C below the objective temperature, and then the control system was set to the objective temperature in mode PID with proportional gain (20), integral gain (375), and derivative gain (93).

After the reactor (1) reached the target temperature, the system was allowed to stabilize for 10 minutes before the reaction started. Once the reaction started, the stirring mechanism (6) was set to 600 rpm (about 80% of motor output) in three steps. The first step was to set the stirring mechanism to 200 rpm and wait for 20 seconds. The second step was to set the stirring mechanism to 400 rpm and wait for another 20 seconds. Finally, the stirring mechanism was set to 600 rpm.

During the reaction, temperature and pressure were recorded in the Parr 4848 controller (2) to monitor the reaction progress. The experiments were carried out for four hours, with temperatures of 90 °C, 120 °C, 150 °C, and 180 °C. Once the reaction time was over, the stirring and heat supply were stopped, and the resultant mixture was allowed to reach room temperature.

After reaching room temperature, the system was depressurized by opening the relief valve (12) to release the pressure inside the reactor. Gas samples were collected from the sample collection valve (11) at three different pressures, 3.44 MPa (500 psi), 2.06 MPa (300 psi), and 0.69 MPa (100 psi), in 500 mL gas bags for further analysis using GC-Gas. Gas bags were labeled correctly to avoid confusion during the analysis process.

The slurry product, which is a combination of liquid and solids resulting from the reaction process, was retrieved by opening the drain valve (21) at the bottom of the reactor. To ensure thorough collection of any remaining slurry product inside the reactor, an additional 50 mL of Milli-Q water was measured using a 50 mL volumetric flask with a tolerance of ±0.05 mL. This water was introduced into the reactor chamber to rinse it and gather any residual slurry product. Then, slurry

was subjected to separation into two distinct components, the residue (solid product) and the extract (liquid product). The separation process is described in detail in Chapter 4.

5.2.3   Analyses

Proximate and elemental analyses and scanning electron microscope (SEM) coupled with energy dispersive X-ray spectroscopy (EDS) performed in this set of experiments were described in Chapter 3. Total organic carbon (TOC) content and density measurements on liquid samples were described in Chapter 4.

Metal elements content in extract samples was carried out with an Agilent ICP-OES 5100. It utilizes the technique of Inductively Coupled Plasma-Optical Emission Spectroscopy to perform an elemental analysis of a sample. The ICP-OES instrument operates through a sequence of steps, beginning with the introduction of the sample into the instrument via a pneumatic concentric nebulizer, which transforms it into an aerosol mist. To ensure a constant sample flow to the instrument, the sample is introduced to the nebulizer chamber via a peristaltic pump and tygon tubing attached to an automatic sampler. These pumps, programmable for consistent delivery, maintain a steady flow of the sample into the nebulizer. The sample pass through a nebulizer and is mixed with argon, creating a fine mist of liquid particles, where larger droplets condense on the spray chamber's walls and are removed through a drain using the same peristaltic pump. Finer droplets, of desired size, continue with the argon flow into the plasma, guaranteeing a uniform flow rate and specific droplet size for accurate analysis [7].

Subsequently, the mist is directed into a high-temperature plasma that decomposes the material and ionizes the elements. The high temperature ionized elements emit light at characteristic wavelengths corresponding to the elements as they cool down and return to a lower energy state. The emission spectrum is recorded by a spectrometer. The spectrometer splits the emitted light into its constituent wavelengths, and the intensity of each wavelength is measured to determine the elemental composition of the sample. The Agilent ICP-OES 5100 is equipped with both radial and axial viewing optical design options. In the analysis, the radial viewing mode was chosen for enhanced sensitivity and precision in elemental analysis.

The operational parameters for an aqueous sample included: Torch (1.8 mm ID injector), plasma flow (12 L.min^{-1}), nebulizer flow (0.7 L.min^{-1}), pump speed (15 rpm), stabilizing time (15 s), read time (5 s) and radio frequency (RF) power (1.2 kW). The emission wavelengths of each element used for the analysis is presented in Table 5-4.

Table 5-4 Emission wavelengths used for ICP-OES

Element	Wavelength (nm)	Element	Wavelength (nm)	Element	Wavelength (nm)
Si	288.158	As	188.980	Ni	230.299
Si	251.432	Ba	455.403	Pb	220.353
Ca	398.847	Be	313.042	Se	196.026
Fe	238.204	Cd	214.439	Ti	276.789
K	766.491	Cd	226.502	U	385.957
Mg	279.553	Cr	267.716	V	292.401
Na	588.995	Cr	283.563	V	309.310
K	769.897	Cu	327.395	Zn	202.548
Ag	328.068	Mn	257.610	Zn	213.857

Gaseous reaction products were analyzed in a 7890A Gas Chromatograph (GC). It is an analytical instrument used for separating, identifying, and quantifying components in a gas mixture. The sample is introduced through an injection port into the system. Inside the GC, there is a column (Hay Sep R column, 2.44 m × 3 mm) with a stationary phase coating. The carrier (hydrogen at a constant flow of 25 mL·min^{-1}) flows through the column, carrying the sample components along. As the sample travels through the column, the different components interact with the stationary phase, causing them to separate based on their properties.

At the end of the column, the thermal conductivity detector (TCD) and the the flame Ionization detector (FID) measure the separated components. The TCD measures the changes in thermal conductivity caused by the presence of different compounds in the gas mixture. The TCD consists of two separate filaments, one being a reference filament and the other being a sample filament. As the gas mixture passes over the filaments, thermal conductivity differences between the reference and sample filaments occur, resulting in a change in electrical resistance that can be measured and used for quantification. The FID works by passing the separated components of the gas mixture through a hydrogen-air flame, where the organic compounds are ionized and produce

electrical currents. The detector measures the magnitude of these electrical currents, which is proportional to the concentration of the compounds, allowing for quantification.

The detector signals are processed by the GC software, which allows the use of a calibration gas to determine the retention time of the different components. Additionally, the calibration gas enables quantification using known concentrations of reference standards. In this case the quantification process is highly influenced by the injection volume. Variations in the injection volume can have a significant impact on the accuracy and reliability of the quantification results. The results are displayed as a chromatogram, a graph showing the peaks corresponding to the separated components. The injections were performed manually using a 500 µL Thermo Scientific Syringe. The injector temperature was set at 200 °C. The temperature program started at 70 °C held isothermally for 7 min, followed by 10 °C·min^{-1} increase to 105°C, then temperature decreased to 70 °C again by 30 °C·min^{-1} where it was held for 6 min. This temperature was then increased by 10 °C·min^{-1} to 250 °C where it was held for 11 min.

For each reaction gas product sample, a total of three runs were conducted in the Gas Chromatograph. During the analysis, the Thermal Conductivity Detector (TCD) successfully detected four distinct peaks at different retention times, indicating the presence of four different components. However, no peaks were detected by the Flame Ionization Detector (FID) during the analysis. Following the completion of the calibration process outlined in section 5.2.5, the components corresponding to the identified peaks were determined. The detected components corresponded to nitrogen (N_2), oxygen (O_2), carbon dioxide (CO_2), and carbon monoxide (CO).

5.2.4   Calculations

Calculations methodology for oxygen weight composition, moisture, ash-free basis elements compositions and heating values based on proximate and elemental analyses results of solid coal (residue) in this set of experiments were described in Chapter 3. Carbon balance, carbon yield and the increase in oxygen content of residue as compared to the oxygen content of the feed were described in Chapter 4.

To calculate the weight of each compound in the gas samples various approaches were considered, such as the ideal gas law, Van der Waals equation of state, and the Peng-Robinson equation of state. However, the results were presented using the Peng-Robinson equation of state. This choice was based on the understanding that the Peng-Robinson equation offers an enhanced description of non-ideal gases compared to the ideal gas law. It achieves this improvement by incorporating the effects of molecular interactions, molecular shape, polarity, and attractive forces between molecules. In contrast, the Van der Waals equation of state, while has an improvement over the ideal gas law, does not account for these additional factors to the same extent. By modifying the attraction pressure term from the Van der Waals equation, the Peng-Robinson equation provides a more accurate representation of real gases [8].

The total gas volume of the reactor was obtained by measuring the reactor's total volume and subtracting the known volumes of water and coal. Assumptions were made that the volumes of water and coal remained unchanged under the reaction pressure conditions. The volume of coal was calculated using an assumed coal density, corresponding to a coal type between subbituminous and bituminous coal, based on Mancal's coal characterization results from Chapter 3. The coal density value selected from Table 2.2 in Chapter 2 was considered as 1.35 g.mL^{-1} [9].

The temperature was measured as the final temperature of the system after cooling down the reaction products (22 °C). The total final pressure was measured at the final temperature after cooling down the reaction.

To determine the composition of the gas product in terms of the volume fraction of each substance, the samples collected at 3.44 MPa (500 psi) are subjected to gas chromatographic analysis, as detailed in the gas analysis section 5.2.3. The area under the curve corresponding to each identified component at specific retention times is measured. Subsequently, the measured area for each component is matched to the corresponding calibration curve developed for that specific component in section 5.2.5, within the specified curve interval calibration. By doing so, the volume percentage of each identified component is determined. To obtain the composition in volume fraction, the volume percentage is then divided by 100.

Calculation of the volume fraction was conducted at a pressure of 3.44 MPa (500 psi) because it was the gas product sample collected at the closest measured pressure to the total final pressure after cooling down the reaction (since there was not sample collected at this pressure). This approach relies on the assumption that the gas-liquid equilibrium at 3.44 MPa closely resembles the equilibrium observed at the actual total final pressure following the reaction cooling process. However, it is important to acknowledge that there might be some variations between the two equilibria in reality.

The partial pressure of each substance is calculated by multiplying the total final pressure measured at the final temperature after cooling down teach reaction products (22 °C) with the calculated volume fraction of the gas sample collected. The molar volume (U) for each specific substance at the specified temperature and pressure was calculated using the Peng-Robinson equation of state (equation 5.1).

$$\mathbf{P} = \frac{R*T}{U-b} - \frac{a*\alpha}{U*(U+b)+b*(U-b)} \tag{5.1}$$

Where a, b and α are given by:

$$\mathbf{a} = \mathbf{0.45723553}\frac{R^2T_c^2}{P_c} \tag{5.2}$$

$$\mathbf{b} = \mathbf{0.07779607}\frac{RT_c}{P_c} \tag{5.3}$$

$$\boldsymbol{\alpha} = (\mathbf{1} + (\mathbf{0.374664} + \mathbf{1.542266}\omega - \mathbf{0.26993}\omega^2)\left(\mathbf{1} - \sqrt{\frac{T}{T_c}}\right)^2 \tag{5.4}$$

And:

P = Partial pressure of each substance (MPa)

T = Absolute temperature after colling down (K)

R = Universal gas constant (mL.MPa.mol^{-1}.K^{-1})

U = molar volume (mL.mol^{-1})

T_c = critical temperature (K)

P_c = critical pressure (MPa)

ω = acentric factor

For all the samples found in the gas product of the reactions including oxygen (O_2), nitrogen (N_2), carbon dioxide (CO_2) and carbon monoxide (CO), critical temperature (Tc), critical pressure (Pc) and the acentric factor (ω) values were extracted from *Reid et al*. [10].

Once the molar volume (U) is known, the weight of each substance in the gas phase is calculated by using the equation 5.5.

$$\text{gas weight} = \frac{V}{U} * PM \tag{5.5}$$

Where:

gas weight = weight of specific gas substance in sample (g)

V = Volume occupied by the gas (mL)

U = molar volume of the gas substance calculated with Peng-Robinson equation ($mL.mol^{-1}$)

PM = molecular weight of each substance ($g.mol^{-1}$)

The solubility of each gas compound in the liquid was calculated assuming pure water as the solvent, using he total final pressure measured at the final temperature after cooling down the reaction and determined by applying Henry's law. However, it is important to note that Henry's law assumes that the system is at dynamic equilibrium, meaning that the rate of dissolution of the gas molecules into the liquid phase is equal to the rate of escape of gas molecules from the liquid phase back into the gas phase. Dynamic equilibrium may not always be completely achieved, especially under high pressures or temperatures, or when the liquid is subjected to stirring as is the case.

Furthermore, the application of Henry's law assumes the presence of only one gas in the system and neglects the potential influence of other dissolved materials. In real-world scenarios, the

131

presence of multiple gases or other solutes could impact the interactions between gas molecules and the solvent, leading to deviations from ideal behavior.

Henry's law equation 5.6 enabled the calculation of the amount of gas substances including carbon dioxide (CO_2) and carbon monoxide (CO) that could dissolve in the liquid under the temperature conditions at which the gas sample was obtained and the final reaction pressure. The Henry's law constant at the reference temperature for all components, were extracted from *NIST* [11].

$$C = k° * P \qquad\qquad (5.6)$$

Where:

C = Concentration of gas in water ($mol.L^{-1}$)

P = Partial pressure of the gas (bar)

$k°$ = Henry's law constant at reference temperature 25 °C ($mol.L^{-1}.bar^{-1}$)

The Henry's law constant ($k°$) from equation 5.6 is intrinsically influenced by changes in the system's temperature, a characteristic that can generally be described through the van 't Hoff equation [12]. In OCD experiments, the temperature of the system was measured at the end of the reaction process when the reaction products had cooled down to 22 °C. Under these conditions, it is assumed that any significant alterations in the Henry's law constant due to temperature fluctuations are minimal and can be disregarded for practical purposes.

5.2.5 Calibrations

ICP-OES

The ICP-OES instrument was calibrated by using the following aqueous standard solutions diluted with water at the specified concentrations:

(Si) in the concentration range 10-80 $mg.L^{-1}$ (20, 30, 40, 50, 60, 70 and 80 $mg.L^{-1}$).

Calibration mix majors standard solutions containing calcium, magnesium, sodium, iron, and potassium (Ca, Mg, Na, Fe, K) was initially performed in the concentration range 10-80 mg.L^{-1} (10, 20, 30, 40, 50, 60, 70 and 80 mg.L^{-1}). During the calibration process, it was observed that the atomization efficiency of calcium in the plasma was significantly higher than that of the other metals. This higher efficiency can be attributed to calcium's low ionization potential, resulting in the efficient conversion of calcium atoms to ions and consequently, the 398.847 nm emission line, which corresponds to calcium's characteristic emission, exhibited a considerably intensified signal intensity wich could not be read at concentrations higher than 40 mg.L^{-1}. Therefore, the calibration measurement was carried out up to a concentration of 40 mg.L^{-1} for calcium. The decision to utilize the 398.847 nm wavelength was based on preliminary experiments developed for the same element, however investigating alternative emission lines by selecting different wavelengths for calcium may provide higher concentration calibration measurements.

Calibration mix 2 majors standard solutions containing silver, arsenic, barium, beryllium, cadmium, cobalt, chromium, copper, manganese, nickel, lead, selenium, thallium, thorium, uranium, vanadium, and zinc (Ag, As, Ba, Be, Cd, Co, Cr, Cu, Mn, Ni, Pb, Se, Tl, Th, U, V and Zn) in the concentration range 10-40 mg.L^{-1} (10, 20, 30, and 40 mg.L^{-1}), all of which were prepared using Milli Q water.

The resulting calibration curves for all calibration standards were analyzed through linear regression, and the coefficient of determination (R^2) was greater than 0.999 for all cases.

GC

The Gas Cromatograph was calibrated by using various gas cylinders and standards, including pure oxygen (O_2), pure nitrogen (N_2), extra pure air (N_2 79 %, O_2 21 %), certified standard mix 1 (CO_2 10.5 %, CO 15.04 %, N_2 10.3 %, CH_4 1 %, O2 0.969 %, H_2 balance), and certified standard mix 2 (CO_2, CH_4, N_2 balance). Furthermore, air was blended in a 50/50 volume percentage with certified standard mix 1, and also in a 50/50 and 90/10 volume percentage with certified standard mix 2 to obtain calibrated concentration curves with ranges close to the concentrated ranges ob served in the reaction gases.

The preparation of these gas mixtures involved specific handling to ensure accuracy and precision. Initial gas samples were collected and stored in gas bags for subsequent use. Using a 500 µL Thermo Scientific Syringe, 250 µL of each gas sample was sequentially collected in the same syringe to create the 50/50 mixture. For the 90/10 volume percentage, 450 µL and 50 µL were collected for each gas sample, respectively.

An important aspect of the procedure involved the specific order of collection. The certified standard mixes were consistently collected first in the syringe, followed by the air sample. This sequential approach was implemented to minimize the potential contamination of the certified standard mixes in the gas bags. In the event of gas bag contamination with the first gas (certified standard mix) due to improper syringe handling, the contaminated content in the air bag was replaced instead of the content in the certified standard mixes.

For each gas concentration calibration point, three individual runs were performed and plotted in pairs of concentration points. The volume gas concentration calibration points for different gases were determined as follows. For nitrogen (N_2), the calibration concentrations included 100 %, 79.0%, and 72.1%. Oxygen (O_2) calibration points comprised 100 %, 21 %, 18.94 %, 10.9 %, 10.5 %, and 0.969 % concentrations. Carbon dioxide (CO_2) was calibrated using concentrations of 40 %, 20 %, 10.05 %, 5.03 %, and 1.01 %. Lastly, carbon monoxide (CO) calibration involved concentrations of 15.04 %, 7.52 %, and 1.5 %. The resulting calibration curves for all calibration standards in the ranges associated to the gas reaction samples were analyzed through linear regression, and the coefficient of determination (R^2) was greater than 0.99 for all cases.

5.3   Results

5.3.1   Material Balance

Table 5-5 shows the measurements used in material balance of the reactants entering the system "in" and the products exiting the system "out" for the OCD reactions over a duration of 4 hours.

These reactions occurred under conditions of 5 MPa pressure and temperatures ranging from 90 to 180 °C.

The mass determination of the feed coal, feed water and washing water, residue, extract and water from residue is similar to the process developed in Chapter 4. The mass determination for both the feed air and gas products involves the application of the Peng-Robinson equation and Henry's law equations, following the steps described in the calculation section and summing up all components.

Table 5-5 Measurements used in material balance of OCD at 5 MPa, 4 hours reaction and temperatures from 90 to 180 °C

Reaction Temperature (°C)	Feed coal	'In' (g) Water		Feed Air	Residue	Extract	'Out' (g) Water from residue	Gas product
		Initial water	Washing water					
90	20.11	499.08	49.91	77.07	16.51	536.36	6.48	77.66
120	20.43	499.08	49.91	77.07	13.52	537.63	3.99	78.96
150	20.70	499.08	49.91	77.07	8.24	541.70	2.78	80.57
180	20.53	499.08	49.91	77.07	5.61	543.80	1.52	88.97

Table 5-6 presents the material balance, encompassing the conversion from reactants to products. On average the material balance closed within a margin of 2 %.

Table 5-6 Material balance of OCD at 5 MPa, 4 hours reaction and temperatures from 90 to 180 °C

Description	Total mass coming 'in'	Total mass going 'out'	Yield to products (%)
Reaction Temperature (°C)			
90	646.17	637.00	98.58
120	646.49	634.09	98.08
150	646.76	633.29	97.92
180	646.59	639.90	98.97

5.3.2 Proximate and Elemental Analysis

Proximate and elemental analyses were performed on the solid OCD products (residue) generated by reactions at 5 MPa and temperature range 90-180 °C (90, 120, 150 and 180 °C). The results of these analyses are presented in Table 5-7 and Table 5-8.

Table 5-7 Proximate Analysis of residue product from OCD at 5 MPa**,** 4 hours reaction and temperatures from 90 to 180 °C

Description	Reaction temperature							
	90 °C		120 °C		150 °C		180 °C	
Proximate Analysis (wt%)[a]	x	s	x	s	x	s	x	s
Moisture	6.7	0.05	6.3	0.02	6.2	0.09	5.7	0.08
Volatile matter	39.4	0.10	40.6	0.16	42.1	0.23	36.3	0.40
Fixed Carbon	40.1	0.06	36.4	0.12	32.4	0.20	25.4	0.57
Ash	13.8	0.00	16.7	0.01	19.3	0.06	32.7	1.05

[a]Averages (x) and sample standard deviations (s) of duplicate analyses

Table 5-8 Elemental Analysis of residue product from OCD at 5 MPa, 4 hours reaction and temperatures from 90 to 180 °C

Description	Reaction temperature							
	90 °C		120 °C		150 °C		180 °C	
Elemental Analysis (wt%, daf)[a]	x	s	x	s	x	s	x	s
Carbon	70.6	0.01	67.4	0.88	63.8	1.20	61.5	0.56
Hydrogen	4.1	0.03	3.5	0.14	2.9	0.07	2.6	0.03
Nitrogen	1.3	0.01	1.3	0.01	1.4	0.02	1.9	0.03
Sulfur	0.4	0.03	0.3	0.03	<0.3	-	<0.3	-
Oxygen[b]	23.6	-	27.5	-	31.7	-	33.7	-
H/C molar ratio (mol/mol)	0.68	-	0.61	-	0.54	-	0.51	-
O/C molar ratio (mol/mol)	0.25	-	0.31	-	0.37	-	0.41	-
Gross heating value[c] (MJ/kg)	25.5	-	22.8	-	20.1	-	18.5	-

[a]Averages (x) and sample standard deviations (s) of duplicate analyses. Calculated on a dry and ash-free basis using elemental and proximate Analysis
[b]Oxygen was determined by difference
[c]Calculated on the basis of Dulong's corelation

The proximate analysis data in Table 5-7 indicates that there is a slight reduction in moisture content as temperature increases. On the other hand, volatile matter content increases between 90 °C and 150 °C, but then decreases notably at 180 °C. The behavior of fixed carbon and ash values

is the opposite, with fixed carbon content decreasing and ash content increasing with temperature. The small standard deviations of the sample analyses suggest that the results are highly precise and reproducible.

As presented in Chapter 4, to assess the internal consistency of the analytical results, a comparison of the ash content from the coal feed to the ash content in the residue product was performed. Assuming that mineral matter did not volatilize or dissolve in the water during the reaction. Table 5-9 shows the change in ash content from the feed to the residue product at different reaction temperatures.

Table 5-9 Change in ash content from feed to residue product from OCD at 5 MPa, 4 hours reaction and temperatures from 90 to 180 °C

Description	Reaction temperature			
	90 °C	120 °C	150 °C	180 °C
Total ash in feed (g)	2.60	2.65	2.68	2.66
Total ash in residue (g)	2.27	2.26	1.59	1.83
Change in ash from feed to residue (g)	0.33	0.39	1.09	0.83
Change in ash from feed to residue (%)	12.7	14.6	40.6	31.1

At lower temperatures of 90 °C and 120 °C, the percentage change in ash content from the feed to the residue product remains relatively moderate, approximately 12.7 % and 14.6 %, respectively. However, a substantial increase in the percentage change in ash is observed at higher reaction temperatures of 150 °C and 180 °C, reaching 40.6 % and 31.1 %, respectively. A factor that could influence the observed variations in ash content is the amount of residue collected during the reactions. At 150 °C and 180 °C, due to the severity of the reaction conditions, the amount of residue collected is smaller compared to lower temperatures. On the one hand, this reduction in the amount of residue collected could lead to increased uncertainty in the data obtained, as a smaller sample size may result in higher variability in the analytical measurements. On the other hand, the lower ash content might also be consequence of the high amount of 'ash' material dissolved with the acids in the aqueous phase.

Regarding the elemental analysis data presented in Table 5-8 indicates that as the temperature increases, the carbon and hydrogen content decreases, while the nitrogen content remains

relatively constant between 90 and 120 °C and then also increases. Sulfur content also decreases with an increase in temperature at 90 and 120 °C before reaching a concentration that is lower than the possible calibrated concentration in the Elemental Analyzer. The oxygen content, on the other hand, increases significantly with increasing temperature. As a result of these changes, the H/C molar ratio and heating value decrease, while the O/C molar ratio increases with increasing temperature.

5.3.3 Total carbon to liquid extract

Table 5-10 Total carbon in liquid extract presents the total carbon content in the liquid extract obtained from the total carbon analysis performed to the liquid extract product during 4 hours reaction at 5 MPa conducted at temperatures ranging from 90 to 180 °C. It shows that as the reaction temperature increases, the total organic carbon (TOC) values show pronounced increase, with the mayor change from 120 to 150 °C with about 0.8 grams of carbon added. The total inorganic carbon (TIC) presents relatively minor variations.

Table 5-10 Total carbon in liquid extract at 5 MPa, 4 hours reaction and temperatures from 90 to 180 °C

Reaction temperature (°C)	TOC (g)	TIC (g)	TC (g)
90	0.171	0.011	0.182
120	0.386	0.011	0.397
150	1.203	0.012	1.215
180	1.381	0.008	1.389

5.3.4 Gases analysis

In the analysis of the gas products generated during the experimental process, the composition of the feed air was assumed to consist of 21% oxygen (O_2) and 79% nitrogen (N_2). The gas analysis, conducted using GC-Gas analysis, identified and quantified four gases, including O_2, N_2, carbon dioxide (CO_2), and carbon monoxide (CO). The calculation was performed using the Peng-Robinson equation as described in section 5.2.4. For calculation of gases dissolved in liquid, Henry's law equation was used and both values were summed up for each component.

Table 5-11 presents the gases balance for the reactions conducted at a pressure of 5 MPa, with a reaction time of 4 hours, and temperatures ranging from 90 to 180 °C. The table provides the mass of the gases involved, both as inputs 'in' and outputs 'out'.

Table 5-11 Gases balance at 5 MPa, 4 hours reaction and temperatures from 90 to 180 °C

Reaction Temperature (°C)	'In' (g)		'Out' (g)			
	N_2	O_2	N_2	O_2	CO_2	CO
90 °C	59.072	17.997	62.127	14.143	1.153	0.236
120 °C	59.072	17.997	60.810	12.132	5.677	0.338
150 °C	59.072	17.997	62.775	1.224	16.135	0.435
180 °C	59.072	17.997	62.991	1.089	24.334	0.558

The gas analysis results presented in Table 5-11 reveal important trends as the reaction temperature is varied. First, N_2 remains relatively stable across different temperatures. This suggests that the nitrogen content in the feed air does not significantly participate in the oxidation reactions during the coal dissolution process as expected. Second, the amount of O_2 shows a noticeable decrease as the reaction temperature increases. This reduction in O_2 can be attributed to its involvement in the oxidation reactions, where it reacts with the coal. The higher reaction temperatures seem to facilitate a more efficient utilization of the oxygen, resulting in a decrease in the amount of remaining O_2. Third, the generation of CO_2 and CO shows a consistent increase as the reaction temperature rises. This indicates that the oxidation of coal becomes more pronounced at higher temperatures, leading to the production of larger quantities of CO_2 and CO.

5.3.5   Carbon balance

Carbon balance to residue

The tabulated data in Table 5-12 shows the carbon balance to residue for the reactions at 5 MPa, as a function of temperature. It details the feed on moisture, ash-free basis, and the quantities of carbon present in the coal feed before the reaction, as well as in the residue after the reaction. The division between these quantities is expressed as the percentage of unconverted carbon, representing the portion that did not react to liquid or gas products during the reaction process.

Table 5-12 Carbon balance to residue at 5 MPa, 4 hours and temperatures from 90 to 180 °C

Reaction temperature (°C)	Carbon in feed (g) 'in'	Carbon in residue (g) 'out'	Unconverted Carbon (%)
90	9.87	9.27	93.3
120	10.03	7.01	69.9
150	10.16	3.91	38.5
180	10.08	2.12	21.1

The data presented in Table 5-12 demonstrates the substantial impact of reaction temperature on the carbon balance to residue. The carbon content in the coal feed exhibits minor variation, primarily dependent on the amount of coal feed. However, the notable changes occur in the carbon content of the coal residue at different temperatures. At 90 °C, a high proportion of unconverted carbon is observed, accounting for 93.3 % of the total carbon. This indicates lower efficiency in carbon conversion to liquid or gas products at this temperature. As the temperature increases to 120 °C, the unconverted carbon decreases to 69.9 %, indicating improved carbon conversion efficiency. At 150 °C, only 38.5 % of the carbon remains unconverted, signifying a significant enhancement in conversion efficiency. Finally, at 180 °C, the carbon balance to residue demonstrates the most promising results, with only 21.1 % of the carbon remaining unconverted. This indicates that higher temperatures promote greater carbon conversion, resulting in a reduced amount of unreacted carbon in the residue.

Carbon balance to liquid extract

Total Organic Carbon (TOC) analysis enables the quantitative determination of the concentration of organic carbon in the liquid phase. This analytical technique is valuable for evaluating the efficacy of oxidative dissolution processes in liberating organic carbon from the coal matrix and transferring it into the liquid medium. The reactivity of coal during oxidation via oxidative coal dissolution and the changes in abundance of organic matter for solid and liquid products have been investigated using TOC analysis in various studies [13][14][15][16].

Table 5-13 shows the carbon balance to liquid products in extract for the reactions at 5 MPa, as a function of temperature. It details the feed on moisture, ash-free basis, and the quantities of carbon present in the coal feed before the reaction, as well as the total organic carbon in the liquid product

after the reaction obtained from the total organic carbon analysis (TOC) and the carbon conversion yield to liquid products.

Table 5-13 Carbon balance to extract at 5 MPa, 4 hours and temperatures from 90 to 180 °C

Reaction temperature (°C)	Carbon in feed (g) 'in'	Carbon in extract (g) 'out'	Carbon yield to extract (%)
90	9.87	0.182	1.8
120	10.03	0.397	4.0
150	10.16	1.215	12.0
180	10.08	1.389	13.8

While TOC analysis does not provide specific information about the individual organic compounds present in the liquid phase, it is capable of monitoring variations in the total organic carbon content as oxidative dissolution progresses. The carbon balance to extract at different reaction temperatures presented in Table 5-13 reveals the distribution of carbon between the coal feed and the resulting liquid products.

As the reaction temperature increases from 90 to 180°C, the total organic carbon in the liquid product experiences a substantial rise. This indicates that the oxidative coal dissolution to liquid products increases at higher temperatures, resulting in increased liberation and transfer of organic carbon into the liquid phase.

The carbon yield to liquid products, expressed as a percentage, presents the effectiveness of the oxidative dissolution process in terms of carbon conversion. At lower temperatures (90 and 120 °C), the carbon yield remains relatively low, with values of 1.9 % and 4.0 % respectively. However, as the reaction temperature is elevated to 150 °C and 180 °C, the carbon yield exhibits significant improvements, reaching 12.2 % and 14.0 % respectively. This might imply that higher temperatures promote greater carbon conversion to the liquid products, which make evident the importance of temperature in the oxidative coal dissolution process.

Carbon balance to gases

Table 5-14 illustrates the carbon balance to gas products for the reactions at 5 MPa, as a function of temperature. Gas chromatography (GC-Gas) was utilized to detect the presence of carbon dioxide and carbon monoxide as products, across all reaction temperatures.

Table 5-14 Carbon balance to gases at 5 MPa, 4 hours and temperatures from 90 to 180 °C

Reaction temperature (°C)	'in' (g)	'out' (g)					Carbon yield to gases (%)
	Carbon in feed	C from CO_2 Gas	C from CO_2 Dissolved	C from CO Gas	C from CO dissolved	Total carbon	
90	9.87	0.24	0.08	0.10	9.48E-04	0.42	4.2
120	10.03	1.16	0.38	0.14	1.36E-03	1.69	16.9
150	10.16	3.32	1.08	0.18	1.74E-03	4.59	45.1
180	10.08	5.03	1.61	0.24	2.24E-03	6.87	68.2

When calculating the concentration of gases dissolved in a liquid, the Henry's law constant for CO_2 is significantly higher at 0.035 mol.kgbar^{-1} [11], compared to the constant for CO which is 0.00099 mol.kgbar^{-1} [11]. This difference indicates that CO2 exhibits much greater solubility in the liquid than CO. As a result, CO2 is the major contributor to the carbon content from gases dissolved in the liquid.

The carbon balance to gases in oxidative coal dissolution reactions exhibits a clear relationship with reaction temperature. Increasing the temperature leads to higher carbon conversion rates to gases, as indicated by the carbon yield to gases in Table 5-14. At 90 °C, the carbon yield is 4.2 %, suggesting a relatively low conversion of carbon into gaseous products. However, as the temperature rises, the carbon yield to gases increases significantly, reaching up to 68.2% at 180 °C due to over-oxidation to CO and CO_2.

5.3.6   Oxygen change from coal feed to residue

Table 5-15 shows the quantitative measurement of oxygen change from solid feed to residue varying reaction conditions. As it is presented in Table 5-7 from the elemental analysis, there is a general increment in the oxygen content of solid residues after reaction with respect to feed (except

the solid residue in reaction at 90 °C which slightly decreases). However, despite the increase in oxygen content for almost all the solid residue after reaction with respect to feed (except the solid residue in reaction at 90 °C which slightly decreases), the total content of oxygen in solid residue decreases with respect to feed contrary to what happens at reactions at ambient pressure. It is attributed to the portion of unconverted coal at reactions at 5 MPa is much lower than at ambient pressure.

Table 5-15 Oxygen gain in coal from feed to residue at 5 MPa, 4 hours and temperatures from 90 to 180 °C

Reaction temperature (°C)	Oxygen in feed[a] (g)	Oxygen in residue[a] (g)	change in oxygen (g)
90	3.41	3.10	-0.31
120	3.46	2.87	-0.6
150	3.51	1.94	-1.57
180	3.48	1.16	-2.31

[a] Calculated on a moisture, ash-free basis as a difference between the weight of feed and residue

5.3.7 pH

To ascertain the level of acidity of the liquid products and the extent of its alteration from the initial state of fresh milli Q water, pH measurement was carried out after the reaction and successive extraction. The results obtained are presented in Table 5-16. The pH values obtained indicate an increase in the acidity of all the liquid products as compared to the initial milli Q water used in the reaction. The level of acidity for the extract increased from 90 °C to 150 °C and then at 180 C the pH increases to an acidity level higher than the liquid product of the reaction at 120 °C but lower than the reaction at 150 °C. Changes in pH can arise from variations in the types and amounts of chemical species generated during the reaction.

Table 5-16 pH of liquid products at 5 MPa, 4 hours and temperatures from 90 to 180°C

Description	Reaction temperature							
	90 °C		120 °C		150 °C		180 °C	
pH[a]	x	s	x	s	x	s	x	s
Fresh Milli Q water	7.26	0.02	7.78	0.04	6.97	0.01	7.21	0.05
Extract	6.32	0.01	4.19	0.01	2.83	0.01	3.36	0.03

[a]Averages (x) and sample standard deviations (s) of duplicate analyses

5.3.8 Mineral matter

Metal content in solid samples

Some secondary electron images were taken using Scanning Electron Microscopy SEM to examine potential variations in residue products resulting from OCD at 5 MPa under different temperatures. The resulting SEM images, as depicted in Figure 5-3 illustrate the residue morphology observed under these conditions.
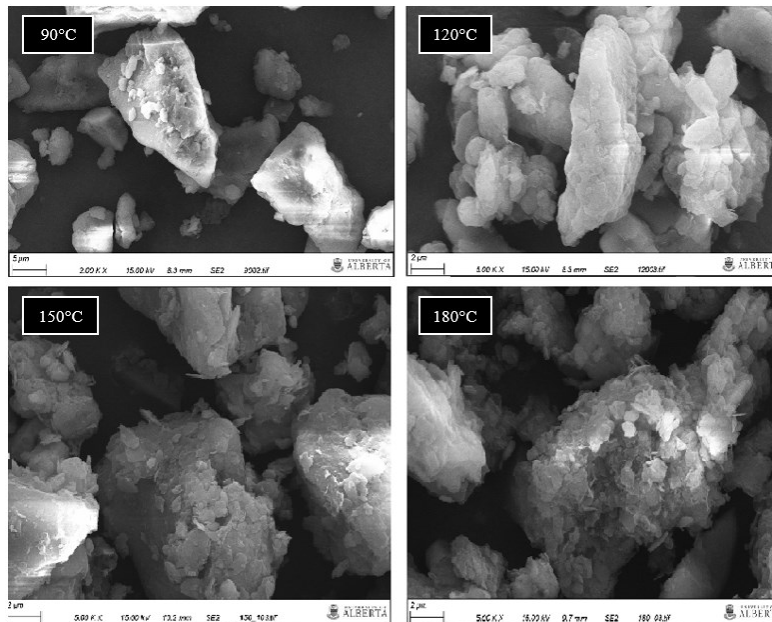
Figure 5-3 Secondary electron images taken to residue after reaction at 5 MPa, 4 hours and temperatures from 90 to 180 °C

To the residue product of each specific reaction, secondary electron images from elemental distribution in SEM-EDS (Map/Spectrum) were also taken. The results showed that as the feed major metals identified seemed to be finely dispersed in the samples with the exception of conspicuous mineral chunks of Silicon, Aluminum or Calcium that where identified. The percentage of the main mineral elements in the sample based on the intensity of the X-ray peaks was also quantified and the results are present in Table 5-17.

Table 5-17 Main mineral elements identified in residue coal after reactions at 4 hours reaction and 5 MPa and temperatures from 90 to 180 °C with SEM-EDS

Element	Wt Percentage in coal (%)							
	90 °C		120 °C		150 °C		180 °C	
	x	s	x	s	x	s	x	s
Si	1.80	1.28	3.78	4.19	3.54	1.75	3.90	2.84
Al	2.01	1.62	3.38	3.83	3.26	1.15	3.85	1.99
Ca	1.26	2.42	1.23	0.60	1.32	1.23	1.76	0.43
Na	0.35	0.14	0.76	0.12	0.70	0.17	0.84	0.04
Fe	0.75	0.55	0.69	0.16	0.89	0.70	1.21	0.43
S	0.51	0.23	0.30	0.11	0.42	0.26	0.23	0.14
Mg	0.34	0.17	0.46	0.06	0.34	0.84	0.21	0.02

Metal content in liquid samples

To determine the metal content in the liquid extract product of oxidative coal dissolution, a meticulous collection of samples was conducted from the aqueous phase of the liquid extract. The collected samples were subjected to Inductively Coupled Plasma -Optical Emission Spectroscopy analysis to determine the concentration of various mineral elements in parts per million (ppm). The concentrations of the main mineral elements identified in the liquid extract after the reactions at a pressure of 5 MPa and temperatures ranging from 90 to 180 °C are presented in Figure 5-4.

During the analysis of the original sample, it was necessary to dilute the samples three times to bring the concentrations of silicon and sodium within the calibration range. Moreover, the sample had to be diluted up to 24 times to achieve measurable concentrations of Calcium within the calibration range. This high level of dilution was required due to the low ionization potential (high intensity) of Calcium.

145

In addition to the elements presented in Figure 5-4, several other elements were analyzed, including silver, arsenic, barium, beryllium, cadmium, cobalt, chromium, copper, manganese, lead, selenium, thallium, thorium, uranium, and vanadium. Among these elements, small amounts of metals (<2ppm) were detected as arsenic, barium, chromium, copper, manganese, lead, selenium, uranium, and vanadium. The emission spectra of each of the aforementioned elements were chosen and calibrated to minimize the potential for interference from neighboring emission lines originating from distinct elemental sources, thereby mitigating the risk of attributing any observed emissions to proximate emissions of dissimilar elements. The emission wavelengths used for each element are shown in Table 5-4.
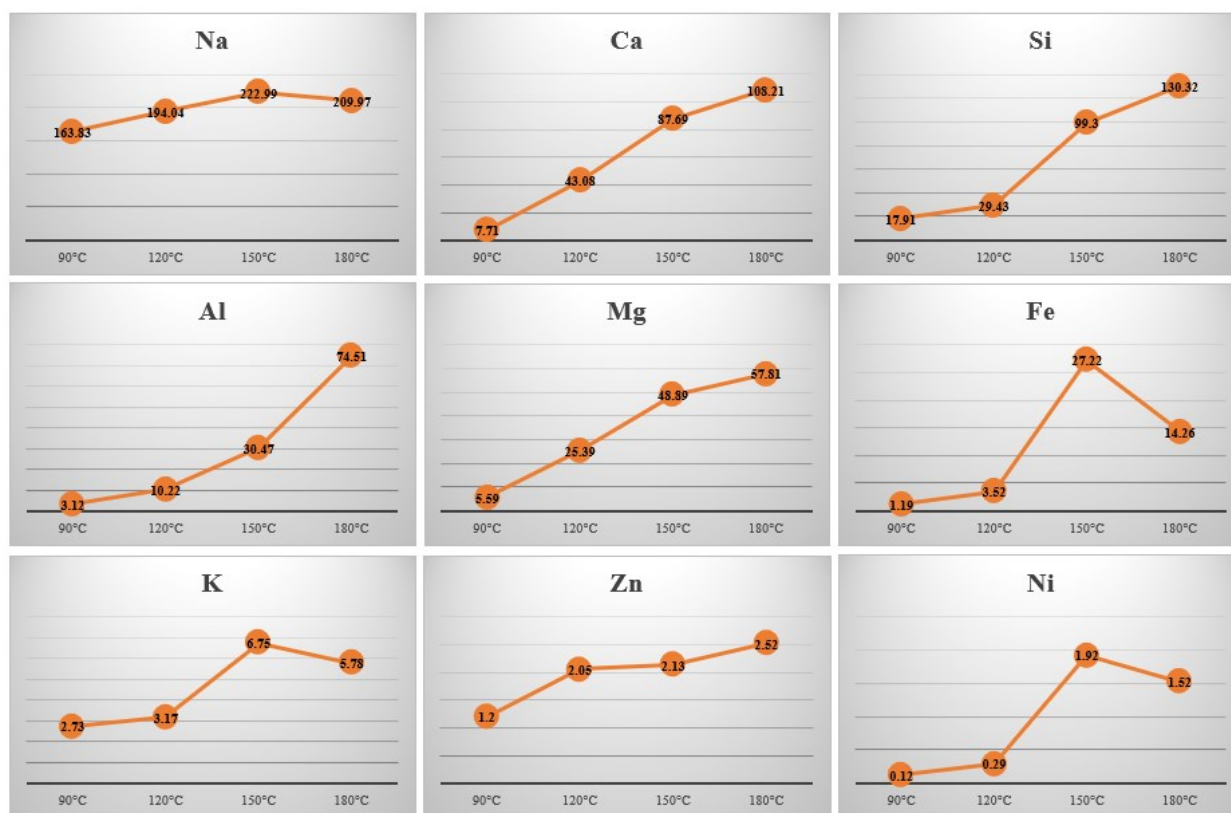
Figure 5-4 Main mineral elements concentrations (ppm) in extract liquid after 4 hours reaction at 5 MPa and temperatures from 90 to 180 °C with ICP

The results presented in Figure 5-4 shows that at 5 MPa, it can be observed that there a general trend of increasing metal concentrations as the reaction temperature increases. Within the

temperature range of 90 to 150 °C, there is an overall increase in the concentrations of all the metals analyzed. This indicates that the reactions are promoting the release and/or dissolution of these metals from the solid feed into the liquid phase. However, at 180 °C, the rate of concentration increases for certain metals, such as sodium, iron, potassium, and nickel, appears to be slightly slower compared to that observed at 150 °C.

Furthermore, while silicon, aluminum, and calcium present higher concentrations in the solid feed and residue as shown in Table 5-2 and Table 5-17, the metal that demonstrates the highest solubility in the extract is sodium. This suggests that sodium has a greater tendency to dissolve in the liquid extract during the reaction process. These observations shed light on the solubility and behavior of various metals during the reaction, indicating their release and presence in the liquid phase.

5.4   Discussion

5.4.1 Effect of changes in oxygen availability compared to experiments at ambient temperature

Before considering the variations in the oxidative coal dissolution process at different temperatures under a constant pressure of 5MPa, it is pertinent to explore the modifications in the availability of oxygen at equivalent reaction temperatures. This comparison specifically focuses on the experiments conducted in Chapter 4, which were performed at atmospheric pressure within the temperature range of 85 °C to 95 °C for 4 hours, and the experiments conducted in the present Chapter at a temperature of 90 °C for 4 hours. While the temperatures are similar, there is a notable difference in the yield of liquid product. The reactions at atmospheric pressure between 85 °C and 95 °C resulted in a yield of 0.5 % to 0.53 %, whereas the reactions at 5MPa demonstrated a comparable higher yield of 1.8 %. This is a nearly four times increase in yield in the latter case.

Even though temperature reaction were similar, in the experiments conducted at atmospheric pressure, the oxidant, which was air, was introduced into the reactor through bubbling at a flow rate of 350 mL.min^{-1}. This approach ensured continuous oxygen supply to the reaction mixture.

However, in the experiments carried out at 5 MPa, the reaction system was pressurized with air, allowing for higher oxygen concentrations within the system.

To explain the observed difference in yield to liquids, there might be different reasons regarding the higher oxidation rate at 5 MPa compared to the use of oxygen bubbling at atmospheric pressure. Firstly, the increased oxygen concentration achieved by pressurizing the reaction system with air at 5MPa may have contributed to the enhanced oxidation. Pressurization may facilitate a greater dissolution of oxygen in the reaction mixture, resulting in a higher availability of oxygen for the oxidative coal dissolution process.

Secondly, the pressurization of the reaction system at 5MPa might have improved the mass transfer of oxygen into the coal matrix. The increased pressure can enhance the amount of oxygen dissolved in the liquid, consequently, this ensures a more abundant oxygen supply for the oxidative coal dissolution process than the oxygen supplied by bubbling air into the reactor at atmospheric pressure , leading to increased oxidation rates.

In addition to the differences in oxygen availability, the stirring process also underwent changes between the experimental setups. At atmospheric pressure, the reaction stirring system was limited to 300 rpm using a magnetic stir bar. In contrast, the Par reactor utilized a stirring system equipped with a turbine type impeller, which generated an excellent mixing action at 600 rpm, representing approximately 80 % of the maximum power output. This is potentially relevant to the reaction if the mass transport rate is higher than the reaction rate.

5.4.2 Proximate and Elemental analysis

Based on the proximate and elemental analysis from the feed presented Table 5-1 and the residue products in Table 5-7 and Table 5-8, there are observations at different reaction temperatures during the oxidative coal dissolution process at 5MPa that are important to discuss. At a reaction temperature of 90°C, the volatile matter and fixed carbon weight percentage increase compared to the feed based on the proximate analysis and it is consistent with the results obtained by *Siddiquee & De Klerk* [17] at similar temperature conditions. This can initially suggest that the mild

oxidative conditions at this temperature promote the increase in volatile matter and fixed carbon content in the residue. This implies the decrease in moisture and/or ash as it is explained below. As the reaction temperature increases beyond 90 °C, a contrasting behavior is observed. The fixed carbon weight percentage starts to decrease and reach a lower value than in the feed at 150 °C. On the other hand, the volatile matter weight percentage continues to increase up to 150 °C, but even when it decreases at 180 °C it is still higher than the value in feed.

The increase in the weight percentage of volatile matter and fixed carbon can be attributed to various factors. One possible factor is the decrease in moisture content from feed to residue. The feed coal has an initial moisture content of 18 %, while the moisture content in all the residue products is around 6 %. As the total percentage of moisture, volatile matter, fixed carbon, and ash represents 100 %, the reduction in moisture content for residue products, may cause a higher apparent increase of weight percentage in volatile matter and fixed carbon, but what might be happening is that the fixed carbon and volatile matter in the coal residue are not increasing at that shown rate, however, due to the larger decrease in moisture, the real percentage in fixed carbon and volatile matter content may not be immediately apparent.

The results of proximate analysis, conducted on a moisture-free basis as presented in Table 5-18, provide evidence of the impact of moisture in the results of volatile matter and fixed carbon weight percentage. The analysis reveals a less pronounced increase in volatile matter content from 90 °C to 150 °C. Additionally, the proximate analysis on a moisture-free basis reveals a significant decrease in the weight percentage of fixed carbon during oxidative coal dissolution. Notably, at 90 °C, the fixed carbon content in the residue is almost identical to that in the feed coal, indicating minimal alteration. Furthermore, as the temperature rises to 120 °C, the fixed carbon content in the residue becomes noticeably lower than that in the feed coal. This observation suggests that the oxidative coal dissolution process at from 120 °C to 180 °C induces a more substantial reduction in the proportion of fixed carbon, resulting in a discernible decrease in its weight percentage compared to the initial feed coal.

Table 5-18 Proximate Analysis on a moisture-free of feed and residue product from OCD during 4 hours at 5 MPa and temperature range 90-180 °C

Description	Feed and reaction temperature				
	Feed	90 °C	120 °C	150 °C	180 °C
Proximate Analysis in a moisture free basis (wt%)					
Volatile matter	41.3	42.3	43.3	44.8	38.5
Fixed Carbon	42.9	43.0	38.8	34.6	26.9
Ash	15.8	14.8	17.8	20.6	34.6

Due to the observation that there is still an increase in weight percentage of volatile matter up to the reaction at 150 °C, another factor that could explain this behavior, might be the incomplete or partial oxidation of coal during the oxidative dissolution process. At these temperatures, the oxidation reactions may not be fully extensive or complete, resulting in the partial oxidation of coal. As a consequence, volatile matter is released from the coal matrix without undergoing complete breakdown or conversion. This partial oxidation process leads to an accumulation of volatile matter in the coal residue, contributing to the observed increase in its weight percentage.

On the other hand, from elemental analysis, the carbon weight percentage in the residue decreases as reaction temperature increases. The decrease in carbon content might be a consequential result of the oxidative reactions occurring during the coal dissolution process. It implies that higher reaction temperatures facilitate more extensive oxidation reactions as it was presented in Chapter 2 section 2.3.4 and presented in experiments at similar temperature conditions [2]. Increasing the temperature of oxidation generally leads to higher rates of reaction and also and more extensive coal decomposition. This can result in greater removal of volatile matter and organic compounds from the coal, leaving behind a relatively lower quantity and quality of solid residue with a high ash content.

5.4.3   Mass loss from feed to residue

Figure 5-5 shows the mass loss of coal from feed to residue at 5 MPa and different temperatures in a moisture free basis. The figure presents the percentage of mass loss for each temperature point, highlighting the influence of temperature on the coal conversion during oxidative coal dissolution.
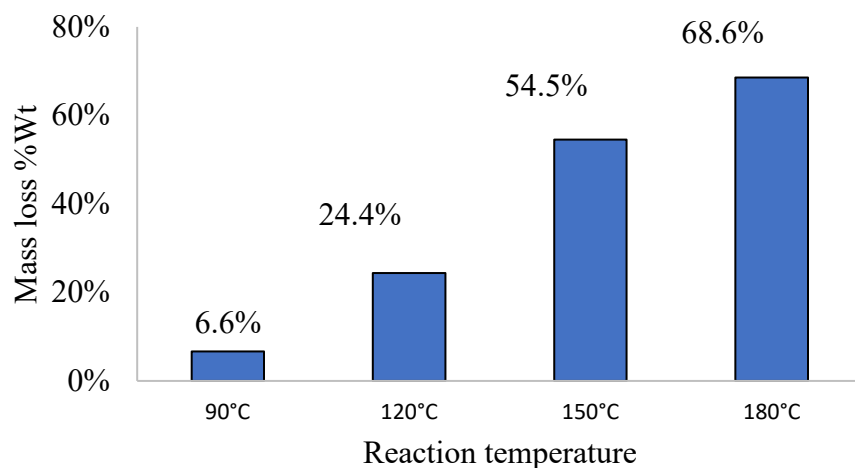
Figure 5-5 Mass loss of coal on a moisture free basis from feed to residue after reaction at 5 MPa and temperatures from 90 to 180 °C during 4 hours

At 90 °C, a relatively low temperature, the mass loss is recorded as 6.6 %. This indicates that only a small portion of the coal has undergone conversion or dissolution under these mild oxidative conditions. Most of the coal remains in the solid residue, suggesting limited oxidation and dissolution of the organic matter at this temperature.

As the temperature increases to 120 °C, a significant increase in mass loss is observed, reaching 24.4 %. This suggests that the coal is more actively undergoing oxidative dissolution, resulting in a substantial reduction in the solid residue. The higher temperature promotes enhanced oxidation reactions, leading to the dissolution and removal of organic compounds from the coal. Further elevating the temperature to 150 °C and 180 °C, the mass loss continues to increase, reaching 54.5 % and 68.6 %, respectively. These weight loss to residue products indicate a significant conversion of the coal into liquid extract and gas products through oxidative dissolution. It can be implied from it that higher temperatures facilitate the dissolution and removal of a greater amount of organic matter from the coal, promoting more extensive oxidation reactions. As the temperature rises, the degree of oxidative dissolution increases, resulting in higher mass loss and a decrease in the solid residue.

5.4.4 Effect of temperature in carbon balance and yield

Figure 5-6 presents the carbon balance yield for residue, extract, and gases all together in oxidative coal dissolution reactions. This comprehensive data provides crucial insights into the efficiency and distribution of carbon throughout the entire reaction process at 5MPa.

The variation observed in the carbon balance, represented by the difference between the sum of carbon in residue, liquid extract, and gas products and 100 % of the feed coal, can be attributed to several factors. One factor is the incomplete collection of residue coal from the centrifuge tubes after separation from the liquid extract in the centrifugation process. Despite efforts to collect all the residue, a small amount of coal residue may have remained in the centrifuge tubes. To mitigate this issue, additional measures were taken, such as placing the centrifuge tubes in the fumehood for an extended period to ensure thorough drying and collecting any remaining coal. However, despite these precautions, a small amount of coal was still lost in the centrifuge tubes, leading to a lower carbon balance in the solid residue and consequently reducing the total carbon content in the products compared to the initial feed.
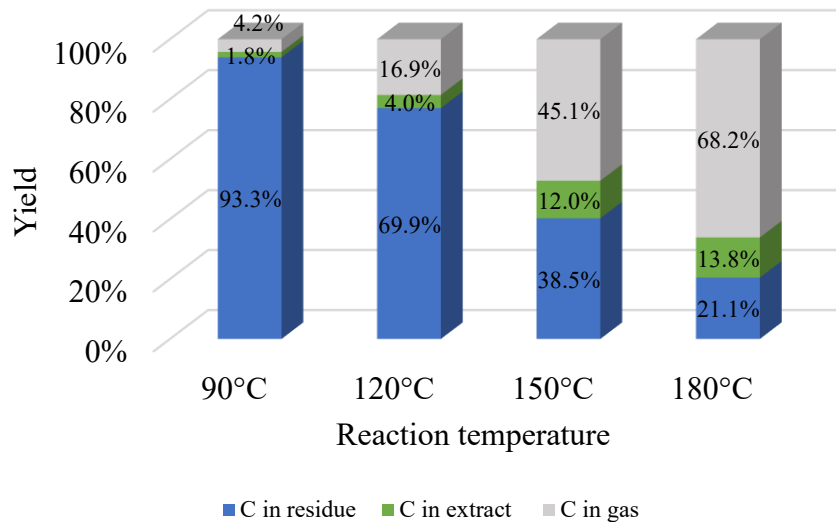
Figure 5-6 Carbon balance yield from residue, extract and gases after reaction at 5 MPa and temperatures from 90 to 180 °C during 4 hours

Another significant factor that can affect the carbon balance calculation is the collection of sample gases after the completion of the reaction. The gas samples were collected at a pressure of 3.44 MPa (500 psi), which is different from the final reaction pressure. This change in pressure alters the equilibrium between the liquid and gas phases, resulting in variations in the composition and partial pressure of the gases. For instance, gases like CO_2, which exhibit significant solubility in water at high pressure, experience an increase in concentration after pressure relief. This change in gas composition and increased partial pressure of CO_2 contribute to a higher calculated total carbon content in the gas products compared to the initial feed.

Despite the factors that may introduce variations in the carbon balance calculation, the results of the study still provide valuable insights into the distribution of carbon in the coal dissolution process. The carbon balance values obtained at different reaction temperatures indicate the overall efficiency of carbon conversion and the relative distribution of carbon among the residue, liquid extract, and gas products.

The analysis of the carbon distribution between liquid and gas products reveals that the carbon yield to liquids is consistently lower than the carbon yield to gases across all reaction temperatures. This indicates that a substantial portion of the carbon undergoes conversion to gaseous products instead of remaining in the liquid phase. At 90 °C, the carbon yield to liquids is merely 1.8 %, while the carbon yield to gases is approximately 2.2 times higher at 4.2 %. As the reaction temperature increases, this disparity becomes even more pronounced. At 120°C, the carbon yield to liquids is 4.0 %, which is 4.2 times lower than the carbon yield to gases at 16.9 %. The trend continues at 150 °C, where the ratio between liquid and gas products decreases to 3.7 times, with the carbon yield to liquids improving to 12.0 %. However, even at this temperature, the carbon yield to gases still significantly surpasses it. Finally, at 180 °C, the ratio reaches its peak of approximately 5 times, as the carbon yield to liquids further increases to 13.8 % and the carbon yield to gases reaches 68.2 %.

The previous analysis may indicate that the best selectivity to liquid products during oxidative coal dissolution at 5 MPa occurs at 150 °C. At this temperature, the relationship between gas and liquid products is the lowest, However, achieving optimal selectivity towards liquid products remains a

challenge because the results obtained from the analysis of carbon distribution at different reaction temperatures indicate a higher selectivity towards gaseous products over liquid products, which suggests overoxidation during the oxidative coal dissolution process. This overoxidation has several notable disadvantages. It results in a loss of desired liquid hydrocarbons as a portion of the carbon is diverted towards the formation of gases, leading to a decreased yield of valuable liquid products. Consequently, the quantity of extractable liquid hydrocarbons from the coal feed is reduced. Overoxidation might also cause a shift in the composition of the liquid products, lowering the concentration of desired liquid products, however it is not possible to prove without a further analysis of the liquid extract product.

The decrease in selectivity towards liquid products due to overoxidation carries also significant economic implications. The reduced concentration of possible valuable liquid hydrocarbons directly impacts the overall value of the product stream. Lower yields of valuable liquid products result in decreased revenue and profitability for the coal dissolution process. The economic viability of the operation may be compromised as the lower value of the product stream affects the cost-benefit ratio and potential return on investment. Additionally, the reduced selectivity towards desired liquid products may limit the commercial viability of the process, potentially discouraging investors and industry stakeholders from pursuing such operations at an industrial level. Therefore, addressing overoxidation and improving the selectivity towards desired liquid products is crucial for maximizing economic benefits and ensuring the sustainability of the coal dissolution process.

5.4.5 Changes in oxygen consumption, carbon monoxide and carbon dioxide generation

O_2 consumption, CO_2 generation, and CO generation in the oxidative coal dissolution reactions at 5 MPa, as a function of temperature, are presented in Figure 5-7. The oxygen content in the feed was determined by assuming a 21 % volume of O_2 in air and calculated using the Peng-Robinson equation for gases and Henry's law for dissolved gases in liquid phase at the initial reaction pressure. It was also assumed that prior to the reaction, there is no CO_2 or CO in feed.

These findings collectively suggest that the oxidation of coal intensifies with increasing reaction temperature. The higher temperatures facilitate greater oxygen utilization and promote more

extensive coal oxidation, resulting in increased production of CO_2 and CO. The decrease in the remaining O_2 content further supports the notion that coal oxidation is enhanced at elevated temperatures.
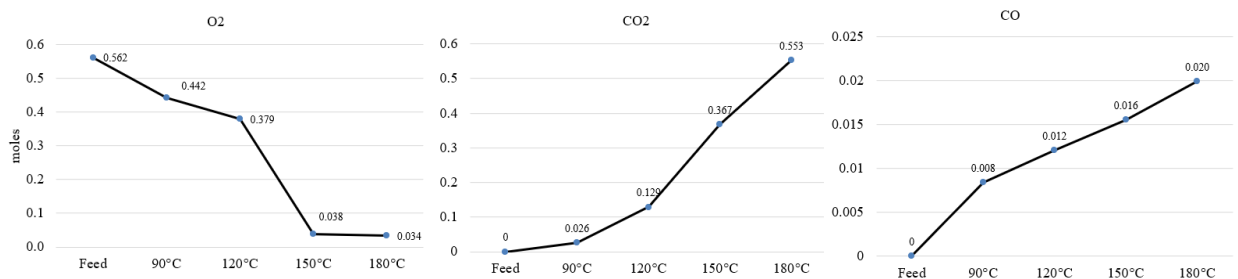
Figure 5-7 O_2 consumption, CO_2 and CO generation for reactions at 5 MPa, 4 hours and temperatures from 90 to 180 °C

As the temperature increases, the generation of CO_2 and CO increases, indicating higher coal conversion to those specific products. The amount of O_2 consumed during the reactions is influenced by temperature, with reduction observed at different temperature levels up to an almost total consumption at the highest reaction temperature (180 °C). The rate of consumption of O_2 moles is different at each specific temperature. It is observed for example that the higher decrease in O_2 moles is observed between 120 °C and 150 °C (0.341 moles) which coincide with the higher increase of CO_2 moles (0.238 moles) for the same interval of temperature. However, regarding to the CO generation, the higher number of moles (0.008 moles) was from feed to 90 °C.

It is also observed that at 150 °C almost all the oxygen is consumed with about 94 % of the initial amount. Between the reactions at 150 °C and 180 °C there is not a significant change in oxygen composition in gases, but the moles of CO_2 and CO are still increasing steadily. The increasing generation of CO_2 and CO in the gas phase suggests a greater extent of carbon conversion to gas products instead of the desired liquid products. Identifying these temperature-dependent changes in gas composition, might be possible to understand the mechanisms involved in coal dissolution and provides insights for developing efficient and controlled coal conversion processes.

155

5.5   Conclusions

- Pressurizing the reaction system at 5MPa in a Parr reactor significantly increases the yield of liquid product compared to experiments at atmospheric pressure at similar temperatures. The higher oxygen concentration achieved through pressurization and the improved mass transfer of oxygen into the coal matrix contribute to enhanced oxidation rates.

- The reaction yield to liquid products represented by the yield to carbon in liquid extract at reaction pressure of 5 MPa and 4 hours reaction increases with an increase temperature from 1.8 % at 90 °C to 13.8 % at 180 °C.

- The carbon yield to gases is consistently higher than the carbon yield to liquids across all reaction temperatures at 5MPa. This suggests that a significantly higher portion of carbon undergoes conversion to gaseous products instead of remaining in the liquid phase.

- Between the reaction temperatures studied, the highest selectivity to liquid products during oxidative coal dissolution occurs at 150 °C, as it has one of lowest ratio between gas and liquid products and the selectivity to liquid products evaluated as the carbon content is 12 %. However, achieving a better selectivity towards liquid products remains a challenge due to the higher preference for gaseous products, indicating overoxidation during the process.

- Metals concentration in liquid extract increase with the increase in reaction temperatures at 5 MPa and 4 hour time, indicating that higher temperatures promote the release and dissolution of metals into the liquid phase. However, at 180 °C, the concentration increases for certain metals, such as sodium, iron, potassium, and nickel, appears to be slightly lower compared to that observed at 150 °C.

5.6   References

[1]   Wang, W.; Hou, Y.; Wu, W.; Niu, M.; Liu, W. Production of benzene polycarboxylic acids from lignite by alkali-oxygen oxidation. *Ind. Eng. Chem. Res.* **2012**, *51*, 14994-15003.

[2]   Savich; T. R.; Howard, H. C. Oxidation of bituminous coal to organic acids by nitric acid and oxygen. *Ind. Eng. Chem.* **1952**, *44* (6), 1409-1411.

[3]   Yang, F.; Hou, Y.; Niu, M.; Lu, T.; Wu, W.; Liu, Z., Catalytic oxidation of lignite to carboxylic acids in aqueous H5PV2Mo10O40/H2SO4 solution with molecular oxygen. *Energy Fuels* **2017**, *31*, 3830-3837.

[4]   Gluskoter, H. J.; Shimp, N. F.; Ruch, R. R. Coal analyses, trace elements, and mineral matter. In *Chemistry of coal utilization, Second Supplementary Volume*; Elliott, M. A. ed; Wiley: New York, 1981, pp. 369-424.

[5]   Speight, J. G. *The chemistry and technology of coal,* 3rd ed.; CRC Press: Boca Raton, 2012.

[6]   Berkowitz, N. *An introduction to coal technology*; Academic Press: New York,1979.

[7]   Dunnivant, F. M; Ginsbach, J. W. Flame Atomic Absorbance and Emission Spectroscopy and Inductively Coupled Spectrometry - Mass Spectrometry, Coal. Typology-Physics-Chemistry-Constitution, 1st ed.; Whitman college: Walla Walla, 2009.

[8]   Peng, D. Y.; Robinson, D. B. (1976). *A New two-constant equation of state. Industrial and Engineering Chemistry: Fundamentals* 1976, 15, 59–64.

[9]   Riley, J. T. *Routine coal and coke analysis: collection, interpretation, and uses of analytical data*, 2nd ed.; ASTM International: West Conshohocken, 2014.

[10]   Reid, R. C; Prausnitz, J. M.; Poling, B. E. *The Properties of Gases and Liquids*, 4th ed.; McGraw-Hill: New York, 1987.

[11]   Shen, V.K.; Siderius, D.W.; Krekelberg, W.P.; Hatch, H.W.; Eds. NIST Standard Reference Simulation Website, NIST Standard Reference Database Number 173, National Institute of Standards and Technology. https://webbook.nist.gov/chemistry/ (accessed 04 23, 2023).

[12]   Atkins, P.; De Paula, J. *Physical Chemistry* [online], 8th ed.; W. H. Freeman and Company: New York, 2006. http://www.rnlkwc.ac.in/pdf/study-material/chemistry/Peter_Atkins__Julio_de_Paula__Physical_Chemistry__1_.pdf (accessed 04 22, 2023)

[13]   Huang, Z.; Urynowicz, M. A.; Haider, R.; Sattar, H.; Saleem, M.; Hoang, L.; Han, N.T.; To, K.A.; Hung, L.Q.; Ali, M.I.; Guo, H. Biogenic methane generation from Vietnamese coal after pretreatment with hydrogen peroxide. *International Journal of Energy Research* **2021**, 45(13), 18713-18721.

[14]   Chen, T.; Rodriguez, S.; Golding, S. D.; Rudolph, V. Improving coal bioavailability for biogenic methane production via hydrogen peroxide oxidation. *International Journal of Coal Geology* **2018**, *195*, 402-414.

[15]   Chen, Q.; Kang, Y.; You, L.; Yang, P.; Zhang, X.; Cheng, Q. Change in composition and pore structure of Longmaxi black shale during oxidative dissolution. *International Journal of Coal Geology* **2017**, *172*, 95-111.

[16]   Yang, S.; Liu, D.; Li, Y.; Yang, C.; Yang, Z.; Chen, X.; Li, H.; Tang, Z. Experimental study on the oxidative dissolution of carbonate-rich shale and silicate-rich shale with H_2O_2, $Na_2S_2O_8$ and $NaClO$: Implication to the shale gas recovery with oxidation stimulation. *Journal of Natural Gas Science and Engineering* **2020**, *76*, 103207.

[17]   Siddiquee, M. N.; De Klerk, A. Heteroatom removal as pretreatment of boiler fuels. *Energy Fuels* **2019**, *33*, 5790-5801.

6. Oxidative coal dissolution at 1 MPa and different temperatures

Abstract

To explore the possibility of enhancing selectivity towards liquid products and mitigating overoxidation noticed at 5 MPa, a new set of experiments was conducted at a reduced pressure of 1 MPa while maintaining the same temperature range (90 to 180 °C) and duration (4 h). Analysis of the reaction yields and carbon distribution among product streams was similar to the 5 MPa reactions.

Findings show that the yield to liquid products increased with temperature, reaching 5.2 % at 150 °C in the 1 MPa oxidative coal dissolution reactions. The temperature range of 150 to 180 °C favored the highest carbon yield to liquid products, but a shift towards higher gas product generation was already observed at 180 °C. Additionally, the heating value of the residue at 90 °C increased after oxidative coal dissolution, suggesting that specific operating conditions induced the liberation of oxygen in some form from the coal molecule, rather than being solely attributed to the process itself. Moreover, higher reaction temperatures at 1 MPa and 4 hour duration led to increased metal concentrations in the aqueous product, indicating greater metal release and dissolution into the liquid phase. A comparison with 5 MPa reactions showed that higher pressures promoted a higher degree of metal dissolution in the liquid phase.

Keywords: oxygen concentration, heating value, reaction temperature, OCD

6.1   Introduction

Oxidative coal dissolution experiments were conducted at a pressure of 5 MPa and temperatures from 90 to 180 °C for 4 hours in Chapter 5. The results revealed a notable increase in the carbon yield to liquid products, reaching up to 14% at 180 °C. This was a significant improvement compared to the previous oxidative coal dissolution experiments in Chapter 4, where lower temperatures at atmospheric pressure were employed, resulting in a carbon yield to liquid products of only about 1%.

However, despite the enhanced carbon yield to liquids, it was consistently observed that the carbon yield to gases, primarily consisting of carbon dioxide (CO_2) and carbon monoxide (CO), remained higher than the yield to liquid products across all reaction temperatures at 5 MPa. This suggests a substantial conversion of carbon to gaseous products, indicating a potential occurrence of overoxidation in the coal oxidation process.

To address the issue of overoxidation and explore the possibility of shifting the selectivity towards the liquid phase, a new set of experiments is conducted. The oxidative coal dissolution reactions are performed at a lower pressure of 1 MPa, maintaining the same temperature range of 90 to 180 °C and a reaction duration of 4 hours. The analysis and evaluation performed in these experiments are similar to those conducted in the 5 MPa reactions, aiming to assess the effectiveness of carbon conversion and the distribution of carbon among the different product streams. This approach enables investigation into the potential benefits of conducting the oxidative coal dissolution process at reduced pressures mitigating overoxidation and improving selectivity towards valuable liquid products.

6.2   Experimental

6.2.1   Materials

Coal from the northwest area of Canada (Alberta and Saskatchewan) was utilized as the feedstock for the oxidative coal dissolution process, which is the focus of this study. The entire coal's characterization is provided in Chapter 3. Table 6-1 presents the proximate and elemental analysis results of the sample feed for experiments under a pressure of 1 MPa, at different temperatures in the autoclave reactor. Additionally, as a reference, it also shows the results of proximate and elemental analyses conducted on the feed samples utilized in the experiments outlined in Chapter 4 at atmospheric pressure (0.1 MPa) varying temperatures (same sample used for characterization in Chapter 3) and time periods, and the experiments from Chapter 5 conducted at 5 MPa pressure. The same batch of coal was used for all the experiments conducted throughout the study in Chapter 6.

Table 6-1 Characterization of Mancal coal feed for reactions at 1 MPa

Description	Feed OCD Temperatures at 0.1 MPa		Feed OCD Time at 0.1 MPa		Feed OCD Temperatures at 5 MPa		Feed OCD Temperatures at 1 MPa	
Proximate Analysis (wt%)[a]	**x**	**s**	**x**	**s**	**x**	**s**	**x**	**s**
Moisture	26.5	0.02	25.8	0.0	18.0	0.02	17.5	0.05
Volatile matter	30.5	0.32	30.4	0.3	33.9	0.32	31.5	0.08
Fixed Carbon	32.8	0.25	30.6	0.3	35.2	0.30	33.6	0.11
Ash	10.2	0.59	13.2	0.0	13.0	0.03	17.4	0.01
Elemental Analysis (wt%, maf)[b]								
Carbon	71.7	0.17	72.3	0.31	71.1	0.36	71.2	0.23
Hydrogen	4.1	0.22	4.4	0.29	2.7	0.41	3.4	0.22
Nitrogen	1.3	0.01	1.4	0.01	1.3	0.01	1.3	0.01
Sulfur	0.8	0.01	0.3	0.00	0.4	0.00	<0.3[e]	-
Oxygen[c]	22.0	-	21.5	-	24.5	-	23.9	-
H/C molar ratio (mol/mol)	0.69	-	0.73	-	0.45	-	0.56	-
O/C molar ratio (mol/mol)	0.23	-	0.22	-	0.26	-	0.25	-
Gross heating value[d] (MJ/kg)	26.3	-	27.0	-	23.5	-	24.6	-

[a]Averages (x) and sample standard deviations (s) of duplicate analyses
[b]Calculated on a moisture, ash-free basis using elemental and proximate Analysis
[c]Oxygen was determined by difference with Sulfur consentration assumed as 0.3 wt% for reactions at 1 MPa
[d]Calculated on the basis of Dulong's correlation
[e]Sulfur is detected in the sample; however, the concentration falls below the detection limit of the calibration method employed (0.3 wt%)

The elemental distribution of Mancal's Coals feed, employed in experiments conducted in this chapter, is presented in Figure 6-1. Additionally, Table 6-2 presents the weight percentages corresponding to individual mineral elements detected in the sample through SEM-EDS analysis. The analysis was conducted utilizing the identical methodology employed in the preceding chapters. Conspicuous bright sites or mineral chunks, such as silicon and aluminum containing minerals were also abundant in the feed as in the feed samples used for experiments in previous chapters.

Figure 6-1 Secondary Electron **SE** image from Mancal's Coal elemental distribution in SEM-EDS (Map/Spectrum) for feed to OCD with changes on temperature at 1 MPa.

Table 6-2 Main mineral elements identified in Mancal's coal for feed to OCD with changes on temperature at 1 MPa.

Element	Wt Percentage in coal (%)	
	x	s
Si	2.04	0.71
Al	1.84	0.34
Ca	1.57	1.24
Na	0.43	0.16
Fe	0.33	0.26
S	0.35	0.17
Mg	0.22	0.17

Averages (x) and sample standard deviations (s) of five different measures

In addition to Mancal's Coals, all materials employed in this chapter were the same as described in chapters 4 and 5.

6.2.2 Equipment and procedure

This set of experiments was performed in batch mode configuration. The equipment and procedures remain consistent with those preformed in chapter 5 where all details are provided. Reaction conditions were, 1 MPa (145 psi) gauge pressure, residence time of 4 hours and a range of temperatures spanning from 90 °C to 180 °C, including intervals of 30 °C (90 °C, 120 °C, 150 °C, and 180 °C). In this set of reactions gas product samples at the end of the reaction were collected at three different gauge

pressures, 1 MPa (145 psi), 0.69 MPa (100 psi), and 0.34 MPa (500 psi), in 500 mL gas bags for further analysis using Gas Chromatography.

Two additional experiments were conducted, maintaining all variables identical to the previous experiments, except for the substitution of air with nitrogen gas. In these experiments, the cylinder of air was replaced with a High Purity 4.8 Nitrogen cylinder to ensure an oxygen-free environment during the reactions conducted at 90 °C. These control experiments were included to differentiate between temperature and oxidation as contributing factors to the observed increase in heating value of the coal residue after conversion at 90 °C at the given conditions.

6.2.3   Analyses

Proximate and elemental analyses and scanning electron microscope (SEM) coupled with energy dispersive X-ray spectroscopy (EDS) performed in this set of experiments were described in Chapter 3. Total organic carbon (TOC) content of extract and the density of liquid feed water and the aqueous phase of the extract of extract samples were described in Chapter 4. Inductively Coupled Plasma-Optical Emission Spectroscopy (ICP-OES) and Gas chromatography (GC) were described in Chapter 5.

6.2.4   Calculations

Calculations methodology for oxygen weight composition, moisture, ash-free basis elements compositions and heating values based on proximate and elemental analyses results of solid coal (residue) in this set of experiments were described in Chapter 3. Carbon balance, carbon yield and the increase in oxygen content of residue as compared to the oxygen content of the feed were described in Chapter 4. The calculation of the gas weight of any specific gas sample was described in Chapter 5.

6.2.5   Calibrations

Calibrations of the analytical equipment were the same for this set of experiments and were described in Chapters 3, 4 and 5.

6.3 Results

6.3.1 Material Balance

Table 6-3 shows the measurements used in material balance of the reactants entering the system "in" and the products exiting the system "out" for the OCD reactions and reactions performed using N_2 over a duration of 4 hours. These reactions occurred under conditions of 1 MPa pressure and temperatures ranging from 90 to 180 °C. The mass determination is the same to the calculations shown in Chapter 5.

Table 6-3 Measurements used in material balance of OCD and reactions performed using N_2 at 1 MPa, 4 hours reaction and temperatures from 90 to   180 °C

Reaction Temperature	'In' (g)				'Out' (g)			
	Feed coal	Water		Feed Air/N_2	Residue	Extract	Water from residue	Gas product
		Initial water	Washing water					
90 °C	20.31	499.08	49.91	15.27	16.88	535.28	5.92	15.16
120 °C	20.37	499.08	49.91	15.27	13.47	537.44	6.02	14.29
150 °C	20.69	499.08	49.91	15.27	15.14	535.67	4.56	14.36
180 °C	20.67	499.08	49.91	15.27	15.15	536.62	4.88	13.94
90 °C with N_2 R1	20.77	499.08	49.91	14.82	18.47	543.18	6.05	14.87
90 °C with N_2 R2	20.57	499.08	49.91	14.82	18.21	542.17	5.94	14.87

Table 6-4 presents the material, encompassing the conversion from reactants to products. On average the material balance closed within a margin of 3 %.

Table 6-4 Material balance of OCD at 1 MPa, 4 hours reaction and temperatures ranging from 90 to 180 °C

Description	Total mass coming 'in'	Total mass going 'out'	Yield to products (%)
Reaction Temperature			
90 °C	584.57	573.25	98.06
120 °C	584.63	574.21	98.22
150 °C	584.95	569.73	97.40
180 °C	584.93	570.59	97.55
90 °C with N_2 R1	584.58	582.58	99.66
90 °C with N_2 R2	584.38	581.19	99.45

6.3.2 Proximate and Elemental Analysis

Proximate and elemental analyses were performed on the solid OCD products (residue) generated by reactions at 1 MPa and temperature range 90-180 °C (90, 120, 150 and 180 °C). The results of these analyses are presented in Table 6-5 and Table 6-6.

Table 6-5 Proximate Analysis of residue product from OCD at1 MPa**,** 4 hours reaction and temperatures from 90 to 180 °C

Description	Reaction temperature							
	90 °C		120 °C		150 °C		180 °C	
Proximate Analysis (wt%)[a]	X	S	X	S	X	S	X	S
Moisture	7.2	0.03	7.4	0.06	6.6	0.03	6.8	0.02
Volatile matter	35.9	0.10	36.3	0.02	37.4	0.57	35.4	0.06
Fixed Carbon	37.9	0.48	37.5	0.07	37.4	0.24	38.2	0.01
Ash	18.9	0.41	18.8	0.15	18.6	0.35	19.5	0.03

[a]Averages (x) and sample standard deviations (s) of duplicate analyses

Table 6-6 Elemental Analysis of residue product from OCD at 1 MPa, 4 hours reaction and temperatures from 90 to 180 °C

Description	Reaction temperature							
	90 °C		120 °C		150 °C		180 °C	
Elemental Analysis (wt%, daf)[a]	X	S	X	S	X	S	X	S
Carbon	72.0	0.61	69.9	0.25	68.8	0.53	70.3	0.76
Hydrogen	3.9	0.10	3.6	0.04	3.4	0.05	3.4	0.03
Nitrogen	1.3	0.00	1.3	0.03	1.3	0.03	1.3	0.01
Sulfur[b]	<0.3	-	<0.3	-	<0.3	-	<0.3	-
Oxygen[c]	22.6	-	24.9	-	26.2	-	24.7	-
H/C molar ratio (mol/mol)	0.64	-	0.62	-	0.58	-	0.57	-
O/C molar ratio (mol/mol)	0.24	-	0.27	-	0.29	-	0.26	-
Gross heating value[d] (MJ/kg)	25.9	-	24.4	-	23.4	-	24.2	-

[a]Averages (x) and sample standard deviations (s) of duplicate analyses. Calculated on a moisture, ash-free basis using elemental and proximate Analysis
[b]Sulfur is detected in the sample; however, the concentration falls below the detection limit of the calibration method employed (0.3 wt%)
[c]Oxygen was determined by difference with Sulfur consentration assumed as 0.3 wt% for reactions at 1 MPa
[d]Calculated on the basis of Dulong's correlation

Table 6-7 shows the change in ash content from the feed to the residue product at different reaction temperatures in order to assess the internal consistency of the analytical results.

Table 6-7 Change in ash content from feed to residue product from OCD at 1 MPa, 4 hours reaction and temperatures from 90 to 180 °C

Description	Reaction temperature			
	90 °C	120 °C	150 °C	180 °C
Total ash in feed (g)	3.53	3.54	3.60	3.60
Total ash in residue (g)	3.19	3.10	2.81	2.96
Change in ash from feed to residue (g)	0.34	0.44	0.79	0.64
Change in ash from feed to residue (%)	9.6	12.5	21.9	17.7

As it was noticed in Chapters 4 and 5, the mass of ash in the residue product was lower than the mass of ash in the feed coal across all reaction temperatures. For the reactions at 1 MPa the percentage decrease in ash content remained relatively moderate, ranging from approximately 9.6 % to 17.7 % at the different reaction temperatures.

Regarding the proximate analysis shown in Table 6-5 similar behavior for volatile matter and fixed carbon is observed as it was described and discussed in Chapter 5. Regarding the elemental analysis shown in Table 6-6 as the reaction temperature increases from 90 to 150 °C, there is a decrease in both carbon and hydrogen content. However, at 180 °C, the carbon content experiences an increase while the hydrogen content remains consistent with the percentage observed at 150 °C. Meanwhile, the nitrogen content remains constant across all the reactions, showing no significant variation.

It can also be observed in Table 6-6 that oxygen content increases as OCD temperatures increase from 120 °C to 180 °C at 1 MPa. This suggests that higher temperatures promote the incorporation of oxygen into the residue during the oxidative coal dissolution process. However, in the reaction conducted at 90 °C the oxygen content actually decreases compared to the feed from 23.9 to 22.6 wt% moisture- and ash-free basis (maf). Consequently, this results in a decrease in the O/C (oxygen-to-carbon) molar ratio and an increase in the gross heating value relative to the feed. This behavior is noteworthy because According to *Van Krevelen* [1] and what was presented in Chapter 2 Section 2.3.1 in coal oxidation processes O/C ratio increases as oxidation proceeds.

The similar behavior of increasing oxygen content with increasing temperatures is also observed in reactions conducted at 5 MPa, as presented in Chapter 5, Table 5-7. In that particular case, as

the OCD temperatures increase from 120 °C to 180 °C, the oxygen content in the liquid extract increases compared to the feed. However, when comparing the feed with the OCD at 90 °C, the oxygen content decreases from 24.5 to 23.6 wt% maf. This behavior is significant because it contradicts the expectations based on *Van Krevelen's* [1] observations and the information presented in Chapter 2, Section 2.3.1, which suggest that in coal oxidation processes, the oxygen-to-carbon (O/C) molar ratio increases as oxidation proceeds.

To comprehensively address the discrepancy observed between the behavior of oxygen content and O/C ratio, additional experiments were conducted to investigate if it is specifically related to the oxidation process of coal in the liquid phase or if there is something else involved. To explore this further, two reactions were performed under identical conditions of 1 MPa and 90 °C, but with the substitution of air by nitrogen (N_2). The objective is to evaluate the impact of oxygen exclusion on the resulting reaction products. The proximate and elemental analysis of feed which is from the same batch of coal used for all the previous experiments conducted, and products are presented in Table 6-8 and Table 6-9.

Table 6-8 Proximate Analysis of feed and residue product from reactions at1 MPa, 4 hours reaction and 90 °C with N_2

Description	Feed		Reaction 1 90 °C		Reaction 2 90 °C	
Proximate Analysis (wt%)[a]	**x**	**s**	**x**	**s**	**x**	**s**
Moisture	16.4	0.04	11.4	0.04	11.8	0.04
Volatile matter	32.4	0.06	34.2	0.08	33.8	0.07
Fixed Carbon	34.2	0.01	37.2	0.50	36.7	0.11
Ash	17.0	0.12	17.2	0.62	17.7	0.08

[a]Averages (x) and sample standard deviations (s) of duplicate analyses

Table 6-9 Elemental Analysis of feed and residue product from reactions at1 MPa, 4 hours reaction and 90 °C with N_2

Description	Feed		Reaction 1 90 °C		Reaction 2 90 °C	
Elemental Analysis (wt%, daf)[a]	**x**	**s**	**x**	**s**	**x**	**s**
Carbon	69.9	0.06	71.1	0.00	71.8	0.20
Hydrogen	2.3	0.05	3.1	0.07	3.2	0.12
Nitrogen	1.3	0.02	1.3	0.01	1.3	0.00
Sulfur	0.3	0.04	<0.3[b]	-	0.3	0.00
Oxygen[c]	26.2	-	24.2	-	23.4	-
H/C molar ratio (mol/mol)	0.40	-	0.52	-	0.53	-
O/C molar ratio (mol/mol)	0.28	-	0.26	-	0.24	-
Gross heating value[d] (MJ/kg)	22.3	-	24.2	-	24.7	-

[a]Averages (x) and sample standard deviations (s) of duplicate analyses. Calculated on a moisture, ash-free basis using elemental and proximate Analysis
[b]Sulfur is detected in the sample; however, the concentration falls below the detection limit of the calibration method employed (0.3 wt%)
[c]Oxygen was determined by difference with Sulfur consentration assumed as 0.3 wt% for reactions at 1 MPa
[d]Calculated on the basis of Dulong's correlation

Table 6-10 shows the change in ash content from the feed to the residue product for reactions with N_2 in order to assess the internal consistency of the analytical results.

Table 6-10 Change in ash content from feed to residue product from reactions at1 MPa, 4 hours reaction and 90 °C with N_2

Description	Reactions at 90 °C with N_2	
	Reaction 1	**Reaction 2**
Total ash in feed (g)	3.54	3.50
Total ash in residue (g)	3.18	3.22
Change in ash from feed to residue (g)	0.36	0.28
Change in ash from feed to residue (%)	10.1	8.1

6.3.3 Total carbon to liquid extract

Table 6-11 presents the total carbon content (TC) in the liquid extract obtained from the total carbon analysis conducted on the liquid extract product during a 4-hour reaction at 1 MPa, with temperatures ranging from 90 to 180 °C. Similar to the observations made during reactions conducted at a pressure of 5 MPa, the most significant change in total organic carbon (TOC) occurs between 120 and 150 °C, resulting in an increase of approximately 0.32 grams of carbon. However,

at 1 MPa and 180 °C, the Total Organic Carbon experiences a decrease compared to the reaction conducted at the same pressure but at 150 °C. The total inorganic carbon (TIC) demonstrates relatively minor variations between 90 and 120 °C but exhibits a significant decrease at 150 and 180 °C.

In relation to the reactions conducted using nitrogen (N_2) at a temperature of 90 °C, the resultant liquid extract exhibited a lower quantity of Total Organic Carbon (TOC) in comparison to all Organic Carbon Distribution (OCD) reactions. However, these TOC levels remain in proximity to those observed in the OCD reaction at 90 °C. Furthermore, the Total Inorganic Carbon (TIC) content is approximately half of the value observed in reactions conducted within the temperature range of 90 to 120 °C.

Table 6-11 Total carbon in liquid extract of OCD and reactions performed using N_2 at 1 MPa, 4 hours and temperatures from 90 to 180 °C

Reaction temperature (°C)	TOC (g)	TIC (g)	TC (g)
90	0.110	0.012	0.122
120	0.173	0.013	0.186
150	0.493	0.001	0.494
180	0.335	0.001	0.336
90 with N_2 R1	0.092	0.007	0.099
90 with N_2 R2	0.096	0.005	0.101

6.3.4 Gases analysis

Table 6-12 presents the gases balance for the OCD and reactions performed using N_2 conducted at a pressure of 1 MPa, with a reaction time of 4 hours, and temperatures ranging from 90 to 180 °C. The table provides the mass of the gases involved, both as inputs 'in' and outputs 'out'.

As with the reactions at 5 MPa, the gas analysis results presented in Table 6-12 reveal similar trends as the OCD reaction temperature changes. N_2 remains relatively stable across different temperatures. The amount of O_2 shows a noticeable decrease as the reaction temperature increases, with the higher change between 120 and 150 °C. The amount of oxygen at the end of the higher temperature reaction 180 °C is minimal. On the other hand, the generation of CO_2 and CO shows

an increase as the reaction temperature increases, particularly evident within the same temperature range where oxygen experiences the greatest decrease.

In the context of the reactions executed under nitrogen atmosphere at a temperature of 90 °C, trace quantities of oxygen and carbon dioxide were identified within the resultant product gas. Carbon monoxide was not detected in the samples analyzed.

Table 6-12 Gases balance of OCD and reactions performed using N_2 at 1 MPa, 4 hours and temperatures from 90 to 180 °C

Reaction	'In' (g)		'Out' (g)			
Temperature (°C)	N_2	O_2	N_2	O_2	CO_2	CO
90	11.698	3.571	12.013	2.895	0.217	0.039
120	11.698	3.571	11.532	1.698	1.002	0.057
150	11.698	3.571	11.053	0.339	2.896	0.073
180	11.698	3.571	10.727	0.205	2.916	0.095
90 with N_2 R1	14.821	0.000	14.638	0.163	0.071	0.000
90 with N_2 R2	14.647	0.000	14.647	0.155	0.067	0.000

6.3.5 Carbon balance

Carbon balance to residue

The tabulated data in Table 6-13 shows the carbon balance to residue for the OCD reactions and reactions performed using N_2 at 1 MPa, as a function of temperature. It details the feed on moisture, ash-free basis, and the quantities of carbon present in the coal feed before the reaction, as well as in the residue after the reaction. The division between these quantities is expressed as the percentage of unconverted carbon, representing the portion that did not react to liquid or gas products during the reaction process.

The carbon balance to residue of OCD reactions at 1 MPa presents the same trend but with a much smaller variation than what was observed in reactions at 5 MPa. As the reaction temperature increases, the percentage of unconverted carbon decreases up to 150 °C. At 90 °C, the unconverted carbon accounts for 95.4% of the carbon present in the feed. However, as the temperature rises to 120 °C, the percentage decreases to 90.1%. Further increase in temperature to 150 °C results in

170

the highest interval reduction, with the unconverted carbon constituting only 81.4%. At the highest temperature of 180 °C, the percentage of unconverted carbon remains similar, standing at 82.0%.

Regarding the reactions conducted using nitrogen, carbon conversion was lower than any OCD reaction with an unconverted carbon of up to 97%.

Table 6-13 Carbon balance to residue of OCD and reactions performed using N_2 at 1 MPa, 4 hours and temperatures from 90 to 180 °C

Reaction temperature (°C)	Carbon in feed (g) 'in'	Carbon in residue (g) 'out'	Unconverted Carbon (%)
90	9.41	8.97	95.4
120	9.44	8.50	90.1
150	9.58	7.80	81.4
180	9.57	7.85	82.0
90 with N_2 R1	9.67	9.38	97.0
90 with N_2 R2	9.57	9.22	96.3

Carbon balance to liquid extract

Table 6-14 shows the carbon balance to liquid products in extract for the OCD reactions and reactions performed using N_2 at 1 MPa, as a function of temperature. It details the feed on moisture, ash-free basis, and the quantities of carbon present in the coal feed before the reaction, as well as the total organic carbon in the liquid product after the reaction obtained from the total organic carbon analysis (TOC) and the carbon conversion yield to liquid products.

Table 6-14 Carbon balance to extract of OCD and reactions performed using N_2 at 1 MPa, 4 hours and temperatures from 90 to 180 °C

Reaction temperature (°C)	Carbon in feed (g) 'in'	Carbon in extract (g) 'out'	Carbon yield to extract (%)
90	9.41	0.122	1.3
120	9.44	0.186	2.0
150	9.58	0.494	5.2
180	9.57	0.336	3.5
90 with N_2 R1	9.67	0.099	1.0
90 with N_2 R2	9.57	0.101	1.1

The results presented in Table 6-14 shows a consistent increase in carbon content as the temperature increases from 90 to 150 °C on OCD reactions. This observation implies that the reaction conditions at 150 °C are conducive to a more efficient conversion of carbon into liquid products. However, it is interesting to note that at 180 °C, the increase in carbon content is comparable to the increase observed at 150 °C. This discrepancy suggests that the optimal temperature for achieving the highest conversion to liquid products at 1 MPa may lie around 150 °C. At this temperature, the reaction conditions seem to be most favorable for the conversion of carbonaceous materials into the desired liquid products, resulting in a higher carbon yield to the extract.

Even though the yield is lower, for the reactions conducted using only nitrogen there is still an important carbon yield to extract, showing an important implication of coal conversion due specifically to the hydrothermal conditions.

Carbon balance to gases

Table 6-15 presents the carbon balance to gas products for the OCD reactions and reactions performed using N_2 conducted at 1 MPa, as a function of temperature.

Table 6-15 Carbon balance to gases of OCD and reactions performed using N_2 at 1 MPa, 4 hours and temperatures from 90 to 180 °C

Reaction temperature (°C)	'in' (g)	'out' (g)					Carbon yield to gases (%)
	Carbon in feed	C from CO_2 Gas	C from CO_2 Dissolved	C from CO Gas	C from CO dissolved	Total carbon	
90	9.41	0.04	0.01	0.02	1.56E-04	0.08	0.8
120	9.44	0.20	0.07	0.02	2.29E-04	0.30	3.2
150	9.58	0.61	0.18	0.03	2.94E-04	0.82	8.6
180	9.57	0.60	0.20	0.04	3.80E-04	0.84	8.7
90 with N_2 R1	9.67	0.015	0.005	0.00	0.00E+00	0.02	0.2
90 with N_2 R2	9.57	0.014	0.005	0.00	0.00E+00	0.02	0.2

It can be observed that as the OCD reaction temperature increases from 90 to 180 °C, there is an overall increase in the carbon yield to gases. This observation suggests that elevated temperatures

facilitate the conversion of carbon into gaseous products. In particular, the carbon content derived from CO_2 gas presents the highest contribution among the different gas components. This finding aligns with the results observed in reactions conducted at 5 MPa. The data implies that the production of carbon dioxide gas plays a key role in the carbon balance to gas products, regardless of the reaction pressure. The control experiments showed that there is also evidence of decarboxylation taking place that is not associated with oxidation.

6.3.6   Oxygen change from coal feed to residue

Oxygen change in coal from feed to residue for the OCD reactions and reactions performed using N_2 at 1 MPa and different temperatures is shown in Table 6-16. As happened in OCD reactions at 5 MPa, it is observed that despite the general increment in the oxygen content of solid residues after reaction with respect to feed (except the solid residue in reaction at 90 °C which slightly decreases) as it can be observed comparing Table 6-1 and Table 6-6, the total content of oxygen in solid residue decreases with respect to feed. Reactions performed using N_2 present a decrease in oxygen content which is even higher that the OCD even though the unconverted carbon is higher. Only some of the loss in oxygen during the control reactions performed under N_2 is due to loss of CO_2 (Table 6-15), which suggests that some oxygenates are also released from the coal at 90 °C.

Table 6-16 Oxygen gain in coal from feed to residue of OCD and reactions performed using N_2 at 1 MPa, 4 hours and temperatures from 90 to 180 °C

Reraction temperature (°C)	Oxygen in feed[a] (g)	Oxygen in residue[a] (g)	change in oxygen (g)
90	3.16	2.82	-0.34
120	3.17	3.02	-0.14
150	3.22	2.97	-0.25
180	3.21	2.76	-0.46
90 with N_2 R1	3.62	3.19	-0.43
90 with N_2 R2	3.58	3.01	-0.58

[a] Calculated on a moisture, ash-free basis as a difference between the weight of feed and residue

6.3.7 pH

To ascertain the level of acidity of the liquid products and the extent of its alteration from the initial state of fresh milli Q water, pH measurement was carried out after the reaction and successive extraction. The results obtained are presented in Table 6-17. The pH values obtained from OCD indicate an increase in the acidity of all the liquid products as compared to the initial milli Q water used in the reaction. The acidity level of the extract shows a consistent trend, aligning with the findings obtained from the reaction conducted at 5 MPa, as documented in Chapter 5. The acidity levels experienced a progressive increase as the temperature escalated from 90 °C to 150 °C. Subsequently, at 180 °C, the pH presents an increment, resulting in an acidity level higher than that observed in the liquid product produced from the reaction conducted at 120 °C, but lower than the reaction at 150 °C. However, the acidity of the aqueous product in reactions at 1 MPa is comparatively weaker, and the pH values are higher across all reaction temperatures, thereby indicating a lower concentration of acid products in the liquid extract as compared to the reactions conducted at 5 MPa. With respect to the reactions conducted using nitrogen, the pH of the liquid extract increased in both cases.

Table 6-17 pH of liquid products from OCD and reactions performed using N_2 at 1 MPa, 4 hours and temperatures from 90 to 180 °C

Description	Reaction temperature											
	90 °C		120 °C		150 °C		180 °C		90 °C with N_2 R1		90 °C with N_2 R2	
pH[a]	X	S	X	S	X	S	X	S	X	S	X	S
Fresh Milli Q water	7.12	0.01	7.24	0.03	7.20	0.01	7.02	0.02	7.12	0.01	7.12	0.01
Extract	6.92	0.10	6.30	0.02	3.96	0.01	4.35	0.00	7.59	0.01	7.57	0.00

[a]Averages (x) and sample standard deviations (s) of duplicate analyses

6.3.8 Mineral matter

Metal content in solid samples

Scanning electron microscopy (SEM) was used to capture secondary electron images, aiming to investigate any potential differences in residue products obtained from OCD or reactions performed using N_2 at 1 MPa, with varying temperatures. The SEM images, presented in Figure

6-2 and Figure 6-3, provide visual representations of the observed morphology of the residues under these specific reaction conditions.

At the same time, secondary electron images using scanning electron microscopy with energy dispersive spectroscopy (SEM-EDS) were captured to analyze the elemental distribution within the residue product of each specific reaction conducted at 1 MPa. The results demonstrated a consistent pattern similar to the residue for reactions at 5 MPa where the major metals appeared to be finely dispersed throughout the samples. However, notable mineral chunks containing Silicon, Aluminium, or Calcium were observed, indicating their distinct presence. The metals were further quantified based on the intensity of the X-ray peaks, allowing for the determination of their respective percentages within the sample and are shown in Table 6-18.
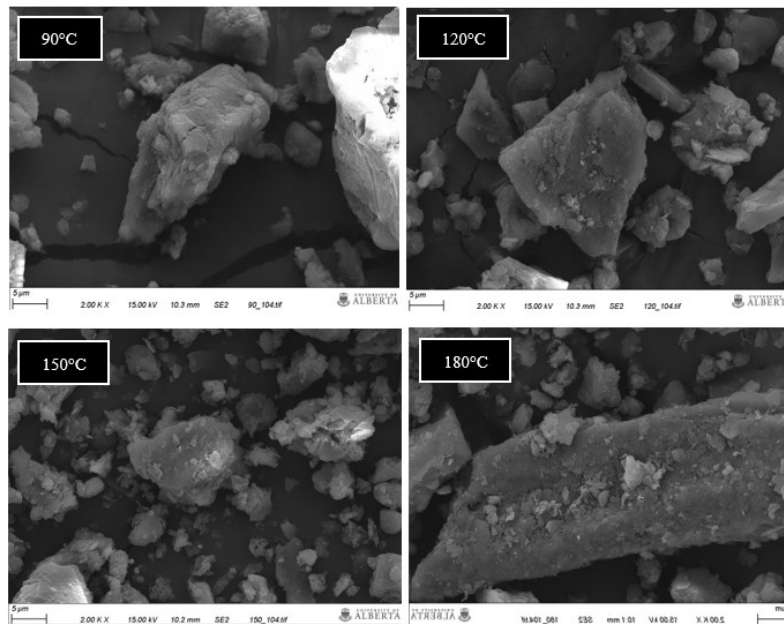
Figure 6-2 Secondary electron images taken to residue after OCD reaction at 1 MPa, 4 hours and temperatures from 90 to 180 °C
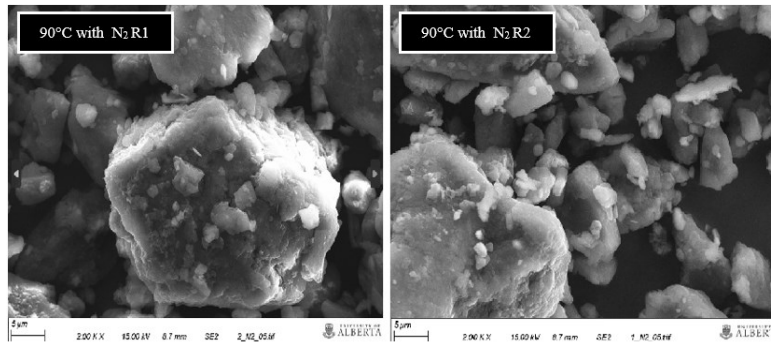
Figure 6-3 Secondary electron images taken to residue after reactions using N_2 at 1 MPa, 4 hours and 90 °C

Table 6-18 Main mineral elements identified in residue coal after OCD and reactions performed using N_2 at 4 hours reaction and 1 MPa and temperatures from 90 to 180 °C with SEM-EDS

Element	Wt Percentage in coal (%)											
	90 °C		120 °C		150 °C		180 °C		90 °C with N_2 R1		90 °C with N_2 R2	
	X	S	X	S	X	S	X	S	X	S	X	S
Si	2.61	1.97	2.15	0.94	2.79	0.48	2.56	2.22	2.10	0.32	2.01	0.81
Al	2.13	1.39	1.82	0.52	2.53	0.48	1.74	0.87	1.70	0.18	1.95	0.76
Ca	0.90	0.45	1.52	0.41	1.28	0.60	1.80	0.89	1.77	1.22	1.94	0.39
Na	0.44	0.24	0.16	0.04	0.13	0.06	0.18	0.08	0.68	0.11	0.62	0.10
Fe	0.33	0.04	0.28	0.05	0.45	0.14	0.47	0.22	0.37	0.67	0.29	0.61
S	0.60	0.17	0.47	0.16	0.34	0.16	0.48	0.25	0.41	0.35	0.54	0.12
Mg	0.29	0.11	0.22	0.10	0.15	0.09	0.23	0.13	0.33	0.07	0.28	0.08

Metal content in liquid samples

The concentrations of the main mineral elements identified in the liquid extract after OCD reactions and reactions performed using N_2 at a pressure of 1 MPa and temperatures ranging from 90 to 180 °C are presented in Figure 6-4. In addition to the elements presented in Figure 6-4, several other elements were analyzed, including silver, arsenic, barium, beryllium, cadmium, cobalt, chromium, copper, manganese, lead, selenium, thallium, thorium, uranium, and vanadium. Among these elements, small amounts of metals (<0.04 ppm) were detected in arsenic, barium, chromium, copper, manganese, lead, selenium, uranium, and vanadium.

Based on the observations from Figure 6-4 and the findings discussed in Chapter 5 concerning OCD reactions conducted at 5 MPa, it can be suggested that there is a general tendency for metal concentrations to increase with rising reaction temperatures. This implies that higher temperatures promote the release and dissolution of metals into the liquid phase. However, there are two notable exceptions at 180 °C, sodium and zinc. In these cases, the metal dissolution in the extract is lower compared to the reactions at 150 °C.

Furthermore, when comparing the different reaction pressures, it is evident that at the lower reaction pressure of 1 MPa, the dissolution of metals in the liquid extract is lower compared to the reactions conducted at 5 MPa (see Chapter 5). This suggests that higher reaction pressures contribute to a higher degree of metal dissolution in the liquid phase.
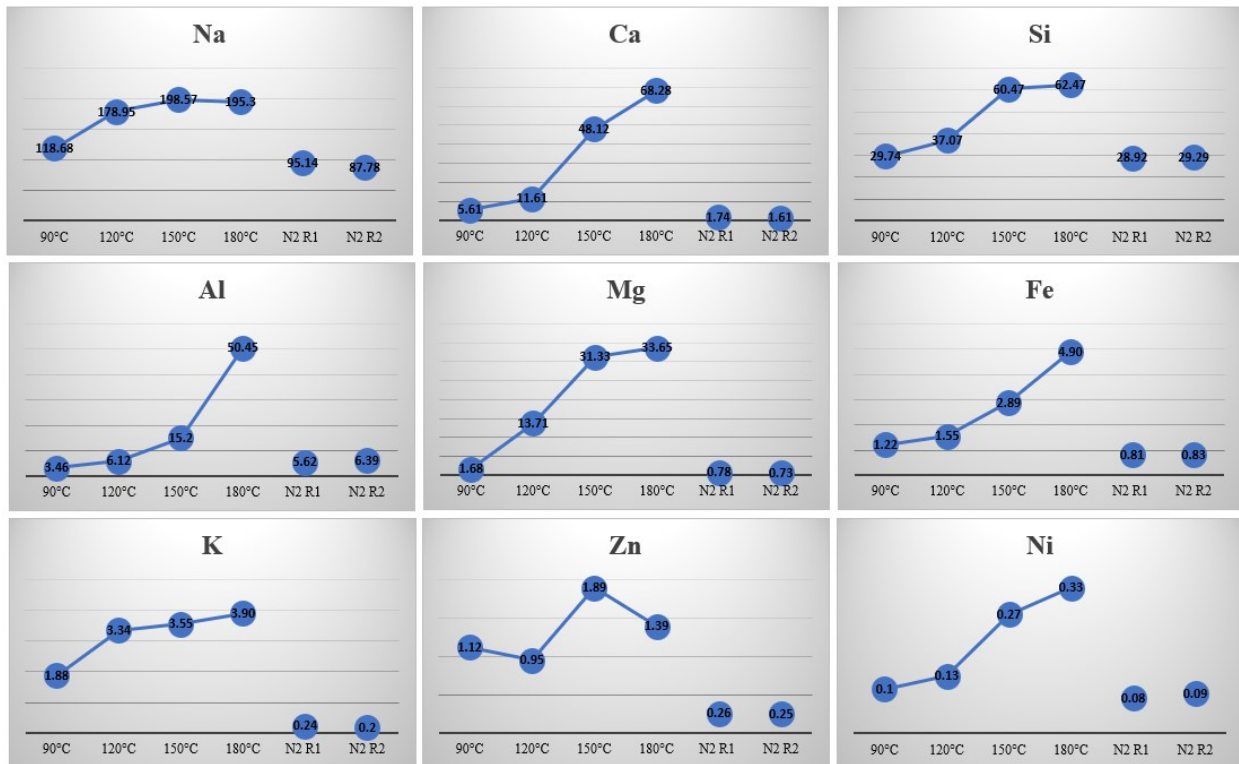
Figure 6-4 Main mineral elements concentrations (ppm) in extract liquid after OCD and reactions performed using N_2 at 4 hours reaction at 1 MPa and temperatures from 90 to 180 °C with ICP

6.4   Discussion

6.4.1   Effect of Temperature in carbon balance and yield

Figure 6-5 shows the carbon balance yield for residue, extract, and gases all together in oxidative coal dissolution reactions at 1 MPa. In this case, carbon conversion is lower than 20% at all temperature reactions, with the best conversion at 150 °C.

The carbon distribution between liquid and gas products reveals that the carbon yield to liquids is higher at 90 °C with 1.3 % against 0.8 % of yield to gases. However, as temperature increases, the yield to gases surpasses the yield to liquids but both increase with the higher conversion to liquids of 5.2% at 150 °C.
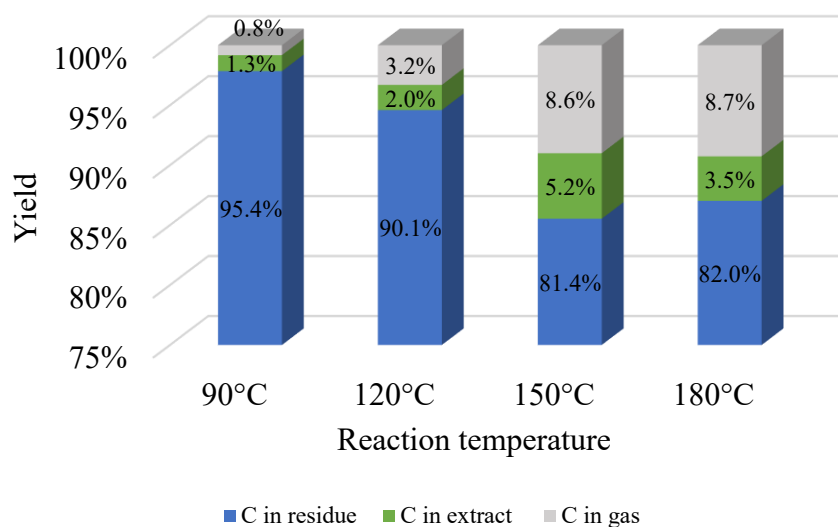
Figure 6-5 Carbon balance yield from residue, extract and gases after reaction at 1 MPa and temperatures from 90 to 180 °C during 4 hours

The comparison of carbon yield to liquid and gas products in OCD reactions at 1 and 5 MPa, across the different temperatures, is illustrated in Figure 6-6. This figure shows the liquid to gas carbon yield ratio for all reactions, providing information about the relative yields between the two product forms.
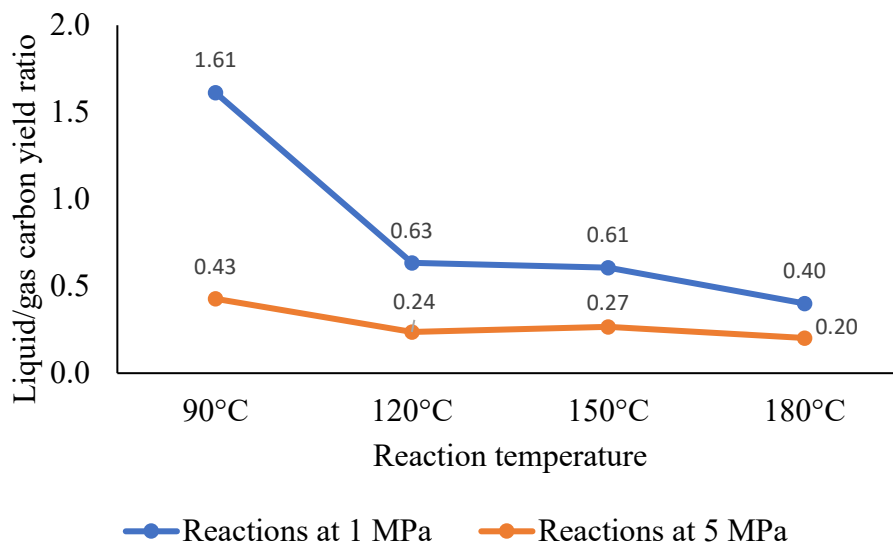
Figure 6-6 Liquid to gas Carbon yield ratio after reaction at 1 and 5 MPa and temperatures from 90 to 180 °C during 4 hours

Figure 6-6 shows that the highest yield ratio to liquids is observed at 90 °C for both pressures. However, according to what is observed in Figure- 5-7 and Figure 6-5 at 90 °C is also the temperature with the lowest yield to liquids among all the reactions. This suggests that while the yield ratio to liquids is higher, the overall conversion to liquid products is relatively low at 90 °C.

At 120 and 150 °C, the liquid/gas carbon yield ratio is similar for each specific reaction pressure. However, the advantage lies in the reactions conducted at 150 °C, where the yield to liquids is consistently 2.5 to 3 times higher compared to reactions at 120 °C. This indicates that 150 °C provides more favorable conditions for the conversion of carbon into liquid products.

At 180 °C, the liquid/gas carbon yield ratio decreases for both pressures. This observation suggests the possibility of overoxidation occurring at this temperature, resulting in a higher selectivity towards the generation of CO_2 and CO as the primary gas products in a reaction temperature between 150 to 180 °C. This shift in selectivity away from liquid products indicates the influence of higher temperatures on the reaction pathways and product distributions.

The obtained results in this study present a contrast with a previous investigation on the oxidation of bituminous coal. In that study, a 1-liter autoclave reactor was utilized to oxidize 20 grams of coal using pure oxygen as the oxidant, along with 200 mL of nitric acid, at a pressure of 2.75 MPa for a duration of 4 hours [2]. Several characteristics of that study align with the experimental setup in this current study, including the use of oxygen as the oxidant, the same reaction time of 4 hours, a comparable pressure range, and a similar liquid-to-coal ratio. In that study, the highest carbon yield to soluble products in liquid extract was achieved at approximately 175 °C, after which it began to decline. Although the peak carbon yield percentage was significantly higher, reaching approximately 38%, the temperature range in which the peak yield was obtained bears similarity to the findings in this study. This suggests a similar trend in the carbon yield response to varying temperatures. Additionally, in other experiments *Yang et al* [3] also found a maximum yield of carboxylic acids at 170 °C of lignite coal in aqueous media with oxygen as the oxidant before conversion started to decrease.

6.4.2 Changes in oxygen consumption, carbon monoxide and carbon dioxide generation

As it was presented for reactions at 5 MPa, O_2 consumption, CO_2 generation, and CO generation in the oxidative coal dissolution reactions at 1 MPa, as a function of temperature, are presented in Figure 6-7.
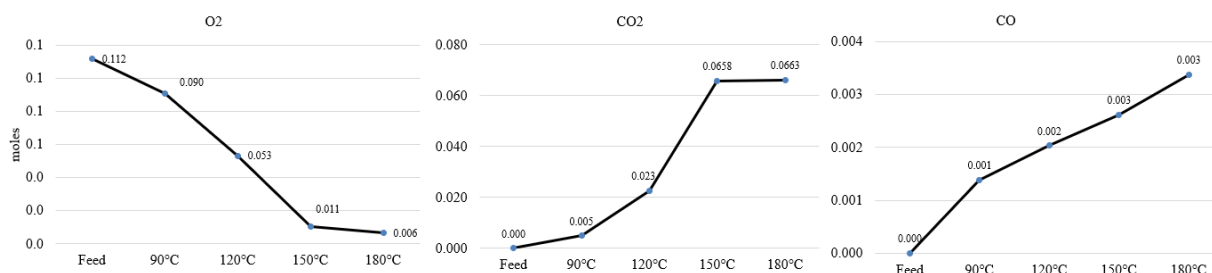
Figure 6-7 O_2 consumption, CO_2 and CO generation for reactions at 1 MPa, 4 hours and temperatures from 90 to 180 °C

Despite the lower mole quantities due to the reduced initial amount of feed air in the reactions conducted at 1 MPa, the tendencies observed in terms of O_2 consumption, CO_2 generation, and CO generation remain largely consistent with the reactions at 5 MPa. Figure 6-7 illustrates that at 150

°C, nearly all of the available oxygen is consumed, accounting for approximately 91 % of the initial quantity. This trend aligns closely with the behavior observed in the reactions conducted at 5 MPa, as shown in Figure 5-6 with 94 % of oxygen consumed according to the initial quantity.

These results indicate that at 150 °C, the majority of the available oxygen is consumed. In contrast, at 180 °C, there appears to be a limitation in oxidant availability, but at the same time there is still a increase in the generation of CO_2 and CO. This observation suggests that at higher temperatures, such as 180 °C, there might be overoxidation of the coal products, leading to the increase in the production of these gas species.

Figure 6-8 provides the ratio of the grams of gases generated after reactions at 5 MPa to the grams of gases generated after reactions at 1 MPa. This includes all the gases analyzed and presented in Chapter 5, Section 5.3.4 Gas Analysis and Table 6-12. The data suggests that there is no significant change in the selectivity towards gas products as a result of varying oxygen availability at different reaction temperatures, as long as oxygen is still readily available up to 150 °C.
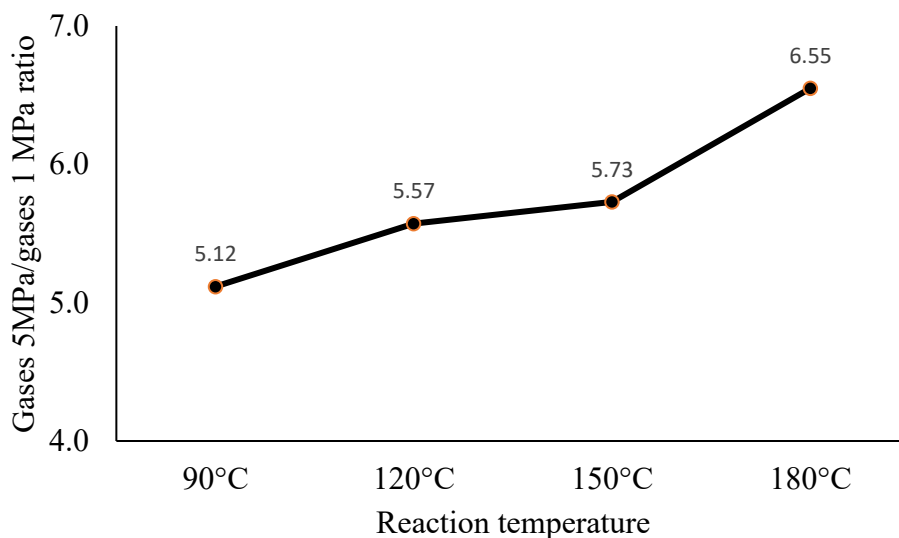
Figure 6-8 Gases at 5 MPa to Gases at 1 MPa C ratio after reactions and temperatures from 90 to 180 °C during 4 hours

However, while *Wang et al.* [4] suggest that the influence of oxygen concentration on coal oxidation does not appear to alter product selectivity, this claim cannot be definitively verified due

to the lack of detailed identification of liquid products in the extract at different pressures in this study. The work by *Wang et al.* [4] provides insights into the general behavior of coal oxidation but falls short in terms of providing a comprehensive analysis of the specific liquid products formed under varying oxygen concentrations. Without detailed identification and characterization of the liquid products in this study, it is not possible to determine the true impact of oxygen concentration on product selectivity in coal oxidation reactions.

In contrast, as described in Chapter 2, *Siddiquee et al.* [5] conducted liquid-phase oxidation of hydrocarbons and demonstrated that the availability of oxygen after hydrogen abstraction from an aliphatic carbon can indeed change the selectivity of product formation.

Additionally, once the availability of oxygen becomes limited, the selectivity towards gas products increases. This can be attributed to overoxidation, where the excess heat and limited oxygen promote the production of gases such as CO_2 and CO. This change in selectivity reflects the influence of oxygen availability on the reaction pathways and the subsequent generation of gas products.

6.4.3 OCD Reactions vs Reactions using N_2

Changes in oxygen content, O/C ratio and heating value in coal residue

The heating value of coal residue after oxidative coal dissolution undergoes changes as a result of the oxidation reactions. Generally, the heating value is a measure of the energy content of the coal and is primarily determined by its carbon content but it also depends on some extent to the hydrogen, sulfur and oxygen content based on Dulong's correlation [6]. During oxidative coal dissolution, as the reaction temperature increases, there is expected a decrease in the carbon content and an increase in oxygen of the residue. However, as observed from the elemental analysis data after reaction at 1 and 5 MPa and 90 °C, for those specific conditions, the oxygen content decreased and therefore the carbon content increased generating a decrease in oxygen-to-carbon (O/C) molar ratio.

Due to that specific behavior on oxygen and carbon content, one additional experiment was conducted to investigate if it is specifically related to the oxidation process of coal in the liquid phase. Two reactions were performed under identical conditions of 1 MPa and 90 °C, but with the substitution of air by nitrogen (N_2). Figure 6-9 presents the oxygen to carbon molar ratio of feed and residue product at 5 MPa and 1 MPa and temperatures from 90 to 180 °C for 4 hours reaction using air and at 1 MPa and 90 °C using pure nitrogen. Oxygen to carbon molar ratio of residue using pure nitrogen is presented as the average of the two reactions performed.
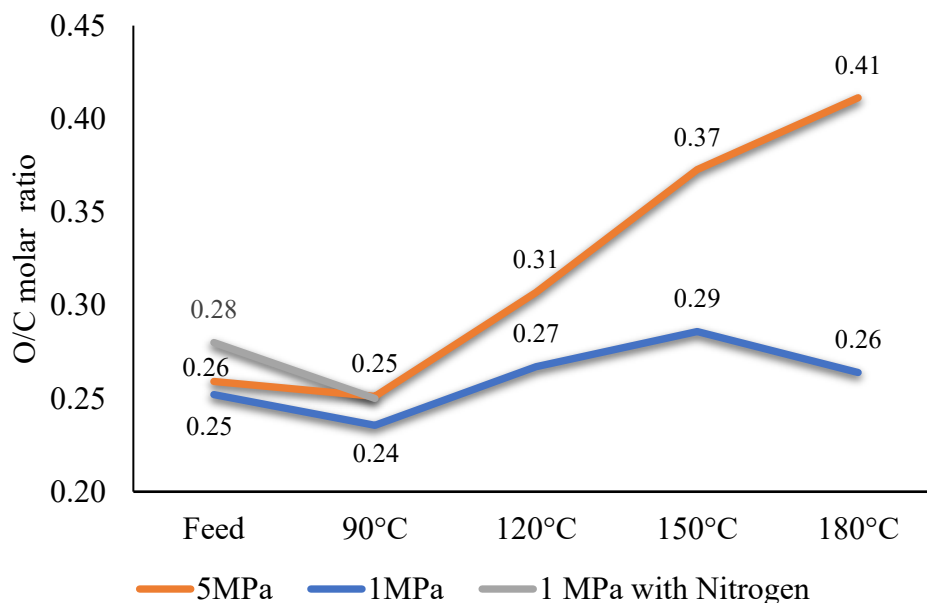
Figure 6-9 Oxygen to carbon molar ratio of feed and residue product at 5 MPa and 1 MPa and temperatures from 90 to 180 °C for 4 hours reaction using air and at 1 MPa and 90 °C using pure nitrogen

The comparative results presented in Figure 6-9 shows that in the reaction with nitrogen at 90 °C there is also a decrease in the oxygen to carbon molar ratio with respect to feed. That implies that the decrease is not a product of the oxidative coal dissolution reaction, since with the absence of oxygen in the feed there is no oxidation of coal. To explain these findings, a possible hypothesis suggests that under the specific reaction conditions of 90 °C, a 4-hour reaction time, stirring at 600 rpm, and a pressure range of 5 to 1 MPa, a small portion of the oxygen bonded within the Mancal's coal is liberated as CO_2 for which evidence was presented (Table 6-15) and oxygenates, which is

only speculated. This phenomenon, possibly related to "coal sweating," could be promoting the exudation of oxygen-rich organic compounds from the coal porous structure, compensating for the expected reduction in heating value by also displacing moisture (Table 6-8). In other words, the conditions seem to promote the release of oxygen from the coal molecule, which leads to the observed decrease in the oxygen-to-carbon molar ratio.

The obtained results have significant importance in the context of the study, as they reveal a notable decrease in the oxygen-to-carbon molar ratio. The decrease in the oxygen-to-carbon molar ratio has direct implications for the heating value of the residue products. The findings indicate that the heating value of the residue at 90 °C, following oxidative coal oxidation reactions, actually increases instead of decreasing as one might expect. This observation, shown in Figure 6-10, presents the heating value of both the feed and the residue at a pressure of 5 MPa and 1 MPa and temperatures ranging from 90 to 180 °C, and a reaction time of 4 hours. The comparison is made between reactions performed using air and reactions performed using pure nitrogen at 1 MPa and 90 °C. The increase in heating value (Figure 6-10) of the product after heating to 90 °C compared to the feed is caused by the heating and it is not related to oxidation.
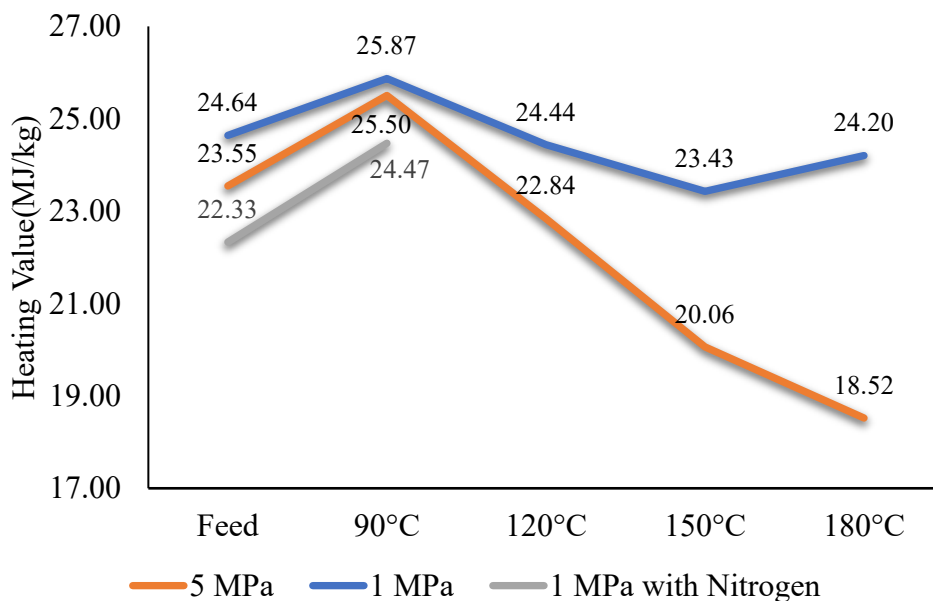
Figure 6-10 Heating value of feed and residue product at 5 MPa and 1 MPa and temperatures from 90 to 180 °C for 4 hours reaction using air and at 1 MPa and 90 °C using pure nitrogen.

Coal dissolution and minerals in liquid extract

According to the results of total organic carbon TOC obtained from the reactions using N_2 compared to the OCD reactions noteworthy observations emerge. While the TOC levels are lower for the reactions using N_2 than any OCD reaction at 1 MPa presented in this Chapter or 5 MPa presented in Chapter 5, it is higher than any of the OCD reactions at atmospheric pressure developed in the Chapter 4. This evidence that on coal dissolutions context, treatment under hydrothermal conditions at 1 MPa is more efficient than oxidative coal dissolution at atmospheric conditions as presented in Chapter 4.

Furthermore, at the same operating conditions (1 MPa and 90 °C) as it is shown in Table 6-11, TOC is similar for OCD reactions and reactions using N_2. Consequently, this similarity in TOC values translates to comparable carbon yields in liquid products, as shown in Table 6-14. This fact evidence that those hydrothermal conditions exert an influence on coal dissolution that is not directly associated to oxidation and therefore extends beyond mere oxidation mechanisms. Additionally, while liquid extract from reactions using N_2 have a basic pH, those from OCD reactions have an acidic pH as it is shown in Table 6-17. This difference in pH may suggest differences in the potential product compositions despite the similarity in coal dissolution trends.

In reference to the mineral constituents dissolved within the liquid extract, for reactions conducted at 5 MPa, there is an overall increase in the concentrations of all the metals analyzed as shown in Figure 5-4. Expanding upon these observations to the reactions at 1 MPa, as shown in Figure 6-4, the trends exhibit a degree of similarity. Nonetheless, the metal concentrations within the liquid extract are comparatively lower than those under the same temperature conditions but at 5 MPa pressure. On the other hand, if the results for reactions using N_2 also shown in Figure 6-4 are compared with the dissolution of metals from OCD reactions at the same temperature and pressure, it is noticed that the dissolution of metals is lower for the hydrothermal treatment with N_2 compared to the oxidative treatment for nearly all the metals as observed in OCD reactions. Silicon and aluminum are the only exceptions showing a similar dissolution in liquid extract for both cases. If this observation is combined with the observation of pH, it can be postulated that the higher metal dissolution of acidic compounds.

6.5   Conclusions

- The reaction yield to liquid products represented by the yield to carbon in liquid extract at reaction pressure of 1 MPa and 4 hours reaction increases with an increase temperature from 1.3 % at 90 °C to 5.2 % at 150 °C.

- The carbon yield to liquid products in oxidative coal dissolution reactions reaches its maximum within the temperature range of 150 to 180 °C. Within this temperature range, the conditions appear to favor the production of liquid products, resulting in higher carbon yield to liquids. However, as the temperature increases beyond this range, there is a noticeable shift towards higher generation of gas products.

- The heating value of the residue at 90 °C at the specific operating conditions in the parr batch reactor increased due to the increased temperature and a comparable increase in heating value was found under air and nitrogen atmosphere.

- There is a general trend of increasing metal concentrations with higher OCD temperatures at 1 MPa and 4 hours time, indicating enhanced release and dissolution of metals into the liquid phase under elevated temperatures. Moreover, a comparison of different reaction pressures shows that higher pressures, such as 5 MPa, promote a greater degree of metal dissolution in the liquid phase compared to lower pressure of 1 MPa.

6.6   References

[1]   Van Krevelen, D. W. Coal. Typology-Physics-Chemistry-Constitution, 3rd ed.; Elsevier: Amsterdam, 1993.

[2]   Savich; T. R.; Howard, H. C. Oxidation of bituminous coal to organic acids by nitric acid and oxygen. *Ind. Eng. Chem.* **1952**, *44* (6), 1409-1411.

[3]   Yang, F.; Hou, Y.; Niu, M.; Lu, T.; Wu, W.; Liu, Z., Catalytic oxidation of lignite to carboxylic acids in aqueous $H_5PV_2Mo_{10}O_{40}/H_2SO_4$ solution with molecular oxygen. *Energy Fuels* **2017**, *31*, 3830-3837.

[4]   Wang, W.; Hou, Y.; Wu, W.; Niu, M.; Liu, W. Production of benzene polycarboxylic acids from lignite by alkali-oxygen oxidation. *Ind. Eng. Chem. Res.* **2012**, *51*, 14994-15003.

[5]   Siddiquee, M. N.; De Klerk, A.; Nazemifard, N. Application of microfluidics to control product selectivity during non-catalityc oxidation of naphthenic-aromatic hydrocarbons. *Reaction Chemistry & Engineering* **2016**, *1*, 418-435.

[6]   Mason, D. M.; Gandhi, K. Formulas for calculating the heating value of coal and coal char: Development, tests and uses. *Prepr. Pap.−Am. Chem. Soc., Div. Fuel Chem.* **1980**, 25 (3), 235−245.

7. Conclusions

7.1 Introduction

The coal industry in Canada has a rich history and significant reserves that are primarily concentrated in the western provinces. However, as environmental concerns grow and alternative uses for coal are sought, oxidative coal dissolution (OCD) emerges as a potentially promising process for generating value-added products. Unlike past studies, OCD in this investigation uses air as the oxidant, for reasons of cost.

To implement OCD on a large scale, understanding the impact of reaction parameters becomes crucial. The six key operating parameters - oxidant type, temperature, time, water-to-coal ratio, pH control, and the use of additives - all influence the conversion, cost, and viability of the process. Analyzing these factors is essential for economic considerations and effective process development. This specific investigation aimed to assess the impact of time, temperature and oxygen availability as key operating parameters on oxidative coal dissolution using oxygen in the air as an oxidant, without making use of additives, keeping the water-to-coal ration constant and monitoring the pH. The experimental scope encompassed coal feed characterization and scoping experiments at atmospheric pressure, exploring changes in temperature and time, as well as reviewing reaction selectivity at 5 MPa and 1 MPa at temperatures over the range 90 to 180 °C.

7.2 Significance, Major Conclusions and Insights

- Mancal's coal is an heterogenous material, and its classification with respect to the heating value falls near the threshold between subbituminous and bituminous coal ranks, depending on the specific sample characteristics.

- The carbon yield from oxidative coal dissolution (OCD) leading to the production of liquid extract at atmospheric pressure, within a temperature range of 65 °C to 95 °C, and with a reaction time span of 15 minutes to 4 hours, is exceedingly low with less than 1% in most of the cases.

- Metal carboxylates are present in the liquid extract (aqueous phase) resulting from the transformation of carboxylic acids as products of OCD at atmospheric pressure, contributing also to the decrease in ash content from coal feed to residue.

- The carbon yield from OCD reaction represented by the yield to carbon in liquid extract at reaction pressure of 5 MPa and 4 hours reaction increases with an increase temperature from 1.8 % at 90 °C to 13.8 % at 180 °C, with the highest selectivity to liquid products at 150 °C.

- The carbon yield from OCD reaction represented by the yield to carbon in liquid extract at reaction pressure of 1 MPa and 4 hours reaction increases with an increase temperature from 1.3 % at 90 °C to 5.2 % at 150 °C. As the temperature increases beyond this range, there is a shift towards higher generation of gas products.

- The heating value of the residue product of OCD at 90 °C, increases due to the increased temperature and a comparable increase in heating value was found under air and nitrogen atmosphere at 1 and 5 MPa.

- The concentration of metals in liquid extract product of OCD is partially related to the increase of the reaction severity (intensity of pressure and temperature) and partially related to the formation and dissolution of acidic compounds.

7.3   Future Work

The research conducted on oxidative coal dissolution (OCD) has provided valuable insights into the process and its potential for adding value to coal through further upgrading. However, there are still several points for future work and research in this area that can lead to advancements and practical applications. Some conclusions about future work include:

- Process Conditions: One key area for future work is the optimization of the OCD process. This includes exploring the operating parameters that were not evaluated in this study, such as water

to coal ratio or the use of alkali. By systematically studying these variables, it will be possible to identify the most favorable conditions for maximizing the yield of valuable liquid products.

- External Mass Transfer Limitations: Detailed studies are required to investigate the existence of external mass transfer limitations at temperatures between 150 and 180 °C during OCD at 1 MPa and 5 MPa, where nearly all oxygen is consumed. Identifying the specific limiting temperature in this range can enhance our understanding of mass transfer effects on the reaction kinetics.

- Constant Oxygen Availability: Evaluating oxidative coal dissolution selectivity with a constant flow of oxygen into the reaction system at various temperatures (90 to 180 °C) can provide valuable insights into oxidation selectivity and yield. This understanding can help optimize the process for specific products.

- Extract Products Identification: Thoroughly identifying and characterizing the products present in the liquid extract obtained during OCD is very important. The liquid extract contains valuable compounds like carboxylic acids, alcohols, and other oxygen-containing species, which hold great potential for various industrial applications. Understanding the composition and properties of these products is crucial for developing efficient separation and purification methods, as well as for tailoring the process to enhance the production of specific high-value compounds. Comprehensive analysis of the liquid extract can provide valuable insights into the reaction pathways and mechanisms, leading to improved process optimization and the development of novel, value-added products from coal.

- Selective Product Formation: Investigating the mechanisms and conditions that favor the selective formation of specific products in the liquid extract during OCD is essential. Understanding the factors that influence the production of carboxylic acids, ketones, phenols, esters, and other valuable compounds can lead to tailoring the process for targeted high-value products.

- Impurity Management: Further research upgrading processes for managing impurities and by-products formed during OCD is essential for ensuring the quality and purity of the final liquid products. Understanding the fate of metals and other impurities in the liquid phase can aid in the development of effective separation and purification techniques.

- Scale-up Studies: To fully understand the economic viability of OCD, the last step, after all the previous work is done, would have to deal with the scale-up potential of the process. This involves conducting cost analysis, assessing the impact of reaction conditions on equipment design, and evaluating the potential for large-scale implementation. Understanding the economic and environmental implications is crucial for practical applications.

Bibliography

- Ahmed, M. D; Kinney, C. R. Ozonization of humic acids prepared from oxidized bituminous coal. *Journal of the American Chemical Society* **1950**, *72*, 559-561.

- Akgün, F.; Arisoy, A. Effect of particle size on the spontaneous heating of a coal stockpile. *Combustion and Flame* **1994**, *99*, 137-146.

- Allardice, D. J.; Evans, D. G. Moisture in coal. In *Analytical methods for coal and coal products, Volume 1*; Karr, C. Jr. ed.; Morgantown, West Virginia, 1978, p. 247-262.

- Alvarez, R.; Clemente, C.; Gomez-Limon, D. 2003. The influence of nitric acid oxidation of low rank coal and its impact on coal structure. *Fuel* **2003**, *82*, 2007-2015.

- ASTM International. ASTM D3173, *Standard Test Methods for Moisture in the Analysis sample of Coal and Coke*; ASTM International: West Conshohocken, PA, 1997.

- ASTM International. ASTM D3174, *Standard Test Methods for Ash in the Analysis sample of Coal and Coke from Coal*; ASTM International: West Conshohocken, PA, 1997.

- ASTM International. ASTM D7582, *Standard Test Methods for Proximate Analysis of Coal and Coke by Macro Thermogravimetric Analysis*; ASTM International: West Conshohocken, PA, 2010.

- Atkins, P.; De Paula, J. *Physical Chemistry* [online], 8th ed.; W. H. Freeman and Company: New York, 2006. http://www.rnlkwc.ac.in/pdf/study-material/chemistry/Peter_Atkins__Julio_de_Paula__Physical_Chemistry__1_.pdf (accessed 04 22, 2023)

- Attar, A.; Hendrickson, G. G. Functional groups and heteroatoms in coal. In *Coal Structure*; Meyers, R. A., Ed.; Academic Press: New York, 1982; pp 131−198

- Berkowitz, N. *An introduction to coal technology*; Academic Press: New York,1979.

- Carras, J. N.; Young, B. C. Self-heating of coal and related materials: models, application and test methods. *Progress in Energy and Combustion Science* **1994**, *20*, 1-15.

- Carrillo-Pedroza, F. R.; Dávalos Sánchez, A.; Soria-Aguilar, M; Pecina Trevino, E.T. Coal desulfurization in oxidative acid media using hydrogen peroxide and ozone: A kinetic and statistical approach. *Energy Fuels* **2009**, 3703-3710.

- Chakrabartty, S. K.; Kretschmer, H. O. Sodium hypochlorite as a selective oxidant for organic compounds. *Journal of the Chemical Society, Perkin Transactions* **1974**, *1*, 222-228.

- Chakrabartty, S. K.; Kretschmer, H. O. Studies on the structure of coals. 2. The valence state of carbon in coal. *Fuel* **1974**, *53* (2), 132-135.

- Chakrabartty, Sujit K. Oxidation of coal by alkaline sodium hypochlorite. In *Organic chemistry of coal*, Larsen, J. W. ed; American Chemical Society: Washington, 1978, pp. 100-107.

- *Chemistry of coal utilization. Vol.1*; Lowry, H. H. ed; Wiley: New York, 1945, pp.346-376.

- Chen, Q.; Kang, Y.; You, L.; Yang, P.; Zhang, X.; Cheng, Q. Change in composition and pore structure of Longmaxi black shale during oxidative dissolution. *International Journal of Coal Geology* **2017**, *172*, 95-111.

- Chen, R.; Wilson, M.; Leong, Y.K.; Bryant, P.; Yang, H.; Zhang, D.K. Preparation and rheology of biochar, lignite char and coal slurry fuels. *Fuel* **2011**, 90, 1689-1695.

- Chen, S.; Zhou, W.; Liu, M.; Zhao, G.; Cao, Q.; Zhao, B.; Kou, K.; Gao, J. Oxidation of zhundong subbituminous coal by Fe^{2+}/H_2O_2 system under mild conditions. *Korean J. Chem. Eng.* **2020**, *37* (4), 597-603.

- Chen, T.; Rodriguez, S.; Golding, S. D.; Rudolph, V. Improving coal bioavailability for biogenic methane production via hydrogen peroxide oxidation. *International Journal of Coal Geology* **2018**, *195*, 402-414.

- Clemens, A. H.; Matheson, T. W.; Rogers, D. E. Low temperature oxidation studies of dried New Zealand coals. *Fuel* **1991**, *70* (2), 215-221.

- Crane, R. *Coal*; Reaktion Books Ltda: London, 2021.

- Davidson, R. M. Molecular structure of coal. In *Coal science Vol. 1*; Gorbaty, M. L., Larsen, J. W., Wender, I. eds.; Academic Press: Orlando, 1982, pp.83-160.

- De Abreu, Y.; Patil, P.; Marquez, A. I.; Botte, G. G.; Characterization of electrooxidized Pittsburgh No. 8 coal. *Fuel* **2007**, *86* (4), 573-584.

- Dryden, I. G. C. Chemical constitution and reactions of coal. In *Chemistry of coal utilization, Supplementary Volume*; Lowry, H. H. ed.; Wiley: New York, 1963, pp. 232-295.

- Dunnivant, F. M; Ginsbach, J. W. Flame Atomic Absorbance and Emission Spectroscopy and Inductively Coupled Spectrometry - Mass Spectrometry, Coal. Typology-Physics-Chemistry-Constitution, 1st ed.; Whitman college: Walla Walla, 2009.

- Francis, W. *Coal. Its formation and composition*, 2ed.; Edward Arnold: London, 1961.

- Ghani, M. J.; Rajoka, M. I.; Akhtar, K. Investigations in fungal solubilization of coal: mechanisms and significance. *Biotechnology and Bioprocess Engineering* **2015**; *20*, 634-642.

- Gluskoter, H. J.; Shimp, N. F.; Ruch, R. R. Coal analyses, trace elements, and mineral matter. In *Chemistry of coal utilization, Second Supplementary Volume*; Elliott, M. A. ed; Wiley: New York, 1981, pp. 369-424.

- Gong, G.-Z.; Wei, X.-Y.; Zong, Z.-M. Separation and analysis of the degradation products of two coals in aqueous NaOCl solution. *Journal of fuel chemistry and technology* **2012**, *40* (1), 1-7.

- Hatcher, P. G. Chemical structural models for coalified wood (vitrinite) in low rank coal. *Organic Geochemistry* **1990**, *16*, 959-968.

- Hatcher, P. G.; Clifford, D. J. The organic geochemistry of coal: from plant materials to coal. *Organic Geochemistry* **1996**, *27*, 251-274.

- Hayashi, J.; Matsuo, Y.; Kusakabe, K.; Morooka, S. Depolymerization of lower rank coals by low-temperature O_2 oxidation. *Energy Fuels* **1997**, *11*, 227-235.

- Hayatsu, R.; Scott, R. G.; Winans, R. E. Oxidation of coal. In *oxidation in organic chemistry. Part D*; Trahanovsky, W. S. ed.; Academic Press: New York, 1982, pp. 279-354.

- Honda, H.; Hirose, Y. Wet oxidizability of coal using phosphoric acid-potassium dichromate solution. *Fuel* **1958**, *37* (3), 323-331.

- Howard, H. C. Chemical constitution of coal: as determined by oxidation reactions. In *Chemistry of coal utilization. Vol.1*; Lowry, H. H. ed; Wiley: New York, 1945, pp.346-376.

- Huang, Z.; Urynowicz, M. A.; Haider, R.; Sattar, H.; Saleem, M.; Hoang, L.; Han, N.T.; To, K.A.; Hung, L.Q.; Ali, M.I.; Guo, H. Biogenic methane generation from Vietnamese coal after pretreatment with hydrogen peroxide. *International Journal of Energy Research* **2021**, 45(13), 18713-18721.

- International Energy Agency. Coal Information.; IEA Publications: France, 2019.

- Itay, M.; Hill, C. R.; Glasser, D. A study of the low temperature oxidation of coal. *Fuel Processing Technology* **1989**, *21*, 81-97.

- Kaji, R.; Hishinuma, Y.; Nakamura, Y. Low temperature oxidation of coals: effects of pore structure and coal composition. *Fuel* **1985**, *64*, 297-302.

- Kapo, G.; Calvert, S. Liquid phase oxidation of coal in alkali. *Ind. Eng. Chem. Proc. Des. Dev.* **1966**, *5*, 97-104.

- Lalvani, S.; Pata, M.; and Coughlin, R. W. Electrochemical oxidation of lignite in basic media. *Fuel* **1986**, *65*, 122-128.

- Liu, F. J.; Wei, X.-Y.; Zhu, Y.; Gui, J.; Wang, Y.-G.; Fan, X.; Zhao, Y.-P.; Zong, Z.-M.; Zhao, W. Investigation on structural features of Shengli lignite through oxidation under mild conditions. *Fuel* **2013**, *109*, 316-324.

- Liu, F. J; Wei, X. Y.; Fan, M.; Zong, Z. M. Separation and structural characterization of the value-added chemicals from mild degradation of lignites: a review. *Applied Energy* **2016**, *170*, 415-436.

- Liu, K.; Yang, J.; Jia, J.; Wang, Y. Desulphurization of coal via low temperature atmospheric alkaline oxidation. *Chemosphere* **2008**, *71*, 183-188.

- Liu, Y.; Zhu, Y.; Li, W.; Zhang, C.; Wang, Y. Ultra micropores in macromolecular structure in subbituminous coal vitrine. *Fuel* **2017**, *210*, 298-306.

- Liu, Z. -X.; Liu, Z. -C.; Zong, Z. -M.; Wei, X.-Y.; Wang, J.; Lee, C. W. GC/MS Analysis of water-soluble products from the mild oxidation of Longkou brown coal with H_2O_2. *Energy & Fuels* **2003**, *17*, 424-426.

- Mackowsky, M.-TH. The application of coal petrography in technical processes. In *Coal Petrology third revised and enlarged edition*; Stach, E., Mackowsky, M.-TH., Teichmüller, M., Taylor, G. H., Chandra, D., Teichmüller, R. eds.; Gebrüder Borntraeger: Berlin, 1982, pp 413-474.

- Mae, K.; Maki, T.; Araki, J.; Miura, K. Extraction of low-rank coals oxidized with hydrogen peroxide in conventionally used solvents at room temperature. *Energy Fuels* **1997**, *11*, 825-831.

- Mae, K.; Maki, T.; Okutsu, H; Miura, K. Examination of relationship between coal structure and pyrolysis yields using oxidized brown coals having different macromolecular networks. *Fuel* **2000**, *79*, 417-425.

- Mae, K.; Shindo, H.; Miura, K. A new two-step oxidative degradation method for producing valuable chemicals from low rank coals under mild conditions. *Energy Fuels* **2001**, *15*, 611-617.

- Mason, D. M.; Gandhi, K. Formulas for calculating the heating value of coal and coal char: Development, tests and uses. *Prepr. Pap.−Am. Chem. Soc., Div. Fuel Chem*. **1980**, 25 (3), 235−245.

- Marion, M. G. Carbonate mineral solubility at low temperatures in the Na-K-Mg-Ca-H-Cl-SO$_4$-OH-HCO$_3$-CO$_3$-CO$_2$-H$_2$O system. *Geochimica et Cosmochimica* **2001**, *65* (12), 1883-1896.

- Maximov, O. B.; Schapovalov, V. E.; Shvets, T. V. Alkaline permanganate oxidation of methylated humic acids. *Fuel* **1972**, *51* (3), 185-189.

- Mishra S. K.; Kanungo, S. B. Factors affecting the preparation of highly concentrated coal-water slurry (HCCWS). *Journal of scientific & industrial research* **2000**, *59*, 765-790.

- Miura, K.; Mae, K.; Okutsu, H.; Mizutani, N. New oxidative degradation method for producing fatty acids in high yields and high selectivity from low-rank coals. *Energy Fuels* **1996**, *10*, 1996-1201.

- Montoya, N.; De Klerk, A. Autoxidation of aromatics. *Applied petrochemical research* **2018**, *8*, 55-78.

- Mraw, S. C.; De Neufville, J. P.; Freund, H.; Baset Z.; Gorbaty, M. L.; Wright, F. J. The science of mineral matter in coal. *Coal Science* **1983**, *2*, 1-63.

- Murata, S.; Hosokawa, M.; Kidena, K.; Nomura, M. Analysis of oxygen-functional groups in brown coals. *Fuel Processing Technology* **2000**, *67* (3), 231-243.

- Nomura, M.; Pugmire, R. J.; Moro-Oka, S. Fletcher, H. T.; Ye, C. *Personal communication report: molecular level characterization of carbonaceous resources of advanced utilization technologies*; *Preprints of Papers,* New Energy, and Industrial Technology Development Organization (NEDO): Japan, 1999.

- O'Keefe, J. M. K.; Bechtel, A; Christanis, K.; Dai, S.; DiMichele, W. A.; Eble, C.F.;Esterle, J.S.; Mastalerz, M.; Raymond, A. L.; Valentim, B. V.; Wanger, N. J.; Ward, C. R.; Hower, J. C. On the fundamental difference between coal rank and coal type. *International Journal of Coal Geology* **2013,** *118*, 58-87.

- Pan, C.-X.; Liu, H.-L.; Liu, Q.; Shui, H.-F.; Wang, Z.-C.; Lei, Z.-P.; Kang, S.-G; Wei, X.-Y. Oxidative depolymerization of shenfu subbituminous coal and its thermal dissolution insoluble fraction. *Fuel Processing Technology* **2017**, *155*, 168-173.

- Pan, C.-X.; Wei, X.-Y.; Shui, H.-F.; Wang, Z.-C.; Gao, J.; Wei, C.; Cao, X.-Z.; Zong, Z.-M. Investigation on the macromolecular network structure of Xianfeng lignite by a new two-step depolymerization. *Fuel* **2013**, *109*, 49-53.

- Parthasarathi, R.; Padmanabhan, J.; Elango, M.; Chitra, K.; Subramanian, V.; Chattaraj, P. K. pK_a prediction using group philicity. *The Journal of Physical Chemistry* **2006**, 110(20), 6540-6544.

- Peña-Méndez, E. M.; Havel, J.; Patočka, J. 2005. Humic substances-compounds of still unknown structure: applications in agriculture, industry, environment, and biomedicine. *Journal of Applied Biomedicine* **2005**, *3*,13-24.

- Peng, D. Y.; Robinson, D. B. (1976). *A New two-constant equation of state. Industrial and Engineering Chemistry: Fundamentals* 1976, 15, 59–64.

- Rahman, M.; Samanta, A.; Gupta, R. Production and characterization of ash-free coal from low-rank Canadian coal by solvent extraction. *Fuel Processing Technology* **2013**, 115, 88-98.

- Raj, S. S. *A study of some chemical structural parameters of coal*; Ph.D. Thesis, Pennsylvania State University, 1976.

- Reid, R. C; Prausnitz, J. M.; Poling, B. E. *The Properties of Gases and Liquids*, 4th ed.; McGraw-Hill: New York, 1987.

- Riley, J. T. *Routine coal and coke analysis: collection, interpretation, and uses of analytical data*, 2nd ed.; ASTM International: West Conshohocken, 2014.

- Roy, A. N.; Howard, H. C. Solvent Fractionation of Polycarboxylic Acids from Oxidation of Coal. *Journal of the American Chemical Society* **1952**, *74*, 3239-3242.

- Sabar, M. A.; Ali, M. I.; Fatima, N.; Malik, A. Y.; Jamal, A.; Liaquat, R.; He, H.; Liu, F.-J.; Guo, H.; Urynowicz, M.; Huang, Z. Evaluation of humic acids produced from Pakistani subbituminous coal by chemical and fungal treatments. *Fuel* **2020**, *278*, 118301.

- Savich; T. R.; Howard, H. C. Oxidation of bituminous coal to organic acids by nitric acid and oxygen. *Ind. Eng. Chem.* **1952**, *44* (6), 1409-1411.

- Schmidt, L.D. and Elder, J.L., 1940. Atmospheric oxidation of coal at moderate temperatures. *Industrial & Engineering Chemistry* **1940**, *32* (2), 249-256.

- Sharma, D.K.; Singh, S. K. Advanced process for the production of clean coal by chemical leaching technique. *Energy sources* **1995**, 17(4):485-493.

- Shen, V.K.; Siderius, D.W.; Krekelberg, W.P.; Hatch, H.W.; Eds. NIST Standard Reference Simulation Website, NIST Standard Reference Database Number 173, National Institute of Standards and Technology. https://webbook.nist.gov/chemistry/ (accessed 04 23, 2023).

- Shinn, J. H. Visualization of complex hydrocarbon reaction systems. *Prepr. Pap. - Am. Chem. Soc., Div. Fuel Chem.* **1996**, *41*, 510-515.

- Shirazi, A. R.; Börtin, O.; Eklund, L.; Lindqvist, O. The impact of mineral matter in coal on its combustion, and a new approach to the determination of the calorific value of coal *Fuel* **1995**, *74* (2), 247-251.

- Siddiquee, M. N.; De Klerk, A. Heteroatom removal as pretreatment of boiler fuels. *Energy Fuels* **2019**, *33*, 5790-5801.

- Siddiquee, M. N.; De Klerk, A.; Nazemifard, N. Application of microfluidics to control product selectivity during non-catalityc oxidation of naphthenic-aromatic hydrocarbons. *Reaction Chemistry & Engineering* **2016**, *1*, 418-435.

- Silverstein, R. M.; Bassler, G.C; Morrill, T.C. *Spectrometryc identification of organic compounds* 4th ed.; John Wiley & Sons Ltda: New York, 1981.

- Singh, H.; Kumar, S.; Mohapatra, S. K.; Prasad, S. B.; Singh, J. Slurryability and flowability of coal water slurry: Effect of particle size distribution. *Journal of Cleaner Production* **2021**, *323*, 129-183.

- Smyrl, N. R.; Fuller, E. L. Chemistry and structure of coals: Diffuse reflectance IR Fourier transformation (DRIFT) spectroscopy of air oxidation. In *Coal and coal products: Analytical characterization techniques*; Fuller, E. L. ed.; Washington, D.C, 1982, p. 133-145.

- Speight, J. G. *Handbook of coal analysis. Chemical analysis: A series of monograph on analytical chemistry and its applications. Vol. 182*, 2ed.; Wiley: Hoboken, New Jersey, 2015.

- Speight, J. G. *The chemistry and technology of coal,* 3rd ed.; CRC Press: Boca Raton, 2012.

- Stach, E. The microlithotypes of coal and their strength. In *Coal Petrology third revised and enlarged edition*; Stach, E., Mackowsky, M.-TH., Teichmüller, M., Taylor, G. H., Chandra, D., Teichmüller, R. eds.; Gebrüder Borntraeger: Berlin, 1982, p140-150.

- Stange, W. The process design of gold leaching and carbon-in-pulp circuits. *The Journal of The South African Institute of Mining and Metallurgy* **1999**, 13-26.

- Stephens, J. F.; Leow, H. M.; Gilbert, T. D.; Philp, R. P. Aqueous sodium dichromate oxidation of australian vitrinite concentrates. *Fuel* **1985**, *64* (11), 1531-1536.

- Stock, L. M.; Obeng, M. Oxidation and decarboxylation. A reaction sequence for the study of aromatic structural elements in Pocahontas No. 3 coal. *Energy Fuels* **1997**, *11*, 987-997.

- Tao, L.; Han, J.; Tao, F. M. Correlations and predictions of carboxylic acid pK_a values using intermolecular structure and properties of hydrogen-bonded complexes. *The Journal of Physical Chemistry* **2008,** 112(4), 775-782.

- Taraba, B; Kupka, J. Subaquatic oxidation of coal by water-dissolved oxygen. *Fuel* **2010**, *89*, 3598-3601.

- Tarafdar, M. N.; Guha, D. Application of wet oxidation processes for the assessment of the spontaneous heating of coal. *Fuel* **1989**, *68* (3), 315-317.

- Thomas, L. *Coal Geology* 3rd ed.; John Wiley & Sons Ltda: Abergavenny, 2020.

- Van Krevelen, D. W. *Coal. Typology-Physics-Chemistry-Constitution*, 3rd ed.; Elsevier: Amsterdam, 1993.

- Wang, H.; Dlugogorski, B. Z.; Kennedy, E. M. Coal oxidation at low temperatures: oxygen consumption, oxidation products, reaction mechanism and kinetic modelling. *Progress in Energy and Combustion Science* **2003**, *29*, 487-513.

- Wang, W.; Hou Y.; Wu W.; Niu M. Simultaneous production of small-molecule fatty acids and benzene polycarboxylic acids from lignite by alkali-oxygen oxidation. *Fuel Processing Technology* **2013**, *112*, 7-11.

- Wang, W.; Hou Y.; Wu W.; Niu M.; Wu, T. High-temperature alkali-oxygen oxidation of lignite to produce benzene polycarboxylic acids. *Ind. Eng. Chem. Res.* **2013**, *52*, 680-685.

- Wang, W.; Hou, Y.; Wu, W.; Niu, M.; Liu, W. Production of benzene polycarboxylic acids from lignite by alkali-oxygen oxidation. *Ind. Eng. Chem. Res.* **2012**, *51*, 14994-15003.

- Wang, Y.; Chen, S.; Ding, M.; Xu, Z. Study of oxidization of coal–pitch by O_3. *International Journal of Mining Science and Technology* **2016**, *26*, 677-681.

- Wender, I.; Heredy, L. A.; Neuworth, M. B.; Dryden, I. G. C. Chemical reactions and the constitution of coal. In *Chemistry of coal utilization, Second Supplementary Volume*; Elliott, M. A. ed; Wiley: New York, 1981, p. 425-521.

- Winter, J.; Bailey, M.; Galley, E.; Joseph, C.; Shaffer, B. A multiple account benefit-cost analysis of coal mining in Alberta. *The school of public policy publications* University of Calgary **2021**, 14, 32

- Yang, F.; Hou, Y.; Niu, M.; Lu, T.; Wu, W.; Liu, Z., Catalytic oxidation of lignite to carboxylic acids in aqueous H5PV2Mo10O40/H2SO4 solution with molecular oxygen. *Energy Fuels* **2017**, *31*, 3830-3837.

- Yang, S.; Liu, D.; Li, Y.; Yang, C.; Yang, Z.; Chen, X.; Li, H.; Tang, Z. Experimental study on the oxidative dissolution of carbonate-rich shale and silicate-rich shale with H_2O_2, $Na_2S_2O_8$ and NaClO: Implication to the shale gas recovery with oxidation stimulation. *Journal of Natural Gas Science and Engineering* **2020**, *76*, 103207.

- Yao, Z.-S.; Wei, X.-Y.; Lv, J.; Liu, F.-J.; Huang, J.-G.; Xu, J.-J.; Chen, F.-J.; Huang, Y.; Li, Y.; Lu, Y.; Zong, Z.-M. Oxidation of shenfu coal with RuO_4 and NaOCl *Energy Fuels* **2010**, *24*, 1801-1808.

- Yoshida, T.; Takanohashi, T.; Sakanishi, K.; Saito, I.; Fujita, M.; Mashimo, K. The effect of extraction condition on HyperCoal production (1) -under room temperature filtration. *Fuel* **2002**, 81(11):1463-1469.

- Zeng, Y.; Chen, X.; Zhao, D.; Li, H.; Zhang, Y.; Xiao, X. Estimation of pK_a values for carboxylic acids, alcohols, phenols and amines using changes in the relative Gibbs free energy. *Fluid Phase Equilibria* **2012**, 148-155.

- Zhou, L.; Yuan, L.; Zhao, B.; Li, Y.; Lin, Z. Structural characteristics of humic acids derived from chinese weathered coal under different oxidizing conditions. *Plos one* **2019**, *14* (5), e0217469.

- Zhumanova, M. O.; Usanboev, N.; Namazov, S. S.; Beglov, B. M. Oxidation of brown coal of Angren deposit with a mixture of nitric and sulfuric acids. *Russian Journal of Applied Chemistry* **2009**, *82* (12), 2223-2229.

Appendices

Appendix A
Density of liquids

The density of the feed water and extract samples was determined using the Anton Paar 4500M digital density meter, with each measurement performed in triplicate. Table A-1 presents the average value of the measured densities, as well as the corresponding standard deviation.

To assess the accuracy of the equipment, the measured deviation for water was compared to the reference water density at 20 °C and 1 atm provided by *NIST* [1], which is 0.99821 $g.cm^{-3}$. The measured deviation was found to be 0.00004 $g.cm^{-3}$, indicating a high level of accuracy for the Anton Paar 4500M digital density meter. The small deviation from the reference value suggests that the instrument provides precise and reliable density measurements.

Table A 1 Density at 20 °C of water used for reaction and extract after reactions

Description	Density ($g.cm^{-3}$)	Standard deviation
Milli-Q Water	0.99817	0.00003
Extract from 4-hour reaction at 65 °C	0.99835	0.00001
Extract from 4-hour reaction at 75 °C	0.99834	0.00003
Extract from 4-hour reaction at 85 °C	0.99844	0.00002
Extract from 4-hour reaction at 95 °C	0.99843	0.00001
Extract from reaction at 95 °C and 15 minutes	0.99847	0.00002
Extract from reaction at 95 °C and 60 minutes	0.99842	0.00001
Extract from reaction at 95 °C and 90 minutes	0.99845	0.00001
Extract from reaction at 95 °C and 120 minutes	0.99847	0.00001
Extract from 4-hour reaction at 5MPa and 90°C	0.99880	0.00001
Extract from 4-hour reaction at 5MPa and 120°C	0.99931	0.00002
Extract from 4-hour reaction at 5MPa and 15°C	1.00130	0.00002
Extract from 4-hour reaction at 5MPa and 180°C	1.00147	0.00001
Extract from 4-hour reaction at 1 MPa and 90°C	0.99866	0.00002
Extract from 4-hour reaction at 1 MPa and 120°C	0.99895	0.00001
Extract from 4-hour reaction at 1 MPa and 15°C	0.99938	0.00001
Extract from 4-hour reaction at 1 MPa and 180°C	0.99928	0.00001
Extract from 4-hour reaction using H_2 at 1 MPa and 90°C	0.99850	0.00001
Extract from 4-hour reaction using H_2 at 1 MPa and 90°C	0.99847	0.00001

Appendix B

Flowmeters calibration and readings

Figure B-1 and Figure B-2 show the calibration results through a linear regression of data recorded in mL.min^{-1} for each flowmeter. Table B-1 shows the flowmeter readings (changes of flow over time) for the 4-hour reaction conducted at temperatures ranging from 65 to 95 °C and for the 95 °C reactions conducted for durations ranging from 15 to 120 minutes.
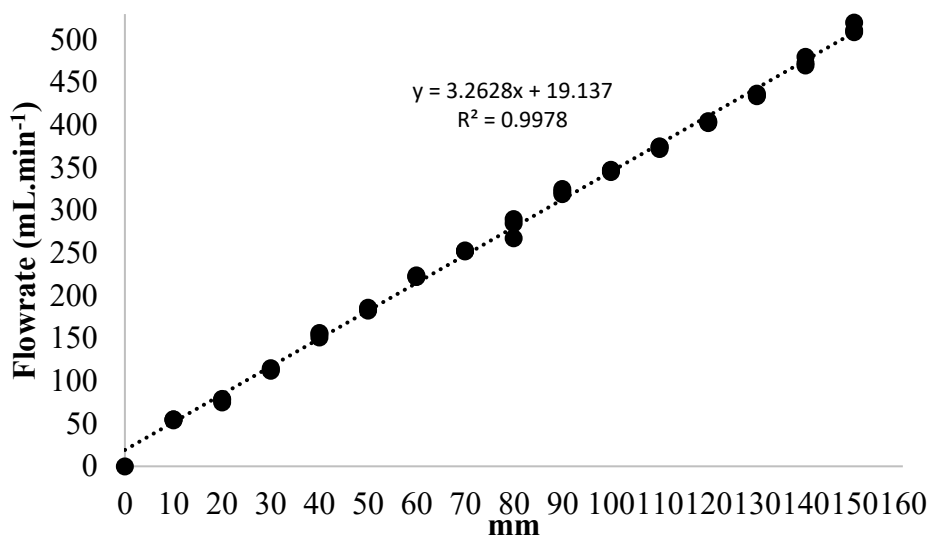
Figure B-1 Calibration results Flowmeter 1.
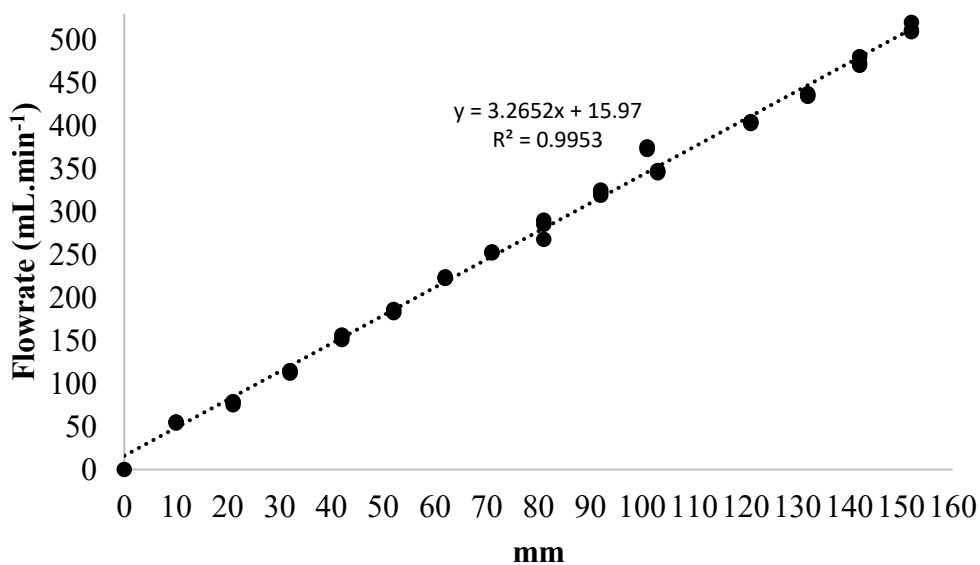
Figure B-2 Calibration results Flowmeter 2

Table B-1 Flowmeters reading at different times for the reactions at atmospheric pressure, as a function of temperature and time

Description	initial time (min)	Final time (min)	FI-1 SS Ball (mm)	FI-1 flow (mL.min⁻¹)	FI-2 SS Ball (mm)	FI-2 flow (mL.min⁻¹)
Flowmeters reading 65 °C	0.0	240.7	101	348.7	101	345.8
Flowmeters reading 75 °C	0.0	238.7	101	348.7	101	345.8
Flowmeters reading 85 °C	0.0	1.3	101	348.7	100.5	344.1
	1.5	2.5	101	348.7	100	342.5
	2.7	4.8	101	348.7	100.5	344.1
	5.0	240.3	101	348.7	101	345.8
Flowmeters reading 95 °C	0.0	1.2	101	348.7	99	339.2
	1.3	2.8	101	348.7	98.5	337.6
	3.0	5.7	101	348.7	99.5	340.9
	5.8	9.0	101	348.7	100	342.5
	9.2	68.8	101	348.7	100.5	344.1
	69.0	241.0	101	348.7	101	345.8
Flowmeters reading 15 min	0.0	1.5	101	348.7	99.5	340.9
	1.7	2.5	101	348.7	99	339.2
	2.7	3.7	101	348.7	99.5	340.9
	3.8	6.0	101	348.7	100	342.5
	6.2	15.5	101	348.7	100.5	344.1
Flowmeters reading 30 min	0.0	0.8	101	348.7	99.5	340.9
	1.0	2.3	101	348.7	99	339.2
	2.5	3.8	101	348.7	99.5	340.9
	4.0	7.5	101	348.7	100	342.5
	7.7	30.3	101	348.7	100.5	344.1
Flowmeters reading 60 min	0.0	1.0	101	348.7	99	339.2
	1.2	2.3	101	348.7	98.5	337.6
	2.5	2.7	101	348.7	99	339.2
	2.8	5.3	101	348.7	99.5	340.9
	5.5	8.3	101	348.7	100	342.5
	8.5	60.2	101	348.7	100.5	344.1
Flowmeters reading 120 min	0.0	0.8	101	348.7	99	339.2
	1.0	2.2	101	348.7	98.5	337.6
	2.3	2.7	101	348.7	99	339.2
	2.8	5.5	101	348.7	99.5	340.9
	5.7	8.8	101	348.7	100	342.5
	9.0	63.5	101	348.7	100.5	344.1
	63.7	120.5	101	348.7	101	345.8

Appendix C
Numerical calculation of gas balance

Tables C-1 to C-8 show the results of the numerical analysis for the gas balance varying temperatures and time. These tables present the average readings of oxygen percentage, carbon dioxide concentration, air coming 'in' to the system, and gas product going 'out' of the system within different time intervals. In addition, the tables also provide the summation of oxygen entering coming 'in' and going 'out' to the system, as well as the corresponding consumption, and the production of carbon dioxide during the same time intervals.

To compute the values for O2 consumption and CO2 production, the densities of oxygen (1.32612 g.L^{-1}) and carbon dioxide (1.82341 g.L^{-1}) were determined using the ideal gas equation. The temperature was assumed to be 22 °C, and the pressure was extracted as an average derived from the *EAS weather Station* [2] data history, corresponding to the months during which the reactions occurred (101.75 kPa).

Table C-1 Numerical calculation of gas balance of OCD reaction at 4 h and 65 °C

| Time (min) | | O₂ % | CO₂ (ppm) | Flow (mL.min⁻¹) | | O₂ (g) | | | CO₂ (g) Production |
Initial	Final			'In'	Out'	'In'	Out'	Consumption	
0	0.8	20.37	320.172	348.7	345.8	9.71E-02	9.34E-02	3.72E-03	2.02E-04
1	1.8	19.94	375.081	348.7	345.8	9.71E-02	9.14E-02	5.67E-03	2.36E-04
2	2.8	19.92	406.572	348.7	345.8	9.71E-02	9.13E-02	5.77E-03	2.56E-04
3	3.8	20.12	339.381	348.7	345.8	9.71E-02	9.22E-02	4.85E-03	2.14E-04
4	4.8	20.32	247.770	348.7	345.8	9.71E-02	9.32E-02	3.94E-03	1.56E-04
5	5.8	20.52	174.117	348.7	345.8	9.71E-02	9.41E-02	3.01E-03	1.10E-04
6	6.8	20.67	118.933	348.7	345.8	9.71E-02	9.48E-02	2.33E-03	7.50E-05
7	7.8	20.71	83.934	348.7	345.8	9.71E-02	9.50E-02	2.14E-03	5.29E-05
8	8.8	20.75	59.230	348.7	345.8	9.71E-02	9.51E-02	1.95E-03	3.73E-05
9	9.8	20.80	43.688	348.7	345.8	9.71E-02	9.54E-02	1.71E-03	2.75E-05
10	19.8	20.88	15.929	348.7	345.8	9.71E-01	9.57E-01	1.37E-02	1.00E-04
20	29.8	20.91	10.585	348.7	345.8	9.71E-01	9.59E-01	1.24E-02	6.67E-05
30	39.8	20.91	13.123	348.7	345.8	9.71E-01	9.59E-01	1.21E-02	8.27E-05
40	49.8	20.91	14.024	348.7	345.8	9.71E-01	9.59E-01	1.23E-02	8.84E-05
50	59.8	20.92	13.779	348.7	345.8	9.71E-01	9.59E-01	1.18E-02	8.69E-05
60	69.8	20.93	17.244	348.7	345.8	9.71E-01	9.60E-01	1.15E-02	1.09E-04
70	79.8	20.94	17.799	348.7	345.8	9.71E-01	9.60E-01	1.08E-02	1.12E-04
80	89.8	20.94	18.876	348.7	345.8	9.71E-01	9.60E-01	1.09E-02	1.19E-04
90	99.8	20.97	20.844	348.7	345.8	9.71E-01	9.61E-01	9.65E-03	1.31E-04
100	129.8	20.97	20.307	348.7	345.8	2.91E+00	2.88E+00	2.92E-02	3.84E-04
130	159.8	20.98	19.907	348.7	345.8	2.91E+00	2.89E+00	2.76E-02	3.77E-04
160	189.8	20.99	14.248	348.7	345.8	2.91E+00	2.89E+00	2.61E-02	2.69E-04
190	219.8	20.99	17.035	348.7	345.8	2.91E+00	2.89E+00	2.53E-02	3.22E-04
220	240.7	21.00	10.241	348.7	345.8	2.02E+00	2.01E+00	1.68E-02	1.35E-04
				Total:		**2.34E+01**	**2.31E+01**	**2.65E-01**	**3.75E-03**

Table C-2 Numerical calculation of gas balance of OCD reaction at 4 h and 75° C

Time (min)		O_2 %	CO_2 (ppm)	Flow (mL.min^{-1})		O_2 (g)			CO_2 (g) Production
Initial	Final			'In'	Out'	'In'	Out'	Consumption	
0	0.8	19.98	393.886	348.7	345.8	9.71E-02	9.16E-02	5.48E-03	2.48E-04
1	1.8	19.85	538.137	348.7	345.8	9.71E-02	9.10E-02	6.07E-03	3.39E-04
2	2.8	19.87	586.156	348.7	345.8	9.71E-02	9.11E-02	6.01E-03	3.70E-04
3	3.8	20.15	443.240	348.7	345.8	9.71E-02	9.24E-02	4.70E-03	2.79E-04
4	4.8	20.28	338.514	348.7	345.8	9.71E-02	9.30E-02	4.11E-03	2.13E-04
5	5.8	20.60	247.243	348.7	345.8	9.71E-02	9.45E-02	2.64E-03	1.56E-04
6	6.8	20.77	171.071	348.7	345.8	9.71E-02	9.52E-02	1.89E-03	1.08E-04
7	7.8	20.70	148.550	348.7	345.8	9.71E-02	9.49E-02	2.17E-03	9.37E-05
8	8.8	20.81	141.638	348.7	345.8	9.71E-02	9.54E-02	1.66E-03	8.93E-05
9	9.8	20.83	137.116	348.7	345.8	9.71E-02	9.55E-02	1.61E-03	8.64E-05
10	19.8	20.78	137.947	348.7	345.8	9.71E-01	9.53E-01	1.82E-02	8.70E-04
20	29.8	20.83	126.256	348.7	345.8	9.71E-01	9.55E-01	1.57E-02	7.96E-04
30	39.8	20.81	115.881	348.7	345.8	9.71E-01	9.54E-01	1.70E-02	7.31E-04
40	49.8	20.85	107.925	348.7	345.8	9.71E-01	9.56E-01	1.50E-02	6.80E-04
50	59.8	20.86	98.287	348.7	345.8	9.71E-01	9.57E-01	1.44E-02	6.20E-04
60	69.8	20.89	92.858	348.7	345.8	9.71E-01	9.58E-01	1.33E-02	5.85E-04
70	79.8	20.81	86.290	348.7	345.8	9.71E-01	9.54E-01	1.68E-02	5.44E-04
80	89.8	20.78	80.580	348.7	345.8	9.71E-01	9.53E-01	1.83E-02	5.08E-04
90	99.8	20.92	73.796	348.7	345.8	9.71E-01	9.59E-01	1.19E-02	4.65E-04
100	129.8	20.86	66.038	348.7	345.8	2.91E+00	2.87E+00	4.40E-02	1.25E-03
130	159.8	20.89	57.132	348.7	345.8	2.91E+00	2.87E+00	3.98E-02	1.08E-03
160	189.8	20.91	48.317	348.7	345.8	2.91E+00	2.88E+00	3.65E-02	9.14E-04
190	219.8	20.93	35.993	348.7	345.8	2.91E+00	2.88E+00	3.42E-02	6.81E-04
220	238.7	20.94	32.126	348.7	345.8	1.83E+00	1.81E+00	2.04E-02	3.81E-04
				Total:		**2.32E+01**	**2.28E+01**	**3.52E-01**	**1.21E-02**

Table C-3 Numerical calculation of gas balance of OCD reaction at 4 h and 85° C

Time (min)		O_2 %	CO_2 (ppm)	Flow (mL.min⁻¹)		O_2 (g)			CO_2 (g) Production
Initial	Final			'In'	Out'	'In'	Out'	Consumption	
0	0.8	20.07	573.188	348.7	344.1	9.71E-02	9.16E-02	5.50E-03	3.60E-04
1	1.8	19.61	1107.878	348.7	343.3	9.71E-02	8.93E-02	7.82E-03	6.93E-04
2	2.8	19.84	1161.205	348.7	343.0	9.71E-02	9.03E-02	6.84E-03	7.26E-04
3	3.8	20.08	956.406	348.7	344.1	9.71E-02	9.16E-02	5.48E-03	6.00E-04
4	4.8	20.32	720.319	348.7	344.1	9.71E-02	9.27E-02	4.36E-03	4.52E-04
5	5.8	20.51	536.213	348.7	345.8	9.71E-02	9.40E-02	3.08E-03	3.38E-04
6	6.8	20.62	418.806	348.7	345.8	9.71E-02	9.46E-02	2.54E-03	2.64E-04
7	7.8	20.66	350.816	348.7	345.8	9.71E-02	9.47E-02	2.40E-03	2.21E-04
8	8.8	20.71	313.863	348.7	345.8	9.71E-02	9.50E-02	2.14E-03	1.98E-04
9	9.8	20.76	294.667	348.7	345.8	9.71E-02	9.52E-02	1.90E-03	1.86E-04
10	19.8	20.80	254.716	348.7	345.8	9.71E-01	9.54E-01	1.73E-02	1.61E-03
20	29.8	20.80	212.361	348.7	345.8	9.71E-01	9.54E-01	1.75E-02	1.34E-03
30	39.8	20.83	179.720	348.7	345.8	9.71E-01	9.55E-01	1.57E-02	1.13E-03
40	49.8	20.84	160.697	348.7	345.8	9.71E-01	9.56E-01	1.55E-02	1.01E-03
50	59.8	20.84	149.616	348.7	345.8	9.71E-01	9.56E-01	1.53E-02	9.43E-04
60	69.8	20.87	139.681	348.7	345.8	9.71E-01	9.57E-01	1.43E-02	8.81E-04
70	79.8	20.90	134.998	348.7	345.8	9.71E-01	9.58E-01	1.29E-02	8.51E-04
80	89.8	20.92	129.609	348.7	345.8	9.71E-01	9.59E-01	1.19E-02	8.17E-04
90	99.8	20.92	122.973	348.7	345.8	9.71E-01	9.59E-01	1.19E-02	7.75E-04
100	129.8	20.92	113.656	348.7	345.8	2.91E+00	2.88E+00	3.59E-02	2.15E-03
130	159.8	20.90	103.006	348.7	345.8	2.91E+00	2.88E+00	3.76E-02	1.95E-03
160	189.8	20.94	93.036	348.7	345.8	2.91E+00	2.88E+00	3.24E-02	1.76E-03
190	219.8	20.93	74.134	348.7	345.8	2.91E+00	2.88E+00	3.44E-02	1.40E-03
220	240.3	20.93	66.720	348.7	345.8	1.99E+00	1.97E+00	2.29E-02	8.62E-04
				Total:		2.34E+01	2.30E+01	3.37E-01	2.15E-02

Table C-4 Numerical calculation of gas balance of OCD reaction at 4 h and 95° C

Time (min)		O_2 %	CO_2 (ppm)	Flow (mL.min⁻¹)		O_2 (g)			CO_2 (g) Production
Initial	Final			'In'	Out'	'In'	Out'	Consumption	
0	0.8	20.01	666.402	348.7	339.2	9.71E-02	9.00E-02	7.07E-03	4.12E-04
1	1.8	19.59	1719.008	348.7	338.1	9.71E-02	8.78E-02	9.26E-03	1.06E-03
2	2.8	19.72	1986.434	348.7	337.6	9.71E-02	8.83E-02	8.80E-03	1.22E-03
3	3.8	20.12	1557.844	348.7	340.9	9.71E-02	9.09E-02	6.18E-03	9.68E-04
4	4.8	20.35	1143.673	348.7	340.9	9.71E-02	9.20E-02	5.13E-03	7.11E-04
5	5.8	20.55	878.122	348.7	341.1	9.71E-02	9.29E-02	4.15E-03	5.46E-04
6	6.8	20.66	718.761	348.7	342.5	9.71E-02	9.38E-02	3.26E-03	4.49E-04
7	7.8	20.64	629.724	348.7	342.5	9.71E-02	9.37E-02	3.35E-03	3.93E-04
8	8.8	20.66	574.300	348.7	342.5	9.71E-02	9.39E-02	3.25E-03	3.59E-04
9	9.8	20.69	542.422	348.7	343.9	9.71E-02	9.43E-02	2.77E-03	3.40E-04
10	19.8	20.78	442.286	348.7	344.1	9.71E-01	9.48E-01	2.29E-02	2.78E-03
20	29.8	20.81	330.542	348.7	344.1	9.71E-01	9.49E-01	2.16E-02	2.07E-03
30	39.8	20.84	272.519	348.7	344.1	9.71E-01	9.51E-01	1.99E-02	1.71E-03
40	49.8	20.84	232.959	348.7	344.1	9.71E-01	9.51E-01	2.01E-02	1.46E-03
50	59.8	20.84	216.317	348.7	344.1	9.71E-01	9.51E-01	1.98E-02	1.36E-03
60	69.8	20.87	211.449	348.7	344.3	9.71E-01	9.53E-01	1.82E-02	1.33E-03
70	79.8	20.90	202.746	348.7	345.8	9.71E-01	9.58E-01	1.29E-02	1.28E-03
80	89.8	20.88	192.781	348.7	345.8	9.71E-01	9.57E-01	1.38E-02	1.22E-03
90	99.8	20.89	180.770	348.7	345.8	9.71E-01	9.58E-01	1.30E-02	1.14E-03
100	129.8	20.91	167.797	348.7	345.8	2.91E+00	2.88E+00	3.69E-02	3.17E-03
130	159.8	20.91	152.055	348.7	345.8	2.91E+00	2.88E+00	3.63E-02	2.88E-03
160	189.8	20.90	142.369	348.7	345.8	2.91E+00	2.88E+00	3.79E-02	2.69E-03
190	219.8	20.92	131.207	348.7	345.8	2.91E+00	2.88E+00	3.59E-02	2.48E-03
220	241.0	20.92	125.459	348.7	345.8	2.06E+00	2.03E+00	2.47E-02	1.67E-03
				Total:		2.34E+01	2.30E+01	3.87E-01	3.37E-02

Table C-5 Numerical calculation of gas balance of OCD reaction at 95° C and 15 minutes

Time (min)		O_2 %	CO_2 (ppm)	Flow (mL.min⁻¹)		O_2 (g)			CO_2 (g) Production
Initial	Final			'In'	Out'	'In'	Out'	Consumption	
0	0.8	20.04	590.143	348.7	340.9	9.71E-02	9.06E-02	6.53E-03	3.67E-04
1	1.8	19.67	1623.851	348.7	340.3	9.71E-02	8.88E-02	8.33E-03	1.01E-03
2	2.8	19.76	1961.667	348.7	339.8	9.71E-02	8.90E-02	8.06E-03	1.22E-03
3	3.8	20.08	1582.565	348.7	341.1	9.71E-02	9.09E-02	6.25E-03	9.84E-04
4	4.8	20.25	1155.990	348.7	342.5	9.71E-02	9.20E-02	5.14E-03	7.22E-04
5	5.8	20.43	879.823	348.7	342.5	9.71E-02	9.28E-02	4.32E-03	5.49E-04
6	6.8	20.60	712.931	348.7	343.9	9.71E-02	9.39E-02	3.16E-03	4.47E-04
7	7.8	20.65	620.159	348.7	344.1	9.71E-02	9.42E-02	2.86E-03	3.89E-04
8	8.8	20.64	561.463	348.7	344.1	9.71E-02	9.42E-02	2.90E-03	3.52E-04
9	9.8	20.59	527.534	348.7	344.1	9.71E-02	9.40E-02	3.13E-03	3.31E-04
10	10.8	20.71	506.084	348.7	344.1	9.71E-02	9.45E-02	2.60E-03	3.18E-04
11	11.8	20.74	480.884	348.7	344.1	9.71E-02	9.46E-02	2.47E-03	3.02E-04
12	12.8	20.70	458.603	348.7	344.1	9.71E-02	9.44E-02	2.66E-03	2.88E-04
13	13.8	20.72	444.076	348.7	344.1	9.71E-02	9.45E-02	2.56E-03	2.79E-04
14	14.8	20.69	433.946	348.7	344.1	9.71E-02	9.44E-02	2.68E-03	2.72E-04
15	15.5	20.70	423.833	348.7	344.1	6.47E-02	6.30E-02	1.77E-03	1.77E-04
				Total:		**1.52E+00**	**1.46E+00**	**6.54E-02**	**8.00E-03**

Table C-6 Numerical calculation of gas balance of OCD reaction at 95° C and 30 minutes

Time (min)		O_2 %	CO_2 (ppm)	Flow (mL.min^{-1})		O_2 (g)			CO_2 (g) Production
Initial	Final			'In'	Out'	'In'	Out'	Consumption	
0	0.8	20.01	621.187	348.7	340.9	9.71E-02	9.04E-02	6.66E-03	3.86E-04
1	1.8	19.73	1654.895	348.7	339.2	9.71E-02	8.88E-02	8.34E-03	1.02E-03
2	2.8	19.72	2007.545	348.7	340.0	9.71E-02	8.89E-02	8.17E-03	1.24E-03
3	3.8	20.10	1613.609	348.7	340.9	9.71E-02	9.08E-02	6.27E-03	1.00E-03
4	4.8	20.24	1187.034	348.7	342.5	9.71E-02	9.19E-02	5.17E-03	7.41E-04
5	5.8	20.51	910.867	348.7	342.5	9.71E-02	9.31E-02	3.95E-03	5.69E-04
6	6.8	20.59	743.975	348.7	342.5	9.71E-02	9.35E-02	3.59E-03	4.65E-04
7	7.8	20.65	651.203	348.7	343.0	9.71E-02	9.39E-02	3.19E-03	4.07E-04
8	8.8	20.64	592.507	348.7	344.1	9.71E-02	9.42E-02	2.93E-03	3.72E-04
9	9.8	20.65	558.578	348.7	344.1	9.71E-02	9.42E-02	2.85E-03	3.50E-04
10	10.8	20.70	537.128	348.7	344.1	9.71E-02	9.45E-02	2.63E-03	3.37E-04
11	11.8	20.73	511.928	348.7	344.1	9.71E-02	9.46E-02	2.50E-03	3.21E-04
12	12.8	20.77	489.647	348.7	344.1	9.71E-02	9.48E-02	2.31E-03	3.07E-04
13	13.8	20.73	475.120	348.7	344.1	9.71E-02	9.46E-02	2.52E-03	2.98E-04
14	14.8	20.70	464.990	348.7	344.1	9.71E-02	9.45E-02	2.63E-03	2.92E-04
15	19.8	20.77	421.792	348.7	344.1	4.86E-01	4.74E-01	1.17E-02	1.32E-03
20	24.8	20.76	366.105	348.7	344.1	4.86E-01	4.74E-01	1.18E-02	1.15E-03
25	30.3	20.80	325.589	348.7	344.1	5.34E-01	5.22E-01	1.20E-02	1.12E-03
				Total:		**2.96E+00**	**2.86E+00**	**9.92E-02**	**1.17E-02**

Table C-7 Numerical calculation of gas balance of OCD reaction at 95° C and 60 minutes

Time (min)		O_2 %	CO_2 (ppm)	Flow (mL.min^{-1})		O_2 (g)			CO_2 (g) Production
Initial	Final			'In'	Out'	'In'	Out'	Consumption	
0	0.8	20.14	631.159	348.7	339.2	9.71E-02	9.06E-02	6.52E-03	3.90E-04
1	1.8	19.73	1672.867	348.7	337.9	9.71E-02	8.84E-02	8.71E-03	1.03E-03
2	2.8	19.80	2041.183	348.7	338.7	9.71E-02	8.89E-02	8.17E-03	1.26E-03
3	3.8	20.30	1635.248	348.7	340.9	9.71E-02	9.18E-02	5.34E-03	1.02E-03
4	4.8	20.31	1198.840	348.7	340.9	9.71E-02	9.18E-02	5.32E-03	7.45E-04
5	5.8	20.57	920.839	348.7	341.7	9.71E-02	9.32E-02	3.90E-03	5.74E-04
6	6.8	20.69	753.947	348.7	342.5	9.71E-02	9.40E-02	3.12E-03	4.71E-04
7	7.8	20.74	661.175	348.7	342.5	9.71E-02	9.42E-02	2.90E-03	4.13E-04
8	8.8	20.72	602.479	348.7	343.3	9.71E-02	9.43E-02	2.78E-03	3.77E-04
9	9.8	20.72	568.550	348.7	344.1	9.71E-02	9.45E-02	2.57E-03	3.57E-04
10	10.8	20.80	547.100	348.7	344.1	9.71E-02	9.49E-02	2.19E-03	3.43E-04
11	11.8	20.83	521.900	348.7	344.1	9.71E-02	9.50E-02	2.06E-03	3.27E-04
12	12.8	20.84	499.619	348.7	344.1	9.71E-02	9.51E-02	2.02E-03	3.13E-04
13	13.8	20.81	485.092	348.7	344.1	9.71E-02	9.49E-02	2.15E-03	3.04E-04
14	14.8	20.78	474.962	348.7	344.1	9.71E-02	9.48E-02	2.26E-03	2.98E-04
15	19.8	20.85	431.764	348.7	344.1	4.86E-01	4.76E-01	9.68E-03	1.35E-03
20	24.8	20.84	376.077	348.7	344.1	4.86E-01	4.75E-01	1.00E-02	1.18E-03
25	29.8	20.87	336.543	348.7	344.1	4.86E-01	4.76E-01	9.42E-03	1.06E-03
30	39.8	20.90	298.269	348.7	344.1	9.71E-01	9.54E-01	1.72E-02	1.87E-03
40	49.8	20.87	258.561	348.7	344.1	9.71E-01	9.53E-01	1.84E-02	1.62E-03
50	60.2	20.90	241.637	348.7	344.1	1.00E+00	9.85E-01	1.79E-02	1.57E-03
				Total:		**5.86E+00**	**5.72E+00**	**1.43E-01**	**1.69E-02**

Table C-8 Numerical calculation of gas balance of OCD reaction at 95° C and 120 minutes

Time (min)		O_2 %	CO_2 (ppm)	Flow (mL.min^{-1})		O_2 (g)			CO_2 (g) Production
Initial	Final			'In'	Out'	'In'	Out'	Consumption	
0	0.8	20.02	605.923	348.7	339.2	9.71E-02	9.01E-02	7.02E-03	3.75E-04
1	1.8	19.63	1639.631	348.7	337.6	9.71E-02	8.79E-02	9.23E-03	1.01E-03
2	2.8	19.73	2006.947	348.7	339.0	9.71E-02	8.87E-02	8.39E-03	1.24E-03
3	3.8	20.17	1598.345	348.7	340.9	9.71E-02	9.12E-02	5.94E-03	9.93E-04
4	4.8	20.31	1171.770	348.7	340.9	9.71E-02	9.18E-02	5.32E-03	7.28E-04
5	5.8	20.55	895.603	348.7	341.4	9.71E-02	9.31E-02	4.05E-03	5.57E-04
6	6.8	20.68	728.711	348.7	342.5	9.71E-02	9.39E-02	3.20E-03	4.55E-04
7	7.8	20.69	635.939	348.7	342.5	9.71E-02	9.40E-02	3.12E-03	3.97E-04
8	8.8	20.68	577.243	348.7	342.5	9.71E-02	9.39E-02	3.16E-03	3.60E-04
9	9.8	20.70	543.314	348.7	344.1	9.71E-02	9.45E-02	2.64E-03	3.41E-04
10	10.8	20.75	521.864	348.7	344.1	9.71E-02	9.47E-02	2.42E-03	3.27E-04
11	11.8	20.78	496.664	348.7	344.1	9.71E-02	9.48E-02	2.29E-03	3.12E-04
12	12.8	20.79	474.383	348.7	344.1	9.71E-02	9.49E-02	2.25E-03	2.98E-04
13	13.8	20.76	459.856	348.7	344.1	9.71E-02	9.47E-02	2.38E-03	2.89E-04
14	14.8	20.73	449.726	348.7	344.1	9.71E-02	9.46E-02	2.49E-03	2.82E-04
15	19.8	20.80	406.528	348.7	344.1	4.86E-01	4.75E-01	1.08E-02	1.28E-03
20	24.8	20.79	350.841	348.7	344.1	4.86E-01	4.74E-01	1.12E-02	1.10E-03
25	29.8	20.82	311.307	348.7	344.1	4.86E-01	4.75E-01	1.06E-02	9.77E-04
30	39.8	20.85	273.033	348.7	344.1	9.71E-01	9.51E-01	1.95E-02	1.71E-03
40	49.8	20.82	233.325	348.7	344.1	9.71E-01	9.50E-01	2.07E-02	1.46E-03
50	59.8	20.84	216.464	348.7	344.1	9.71E-01	9.51E-01	1.98E-02	1.36E-03
60	89.8	20.88	202.492	348.7	345.6	2.91E+00	2.87E+00	4.25E-02	3.83E-03
90	120.5	20.90	174.301	348.7	345.8	2.98E+00	2.94E+00	3.90E-02	3.37E-03
				Total:		1.17E+01	1.15E+01	2.38E-01	2.31E-02

Appendix D
ICP Calibration Data

Calibration of Silicon (Si) solution with a initial concentration of 1000 µg.mL^{-1} was performed in the concentration range 10-80 mg.L^{-1} to obtain about 25 mL of final solution. The specific measurements of water and the standard for the dilution process whit the corresponding concentrations of each element are presented in Table D-1.

Table D-1 Measurements for calibration of Silicon (Si) solution

Standard Silicon (g)	water (g)	Final Solution concentration (mg.L^{-1})
0.2511	24.7544	10.0418
0.5138	24.5033	20.5380
0.7535	24.2536	30.1314
0.9991	24.0024	39.9616
1.2508	23.7565	50.0174
1.5040	23.5084	60.1302
1.7515	23.2519	70.0505
2.0139	22.9984	80.5164

Calibration of mix majors standard solution containing calcium, magnesium, sodium, iron, and potassium (Ca, Mg, Na, Fe, K) with a initial concentration of 500 mg.L^{-1} was performed in the concentration range 10-80 mg.L^{-1} to obtain about 25 mL of final solution. The specific measurements of water and the standard for the dilution process with the corresponding concentrations of each element are presented in Table D-2.

Table D-2 Measurements for calibration of mix majors solution

Standard mix majors (g)	water (g)	Final Solution concentration (mg.L^{-1})
0.5012	24.4971	10.0247
1.0242	24.0023	20.4623
1.4946	23.5026	29.8953
2.0099	23.0046	40.1747
2.5098	22.5076	50.1611
3.0081	22.0039	60.1331
3.5035	21.5017	70.0554
4.0066	21.0058	80.0923

Calibration of mix 2 majors standard solutions containing silver, arsenic, barium, beryllium, cadmium, cobalt, chromium, copper, manganese, nickel, lead, selenium, thallium, thorium, uranium, vanadium, and zinc (Ag, As, Ba, Be, Cd, Co, Cr, Cu, Mn, Ni, Pb, Se, Tl, Th, U, V and Zn) with a initial concentration of 100 mg.L^{-1} was performed in the concentration range 10-40 mg.L^{-1} to obtain about 25 mL of final solution. The specific measurements of water and the standard for the dilution process with the corresponding concentrations of each element are presented in Table D-3.

Table D-3 Measurements for calibration of 2 solution

Standard Mix 2 (g)	water (g)	Final Solution concentration (mg.L^{-1})
2.5082	22.0598	10.2092
5.0022	20.0138	19.9960
7.5146	17.5019	30.0386
10.0053	15.0104	39.9961

Appendix E

GC-Gas Calibration

Table E-1 presents the retention time and corresponding peak areas obtained for each compound at their specific concentrations. For hydrogen, which served as the carrier gas, no peak areas were identified. The retention time represents the time required for each compound to travel through the chromatographic column and be eluted for identification in one of the detectors. It serves as a characteristic parameter for compound identification and differentiation.

214

Table E-1 GC-Gas Calibration Data

Calibration Standard	Retention time	Component	Vol. Percentage	Area		
				run #1	run #2	run #3
Nitrogen 100%	14.8	N_2	100.00	105361.7	105748.8	104826.5
Air	14.8	N_2	79.00	83624.5	82387.6	82743.8
	14.45	O_2	21.00	12550.1	11853.6	12792.2
Oxygen 100%	14.45	O_2	100.00	84535.1	82360.3	82009.3
Mix 1	1.25	CO_2	10.05	14880.0	14796.3	15272.9
	16.075	CO	15.04	18252.0	18571.0	19421.0
	14.8	N_2	10.03	16298.1	15833.3	18926.5
	15.9	CH_4	1.00	16835.8	18215.3	18046.7
	14.45	O2	0.97	85.6	62.2	88.7
		H_2	62.91	-	-	-
Mix 2	1.25	CO2	40.00	56246.0	55595.7	52156.3
	15.79	CH_4	40.00	935547.8	876795.1	811763.3
	14.8	N_2	20.00	27111.0	28269.0	29695.5
Mix 2(50%) + Air (50%)	1.25	CO_2	20.00	24881.9	23765.6	23726.7
	15.79	CH_4	20.00	479802.2	450708.5	442394.5
	14.8	N_2	49.50	61207.4	59339.6	61305.6
	14.45	O_2	10.50	3894.4	3415.5	3725.7
Mix 1(50%) + Air (50%)	1.25	CO_2	5.03	6804.4	6309.3	6947.7
	16.075	CO	7.52	9013.0	9437.1	9259.9
	14.8	N_2	44.52	53639.0	63187.0	54874.9
	15.9	CH_4	0.50	8739.2	9293.6	9009.6
	14.45	O_2	10.98	2696.9	3894.3	3155.6
		H_2	31.46	-	-	-
Mix 1(10%) + Air (90%)	1.25	CO_2	1.01	1114.7	1193.7	1194.0
	16.075	CO	1.50	2383.2	2448.2	2361.0
	14.8	N_2	72.10	137001.3	139369.0	139748.0
	15.9	CH_4	0.10	1810.3	1850.4	1862.4
	14.45	O_2	19.00	16526.9	16691.1	16707.0
		H_2	6.29			

Appendix F
EOS

Gas analysis quantification between the feed air and gas products was performed using various equations of state (EOS), including the ideal gas law, Van der Waals equation of state, and the Peng Robinson equation of state. The calculations involved determining the number of moles and grams for each component. The results obtained using each equation of state are presented in Table F-1.

Table F-1 Gas quantification with EOS at 5 MPa, 4 hours and temperatures from 90 to 180°C

Description	Reaction Temperature (°C)	Ideal Gas Equation		Van der Waals Equation		Peng Robinson equation	
		moles	grams	moles	grams	moles	grams
Feed Air							
N2	-	2.069	57.950	2.120	59.383	2.096	58.728
O2	-	0.550	17.596	0.556	17.788	0.555	17.771
Gas Products							
N_2	90	2.175	60.935	2.231	62.490	2.205	61.778
	120	2.129	59.653	2.183	61.149	2.159	60.469
	150	2.198	61.565	2.254	63.150	2.228	62.422
	180	2.205	61.776	2.262	63.371	2.236	62.638
O_2	90	0.433	13.862	0.437	13.976	0.437	13.971
	120	0.372	11.904	0.375	11.988	0.375	11.984
	150	0.038	1.208	0.038	1.209	0.038	1.209
	180	0.034	1.075	0.034	1.076	0.034	1.076
CO_2	90	0.020	0.863	0.020	0.864	0.020	0.864
	120	0.096	4.222	0.097	4.256	0.097	4.266
	150	0.269	11.826	0.275	12.100	0.277	12.184
	180	0.401	17.630	0.415	18.252	0.419	18.443
CO	90	0.008	0.234	0.008	0.234	0.008	0.234
	120	0.012	0.335	0.012	0.335	0.012	0.335
	150	0.015	0.430	0.015	0.430	0.015	0.430
	180	0.020	0.553	0.020	0.553	0.020	0.553

Table F-2 Gas quantification with EOS at 1 MPa, 4 hours and temperatures from 90 to 180°C

Description	Reaction Temperature (°C)	Ideal Gas Equation		Van der Waals Equation		Peng Robinson equation	
		moles	grams	moles	grams	moles	grams
Feed Air							
N2	-	0.414	11.590	0.416	11.653	0.415	11.631
O2	-	0.110	3.519	0.110	3.528	0.110	3.526
Gas Products							
N_2	90	0.425	11.901	0.427	11.967	0.426	11.945
	120	0.408	11.426	0.410	11.487	0.409	11.466
	150	0.391	10.953	0.393	11.009	0.392	10.990
	180	0.380	10.631	0.381	10.684	0.381	10.666
O_2	90	0.089	2.855	0.089	2.860	0.089	2.859
	120	0.052	1.675	0.052	1.677	0.052	1.677
	150	0.010	0.335	0.010	0.335	0.010	0.335
	180	0.006	0.202	0.006	0.202	0.006	0.202
CO_2	90	0.004	0.163	0.004	0.164	0.004	0.163
	120	0.017	0.750	0.017	0.751	0.017	0.751
	150	0.046	2.013	0.046	2.020	0.051	2.224
	180	0.049	2.177	0.050	2.186	0.050	2.188
CO	90	0.001	0.038	0.001	0.039	0.001	0.038
	120	0.002	0.057	0.002	0.057	0.002	0.057
	150	0.003	0.073	0.003	0.073	0.003	0.073
	180	0.003	0.094	0.003	0.095	0.003	0.094

Appendix G

Solubility of gases in liquid

The solubility of each gas compound in the liquid was calculated assuming pure water as the solvent, using the pressure of each reaction and determined by applying Henry's law. the number of moles and grams for each component are presented in table E-1.

Table G-1 Gas in liquid quantification applying Henry's law at 5 MPa, 4 hours and temperatures from 90 to 180°C

Description	Temperature (°C)	moles	grams
Feed Air			
N2	-	0.012	0.343
O2	-	0.007	0.226
Gas Products			
N2	90	0.012	0.349
	120	0.012	0.342
	150	0.013	0.353
	180	0.013	0.354
O2	90	0.005	0.172
	120	0.005	0.148
	150	0.000	0.015
	180	0.000	0.013
CO2	90	0.007	0.288
	120	0.032	1.411
	150	0.090	3.952
	180	0.134	5.891
CO	90	0.000	0.002
	120	0.000	0.003
	150	0.000	0.004
	180	0.000	0.005

Table G-2 Gas in liquid quantification applying Henry's law at 1 MPa, 4 hours and temperatures from 90 to 180°C

Description	Temperature (°C)	moles	grams
Feed Air			
N2	-	0.002	0.067
O2	-	0.001	0.044
Gas Products			
N2	90	0.002	0.068
	120	0.002	0.065
	150	0.002	0.063
	180	0.002	0.061
O2	90	0.001	0.035
	120	0.001	0.021
	150	0.000	0.004
	180	0.000	0.003
CO2	90	0.001	0.054
	120	0.006	0.251
	150	0.015	0.673
	180	0.017	0.727
CO	90	0.000	0.000
	120	0.000	0.001
	150	0.000	0.001
	180	0.000	0.001

Literature cited

[1]   Shen, V.K.; Siderius, D.W.; Krekelberg, W.P.; Hatch, H.W.; Eds. NIST Standard Reference Simulation Website, NIST Standard Reference Database Number 173, National Institute of Standards and Technology. https://webbook.nist.gov/chemistry/ (accessed 06 20, 2023).

[2]   Department of Earth and Atmospheric Sciences. University of Alberta, Weather station https://www.ualberta.ca/earth-sciences/facilities/weather.html (accessed 06 21, 2023).